Electrical Performance and Economic Feasibility Analyses of Hybrid and Battery Storage Devices used in Remote Area Islanded Renewable Energy Systems

Prepared by:

Imran Chotia

CHTIMR001

Department of Electrical Engineering
University of Cape Town

Prepared for:

Dr S Chowdhury

Department of Electrical Engineering
University of Cape Town

2 April 2016

Submitted to the Department of Electrical Engineering at the University of Cape Town in partial fulfilment of the academic requirements for a **Master of Science** degree in Electrical Engineering

Key Words: Battery, Operating Reserve, Renewable Energy System, Supercapacitor

Declaration

1. I know that plagiarism is wrong. Plagiarism is to use another's work and pretend that it is one's own.
2. I have used the IEEE convention for citation and referencing. Each contribution to, and quotation in, this final year project report from the work(s) of other people, has been attributed and has been cited and referenced.
3. This final year project report is my own work.
4. I have not allowed, and will not allow, anyone to copy my work with the intention of passing it off as their own work or part thereof

Name: **Imran Chotia**

Signature: _____ **Date:** 2 April 2016

Terms of Reference

The aim of this dissertation was to identify the need for remote area, renewable energy systems operating with storage device reserves. The aforementioned systems were then tested based on their electrical performance and the economic feasibility of deployment.

Acknowledgements

All praise is due to Allah. There is no quantifiable way for me to express my gratitude as nothing takes place without His will. I truly hope to use what I have learnt here to serve this Ummah as an expression of my gratitude and as a form of ibadah.

I would like to thank my Mommy for being my pillar of strength and my Daddy for being my pillar of calmness. I am truly blessed to have you as my role models.

Thank you to Dr Sunetra Chowdhury for your support and guidance throughout this journey. I thank you for the opportunities and knowledge I received under your supervision. You are the perfect example of what a supervisor should be.

Shukran to my beloved siblings; Yusuf, Nadia, Tasneem, Hasan and my nieces, nephew uncles and aunties.

Thank you to all of my friends from the Menzies room 5.26, UCT caf, High School, Twitter, Madrassa and Eskom. I look forward to spending more time with you now that I am free.

Thank you to my beloved Nurunisa, I am so grateful to have done Masters as it gave me the opportunity to meet such a beautiful, positive and caring person. I look forward to spending the rest of my life with you. Thank you for your boring jokes and for bringing porridge to my office.

Thank you Bilqis Rawoot, you are an absolute queen. I am very lucky to have you as a friend and I truly appreciate the hours you put into editing this thesis.

Special thanks must be given to my employer Eskom and the National Research Fund for granting me the funding and resources opportunity to study at University.

I would also like to thank UCT in all of its aspects, my office colleagues, friends, the NEB, EBE, cafeteria, cleaning and sports centre staff, the MSA, PSF, RMF, Student activists, and not to mention the vending machine.

I would also like to send a special thanks to those have kept me motivated and inspired throughout my studies namely, John Cena, Seth Rollins, AJ Styles, Young Thug, Future, DJ Khaled, Chris Brown, Lil Wayne, and the McDonalds R30 meal. You all mean so much to me.

Lastly, I would like to thank my younger brother Sadiq. You are truly my best friend and have made countless sacrifices without complaint during this academic journey. I will never be able to repay you but I do sincerely share this moment with you. The same way we share all our clothes, the car and everything else, I share this accomplishment with you. This is truly OUR MASTERS.

This Master's Thesis is dedicated to my Parents.
Shukran for all of your advice, love, support and duas.

Abstract

South Africa has the fifth largest coal based utility grid in the world, unfortunately many regions in the country are simply too remote for connection with this grid thus have no electricity access [1]. Many remote areas possess high wind speeds and solar irradiance exposure, which makes them ideal for Renewable Energy Systems (RES) but the electrical and economic viability of this deployment, is still in question. Based on these observations, an electrical performance analysis and economic feasibility study based on islanded RES deployment in remote areas of SA is conducted. RES growth is restricted to the effectiveness of its energy management strategy. Pumped Hydro Storage (PHS) is the cheapest islanded large scale storage option but its assignment is restricted to applicable an landscape and terrain [2], [3]. After conducting a critical review, the Lead Acid Battery Storage System (BSS) and Hybrid Battery Supercapacitor Storage (HBS) were over the PHS. A theory development study on established generations systems and storage models was used to compare software designs which resulted in the selection of Matlab software for electric performance analysis and HOMER for the economic feasibility study.

The electric performance analysis was divided into three case studies based on the input power supply, viz. ideal voltage source, Solar Photo Voltaic (PV) and Wind Energy Conversion System (WECS), with each case being connected to a BSS and HBS. A load profile and solar and wind resource investigation was conducted using the NASA, Wind Atlas of South Africa (WASA) and Solar GIS database. Electrical cases were modelled in Matlab and evaluated in terms of power security, load matching, power response and charge algorithm accuracy. The results showed that deploying an islanded RES in South Africa is indeed electrically feasible based on the high power security, load matching accuracy, and disturbance response seen in the solar-RES cases. The wind-RES maintained an uninterruptable power supply but failed to match the load as accurately. Cases which used the HBS showed improvements in power stability; load fluctuation response and an extension of storage device lifespan when compared to the BSS connected cases. This was due to the supercapacitor high power density which made it ideal for the compensation of RES and load fluctuations.

Three new cases were established for the economic study as follows; solar, wind and hybrid solar-wind generation all tested under BSS and HBS conditions once again. A socio economic study established the region of deployment, natural resources, terrain, landscape as well as the price of WECS, PV, storage, and converter components. These findings were used in HOMER to construct an optimised combination of components required for the supply of a 5MWh/d average load. This was followed by a sensitivity analysis which conducted 14 different optimisations at loads ranging from 1-10MWh/d. Economic benefits of the supercapacitor power density was uncovered through a reduction of the required RES Peak Operating Reserve (POR) capacity. This is especially significant in islanded RES, as they demand large POR in order to maintain autonomous power supply. This amounted to substantial NPC savings ranging from $1 - $7.5 million for the 25 year project. What was more interesting was the hybrid wind-solar generation results of the last case which extended total NPC savings, by up to $10 million. The hybrid-HBS does show some POR reductions which brought the COE to 0.3$/kWh on average, with the hybrid-BSS at 0.35$/kWh. The hybrid-BSS is slightly more expensive but has a reduced complexity which can be more inviting to project engineers therefore both hybrid cases are exceptionally feasible for local RES deployment.

Single source RES is indeed electrically and economically feasible and shows extended sizing and performance benefits when implementing HBS. However, the cost reductions and performance benefits of hybrid generation make it the most practical solution to islanded RES in South Africa.

Contents of Thesis

List of Illustrations

List of Figures

List of Tables

1. Chapter 1 - Introduction

1.1 Background to the Study

South Africa is one of the more geographically privileged nations of the world, benefitting from high wind speeds and high solar irradiance. In the last 30 years, most countries have established substantial methods of harnessing and generating sustainable energy. Energy generation accounts for approximately 15% of the South African economy and is a major stakeholder in job creation [1]. Due to previous political influence, South Africa's national grid was severely restricted, only supplying full electricity access to 21% of all households [4]. Since democracy was established, in 1994, the electricity grid was extended in order to cater to a major increase in electricity demand and to support increasing economic growth. As a result, a backlog in electricity generation was observed [5].

The solution to this backlog was proposed by the Renewable Energy Independent Power Producer Procurement Program (REIPPPP), in the form of renewable energy generation. The program sustainability, feasibility and reliability will be subject to on-going inspection before any full-fledged rollout of Renewable Energy Systems (RES) becomes possible in the country [4]–[7]. For this rollout to take place the current public perception and lack of knowledge on RES needs to be addressed to facilitate investment in these generation sources [8].

A pertinent factor relating to mainstream penetration of RES is suitable resource extraction and energy provision. Many areas in South Africa are simply too remote for utility grid connection, and thus have no electricity access at all. Renewable energy and low-carbon microgrids can effectively distribute electricity to these regions, but concerns arise when considering the feasibility of uninterrupted autonomous supply through intermittent natural resources [6], [9].

RES pose a clean energy alternative to coal based utility grids. They are either connected to the utility grid for use as a secondary generation source, or they operate without any connection from the main grid thereby supplying loads autonomously [10]–[12]. In grid connected generation, when excess Renewable Energy (RE) is generated it is usually dumped or sold for cheap to the utility grid. During times of high electricity demand the utility grid energy would then be purchased by the RES provider at more expensive rates [13], [14]. Through storage, the natural resources used can be further extracted at times of high sunlight and increased wind speeds and then employed during these high demand times, thereby reducing the need for additional grid energy purchasing. In most cases, autonomous or islanded RES will require some form of backup energy supply and stabilisation means. This is essential due to the intermittency of generation resources such as wind gusts and sunrays. Observed fluctuations and irregular resource availability means that renewable energy is not continuously generated in islanded RES [15]–[17]. In addition, islanded RES irregularities can lead to a misalignment of supplied frequency and power stability. For this reason storage devices are required to sustain feasible supply mechanisms, with adequate power quality and continuous supply [18], [19].

Through connection with storage devices, both grid and islanded RES systems show an improved electrical performance. Extracting from South Africa's abundance of wind and

solar irradiance resources is a priority for this country, but this should be done while considering the lack of facilities in areas too far for grid connection. For this reason, an electrical performance analyses and economic feasibility study on remote area islanded RE storage devices is conducted.

1.2 Objectives

1.2.1 Aspects to be investigated

The aim of this thesis is to carry out an economic feasibility study and performance analysis of remote-area islanded RES in South Africa, through the use of different storage devices namely, battery and hybrid storage. The performance analysis and feasibility study is conducted through the modelling and the simulation of microgrids with BSS and HBS, in remote area regions of South Africa. Although this goal may form the fundamental objective of this project, additional objectives include:

- A background study highlighting the potential of RES implementation with the purpose of supplying remote area off-grid and rural area loads
- A review of general storage devices and specific battery and supercapacitor storage device literature
- The development of a mathematical and electrical model framework, justifying the selection of simulation software for electrical performance and economic feasibility analyses of RES
- Modelling, simulation and performance analysis in Matlab, of RES with different sustainable energy sources and different storage device options
- Selection of suitable locations for deploying a RES in the Western Cape, South Africa
- Collection of wind and solar resources from the selected location, and relevant load and electrical component data to model and simulate the RES with storage, for economic feasibility analysis
- Economic feasibility study of RES with hybrid and battery storage systems in HOMER
- Analyses of technical and economic results, from which conclusions are drawn with the sole aim being to identify the most feasible South African remote area RES and storage device pair
- Making recommendations on possible design, simulation and strategy improvements

1.2.2 Purpose of Study

The current state of renewable energy generation in South Africa does not promote a sustainable environment. The country is ranked as the 24th worst polluter in terms of carbon emissions globally, and is currently experiencing a backlog in electricity generation [6], [8]. A reason for the high carbon emission is the abundance of coal reserves available within the country (specifically Mpumalanga), which is a result of South Africa being the fifth largest coal producer in the world [1]. Previously, South Africa had no established democracy and operated under academic and economic isolation due to international embargos. A study conducted by the National Electricity Regulator of South Africa (NERSA) showed that 79% of

rural households and 50% of all households, had no access to electricity in 1995 [4]. After significant pressure, democracy was established and provision of electricity was made to more of the country's poor regions. The study further showed that 8 years after 1995, electricity was provided to an additional 19% of households across the country [4]. As a result, the national load was tremendously increased in a short period of time, but the infrastructure implemented was still out-dated, under strain and not well maintained. Delays in construction, shortage of diesel and the collapse of generation infrastructure have all contributed to the current energy backlog. The results of this backlog are more pertinent at present, with SA experiencing more than 30 days of load shedding between 1 Dec 2014 and 17 May 2015 [20].

In order to facilitate investment in renewable energy, this thesis aims to establish the importance of renewable energy storage for autonomous RES designed to supply electricity to remote off-grid load areas. This is to show that small scale, localised storage and autonomous sustainable energy can be provided to remote areas without grid connection, or to terrains which do not accommodate for larger and more elaborate PHS or Compressed Air Energy Storage (CAES).

Since storage devices are essential to extracting the full benefits of RES when no grid connection is possible. Since connection with the grid and specific terrains for CAES or PHS is not always possible, BSS and HBS make up the best deployable alternatives. RES have long off-times, which require time scaling and load shifting. Batteries are ideal for these provisions due to their high energy density and low self-discharge. In addition, RES suffer from high generation fluctuations and often require high power density for impulse absorption and maintaining power quality. Batteries are not renowned for their power density but supercapacitors (used in the HBS) are. However, supercapacitors also have low energy density and high leakage, meaning they cannot completely replace battery provisions. Consequently, it is clear that batteries and supercapacitors have ideal opposing strengths, and that through their combination they can potentially provide a high energy and high power density storage alternative. This alternative is known as Hybrid Storage and promotes power quality, reliability and uninterrupted electricity supply for isolated RES. The novelty of using hybrid storage devices to combine the complimentary characteristics of batteries and supercapacitors in providing uninterrupted quality power, poses an exciting venture.

The research on feasibility and performance analyses of RES with BSS and HBS begins with a study which identifies the relevant issues and potential for growth in South African RES. The importance of storage is then identified, and an electrical performance analysis and comparison of hybrid and battery storage systems is carried out. After this, a novel economic supercapacitor model is designed in HOMER and used as part of the feasibility study, which will assess the battery and hybrid storage device's potential for practical application. The prospect of implementing remote area islanded or autonomous generation systems in South Africa is the main motivation for this study. The outcome of this research on energy storage is then expected to contribute to the research and implementation of storage devices in South Africa, and abroad. Scope and limitations of this study are listed below.

1.3 Scope and Limitations

The scope of the study includes:

- Conducting a review and identifying the potential for solar and wind energy generation systems in South Africa, as well as issues preventing its implementation
- Expressing the significance of storage in South African RES by analysing battery, supercapacitor and hybrid storage characteristics and the provisions they bring forth
- Clearly defining and comparing the electrical and mathematical architecture of battery and supercapacitor systems, in order to select the modelling strategy and modelling software required. Additionally, identification of software shortcomings are noted, and necessary assumptions in the design algorithms are made
- Dividing the performance analyses into three case studies, namely an ideal cell voltage source, solar PV and wind turbine generation systems. The electrical simulation methodology of each case study is then explained
- Carrying out the electrical performance analysis and presenting the results for each case study, necessary for when comparing the BSS and HBS
- Establishing the electrical feasibility of remote area RES and whether electrical operation can be sustained, when replacing the utility grid with South African based wind or PV power systems coupled with BSS or HBS
- Conducting a socio-environmental study in order to find a suitable region for RES deployment
- Dividing the economic feasibility study into six case studies of solar BSS, solar HBS, wind BSS, wind HBS, wind and solar hybrid resource BSS as well as wind and solar hybrid resource HBS
- Based on the location and case study requirements established, explaining the procedure for the economic feasibility modelling using HOMER; with special mention of the assumptions made for the proposed supercapacitor model
- Carrying out the economic feasibility study, and presenting and analysing the results with tabulation and discussion on the constant averaged load optimisation study. This is then followed by a sensitivity analyses considering all averaged loads tests and optimised cases, collectively
- Drawing conclusions on the choice of storage devices for islanded generation systems, and identifying which generation procedures and storage systems are most applicable for efficient and cheap energy generation in remote areas of South Africa
- Providing recommendations on modelling, design selection and strategy criteria for future RES storage device research

The study was limited to the above scope but was constrained by:

- High sample time requirements for electrical simulation, which were limited by the computer processor computational constraints

- Large test matrices requirements for sensitivity analyses in economic studies, which were also limited to the computer's processing capabilities

1.4 Thesis Outline

The report is structured as follows:

Chapter 1: Presents a brief background to research proposed, motivation for the study, scope and limitations associated with the study and an outline of the thesis.

Chapter 2: Explains a brief history leading to the current energy state of South Africa, and reviews the latest storage contributions, device types and applications in renewable energy literature.

Chapter 3: Discusses the research methodology for electrical performance analysis of hybrid and battery storage. This chapter first explains the development of theory for electrical and mathematical models, followed by a comparative software model validation of proposed devices. This is followed by an explanation of the procedure in modelling the electrical systems in Matlab.

Chapter 4: Presents and analyses the electrical performance results of the Matlab simulation study for system validation.

Chapter 5: Discusses the methodology followed for conducting the economic feasibility analysis of renewable energy systems and microgrids, with hybrid and battery storage. Firstly, the selection of a suitable location for a microgrid and its corresponding resource and load data acquisition is conducted and presented. Secondly, the selection of electrical components for microgrid and storage are detailed and presented, along with their technical and cost data. Finally, the modelling of microgrid test systems and case studies are explained, along with the strategy used for the economic feasibility analysis in HOMER.

Chapter 6: Presents analyses, and compares economic feasibility study results for various optimal solutions obtained for the case studies. The results are initially compared on the basis of optimal solutions, and then through a collective case sensitivity analysis.

Chapter 7: Presents the concluding remarks associated with the final outcomes of the research project, and provides recommendations to develop a platform for further research in the field of renewable energy storage systems.

2. Chapter 2 - Literature Review

South African Energy and Storage Potential

This chapter reviews the potential for growth and expansion in South African renewable energy, as well as those factors which contribute to it in positive and negative ways. Distributed generation (DG) systems are presently expanding and seen as a stakeholder in the future of sustainable energy production. Key generation factors such as protection, energy conservation, system operation, resource forecasting, uncertainty analysis, storage devices, mathematical models, energy management systems and market and environmental aspects are essential to its expansion.

This literature review is also focussed on applications used which further harness renewable and low-carbon resources through the use of effective storage devices and energy management techniques. Upon reviewing different energy management systems a novel Hybrid Battery-Supercapacitor Storage System or HBS is proposed and compared to a conventional Battery Storage System (BSS) for implementation in a renewable energy generation system. The benefits of both systems are explained and a comparative review of existing and potential storage architecture is discussed in this chapter.

2.1 Resource and Renewable Energy Potential in South Africa

In recent decades the growth of worldwide technology has facilitated an accelerated demand for energy. This growth is illustrated in Figure 2.1 which shows that the anticipated global energy consumption is expected to double in the fifty year span of 1990-2040. Electricity demand is rapidly increasing across the world, but in many developing countries the growth of energy infrastructure is not increasing at the same rate. In South Africa, issues of accessibility to energy still need to be addressed to completely satisfy the growing demand. Another aspect that needs to be considered is the impact this demand has on the planet. All of these influences have led to the culmination in advancements and growth in the field of Renewable Energy Systems (RES) research [21], [22].

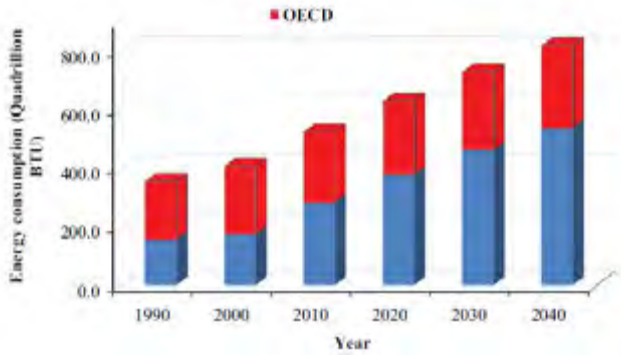

Figure 2.1 Total Global Energy Consumption from 1990-2040 in Quadrillion British Thermal Units [23]

South Africa has abundant wind and solar resources hence the scope of harnessing these technologies is gradually growing in the country. Still some references such as [9] tend not

to consider solar or wind as potentially viable energy sources in the country. Most African nations show an abundance of irradiance rays, including South Africa. The African continent literally outshines the rest of the world in terms of solar energy potential. South Africa's potential for wind generation is estimated at 70% of the nation's electricity needs of 80TWh of energy [24]. Considering the global Photovoltaic (PV) and wind resource maps in Figures 2.2 and 2.3, this is easy to believe.

Nations based along the equator experience low air pressure, due to increased sunlight exposure and higher temperatures. Wind blows from regions of high pressure to low pressure. In most cases, this means that wind travels from the Southern and Northern hemispheres towards the equator. The problem is that once the wind gets there it essentially stops blowing due to the earth's rotation. When the earth rotates it generates an opposing Coriolis force. This force deflects all of the wind which travels towards the equator which results in these nations having low wind speeds. Fortunately, South Africa is based on latitude of 40^0 S. This means that South Africa's wind resources are not near the equator line and are still substantially high. In addition, South Africa is situated in the African continent which means the irradiance values are in abundance as well. Having an abundance of both wind and solar resources makes the prospect of renewable and hybrid generation more beneficial in South Africa [16]–[19].

In terms of wind energy generation, between the years 1980 – 2005, the wind turbine rotor blade diameter underwent a substantial increase in length from 20m to 120m. Since then, the average rotor blade diameter has remained fixed. Previously wind energy research literature suggested that the goal was to extract as much power from the wind as physically possible [25], [26]. This resulted in issues of stability, reliability, control, quality and integration of supply. With large scale wind energy systems being established, the current trend in research is toward an improvement in the extraction capacity of the wind turbines [26]–[28]. This subsequently increases its feasibility in areas where high resources and low investor confidence is observed, particularly South Africa.

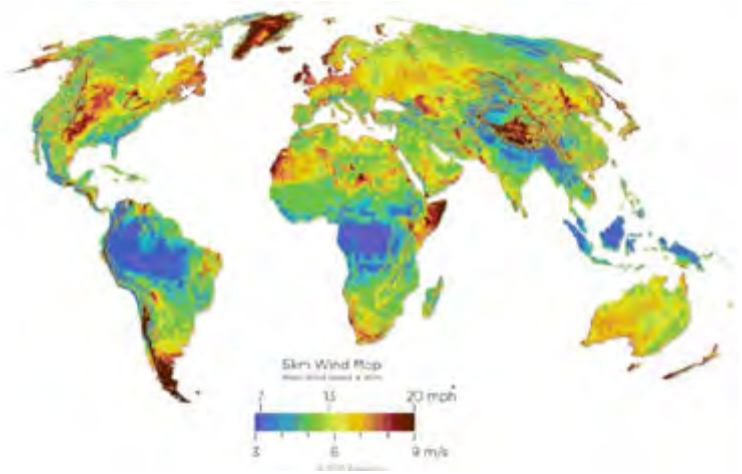

Figure 2.2 5km World Wind Speed Map [29]

Unlike wind energy, solar energy does not present potential noise or visual disruption, but is still overlooked in terms of its feasible potential in the country [30]. Figure 2.3 shows that South Africa's global solar irradiance values are seen to be above the average values

measured across the world, and that it has the potential to become a sustainable source of clean energy in the near future [29]. Section 7.1 of the South African Integrated Resource Plan (IRP) for electricity from the years 2010 -2030 states that: when the cost of storage is neglected, PV generation in remote areas can present costs which are similar to current tariffs. The department of energy goes on to seriously recommend solar generation due to this economic potential [31].

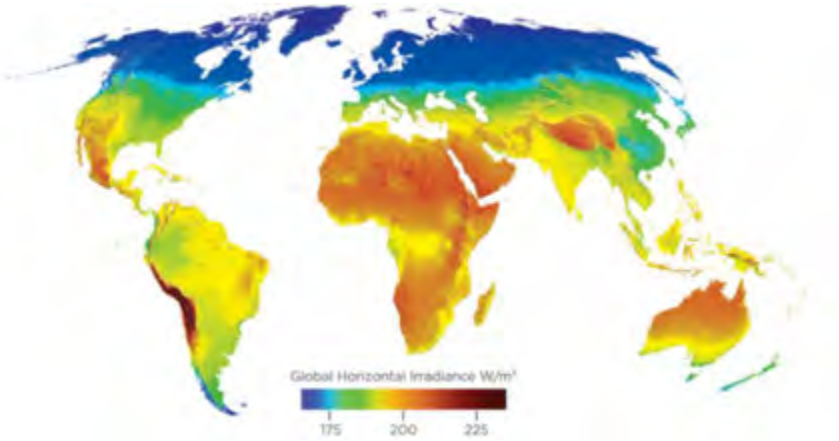

Figure 2.3 Global Horizontal Solar Irradiance W/m² [29]

A South African study comparing coal based generation systems to solar energy was conducted in [32]. The study made use of learning curves for the coal and solar energy comparison. Learning curves are a generalisation method used to predict future costs of products based on historical behaviour. The learning rates are used as a future cost prediction tool based on previous cost trajectories. The study showed that, based on the present decline in PV prices, solar generation can reach parity with coal based generation costs if the current learning rates of PV modules are maintained [32]. This claim has been validated via the potential evident in other countries such as Thailand and Vietnam, where PV energy is currently measured to be lower than alternative fossil-fuel based grid generation [33]. In order to validate this estimation the learning rates of PV power needs to be maintained by effectively managing the energy generation of the systems and through developments of efficient energy extraction [22], [34]. With the demand of energy and potential growth being established, current and future wind and solar RES projects are now considered.

2.2 Current and Future Wind and Solar RES in South Africa

The abundance of solar and wind sources observed in South Africa has been used in certain instances, in the form of planning and commissioning of various energy generation schemes. Considering the wind profile map in Figure 2.2 a few small scale wind RES have been implemented as confirmed in Figure 2.4. Interestingly nine of the RES projects are located in the Eastern Cape Province. This shows the importance of resource assessment and selecting a location before deployment, when working with sustainable energy resources. According to Figure 2.4 the locations of PV RES also correlate to the abundance of irradiance in the Northern Cape and Free State provinces of South Africa.

A few concentrated solar power (CSP) plants are currently being implemented as seen in Figure 2.4 and Table 2.1; this is still a relatively new generation technology though it shows potential for cost reductions according to [32]. Furthermore, Figure 2.4 shows two hydroelectric power generation systems that are implemented but are still restricted on the applicable terrain and resource availability [33], [35]. Some wind and solar RES in South Africa and their capacities are now listed in Table 2.1 below.

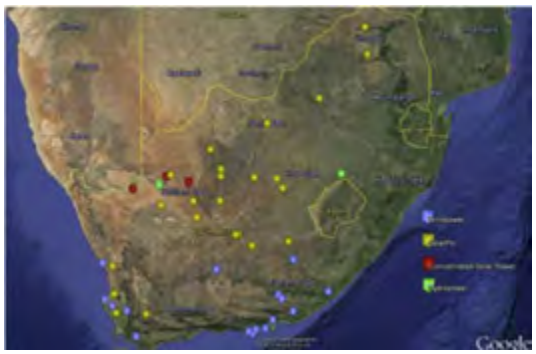

Figure 2.4 Renewable Energy Generation Systems in South Africa [11]

Table 2.1 List of Current and Future Wind and Solar Projects in South Africa [20]

Projects Awarded Bid Windows				Currently Running	
Wind	**Capacity (MW)**	**Solar PV**	**Capacity (MW)**	**Concentrated Solar PV**	**Capacity (MW)**
Nobelsfontein Phase 1	75	Letsatsi Solar Photovoltaic Park	64	Bokpoort	54.5
Dorper Wind Farm	97.5	Lesedi Solar Photovoltaic Park	64	KaXu Solar One	100
Dassieklip Wind Energy Facility	27	Witkop Solar Park	30	Khi Solar One	50
Metrowind Van Stadens	27	Touwsrivier Solar Park	36	Xina Solar One	100
Kouga Red Cape Oyster Bay	80	Soutpan Solar Park	28	Undisclosed	100
Jeffreys Bay Onshore Wind	138	Mulilo Solar PV De Aar	10		
Hopefield Wind Farm Onshore	65.4	Mulilo Solar PV Prieska	20	**Wind**	**Capacity (MW)**
Cookhouse Wind Farm Onshore	138.6	Konkoonsies Solar Energy Facility	9.7	Amakhala Emoyeni	134.4
Gouda Wind Project	135.5	RustMo1 Solar Farm	6.9	Coega	43.2
Amakhala Wind Project	133.7	Kalkbult	72.5	Cookhouse	138.6
Tsitsikamma Community Farm	94.8	Aries Solar Energy Facility	9.7	Dorper	100
Wind Farm West Coast 1	90.8	Slimsun Swartland Solar Park	5	Eastern Cape	80
Waainek Wind Power	23.3	Mainstream De Aar PV	45.6	Eastern Cape #2	27
Grassridge Onshore Wind	59.8	Greefspan PV Power Plant	9.9	Grassridge	61.5
Chaba Wind Power	21	Kathu Solar Plant	75	Hopefield	66.6
Longyuan Mulilo DeAar 2	139	Solar Capital De Aar	75	Klipheuwel	30.1
LongyuanMulilo Maanhaarberg	96.5	Mainstream Droogfontein	45.6	Klipheuwel	3
Nojoli Wind Farm	96.5	Herbert PV Power Plant	20	Nobelsfontaine	73.8
Loeriesfontein 2	138.2	Solar Capital De Aar 3	75	Sere	100
Noupoort	79.1	Sishen Solar Facility	74	Van Stadens	27
Khobab Wind	137.7	Aurora-Rietvlei Solar Power	9		
Red Cape Gibson Bay	110	Vredendal Solar Park	8.8		
		Linde	36.8		
		Dreunberg	69.6		
		Jasper Power Company	75		
		Boshoff Solar Park	60		
		Upington Airport	8.9		
		Adams Solar PV 2	75		
		Electra Capital (Pty) Ltd	75		
		Mulilo Sonnedix Prieska PV	75		

	Mulilo Prieska PV	75	
	Tom Burke Solar Park	60	
	Pulida Solar Park	75	

As previously mentioned solar generation costs are steadily declining in South Africa. This is reflected by the increase of proposed PV, wind and CSP systems currently under construction, which are marked in green in Table 2.1. Project bids awarded in Table 2.1 show that small scale solar PV and wind RES are gathering interest, especially on a medium voltage scale. These systems are ideal for incorporating battery storage and to then be utilized for generation in remote areas. Large-scale RES of over 100MW are commonly connected to the utility grid but this is not always plausible. Potential factors which could hinder the implementation and operation of solar and wind RES projects mentioned thus far are now discussed in the next section in the context of South Africa.

2.3 Factors Affecting Solar and Wind Generation in South Africa

Distributed Generation and RES are seen as the crucial solutions to the current electricity backlog observed in South Africa. DG is being helped by growth in distributed wind and solar energy generation and their complimentary technologies [26], [28], [37]. Despite the large capacity in terms of natural resources available in South Africa, there are certain factors that restrict PV and wind power expansion locally.

2.3.1 PV Generation Factors

Penetration of solar energy is often associated with availability of solar irradiance rays and spectral analyses. In addition to this, environmental and climatic factors in the selected region must also be considered for local PV energy generation. Moreover, there are some other factors which are not as obvious but can have significant impact on supplied load. In most cases these factors can be seen as trivial but upon further investigation are found to significantly affect operational efficiency, cost and continuity, or the quality of supply in some instances [38], [39]. Key factors affecting solar PV generation are discussed below:

a) Shading & Seasonal Effects

Partial covering or shading of the solar panels due to movement of animals, people or cloud cover can reduce the solar irradiance captured by the panels and hence their energy output. Human and animal movement which cause partial or complete shading is far more apparent and significant in solar PV RES in remote areas; unless restricted by securing the generation system and its associated substation.

The problem with cloud cover is that it is an uncontrollable external factor that will still have large bearing on PV supply. Potential cloud cover, even for a short duration, can cause large and abrupt drops in instantaneous and short-term output power generated [38].

b) Terrain and Dust

Geographical terrain in which the PV farm is located can have significant impact on its energy production. Soiling is commonly underestimated but can be the deciding factor in the viability of the PV installation [39]. A test conducted in the Sahara and measured the difference in power outputs for clean and dirty PV modules in Figure 2.5 [40].

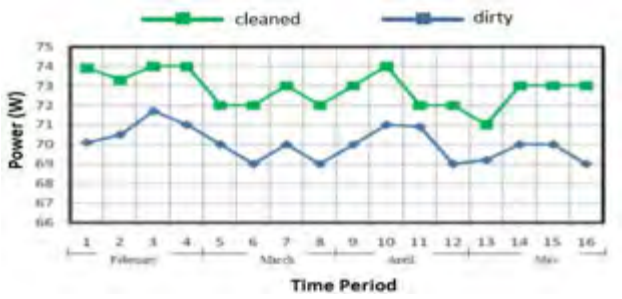

Figure 2.5 Power Measurement of Clean and Dusty PV Modules [40]

Figure 2.5 shows a substantial difference in power measured when comparing a clean and a dirty solar panel. The result of Figure 2.5 will be amplified when using a large scale PV bank for microgrid or RES supply. Some PV models have used automated sprinklers but this is not cost effective since each module consumes around 5 litres of water per wash [40]. The best solution reported by *Sarver et al.* states that manual water spraying is the most effective for solar panel maintenance especially in during dry climatic conditions [39].

c) Theft and Angle of Exposure

A possibility of theft of solar panels poses a major challenge to the viability of solar PV systems in South Africa. Different approaches are taken to counter this threat. This is evident in some communities where PV panels are mounted flat on the ground and are then taken in at night for safekeeping. Additionally, mounted panels with coupled security sensor lights have been implemented but the lights are run off the PV panel supply which reduces its efficiency. Even if the PV equipment is not completely lost/stolen, threat of theft still affects the PV generation productivity [33].

In order to gain maximum exposure of solar irradiance, the solar panel must be laid firmly at an optimum angle. In advanced systems PV farms, angle tracking panels are often employed but the most cost effective rural area solution is to lay the panel at the effective angle based on latitude and climate. This is often difficult when the threat of component theft is imminent. A study conducted in the Thlataganya Village in the Polokwane province in South Africa has shown that the highest overall energy output locally occurred at a 24° tilt [33]. With this angle being established a solar home system (SHS) optimisation study was conducted in Polokwane which showed that by simply using the optimised angle and monitoring the coupled battery SOC, the lifecycle cost was reduced by 19-26% per SHS when compared to a flat mounted panel without battery SOC monitoring [33], [41].

2.3.2 Wind Speed, Energy Cost and Generation Factors

Many factors currently hinder the growth of wind energy generation in industry. The unpredictability of this resource often reduces investor confidence. A selection of common issues which occur with wind energy have been identified, and a review of previous literature which pose potential solutions is presented.

a) Wind Speed Fluctuation and Forecasting

The biggest factor influencing renewable energy generation and penetration is its intermittency. Variation in wind speed means that the generation capacity of a wind farm

and its capability to cater to its allocated load will constantly vary, leading to fluctuations in energy costs. The effect of resource fluctuation is presented in the price curve in Figure 2.6.

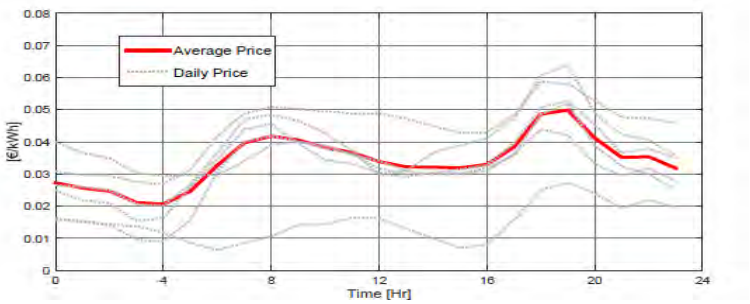

Figure 2.6 Wind Price Fluctuation in a Single Day [42]

Figure 2.6 considers one week of price data from the European Electricity Index market price (ELIX Spot) [42]. The price is measured for a single day and fluctuates substantially considering the fact that the Y-axis is measured in Euros per kilowatt hour. Despite the intermittency the curve still represents a predictable daily pattern which means forecasting methods can be employed.

b) Wind Speed Prediction and Component Sizing

In order to reduce or at least manage the previously mentioned wind price and energy variations the speed and mass of wind anticipated must be found. Forecasting is a common tool used for short term prediction in the range of one hour to one day and is based on resource anticipation [2,22]. Data acquisition accounts for long term models applied to time spans of around 10-20 years. An example of data acquisition is the Wind Atlas of South Africa (WASA) observational report [44]. Data compression and acquisition techniques have improved significantly in recent years which has facilitated improvements in resource predication and component sizing for RES [26, 27].

Due to resource intermittency it is often difficult to accurately predict the ratings of additional components such as storage devices, converters and protection circuits when deploying a RES. In some cases accurate resource prediction is coupled with the respective sizing of power system components. This has been demonstrated through Power Distribution Control Strategies (PDCS) for Hybrid Electric Vehicles (HEV) and statistical models based on historical data of wind speed for RES. This prediction method is built around reducing the amount of cycles required for batteries, which improves sizing and lifespan of components [34, 35].

2.4 Review of Renewable Energy Storage

The potential for penetration as well as weakness of RES has been identified in chapters 2.1 and 2.3 respectively. The influence storage devices have on RES is now discussed in chapter 2.4

2.4.1 Contributions of Storage in RES

In South Africa many areas do not have connection to the national grid and can subsequently benefit from islanded RES. When operating in islanded mode with a single

energy source it is almost impossible to continuously supply electricity without facing energy shortages.

A fundamental requirement of electricity delivery is uninterrupted power supply. Natural resources such as sunlight are only available for half the hours in a day, which limits PV generation. A common solution for large scale storage is Pumped Hydro Storage (PHS) or Compressed Air Energy Storage (CAES). The former has been implemented in three documented cases in South Africa and is rated as the cheapest form of large scale storage as seen in Figure 2.7 [20]. PHS and CAES types are land and terrain dependant which limits their deployment and versatility. In remote and rural areas the South African utility grid does not always extend to supply electricity to consumers [49]–[51].

Since PHS and CAES are restricted to applicable terrains and are based mainly on large scale storage of above 2MW, the provisions of more applicable RES storage alternatives are now considered [3].

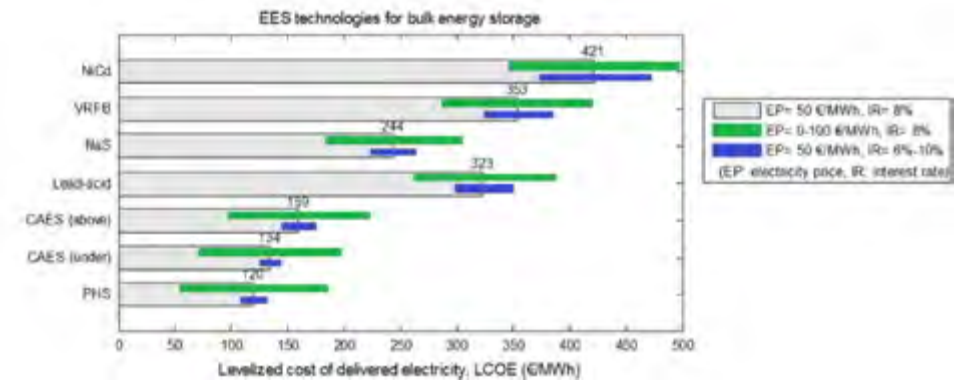

Figure 2.7 Bulk Storage Cost Comparison [20]

a) Renewable Energy Backup

The fundamental purpose of energy storage is to provide an alternative energy source when the primary source is inadequate. In RES this is often the case since renewable resources have stochastic tendencies. When supplying loads in isolation, a storage device is essential to maintaining a constant power supply. When excess renewable energy is generated in grid connected mode the energy can be absorbed and used at a later stage, reducing the need for utility grid purchases [52], [53]. Batteries and other non-disposable storage devices offer cheap but matured technologies which, through charge/discharge cycle management, can absorb excess energy and therefore supply it back to the customers in peak demand times. This benefits renewable energy supplies in islanded or grid connected mode, especially when grid power is not available due to blackouts, maintenance or load shedding [2], [18], [38].

b) Power Quality and Fluctuation Suppression

Based on the nature of the sun, irradiance availability varies throughout the day which results in generated fluctuations. The general consensus between RES modelling authors is to set an additional operating storage reserve value, of 25% for solar energy and 50% for wind energy, in order to compensate for fluctuations [53]. PV panels require direct exposure to sunlight for electricity generation. This makes it very susceptible to shading which can

cause large spikes in energy generation at any time [38]. Furthermore wind energy can increase or decrease within a range of 50% of its generated capacity in merely three hours due to its inherent intermittency [49]. Power quality and suppression of these fluctuations are pertinent to maintaining RES operation.

Generally the utility grid would be used to stabilise power and maintain the required operational frequency upon integration and supply. When no grid is available the cheapest alternative would be the use of battery or hybrid battery supercapacitor storage. A largely accepted means of suppressing fluctuations is by connecting an energy storage system parallel to a DC-DC Buck-Boost converter for solar panels or at the DC link of the back to back AC –AC converter used for adjusting the voltage and frequency of the AC wind energy generated [54], [55]. Since the frequency and voltage needs to be maintained under highly fluctuating conditions, the storage device connected across the DC link or AC-AC converter needs to be able to deliver high magnitudes of energy in short times. High power density systems such as the Lithium Ion (Li-ion) battery or supercapacitor is applicable in these instances [49].

c) Load and Time Shifting

Load shifting refers to the allocation of a mass of electricity from one energy source to another. This could be during maintenance, peak hours or when the primary generation source is inadequate. Load shifting is different to disturbance rejection since it usually considers a substantial mass of electricity which needs to be supplied for approximately two to four hours. This is common during peak hours when the utility grid is inadequate or during off peak renewable energy generation hours.

It is well understood in storage device literature such as [29] and [43] that PHS presents the best option for responding to load shifting. However, when geographical limitations do not permit this, lead acid batteries and sometimes thermal storage is preferred. For a few hours of the day renewable energy resources are readily available, which increases supply thereby reducing generation costs. Unfortunately in wind energy systems, the times of low cost generation are often unaligned with periods of high energy demand. In many cases wind generation demonstrates an anti-peak feature wherein its high cost generation hours actually align with peak demand hours. This issue is not as prominent in PV generation but can be problematic for loads with late night or early morning operation hours [57], [58].

Time shifting is the scheduled reallocation of generated energy for use at a more effective and economical time. The lead acid battery is an ideal storage candidate for time shifting provisions since it possesses a high energy density as well as low self-discharge, which allows for energy retention in long periods [13], [59]. Time shifting can facilitate substantial savings in RES when connected in islanded and grid-connected modes. Through storage devices, low cost energy can be generated and stored then distributed to the load at peak times for island mode operation, or can be sold to utility at more competitive prices in grid connected mode. Time shifting reduces the need for additional energy purchases at peak prices and encourages autonomy of RES [3], [17], [34], [60]. Load shifting refers to the allocation of resources when electricity is essential. Time shifting is a more strategic method of load shifting which involves storing excess energy at off peak times and deploying the

energy at peak hours with the intention of reducing costs. In both cases storage devices are essential to maintaining supply.

d) Spinning Reserve

An essential requirement of renewable energy is to maintain power supply at times when the generation source is momentarily inoperable. This can be seen in cases of shading, wind spikes or general electrical disruption when systems fall out of synchronism. Instead of using additional generators or grid-connections one can alleviate this by using storage devices which operate under a spinning reserve.

The technical definition of spinning reserve is the unused electrical capacity that can be immediately called upon by a system operator or through a controller instruction. Spinning reserve is provided by a synchronised network of devices that are capable of affecting the active power of the system [54]. The spinning reserve is thus a certain amount of energy that is available online while the device is operating considerably below its full capacity. It can therefore supply loads quickly when generation failure occurs [60].

e) End User Peak Shaving

When operating in industry settings, customers run machines which require significant amounts of power over relatively short times. This can happen in residential supply for the initial heat up of a geyser for instance. Some transmission and distribution suppliers became aware of this and started billing clients separately based on the highest power demand averaged over a 15 minute period. The additional high demand charges considered can constitute half the actual energy bill [60].

In terms of RES, these high demand regions may at any time cause the load to exceed available renewable generation. In such cases, storage devices can be used to reduce this demand on the RES. The supercapacitor has especially high power density and is particularly useful for instances like these. Using a supercapacitor for peak shaving can reduce the cost of the additional energy bill and can reduce the cost of using an oversized battery [58].

f) Voltage Control Support and Ride Through

RES such as solar PV systems and squirrel cage induction type wind generators consume large amounts of reactive power. In order to maintain an operable voltage level, reactive power must be effectively controlled. Batteries, flywheels, supercapacitors and Superconducting Magnetic Energy Storage (SMES) are ideal for reactive power control due to their high ramp rates [54].

Using energy storage allows for the serving of short term loads and the elimination of random fluctuations in demand. This can prevent/deter the need for frequency regulation through grid interconnection. Due to the fluctuation often accompanied by RES generation, grid codes state that the wind and solar RES should be able to withstand voltage dips of up to 0% of the rated voltage. This is known as low voltage ride through [54], [55]. By adjusting the storage device output through power electronic converters it is possible to regulate the reactive power injected into the system during voltage dips. This will reduce the dip magnitude and will allow the storage device to momentarily ride through low power outages and eliminate large voltage sags and surges [61].

g) Oscillation Damping and Voltage Fluctuation

When the wind-based RES undergo high penetration levels of wind power, system stability is compromised. This is compromised due to the power oscillation accompanied by excessive amounts of generation. In order to mitigate these oscillations the system needs to maintain synchronisation. This can be done by employing batteries, supercapacitors or SMES devices. The storage device employed detects the oscillation within 20 milliseconds and injects or absorbs active power at a frequency between 0.5Hz and 1Hz. The active power injected or absorbed opposes the oscillation for up to 20 cycles thereby mitigating the oscillation and maintaining the systems angular stability [54].

Solar applications also benefit from storage devices during high and low penetration levels. This is because PV systems are susceptible to short and long term irradiance changes, due to climatic conditions such as cloud cover or exposure to excessively high levels of sunlight. At high penetration levels the PV generation system can inject power to the transmission network which affects the voltage level and protection setting of the RES [38]. At low energy penetration the voltage levels might fluctuate leading to the malfunctioning of other components [62]. It is important in both high and low level penetration cases to maintain the voltage level in PV systems since the loads are connected at a single common place known as the point of common coupling [63]. In order to protect the system and power electronic or protection components from excess power injections, or customers from voltage level imbalances, storage devices are employed and connected in parallel across the converter before transmission can take place [62]. This maintains the voltage and injects active power when necessary.

2.4.2 Observations

Through the use of storage for islanded RES one can eliminate the complex conditions of grid connection and the need to sell energy back to the utility grid at lower prices. Since storage devices absorb the excess energy for supply back to the system.

Optimised conditions mentioned in the best angle operation region for PV connection is subject to the connection of a lead acid battery storage device. It was tested in South Africa with results revealing that with battery operation knowledge and effective energy management systems, significant component lifespans and cost reductions occur [33].

The benefits of time and load shifting show that the battery can easily compensate for any shortages which occur as a result of non-availability of solar or wind resources (e.g. shading of solar PV panels). Wind and solar energy prices fluctuate based on the load demand as well as the resource availability. Considering Figure 2.6, at peak demand hours of between 5pm and 7pm the wind energy price is at its highest. The price then steadily declines into the night. Wind energy availability actually decreases at night but since the demand is dramatically reduced later in the evening, the cost of energy declines. Through renewable energy backup and time shifting, energy can be stored at the cheapest times and deployed at times of price hikes. The wind and solar energy price is less susceptible to sudden fluctuations making it more feasible for implementation and purchase [42].

A study on the use of lead acid batteries in domestic PV lighting systems, found that despite the battery being cheap, overloading by the user caused significant reduction in battery life. A lack of user awareness and knowledge results in poor handling and

maintenance of the batteries and therefore in many cases users go back to the reliable gas-based or coal-based generation systems. This shows the fundamental motivation behind conducting a study on battery storage devices for RES. Through the understanding of resources and established components as well as research into new ones, the penetration of renewable energy in South Africa and other developing nations can be fast tracked[33]. Battery and hybrid storage research and implementation show the potential to resolve many of the issues identified with renewable energy deployment in the South African context. This can increase the reliability, sustainability, economic gains, and openness of investors to RES in South Africa.

2.5 Types of Batteries

Battery storage systems are one of the most established and well researched storage devices available. The device has remained relevant and applicable to industry by constantly undergoing minor adjustments which result in cost reductions and performance improvements. Insight on the most common batteries available and their provisions are now reviewed in this section.

2.5.1 Lead Acid Battery

Lead acid batteries have invariably been chosen as the ideal battery. Since their development in the 19th century, they have undergone steady development in technology; though in most cases their electrochemistry basis has remained unchanged. Material science improvements and engineering design advancements have contributed significantly to this battery composition and technology. An example of a very recent development is the plate grid modification in the battery. It uses an improved lead alloy design and larger honeycomb shaped negative carbon plate electrode with industry grade precursors. This improves and scales the negative active material which has shown an improvement in autonomous battery supply [64]. The material separators, cell battery construction and the replacement of glass packaging with polypropylene are just a few of the recent advancements made to lead acid batteries [61].

The developing sectors of wind and solar energy generation have facilitated the emergence of lead acid batteries as a key component of RES. Due to their penetration in industry and cheap costs, lead acid batteries possess a very large target market. According to a storage device review conducted in [3], this battery is ideal for loads of between 30-500kWh. The major weakness found in lead acid batteries is of course the limited lifespan which is rated at 3-12 years. This short lifespan is due to the low cycle life of the battery which is measured at less than 1500 cycles. In addition, they are susceptible to lifespan degradation as a result of frequent shallow discharge cycles. High power disturbance response often required from the battery leads to oversized components in order to protect the battery from undergoing deep discharge [56], [65]–[67].

Recently the recyclability of lead acid batteries has improved in addition to reduced replacement costs. They are reasonably efficient at an average value of 80% and have a distinct benefit of very low self-discharge figures, of under 0.1% [56]. A large amount of research and models of lead acid batteries are available which has essentially made them the preferred general battery storage device.

2.5.2 Nickel Cadmium Battery

Nickel Cadmium (Ni-Cd) batteries present good technical characteristics. They were invented in the 19th century which makes them as old as the lead acid battery. The batteries range from 1500 cycles for pocket plate vented categories and 300 cycles in sinter vented designs. The energy density presented in this battery is 80Wh/kg. Ni-Cd batteries use a Nickel Hydroxide material for the positive electrode and electrolyte, and an aqueous solution of Potassium Hydroxide and a Lithium Hydroxide alloy. The negative electrode uses Cadmium Hydroxide but can also use Metal Alloy (Ni-MH) or Zinc Hydroxide (Ni-Zn). However, both alternative electrode connections present far lower cycle life and energy densities than Ni-Cd [17], [54]. A study which considers the life cycle cost price for charging power is presented in Figure 2.8. The first red block in this figure shows that Ni-Cd batteries have a lower cost compared to the lead acid and flow batteries in the first hour of discharge. The second red block shows that the Ni-Cd battery is clearly the most expensive storage device compared to the other batteries after 3 hours of discharge time. The plot of Figure 2.12 is helpful in selecting the ideal storage device based on the application constraints required. It does not, however, consider the inefficiencies of storage devices which will have an effect on overall costs [51].

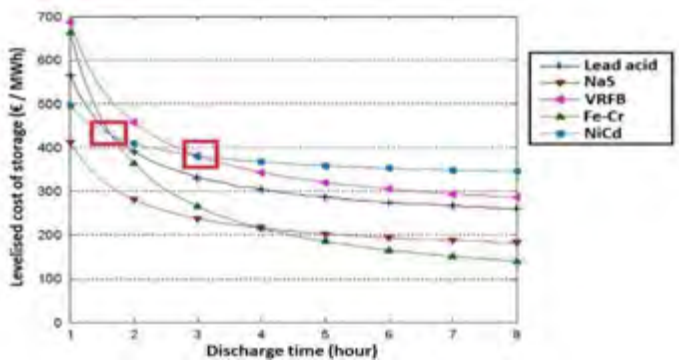

Figure 2.8 Levelised Cost Added by Storage versus Discharge Times [51]

Despite these promising characteristics Ni-Cd batteries presents fundamental weaknesses which have hindered its success. Regardless of its old architecture, no attempt has been made to make it more environment-friendly. The disposal of toxic cadmium is still a major issue which is problematic for sustainable energy usage [61]. Depending on the plate design its efficiency spans from 65% to 83%. The self-discharge value of 10% of the rated capacity per month severely reduces its time scaling and load shifting capabilities. The proprieties mentioned are generally inferior to the lead acid battery yet the price of Ni-Cd is 10 times higher than the lead acid battery [54], [67].

2.5.3 Sodium Sulphur Battery

The Sodium Sulphur battery was developed in the 1970s with several designs having been proposed throughout its lifespan. The most important features of this device are:

1. The liquid sodium used as the active material in the negative electrode
2. A liquid sulphur material used for the positive electrode
3. The beta aluminium ceramic separator which functions as an electrolyte.

Sodium Sulphur is a type of molten metal battery which has a high energy density and high efficiency of 83-92%. The battery also has a long cycle life and is fabricated from cheap sodium beta and liquid sulphur material. It is a rechargeable metallic battery which provides a promising energy utility option for applications which require load levelling, power quality enhancement and peak shaving [68].

During discharge the battery dissipates sodium polysulfide which is highly corrosive. In addition, the discharge process is an exothermic reaction which results in high level heat dissipation as well as an operating temperature of 300-330^{0}C. Because of the corrosive discharge produced and high operating temperature this device is not used in mobile applications but is still suitable for grid energy storage [54], [68].

2.5.4 Lithium Ion Battery

In today's era the reliance on cell phones, tables and laptops is constantly growing. As a result the need for compact extended battery life storage is increasing the development of Lithium Ion (Li-ion) batteries has been accelerated by the increased reliance on electronics.

These batteries are amongst the ones with the highest power density and are used for small scale hand held storage or even efficient electric vehicle (EV) operation. Their energy density is rated at 75-125 Wh/kg and they can reach 90% of rated power at 0.2 seconds, resulting in a high power density as well. The round trip efficiency of 78-90% within 2500 cycles makes this battery very efficient and yields a significant lifespan [69], [70].

Li-ion batteries are expensive and are suitable for mostly small scale storage systems ranging from small scale electronics to 10kWh [3]. Despite recent price reductions their application in large scale generation is still not practical [51]. Li-ion batteries can perform the RES's needs of load levelling and voltage stabilisation due to their high power density and fast response, but they are still not the ideal choice since RES applications require time shifting yet li-ion batteries suffer from high self-discharge. In addition, while being used on a large scale basis they can be seen as dangerous since they do not possess internal protective circuits and are susceptible to overcharging [3].

2.5.5 Flow Battery or Regenerative Fuel Cell

One of the clear benefits of flow batteries is that their energy capacity is easily scalable as it is dependent on the electrolyte volume. The flow battery contains an electro-active substance dissolved in electrolytes which flows through an electrochemical cell and subsequently converts the chemical energy directly into electricity , as seen in Figure 2.9 [54], [61]. They are rechargeable but Figure 2.9 shows that their electrodes and electrolytes are coupled differently in comparison to other electrochemical batteries. They are fundamentally the hybrid product of a fuel cell and a secondary battery, and are more volumetrically efficient. The amount of electro-active substance stored in tanks determines the capacity of the battery in Wh. This creates a considerable benefit in stationary applications [54], [61], [71].

Flow batteries are available in Vanadium redox, Polysulphide-Bromide or Zinc-Bromine types and all possess high specific energy of around 70-80 Wh/kg. This is 2-3 times higher than that of lead acid batteries; but their efficiency at 75-85% and number of charge /discharge cycles between 1000-2000 times are both lower than in lead acid batteries. It is

important to note that their cycles differ from other batteries since they have the capability of full discharging or charging per cycle [54], [61]. This is an essential development since previously, depth of discharge was perceived as a limit on Li-ion battery lifespan, only recently being established as the number of cycles over time, which actually contributes to cell degradation [69], [72].

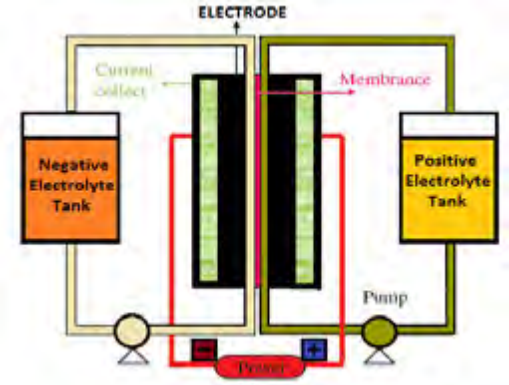

Figure 2.9 Flow Battery Schematic Diagram [71]

Unlike fuel cells the flow battery can be directly recharged and is far cheaper than its counterpart (with the exception of the Polysulphide-Bromide flow batteries). The only major disadvantages noted with this system are the high discharge rates, but this is only apparent during initial stages. It is a promising but complex storage system with minimal literature available thus far [61], [68].

2.6 Supercapacitors

The supercapacitor is one of the fastest energy storage technologies currently available. It has a high initial capital but when used effectively can result in substantial cost benefits due to its long lifespan and power density. In order to capitalise on this system's potential the properties and provisions of the supercapacitor is explained in this chapter.

2.6.1 Model Architecture

Supercapacitors are also known as the ultra-capacitors or the electric double layer capacitors (EDLCs). One supercapacitor electrochemical cell contains two conductor electrodes, a porous membrane and molecule thin layer electrolyte dielectric separator, whereby ion transit between the two electrodes takes place. The supercapacitor electrochemical design is illustrated in Figure 2.10.

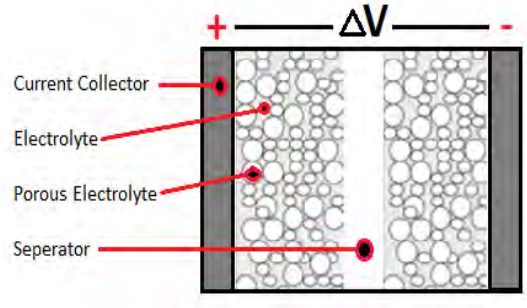

Figure 2.10 The Supercapacitor Cell Architecture [67]

The stored energy in a supercapacitor is directly proportional to the square of the voltage observed between terminals of the cell. The actual Farad capacity is proportional to the very proximity of the electrodes as well as to their surface area. The simple distinguishing factor between a normal capacitor and supercapacitor is that the latter uses porous electrodes with a high surface area and distinctively thin layer. This large area and molecular thickness is what attributes the larger capacitances observed when compared to a normal capacitor [73]–[75].

2.6.2 Lifespan

Supercapacitors are electrochemical storage device which rely on electrostatic action. Since no chemical actions are involved the effect is easily reversible. Hence, the supercapacitor has the advantage of deep discharge and over charge with minimal degradation. Minimal degradation means the supercapacitor has a tremendously long lifespan and can undergo over 500 000 charge/discharge cycles [67].

2.6.3 Thermal Dependence

Much like the battery applications, it is important to understand thermal dependence of supercapacitors. The thermal profile of every storage device is what limits its appropriate storage applications. The capacitance-frequency dependence of a supercapacitor for various temperatures is shown in Figure 2.11.

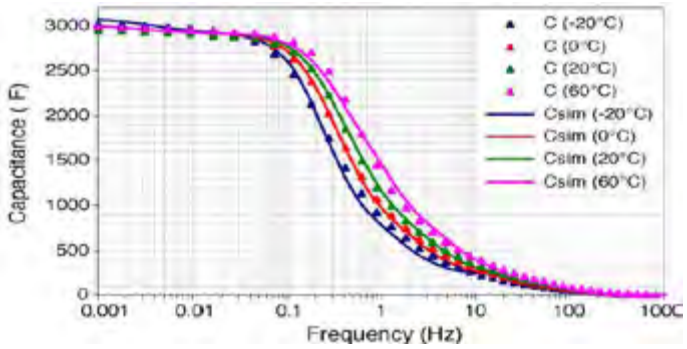

Figure 2.11 Capacitance Frequency Dependence for Different Temperatures [76]

This figure indicates that at very low frequencies of under 0.1 Hz the capacitance is almost constant with temperature, since the ions penetrate in the depth of the pores of the electrode. Basically at very low frequencies the capacitance and temperature contribution is the same regardless of temperature. In the frequency range of 0.1 – 10Hz the capacitance substantially declines. This decline is observed for all measured temperatures in this frequency region but capacitance is lower for lower temperatures. The reason for this is the shift in cut-off frequency due to reduced ion mobility, which implies an increase in the series resistance [76].

2.6.4 Voltage Balancing

Series supercapacitor stacks lead to unequal voltage distributions as the capacitance of each supercapacitor can vary slightly due to the physical structure of each cell. Since the stack of supercapacitors contains a series capacitance value at each electrode, the cells with

higher capacitance will be charged to lower voltages, and the cells with less capacitance will be charged to higher voltages [76]. This is on the grounds that every cell delivers the same current, and that the voltage is a function of current and capacitance. A capacitor with less capacitance needs a smaller charging time and, in this manner, achieves its highest voltage quicker than a larger sized capacitor. Voltage balancing or equalling circuits are used to protect the smallest capacitor from damage [74].

2.6.5 Power Density and Power Quality

By adding a supercapacitor as an alternative storage device, the potential power quality of systems can be immediately enhanced. A supercapacitor has a high power density and can undergo deep discharge cycles without damage. This makes it capable of constantly responding to high power disturbances. Because of the previously mentioned low voltage ride through regulations and intermittency issues associated with wind and solar energy generation, fast high power responses are required to ensure that these RES intermittency issues do not affect the quality of power supplied to customers. The high power density and robust response capabilities of supercapacitors can ensure system voltage and frequency values are kept within stipulated grid codes therefore ensuring the reliability and quality of power supplied [49], [74], [76].

2.6.6 Renewable Energy Applications

In solar PV applications batteries have to be replaced every 3 - 7 years due to the continuous cycling which has a detrimental effect on the battery lifespan. This comes from the continuous weather fluctuations observed. The same can be said to an even greater extent with wind applications. But with supercapacitors, their capacity to undergo many cycles, minimal degradation and fast reactions cause them to be replaced every 20-25 years. This is ideal since it matches the lifetime of the PV panel often used in RES [74], [77].

As a result overall life cycle costs are reduced through the elimination of frequent operation and maintenance cost requirements. In addition, the robustness, fast response to voltage fluctuations and high power density of the supercapacitor makes it ideal for power quality enhancement in RES. Energy efficiency is often the primary concern in RES, fortunately supercapacitors generate higher charging efficiency than lead acid batteries. For instance, lead acid batteries can lose up to 30% of energy during charging while supercapacitors only lose 10% [74], [78].

Since the supercapacitor can use protective circuits and can operate at higher temperatures with reasonable frequency, they are ideal for PV systems. In many cases renewable energy generation can be observed in cold climates as well, but the potential temperature independence makes the supercapacitor more reliable for renewable energy. Another promising observation is that supercapacitor research suggests a significant price decline in coming years [74], [76].

2.6.7 Disadvantages

The supercapacitor requires voltage balancing when used in series cells. As seen in Figure 2.11 the capacitance value of the supercapacitor slightly increases with temperature but this is only observed at the cut-off frequency region. The major weakness known in

supercapacitors is that it has a high self-discharge. The self-discharge makes it incapable of time shifting. In most instances, the supercapacitor has a small energy density therefore it is preferred as a secondary storage device. High power and energy density supercapacitors are available but this adds to overall component costs. A supercapacitor is usually five times more expensive than a lead acid battery but compensates for costs with long lifespan[75], [76], [79].

2.7 Battery and Hybrid Battery Supercapacitor Storage

The HBS is undergoing major growth as it is primarily designed for the emerging technologies, such as renewable energy based sustainable or low carbon generation systems [80]. As a result the application benefits and optimisation techniques of hybrid storage are a major topic of interest in recent publications [81], [82]. The feasibility and practicality of this system is still in question as the isolated battery storage system (BSS) is already a well-established option for medium voltage applications [49], [83]. By critically reviewing the distinctive operation, application, configuration and economic differences between the isolated BSS and the HBS, one can determine the most applicable storage device for the emerging technologies of wind and solar applications. Establishing the feasibility of storage devices will assist the drive towards fully utilizing the mass of renewable energy sources currently available in South Africa. Section 7.2 of the South African Integrated Resource Plan for 2010-2030 states that storage devices are essential in assisting RES with demand management and balancing capabilities for future projects [31]. Based on this recommendation the following critical review of prominent battery and hybrid storage takes place[84].

2.7.1 Complimentary Characteristics

Battery storage systems have dominated the medium voltage RES industry as an established storage device [85]. Many authors argue that the BSS provides high energy density and requires simple control methods with minimum complex power electronic interfaces and computation methods. In most RES a standard BSS is often used while the primary focus tends toward energy extraction and conversion. Often factors such as time shifting, spinning reserve and peak shaving are not considered for RESs because of the assumption that grid connection is adequate for sufficient power quality. This is true in some cases but it has been established that storage devices can pose benefits to grid connected systems and more importantly allow for autonomous islanded RES [13], [84].

Díaz-González et al. argue in [54] that the issues of short service life and low power density strain the battery and limit its high speed response capabilities, thus they recommend alternatives to the autonomous BSS [54], [82]. In remote areas in South Africa the autonomous RES with a BSS is essential to electricity provision, hence ways to facilitate its autonomy without grid connection needs to be considered. The supercapacitor proposes an alternative since it can compensate for battery weaknesses through its high power density and high cycle life. However, its implementation requires complicated power electronic interfacing and system control techniques used for energy management. In addition to a more complex system the use of a supercapacitor can also bring about higher initial capital costs when compared to older storage devices [79]. One needs to determine

whether the intricate configuration and control techniques of hybrid storage is worth implementation and if so, which of these configurations and benefits are best suited for the RES in question.

Batteries vary in technical maturity, weight, price, degradation proprieties and speed of discharge and charge. These distinctions affect the decision of using a BSS or HBS per application [86]. In this thesis the focus on wind, solar and EV applications means that the most common batteries considered are Nickel-metal hydride (NiMH), Ni-Cd, $NaSO_4$, PbO_2 and Li-ion batteries. Ni-MH has dominated the HEV storage market but recent publications agree that Li-ion batteries are replacing them, since Li-ion batteries possess high electrical and thermal stability and have undergone a cost reduction in the past decade [87]. The specific energy density and power density capacities of the batteries mentioned are compared using the Ragone plot shown in Figure 2.12. The power density defines the speed of reaction of the device, with the energy density determining the capacity of electricity the device is capable of dissipating and absorbing.

Lead acid batteries have been implemented in HEV and small scale applications but Li-ion is commonly preferred as it lasts significantly longer and weighs less. In their defence, lead acid batteries are the most prominent choice in medium voltage renewable storage applications when accessibility to reservoirs for pumped hydro storage is not available or feasible. This is confirmed by the cost analysis bulk storage comparison shown in Figure 2.7. Lead acid batteries are seen to have a significant role in the future of renewable energy storage as they are a mature, reliable and easily obtainable technology with high energy density and well understood recyclability procedures [49], [88].

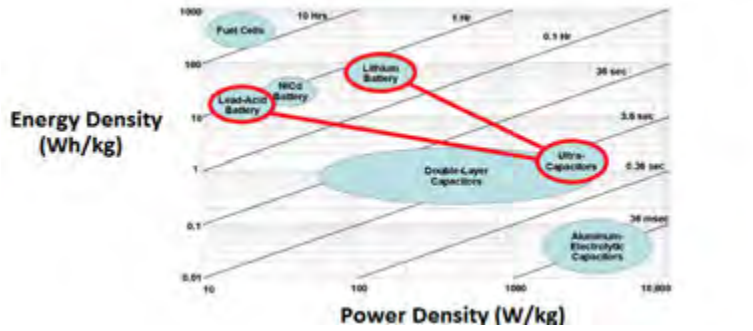

Figure 2.12 Ragone Plot for Storage Devices [84]

Despite lead acid batteries' high availability in industry and low initial cost, their lifespan of under 1000 full cycles constitutes a large part of the application cost through replacement and servicing [89]. Lead acid batteries have a significantly low power density of under 100W/kg which limits its response time to severe load fluctuations and renewable energy variations [85]. Considering Figure 2.12, the supercapacitor offers power densities of between 1000-5000W/kg and a service life of over 500,000 cycles allowing rapid response to short term load fluctuations despite their low energy density [75], [85]. The complementary energy and power density properties of the battery and supercapacitor, as seen in Figure 2.12, facilitate their union as an ideal high energy and high power density storage device.

2.7.2 Potential Applications

It is well established that batteries hold a strong place in the renewable energy and HEV sectors. Batteries are especially effective in supplying steady loads but Renewable Energy Power outputs and price can fluctuate due to weather changes [89]. Model Predictive Control (MPC) and BSS scheduling systems are designed to compensate for these variations from their specified values. A cost effective integration of wind energy and the centralised grid was proposed [90]. By employing MPC the grid can eliminate power fluctuations which allows the battery to be used as the primary storage device [90]. As mentioned, in this instance the RES is fixed to the grid such that fluctuations, lifetime extension and power quality needs are compensated for by the grid, therefore a BSS was sufficient. Conversely, in an autonomous (islanded) RES the HBS is preferred as the supercapacitor will compensate for stabilisation of the unbalanced load, peak shaving, spinning reserve and voltage fluctuation suppression [47]. An example of a small scale PV-wind islanded RES using hybrid storage is shown in Figure 2.13 [68]

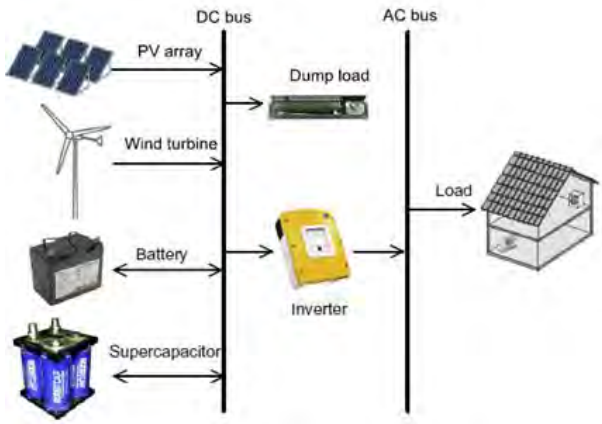

Figure 2.13 Autonomous PV Wind Islanded RES with Hybrid Storage [84]

RES can transfer their operation from grid-connected mode to islanded mode. The autonomous or islanded mode considered in Figure 2.13 would be more applicable to the remote off-grid rural customers of South Africa, and in many other countries in the African continent. However, in the South African context, the grid-connected generation is equally as significant. Considering South Africa's current electricity backlog situation, the addition of RES can be used in connection with the grid as a secondary generation source. When integrating wind and solar RES with the utility grid, an interfacing technique needs to be implemented to ensure successful load allocation and scheduling. Storage devices can be essential to this integration process with the previously mentioned provisions of load shifting, time shifting and peak shaving [32], [91], [92].

The transition between grid-connected and islanded mode of operation can be smoothened via the supercapacitor's dynamic response [84]. Supercapacitors provide fast discharge for transition variations and act as a buffer to the battery thus protecting it from shallow discharges or current peaks found in wind and solar energy, which in turn extends battery service life and system reliability [79], [85], [89].

In RES with frequent power fluctuations the BSS is incapable of reacting and compensating for the deficit in power without severely damaging itself. When the BSS undergoes shallow discharge cycles its lifespan is shortened thus the HBS or grid connection is essential in these case [38]. The published works show that a fully or semi grid connected RES can operate with the HBS or BSS depending on the precision required. However, if an autonomous or islanded RES is used, then the HBS is quintessential in maintaining an uninterrupted power supply with sufficient quality power.

In an attempt to improve simplicity of configuration, operation, lifespan and cost, the Ultrabattery was introduced [88]. The composition of the ultrabattery is illustrated in Figure 2.14 where it is presented as a combination of lead acid battery and supercapacitor. With the addition of two porous electrodes soaked in electrolyte, this system combines the properties of the supercapacitor and lead acid battery in order to compensate for acceleration, cold cranking, and regenerative breaking issues in HEV applications [93]. Ultrabattery reduces the need for complex power electronics interfacing previously mentioned and does not suffer from the high self-discharge which the supercapacitor is notoriously known for [65].

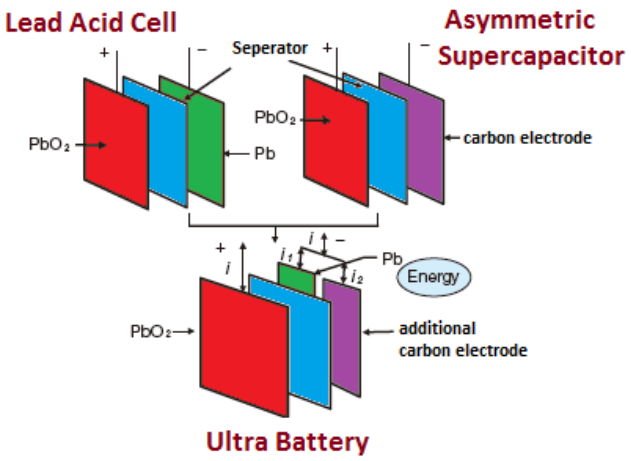

Figure 2.14 Lead Acid Battery Supercapacitor and Ultrabattery [84]

The ultrabattery was originally designed to improve on the HEV storage, but has been implemented in wind and solar applications generally for load levelling [65]. Despite its promise this device is still in its infancy; thus more matured standard BSS and HBS technology are preferred for existing RES and similar application.

2.7.3 Configurations and Energy Management Systems

The HBS and BSS applications discussed and compared above all require relevant interfacing configurations and control methods. The configuration selected is essential to the storage success as it is responsible for connecting the load supply and storage device(s) together with the end goals of enhancing lifespan, efficiency, power quality, and feasibility of the system [94]–[96]. In the isolated BSS, the onus is solely on the battery to respond to all loads, whereas in the HBS, high frequency loads are sent to supercapacitor to relieve battery discharge cycling strain [85]. By using Fast Fourier Transforms (FFT) or Hysteretic

Current Loop (HCL) control, loads can be absorbed by the supercapacitor thus avoiding shallow cycles on the battery which in turn can extend its service life [47].

In BSS, the battery is usually coupled with a grid or dump load to alleviate the potential strain of operating outside of the allocated state of charge region of between 60-90%. Using a dump load is inefficient but many argue that it is well worth the supercapacitor capital cost. The BSS uses a bidirectional DC-DC converter which regulates charging while the HBS connects the devices in parallel and applies one bidirectional DC-DC converter on the battery, supercapacitor or load. An example of this is shown in Figure 2.15 with the DC-DC converters each illustrated by a red block.

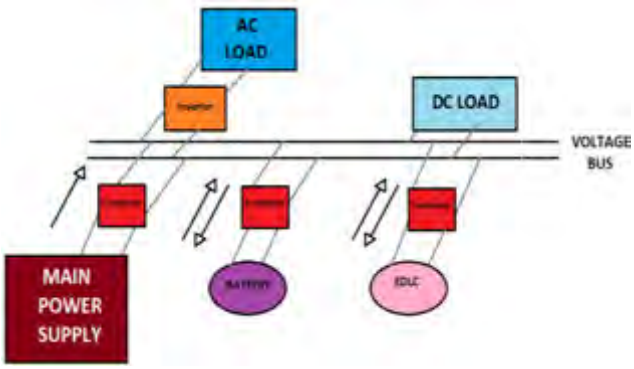

Figure 2.15 Hybrid Storage Interfacing Architecture using Unidirectional and Bidirectional Converters [84]

Primarily there are three types of connections in which the battery and supercapacitor are interfaced; namely passive, semi-active and fully active. The passive connection refers to the parallel connection of the battery and supercapacitor. The storage devices in this case therefore share a converter, resulting in component cost savings as seen in Figure 2.13 [89]. Semi-active is the most common configuration selected for both HBS and BSS as it provides a form of control with reduced switching losses and converter costs [13], [89]. The fully active system uses multiple bidirectional DC-DC converters and is popular in EV and RES applications as they demand fast responding bidirectional current flow, load levelling, high power and energy density and extended storage lifespan [47], [95]. The fully active connection is mainly implemented in large scale HBS applications, often requiring a high voltage DC link. Since a single battery cannot supply this high voltage, a series battery bank is formed [89]. *Zhou* argues that when a series bank is formed the battery with the lowest state of charge (SOC) is susceptible to deep discharge which causes non-linear charging and reduced lifespan [79]. *Ding et al*. suggests a soft switching, multiport converter showing promising loss reduction but it has only been tested on a small scale and does not consider battery SOC [95]. An alternative configuration using dual active bridges (DAB) in a modular connection is proposed. By allowing the voltage to be amplified per module, the batteries are protected and a flexible power control method for high energy applications is achieved [79]. Much like soft switching DAB compensate for switching losses but the primary Energy Management System (EMS) input is SOC making it more applicable for hybrid storage. A case can be made for all HBS and BSS converters required but a trade-off of high power quality, response, efficiency ,system complexity and component costs always needs to be made with the application necessities in mind.

2.7.4 Battery Lifespan Extension

One of the significant arguments made in support of preferring HBS over BSS is the extension of the battery lifespan. As mentioned previously the supercapacitor has a substantially higher cycle life than any battery, with a life expectancy of over 50 000 hours [82], [97]. In order to understand how the battery lifespan can be extended the actual deterioration process must be observed. Equation (2.1) presents the charge (left to right) and discharge reactions of a lead acid battery. If charge to a battery is removed and a discharge immediately applied there is a defined time for transition to occur. This depends on factors such as temperature and SOC of the battery. *Peukert's Law* states that the discharge current and discharge length is proportional to the actual capacity lost. It is defined by the *Peukert* constant for the specific battery [88]. Considering this equation, it follows that any engineering notion to increase the reaction speed of the battery for faster discharge and charge will accelerate the rate of plate corrosion, which in turn shortens battery lifespan.

$$Pb + PbO2 + 2H2SO4 \Leftrightarrow 2PbSO4 + 2H2O \quad (2.1)$$

Since it is inevitable that the charging and discharging of a battery must take place in course of its operation, the observation made is that the battery lifespan is a direct reflection of the number of cycles undergone. In order to prevent this plate corrosion reaction, the addition of a carbon electrode layer to the lead acid battery is proposed in [65]. This improved lead acid battery is known as the ultrabattery [88]. Unfortunately, limited ultrabattery literature is currently available to validate its implementation and feasibility as a solution to the conventional BSS lifespan problem. However, several authors have shown that HBS implementation can extended the lead acid battery lifespan and a yield a faster system response [38], [75], [79], [98]. This HBS argument has been confirmed in solar applications via a support vector machine which improves power reliability [82]. Additionally, a model for stabilized energy provision in fluctuating remote area RES loads has been developed [89]. In HEVs, adding the supercapacitor can act as a buffer for the lead acid batteries which alleviates the strain of high rate charge/discharging hence extending the lifespan of the battery [93]. *Bouharchouche et al.* shows how modelling the HBS for a wind power application has improved dynamic performance and extended lifespan of the battery by setting EMS operating intervals. The operating intervals are based on the batteries' SOC which then maintains the operable depth of discharge (DoD), allowing optimised supply and storage without battery strain [99]. Within all applications considered in this review the cheap, easily accessible and highly recyclable lead acid battery benefits the most from the supercapacitor addition in terms of significant protection, life extension, instantaneous load response and energy absorption.

Prominent storage devices for BSS or HBS in the wind, PV or HEV applications on a medium scale are Ni-MH, and Li-ion batteries. *Peterson et al.,* however, states that degradation factors for Ni-MH and lead acid batteries are well understood but not for li-ion thus far [72]. It is reported that the li-ion battery is tested in an EV under driving and Vehicle to Grid Energy Transfer (V2G) operation, whilst both at constant temperature [72], [100],

[101]. Interestingly, the results show that DoD has no effect on capacity fade but higher rate cycling does cause capacity loss in Li-ion batteries. At higher rates, greater over potentials are observed at the electrode surfaces, which marginally enhance the Solid Electrolyte Interface (SEI) layer build-up. SEI build-up has a square root of time relationship with capacity fade, representing irreversible capacity loss [69], [87]. Despite the convincing result of DoD having no effect on lifespan, the addition of the supercapacitor can still extend li-ion BSS lifespan by alleviating high discharge rates as seen in [101].

2.7.5 Cost Analyses

When deciding between the feasibility of the HBS or the regular BSS, some of the primary motives are the operation and component costs. A review of multiple studies on the lead acid, Li-ion and supercapacitor storage device lifespans and cost of operation has been compiled and presented in Table 2.2.

Table 2.2 Lifespan and Cost Analysis for Lead Acid Battery, Li-ion Battery and Supercapacitor [84]

		Eff. (%)	Lifespan (yrs.)	Trade Period (yrs.)	Trade Cost ($/kWh)	Power Cost ($/kW)	Energy Cost ($/kWh)
Lead Acid Battery	Min	60%	5	5	26.61	175	150
	Max	90%	16	6	23.79	4600	3800
Li-ion Battery	Min	78%	5	10	-	175	500
	Max	99%	16	10	27.63	7850	6200
Super capacitor	Min	70%	8	-	-	100	300
	Max	98%	20	-	-	2355	20000

The Li-ion battery offers a costly storage alternative but does not require as frequent replacement when compared to the lead acid battery, specifically in isolated BSS [49], [75]. The addition of a supercapacitor has been proven to reduce the need for frequent replacement through DoD maintenance in lead acid batteries and buffering for overcharge protection in Li-ion batteries, which implicitly reduces operational costs [99], [101].

Tehrani et al. believes the biggest problem with HBS is its high cost and suggests Li-ion batteries for HEV applications as they can compensate for HEV demands through their thermal and chemical stability [87]. Authors in [85], [87], concede that there is a knowledge gap in literature available on the economic evaluation of the HBS. The literature covered in this review shows that in many applications the benefits of the supercapacitor addition in terms of energy extraction, power quality, load fluctuation response, fault reduction and lifespan extension easily compensates for the additional component costs [48], [96]. Conversely, *Sparatu et al.* recently conducted a cost and applicability analysis which showed that li-ion and lead acid batteries are significantly robust for many applications [49]. This analysis suggests that the BSS offers an adequate and cheap storage alternative for low to medium voltage applications despite their replacement costs.

2.7.6 Current Models Considered

The perfect storage device is technically mature, low-priced, long lasting, easily implemented, and efficient with high energy and power density [102]. No storage device can meet all of these demands completely but based on application criteria an ideal storage device can be selected for most cases. Using reviewed literature, factors such as load

shifting, renewable integration, electrical interfacing and power quality are considered, with previous examples of storage implementation per application are listed in Table 2.3.

The needs and criteria mentioned are ranked as low, medium or high and are used to suggest each application's ideal storage device and respective electrical configuration. Table 2 considers the relevant control, power quality accuracy level, load shifting, weight, configurations and electric capacity of the overall system. This electric capacity refers to the size of the storage device specifically.

Based on the results compiled in Table 2.3 it is clear that lithium ion batteries dominate the HEV storage industry due to their high power quality and volumetric efficiency [49], [72]. Since large wind and solar generation systems remain on a fixed location the volumetric efficiency is not as important; hence the cheaper lead acid batteries are selected in most cases considered [3], [103], [104]. Based on Table 2.3 the distinction between hybrid or battery storage is mainly based on the application's power quality and control accuracy demands required, regardless of the battery selected. Based on Table 2.3, HBS is preferred over BSS when a higher initial capital is available and a more reliable storage system is required[38], [74].

Table 2.3 Ideal Storage Device Selection based on Application Specifications [84]

Application	Control / PQ	Electric Capacity	Load Shifting	Relative Cost	Weight / Size	Storage System	Configuration
Micro/Mild HEV	Medium	Low	Low	Low	Low	Li-ion BBS	DC-DC
Medium/Full HEV	Medium	Medium	Medium	Low	Low	Li- ion BSS	3 DC-DC
Plug-in HEV	High	Medium	High	High	Low	Li-ion HBS	Modular Conv.
Island PV / Wind MG	Low	High	Low	Low	High	LA BSS	DC-DC
Island PV / Wind MG	High	High	High	High	High	LA HBS	Modular Conv.
Ancillary / V2G	High	High	High	High	Low	Li-ion HBS	Modular Conv.
Fast PV Charger	High	Low	High	Medium	Medium	LA HBS	SLM
Grid PV / Wind MG	Medium	High	Medium	Medium	High	LA BBS	DC-DC
PV Sensor networks	High	Low	Medium	Medium	Low	Li-ion HBS	3 DC-DC

Table 2.3 provides a good overview with regard to battery and hybrid storage device applicability. The literature digested which formulates Table 2.3 concedes that HBSHBS requires a higher initial capital, but it does not consider the system's economic viability after establishment in terms of energy generation savings, component sizing and lifespan reduction.

2.8 Conclusion

Based on the literature reviewed it is clear that South Africa has a mass of untapped renewable energy potential which is essential to reducing the current backlog in energy demand. It has clearly been established that storage devices contribute and facilitate the implementation and integration of RES. This is completed through time scaling, load shifting, spinning reserve provision, voltage balancing, power quality enhancement and many other benefits. Despite all of the technical and environmental benefits, fossil fuel generation is still observed as the cheapest form of energy. For RES to significantly penetrate South Africa's energy profile, unelectrified areas with a mass of renewable sources must be competitively priced in order to challenge the extension of the coal based utility grid.

The comparison of storage devices considered has shown that no perfect storage device exists but the most applicable device can be selected depending on application criteria. This thesis aims to compare the feasibility of RES deployment when using either the BSS or HBS.

Since it has been established that many unconnected regions in South Africa require electricity, the comparative study will be based upon regions which can benefit South Africa's remote generation profile[84].

3. Chapter 3 - Research Methodology for Electrical Performance Analyses

Storage Device Modelling Theory

The procedure followed for modelling the electrical performance of islanded RES and their storage devices, is explained in Chapter 3. Firstly, the storage device modelling theory is discussed and improvements on proposed storage models are explained. After defining constraints and model improvements, the procedure followed for modelling the RES in Matlab-Simulink is presented.

3.1 Previous Battery Models

Lead Acid batteries are well established in industry and are widely preferred in RES storage due to their low cost and maturity. Since these batteries are very popular a large body of literature has been established explaining their strengths, weaknesses and ways to model them for simulation and design improvements. This chapter reviews three of the common battery models and compares them to the Matlab Simulink software model used. Based on this comparison, the shortcomings and strengths of the Matlab software model are identified. Improvements to the Matlab model are then proposed and constraints are defined, in order to develop a RES-related storage model for facilitating an accurate electrical performance analysis.

3.1.1 Simple Battery Model

The simple electrical model, as shown in Figure 3.1, uses an ideal voltage source E_0 in series with an internal resistance R_b. The Open Circuit Voltage V_{OC} supplies a voltage across the ideal battery. When we consider the ideal source, E_0 and a voltage drop across the internal resistor R_b, the output is measured as V_b [105].

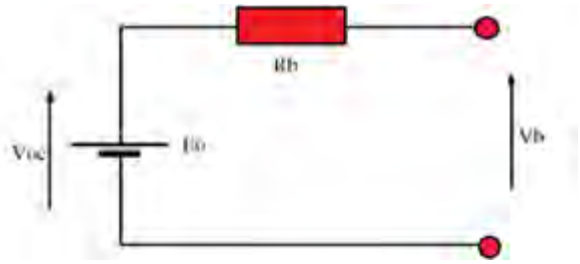

Figure 3.1: Simple Battery Model [104], [106]

This model is easy to understand but does not consider true internal resistance of the battery. State of charge (SOC) and electrolyte concentration is strongly related to the true

internal resistance, making the simple battery circuit rather unsuitable for accurate modelling [107].

3.1.2 Thevenin Battery Model

A common battery model, as shown in Figure 3.2, is known as the Thevenin battery model. It represents the battery as an open circuit, with a few adjustments made to the simple model previously mentioned in section 3.1.1. In this model, the ideal voltage source E_0 is still retained, but reactive impedance in the form of a capacitor C_0 and a parallel resistor R_0 is added in accordance with the series internal resistor/rheostat, R [89], [107].

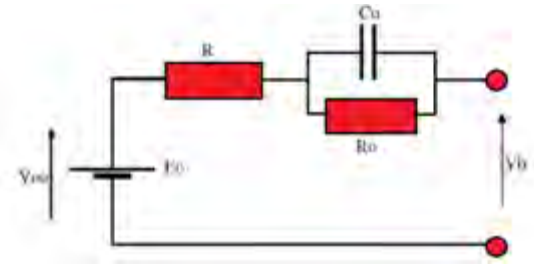

Figure 3.2: Thevenin Battery Model [106]

This model however possesses two fundamental shortcomings. For one, battery electrochemistry components are completely neglected in the Thevenin model. In addition, the model assumes that characteristics are linear but in reality the C_0, R_0 and V_b values are highly dependent on the SOC, storage capacity, temperature and rate of discharge [106], [107].

3.1.3 Non-Linear Dynamic Battery Model

In an attempt to rectify the linear assumptions made in the Thevenin model the non-linear dynamic battery model is introduced, as shown in Figure 3.3. In this model the charging and discharging processes are separated. A clear demonstration of charge separation is through the use of diodes in the circuit diagram of Figure 3.5.

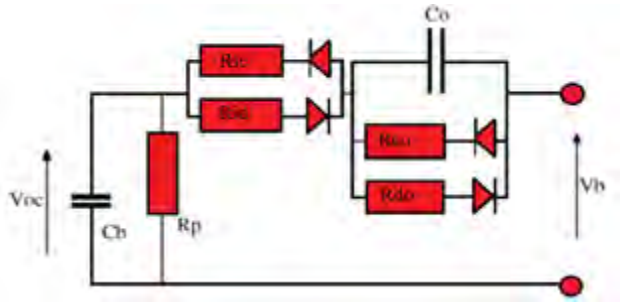

Figure 3.3: Non-linear Dynamic Model [107]

Instead of the ideal constant power supply, this model uses the capacitor C_b as the voltage source. A capacitor is more accurate than the common ideal voltage supply since it

is an electrical storage device which keeps track of its capacity [107]. The SOC is therefore expressed in terms of stored charge in the capacitor C_b. The internal resistance in the battery considers the over potential voltage drop, hence it is represented by the resistors R_{co} and R_{do} [67], [107]. An issue observed with the non-linear dynamic model is the assumption that the capacity tracking is done by using an ideal capacitor. This means that the charging accuracy is overlooked [107].

3.2 Battery Software Model Evaluation

After considering the three previous battery models it is clear that each approximation is not without fault. The electric performance analysis requires accurate monitoring of charge dynamics, due to the abrupt variations which occur when a battery is used in RES. Since the electrical performance analysis compares the HBS and BSS, the battery capacity needs to be effectively monitored as well, in order to see the storage device lifespan and performance improvements. As a result, the software model considered is not evaluated. The new dynamic model which was designed and implemented in Matlab is explained, and then compared to real batteries operating under the same charge conditions [108].

The review of previous electric battery models shows that a battery model can always be improved. Since this chapter considers the electrical performance analysis of lead acid batteries in RES, the storage devices will need to be effectively modelled to represent load shifting, capacity monitoring and battery lifespan properties. As mentioned in the previously conducted lead acid battery model reviews of [107] and [106], the non-linear dynamic model provides an effective improvement on the Thevenin model by using a separate charging and discharging process but which then models the storage capacity with a capacitor. As a result, the load shifting properties of the battery will be accurately represented in any simulation study, but storage capacity will not be accurate enough for analysis. The SOC is important to the electrical study lifespan extension through SOC regulation, which is a major benefit of hybrid storage. Due to this limitation the Ceraolo model used in Matlab Simulink will now be evaluated, by comparing its circuit provisions and performance in comparison to a real lead acid battery. Based on the evaluation it will become clear whether the Matlab software has the necessary SOC, load shifting and non-linear modelling properties needed for the electrical performance analysis. The Ceraolo model used in Matlab provides an improvement to the non-linear dynamic model, by using an input regulated voltage source instead of a capacitor. This circuit is shown in Figure 3.4.

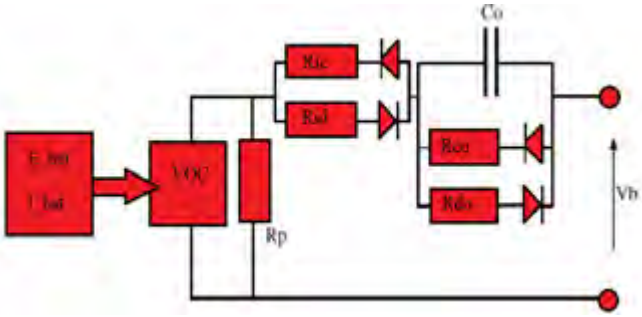

Figure 3.4: Ceraolo Battery Model for Simulation [107]

The Matlab model considers multiple factors often overlooked by other mathematical designs. Primary contributions of the model are:

1. The modelling of electrolyte temperature
2. Using an electric bi-pole model to allow for a more accurate charge efficiency
3. Represents battery in an electrical sense whilst still maintaining accuracy of electrochemical model

The study conducted in [108], provides a good analysis on the performance of the Matlab model. Massimo Ceraolo tested his model by comparing the voltage response under long and short term discharge. Extensive tests were conducted on various types of lead acid batteries, such as flooded and valve regulated (gelled), in order to discover an optimised general lead acid battery model. The discharge and charge parameters were uncovered and are displayed in terms of the inputs which are entered into the Ceraolo model equations (3.1) and (3.2), as shown below [108].

Charge:

$$V_{bat} = E_0 - Ri - K\frac{Q}{it - 0.1Q}i^* - K\frac{Q}{Q - it}.it + e^{(t)} \tag{3.1}$$

Discharge:

$$V_{bat} = E_0 - Ri - K\frac{Q}{Q - it}.(it + i^*) + e^{(t)} \tag{3.2}$$

The charge and discharge parameters are illustrated using different curves, since the lead acid battery chemical transfer is a non-reversible reaction. The $i*$ value represents the low frequency current dynamics which are included in the discharge curve of Equation 3.2. This in turn changes the capacity measuring term of the equation. The constant voltage E_0, the resistive voltage dropped Ri, and the exponential curvature $e^{(t)}$ all remain the same in both battery equations [108], [109]. The battery discharge parameters for two tested lead acid batteries are now specified in Table 3.1 below. In the table, 'gelled' refers to the valve regulated gel base lead acid battery, and 'flooded' represents the flooded lead acid cells used in the second battery. The commercialised titles of the batteries are not provided in the test but the relevant storage device parameters are shown.

Table 3.1 Battery Discharge Parameters [108]

Description	Actual Parameter	Battery 1 - Gelled	Battery 2 - Flooded
Parameters referring to battery capacity	I^*	51.5A	49A
	K_c	1.11	1.18
	C_0	317.9Ah	261.9Ah
	ε	1.19	1.29
	∂	1.75	1.40
	θ_f	-40°C	-40°C
Parameters referring to the main branch of the electric equivalent circuit	E_{m0}	2.18 V	2.135 V
	K_E	0.839e^{-3} V/C	0.580e^{-3} V/C
	R_{00}	2 mΩ	2 mΩ
	R_{10}	0.4 mΩ	0.7 mΩ
	τ_i	7200s	5000s
	A_0	-0.2	-0.3
Parameters referring to thermal model	C_0	15 Wh/°C	15 Wh/°C
	R_0	0.2°C/W	0.2°C/W

The parameters shown in Table 3.1 refer to the charge and discharge equations, with (3.1) and (3.2) used as inputs for mathematical modelling of the batteries. The equations defined are used in Matlab for simulation of batteries as well. By testing the two batteries shown in Table 3.1 in a lab, a comparison between Matlab and real life application is made.

The gelled and flooded batteries were charged using the constant current - constant voltage (CC-CV) discharge procedure shown in Figure 3.5. In this discharge method the battery first operates in a constant current (CC) region and increases its voltage, this is then followed by the constant voltage (CV) region. Battery 1 is discharged at 58A for 8.6 hours and battery 2 is discharged at 63A for 7.2 hours. At the respective battery discharge times it was noted that the voltage reached 1.75V, and then settled at 2.1V as the constant voltage region for both the batteries. The mathematical discharge equation (3.2) used for Matlab simulation was then tested under the same conditions. The batteries input parameters used were as defined in Table 3.1, but the current and time frames were adjusted to match the real life test conditions for the CC-CV charge protocol.

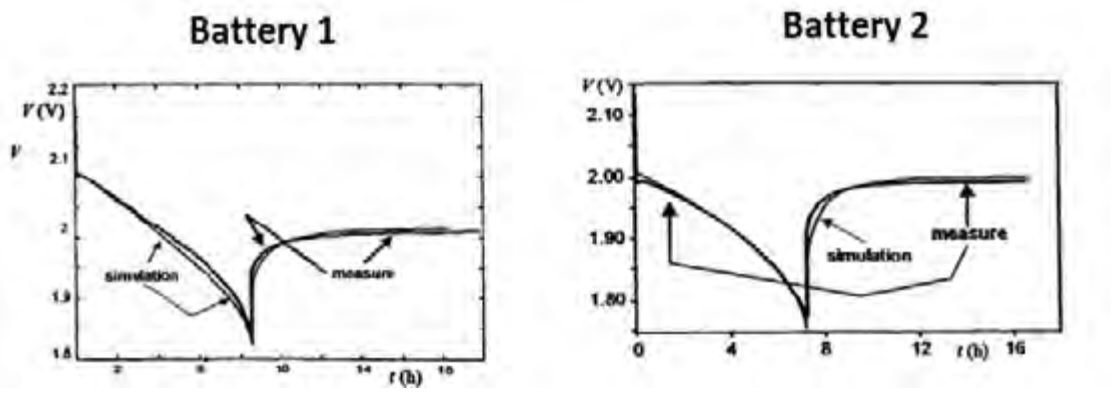

Figure 3.5: Mathematical and Measured Battery Model Comparison Over Full Time Period [108]

The Matlab model equation and the real lab tested discharge curves were then compared in Figure 3.5. In the first 7 seconds of the voltage plots for battery 1 and battery 2, as seen in Figure 3.5, the voltage is steadily decreasing. This is a result of the Constant

Current (CC) battery discharging phase. When the battery discharges this constant current, the voltage is reduced at the rate shown in the first 7 seconds of Figure 3.5. The battery has a finite amount of energy in its reserves, as a result its depletion will never be constant for both current and voltage at the same time. During discharge, if the voltage is constant the current is decreasing and vice versa. After 7 seconds the battery voltage is fixed and the current will vary accordingly, therefore, the region after 8 seconds is known as the constant voltage (CV) region.

Figure 3.5 shows that at a CC discharge, the initial region where the voltage is decreasing, the flooded battery (battery 2) matches the simulation curve with minimal error. When the flooded battery transitions to CV discharge, the simulated curve has a slight misalignment. In the gelled battery 1, the Matlab model (New dynamic battery model) shows a slight misalignment in the initial CC region, but successfully mirrors the transition and operation of constant voltage. The software has also been evaluated under transient response conditions in [108], and shows accurate modelling of the CC and CV region for both types of lead acid batteries. In addition, the new dynamic model tested in Figure 3.5 is the only design which effectively monitored the CV region. The results of the comparison reveal that both lead acid battery types show minimal variation between real and simulated results, making the Matlab software an accurate approximation in terms of charge dynamics and transient response modelling [108].

The Matlab model employs a dynamic control strategy which monitors the battery capacity, unlike the capacitor approximation used in the non-linear model [107], [108]. Since the measured and simulated results both reach 1.75V concurrently, the capacity of the batteries are being effectively modelled in the Matlab software. This is essential to the electrical performance analysis which follows in Chapter 4. New dynamic model curves also accurately match changes in current and voltage, which means sudden variations such as short term load shifting are successfully presented. The simulated model concedes minor variations in voltage at the transitional phase, between constant current and constant voltage regions.

The properties of charge, transient response and capacity monitoring are priority parameters for the electric performance evaluation of RES storage. Therefore the Matlab battery model is deemed ideal for simulation. The identified limitations of the model and proposed improvement will be made in Chapter 3.5, before the simulation description can take place.

3.3 Established Supercapacitor Models

Existing supercapacitor models are now discussed in order to evaluate the accuracy of the Matlab Simulink model used.

3.3.1 Types of Supercapacitors

Electric Double Layer Capacitors (EDLC) are categorised into two types, the first of which involves the storage of charge in the electrical double layer, at or near the electronic material interface or electrolyte i.e. the ultracapacitor. The second type is known as the supercapacitor, which utilizes the transient absorption of atomic species. This absorption takes place within a crystal structure of the electricity conducting compact electrode [75],

[81]. Charging and discharging of the supercapacitor compact electrode is shown in Figure 3.6.

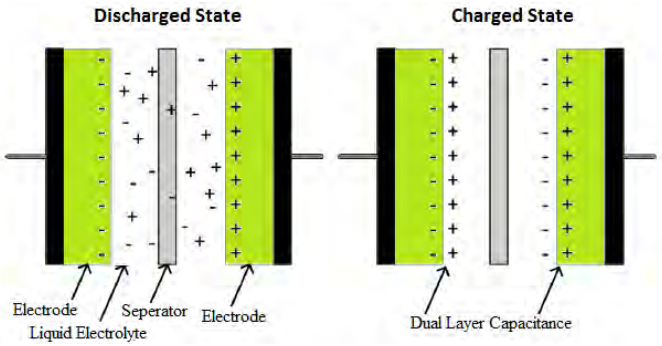

Figure 3.6: Electrochemical Supercapacitor During Charged and Discharged States [102]

The combination of a solid electrode and electrolyte solution, has a greater capacitance density when compared to any other storage device. The reason for this can be deduced by considering the electrochemical structure of the device [102], [110]. In Figure 3.6, charges collect at the interface between the two electrodes. The electrostatic charge is stored in the double layer with an effective distance between the each charge, in the order of 1nm (10^{-9} m) [74], [111].

It is important to distinguish between different EDLCs, but the use of an electrochemical supercapacitor model is far too complicated to be considered feasible for electric performance analysis [74]. The use of common equivalent circuit models are now shown and compared to the software model.

3.3.2 Classical Equivalent Circuit Model

A classical equivalent circuit model consists of an equivalent series resistance (ESR), equivalent parallel resistance (EPR) and capacitor C which represents the equivalent capacitance. The simple electrical structure of this model is shown in Figure 3.7.

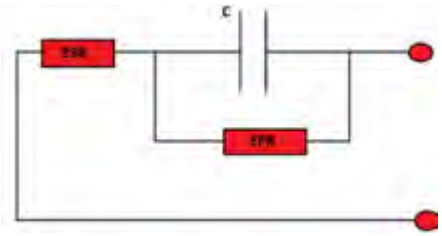

Figure 3.7 Classical Equivalent Circuit Supercapacitor Model [74]

The classical model is suitable for applications where the supercapacitor is allowed to discharge slowly, for a period of less than a minute. For multiple reasons, such as short discharge inaccuracies for durations of a few minutes and the limitation of first order approximation, the classical circuit is an inadequate electrical performance analysis [74].

3.3.3 Three Branch Model

A common model used for improving the low order limitations of the classical model is known as the three branch model. In this design, the R_i branch dominates behaviour in the first few seconds of current flow and so is labelled the initial branch. The delayed branch R_d, influences the range of the circuit in minutes and the third branch is responsible for the long term circuit response for after 10 minutes [74].

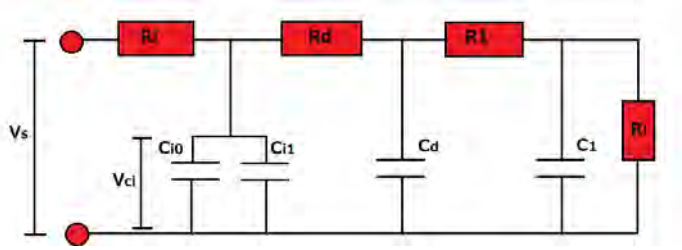

Figure 3.8: Three Branch Transmission Line Equivalent Circuit Model [112]

C_{i1}, models the voltage reliance of the double layer's capacitance. The leakage current is the most prominent weakness of the supercapacitor and is modelled by R_l, [82].

3.4 Supercapacitor Software Model Evaluation

The Matlab supercapacitor model neglects factors such as temperature, resistance and charge distribution. The software model also overlooks the aging effect and continuous charge, but these are fair assumptions for simulation because most electric circuit models also neglect these factors [113].

Despite the assumptions acknowledged in this model, the results of a software accuracy study conducted in [113] showed that the maximum error of the Matlab model, when compared to an actual supercapacitor reading, was found to be at a maximum of 5% with an averaged error of below 2%. These readings make this simulation reliable enough to model most supercapacitors on [109], [113].

The electrical performance analysis, reported in this thesis, uses the supercapacitor as a secondary storage device. This means the study is heavily reliant on the supercapacitors for high power responses and high frequency disturbance rejection. In order to observe the applicability of the supercapacitor model used for the electric performance analysis, its potential provisions need to be evaluated.

Supercapacitor charge profile has a reported maximum error of 5%, which means the high power density properties of the Matlab model is effectively displayed. However, the high frequency operation still needs to be effectively presented for dynamic supercapacitor performance analysis in RES disturbance rejection. This property is evaluated by establishing the RES frequency band of operation. This is then used as the necessary benchmark for supercapacitor selection. Using the equivalent circuit operating order and frequency bands shown in Figure 3.9, the applicable supercapacitor can be found. Once this is found the order of the Simulink model will be evaluated.

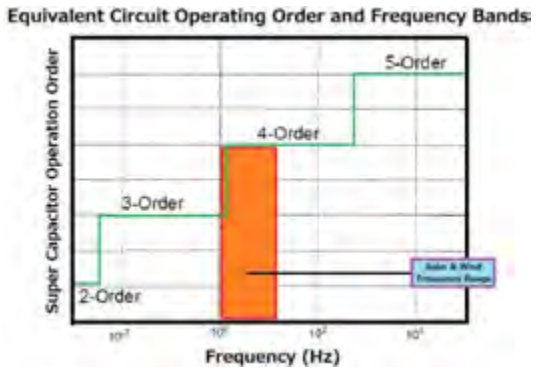

Figure 3.9: Operating Frequency Band with Corresponding Operating Order Comparison [106]

Figure 3.9 is used to evaluate the Matlab supercapacitor frequency band for solar and wind RES storage. Figure 3.9 shows the equivalent operating order and its relationship with the frequency bandwidth of the supercapacitor. The Y-axis of the figure rates the exponential order of the supercapacitor model being used. The X-axis then shows the effective frequency band (and differential order) within which the supercapacitor model lies. According to [106], solar and wind RES require storage devices which can respond within 0.5 to 10 seconds, for optimised operation. However, in [54] a detection and disturbance response of 20ms is recommended for optimised load balancing. Since the electrical performance analysis herein requires sufficient average operation and load balancing, Figure 3.9 has used both the minimum times recommended and has set an operable frequency band.

Based on Figure 3.9, it is clear that a 4^{th} order model will work best for supercapacitor RES storage. A 3^{rd} order model such as the three branch circuit is potentially operable but only for averaged load storage, and it would still be operating on its bandwidth limit.

However, Simulink manages to combine the relatively new Stern Model and classic Tafel model to display the supercapacitor parameters on a 5^{th} order level. This makes it ideal for modelling even higher order potential fluctuations, which would be its main priority in the electrical performance analysis [106].

3.5 Proposed Model

Based on the evaluation, the software models can accurately represent majority of the required RES storage device dynamics. However, some characteristics such as temperature effects, self-discharge and continuous current flow are neglected. Potential improvements and constraints are now defined in order to make the Matlab models more conducive to RES storage.

3.5.1 Storage Device Limitations

Before one can make improvements to the Matlab models, some of their important limitations are identified and discussed in this section.

a) Battery Model Limitations

All of the battery models considered are compiled in Table 3.2 in terms of important provisions and compared to the Matlab Simulink model. 'Yes', 'No' and 'Moderate' indicate to what extent the applications listed in Table 3.2 can be performed by these models.

Table 3.2 Properties of Battery Models [104], [108], [109], [114]

Application	Simple	Thevenin	Non-linear Dynamic	Matlab Simulink
AC Prediction	Moderate	Moderate	Yes	**Yes**
DC Prediction	No	No	Moderate	**Yes**
Internal Resistance	No	Moderate	Yes	**Moderate**
Capacity Tracking	No	No	Yes	**Yes**
Temperature	No	No	Moderate	No
Self-Discharge	No	Moderate	Yes	No
Transient Behaviour	No	Moderate	Yes	**Yes**
State of Charge	Moderate	Moderate	Yes	**Yes**
Separate Charge and Discharge Profile	No	No	Yes	**Yes**

The Matlab Simulink battery model is outcome based in comparison to the electric circuit models. It is one of the few models which can represent charge and discharge profiles using separate equations, whilst aligning with the electrochemical characteristics of the battery. Important shortcomings of the model are as follows:

1. Temperature effects, which influence internal resistance and lifespan, are neglected.
2. Internal resistance remains constant for charge and discharge cycles.
3. Unlike the new dynamic model, the Matlab model does not show battery capacity changing with current amplitude.
4. The self-discharge is not represented in the battery behaviour [108], [109].

b) Supercapacitor Model Limitations

Matlab Simulink combines the relatively new Tafel and classical Stern equations to model both the current and voltage respectively. The Tafel model is a generalised plot which can be used for different applications. In this instance it is used to model the current waveform of the supercapacitor. This current is shown in Equation 3.3.

$$i = i_0 \exp(2 \propto \frac{F\Delta V_{act}}{RT}) \tag{3.3}$$

The Stern Model uses a modified capacitance value which portrays an accurate ion alignment, by including the surface charge of ions and charge density. The capacitive summation of this improvement is shown in Equation 3.4.

$$\frac{1}{C} = \frac{1}{C_1} + \frac{1}{C_G}\left(1 + \frac{\partial \sigma_A}{\partial \sigma}\right) \tag{3.4}$$

After considering the more accurate capacitor design, the combined Stern-Tafel model can be represented in voltage form in Equation 3.5.

$$V = N\left(\frac{N_s N Q x_2}{N_p N^2 \varepsilon\varepsilon_0 S} + \frac{N_s N 2RT}{F} \times \operatorname{arsinh}\left(\frac{Q}{N_p N^2 S\sqrt{8\,RT\varepsilon\varepsilon_0 c}}\right)\right) \quad (3.5)$$

It is worth noting that the voltage seen in Equation 3.5 is substituted into the Tafel model, shown in Equation 3.3, in order to model the supercapacitor current. The key parameters which define the above equations are now described in Table 3.3.

Table 3.3 Supercapacitor Matlab Model Equation Parameters [109]

Parameter	Unit	Description
i	$Am-2$	Current density
i_0	$Am-2$	Exchange current density i0 = if/A
RT	℃	Ideal gas constant and temperature
ΔV_{act}	V	Over-potential
F	/	Faraday constant
C_1	F	Model capacitance
C_G	F	Thermal motion capacitance
$\partial\sigma_A/\partial\sigma$	/	Ion alignment factor
N_p or N_s	/	Number of parallel & series supercapacitors
N	/	Avagadros constant
Q	C	Charge in Coulombs

The Tafel model represents an averaged curve which can be used across academic fields for different curve modelling practices. In this case, the supercapacitor current is modelled with this curve while using over-potential, ideal gas constant and a temperature ratio is to vary the exponent of the curve [115]. The Gouy-Chapman model is improved upon in Equation 3.2 by including the thermal motion of ions influence on capacitance. From these values, the rest of the parameters found in Table 3.3, such as the ion alignment factor $\partial\sigma_A/\partial\sigma$, number of parallel and series supercapacitors N_p or N_s and charge Q, are used to define the combined Stern-Tafel model in Equation 3.5. The supercapacitor model was only released in the recent Matlab 2013 version [74], [77], [116]. Despite this being the first Matlab supercapacitor model, a few shortcomings are still noted:

1. The model does not take into account the temperature effect.
2. No aging effect and cell balancing is considered.
3. Internal resistance and capacitance are assumed constant.
4. Supercapacitor current is assumed to be continuous according to Equation 3.3.
5. Charge distribution is constant for all voltages

The temperature, resistance, capacitance and charge distribution assumptions are all significant with regard to impacting modelling accuracy of results; this shows that the model can be improved for electrical studies [109], [113].

3.5.2 RES and Storage Model Assumptions, Constraints and Improvements

I. Assumptions and Constraints Observed:

After researching the composition of the battery and supercapacitor Matlab-SimPowerSystems model and comparing them to previous electrical models, the following

assumptions and constraints were proposed in order to facilitate accurate electric performance analysis.

1. A discrete simulation was used for system calculation instead of real time units.
2. The simulation was restricted to a single day of RES operation of 25 hours.
3. In Case 1, the utility grid supply was modelled by an ideal voltage source.
4. Resources modelled will vary at hourly values using the data collected in [44] and [117].
5. A 2x2 battery bank and one supercapacitor is utilised to model storage contributions.
6. Load shifting properties were tested by allocating the load to different storage devices and the power supply during peak load demand or low energy generation times.
7. Four load and five supply fluctuations were assumed in a single 25 hour day simulation.
8. Disturbances observed in the load and supply are assumed to be rectangular with a period of 60 seconds and high amplitude of over 100% of the averaged load. This allowed the supercapacitor to be tested extensively.
9. A proportional integral (PI) controller was used for energy management.
10. A separate PI controller was designed to filter resistive noise.

II. Limitations:

Important component, software, storage and computational limitations are now drawn:

a) Storage Device and Resource Limit:

The electric performance analysis is restricted to a comparison of battery storage and hybrid storage systems based on the study limitations reviewed in Chapter 2. The simulation has acquired data from the town of Napier, in the Western Cape region, for RES deployment. Due to its complementary low power density and experience in industry, only the lead acid battery is considered for the three cases.

b) Software Modelling Limits:

Only components which can be interfaced with SimPowerSystems and SimScape block sets are used. A short 50µ second sample time is required for accurate high frequency modelling, resulting in a large number of iterations with long computation time during one simulation, and running the risk of exceeding the memory capacity of the computer. Hence, the simulation will be limited to a single day model of 25 units. A single day simulation period means that no long term properties, such as load shedding and system maintenance, could be evaluated.

c) Signal Quality

Another observation is that the energy generated and supplied tends to vary. This is due to the converters and passive components being used, such as resistors and inductors, which can cause voltage fluctuations.

III. Improvements Made

Based on limitations observed throughout the model comparison, the following improvements have been made to compensate for software limitations and model assumptions:

a) State of Charge Tracking Comparison

Battery lifespan cannot be directly modelled in Matlab but is essential to the HBS and BSS device comparison. After conducting research on lead acid batteries it was established that the optimum SOC is between 60-80% [55], [107], [118]–[121]. Operation outside of this range and shallow discharges have a negative effect on the battery lifespan and response [55], [69], [121]. A measuring scope was therefore connected at both simulations (HBS and BSS), and the SOC plot data was saved in Notepad and presented on the same axes in a Matlab database plot. This allowed for presentation of the SOC enhancement property exhibited when using HBS, and as a result an indirect lifespan extension comparison.

b) Fluctuation Suppression

Supply and load power spikes need to be detected and isolated through storage devices. In order to isolate both signals and allocate the impulse response to the supercapacitor, a PI controller with disturbance rejection is used on the initial signal, thereby filtering out disturbances and distributing the average load signal to the battery. By subtracting the original signal from the controlled value, excess disturbances are detected and sent to the supercapacitor.

c) Battery Degradation and Protection

The battery needs to be protected from operating at an SOC of below 30%. Furthermore, the batteries require a charging protection scheme due to RES intermittency [55], [107], [118]–[122]. After employing the disturbance detection and fluctuation suppression scheme the filtering process shown in Figure 3.10 is implemented. In order to prevent storage degradation during the simulation, parameters are limited to a single day.

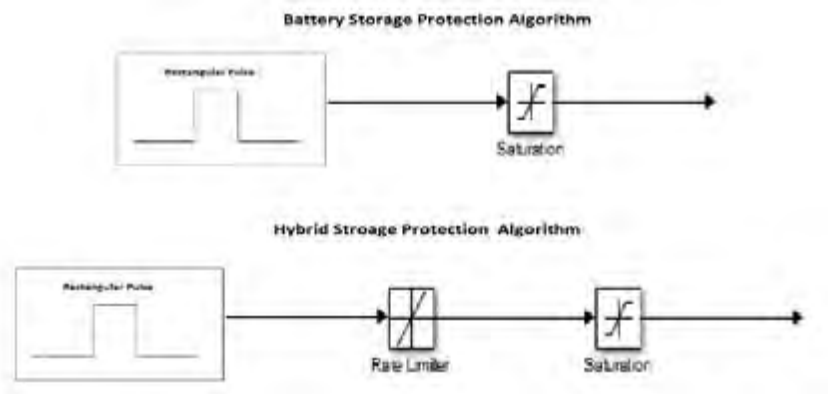

Figure 3.10 Battery Protection and Supercapacitor Allocation Methodology

Through the use of hysteresis blocks shown in Figure 3.10, the battery discharge is limited depending on the capacity observed. The rate limiter block measures the gradient of the disturbance before allocating it to the supercapacitor in HBS mode. A saturation block is used in both HBS and BSS cases, for limiting battery charge and discharge values to within 200% of peak power amplitude and a gradient of below 1000.

d) Resistive Noise Filtering

The solar panels needed to be modelled using the SimScape solar cell. The only way to interface SimPowerSystems and SimScape is through a resistor current interface, since it is common in both block sets. This generated problematic resistive noise fluctuations. After

consulting multiple online articles it was found that by modelling the SimScape solar cell output as a current source, using a resistor and current measurement block, one could interface the dual toolbox RLC block as seen in Figure 3.11 [123].

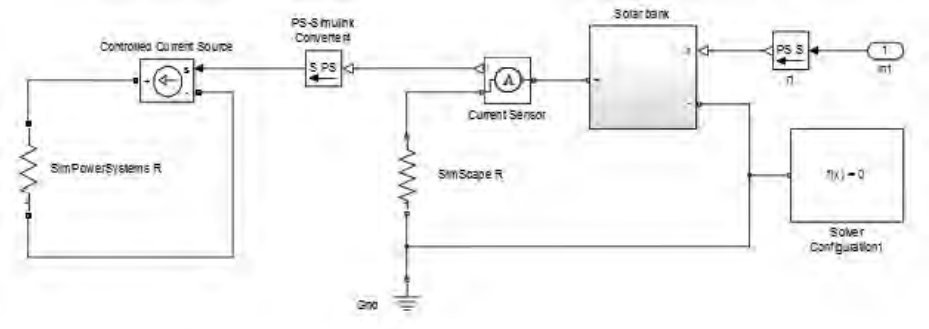

Figure 3.11 Software Conversion between Platforms for Improved Solar Modelling

A disturbance rejection PI controller is used to filter out the observed noise, and to re-establish the original SimScape voltage signal. The signal is filtered through the controller before connection with the DC-DC converter, ensuring no noise amplification could take place.

3.5.3 Final Modelling Remarks

By limiting the time frame for simulation, battery degradation will not be observed in the study. The evaluation of the storage devices revealed that both charge processes in the battery can be used during the study. The evaluation also showed that the software model has a large enough frequency range to accurately model load fluctuations and disturbances. This makes up for the supercapacitor software weaknesses identified, such as constant temperature, resistance and capacitance assumptions. Due to the high frequency band of the model, the supercapacitor effect for high power and high frequency response will be evaluated. Since the battery lifespan cannot be directly monitored in the software, its extension, due to supercapacitor addition, will be evaluated through the software's accurate state of charge monitoring provisions. In addition to monitoring the success of autonomous supply, both storage systems will be separately designed and compared.

3.6 Case Study Layout

This section explains the layout of the following three case studies, namely ideal voltage source, solar PV panel and wind PMSG generation cases. The supply input source and storage device pair varies across all cases to provide a large test matrix of results. The first case compares the storage device performance with an ideal voltage source input, thereby modelling a voltage bus connection. The second case models solar PV panel as a RES generation input. The third uses wind turbine PMSG power supply, obtained on the Matlab MathWorks open source demo site [109], [124], [125]. Each case is tested under HBS and BSS conditions. The cases are modelled over a 24 hour period and results are extrapolated to give weighting to the HOMER techno-economic study. The case study layout is shown in Table 3.4 below. In Table 3.4, "SC" means the supercapacitor.

Table 3.4 Subsystem Interfacing per Case Study

Case	Input Supply	Storage Device	Converter	Control Block
Case 1a	Ideal Voltage Source	Battery	Subsystem 2a	Subsystem 3a
Case 1b	Ideal Voltage Source	Battery and SC	Subsystem 2a & 2b	Subsystem 3b
Case 2a	Solar PV Panels	Battery	Subsystem 2a	Subsystem 3a
Case 2b	Solar PV Panels	Battery and SC	Subsystem 2a & 2b	Subsystem 3b
Case 3a	Wind PMSG	Battery	Subsystem 2a	Subsystem 3a
Case 3b	Wind PMSG	Battery and SC	Subsystem 2a & 2b	Subsystem 3b

Table 3.4 shows the allocated subsystems for the modelling of each case. It is worth noting that Case 1 uses an ideal voltage source to evaluate the storage device performance, as a result the load is solely supplied by the BSS or HBS. All cases are divided into subsections, for example the system in Case 1a which use the BSS and the system in Case 1b which then uses the HBS with the battery and the supercapacitor. Similar subdivisions are also made for Case 2 (2a and 2b) and Case 3 (3a and 3b).

As seen in Table 3.4, different BSS cases will use different controller and converter interfaces compared to the HBS cases. The modelling and simulation of these cases in Matlab are now explained, with relevant schematic and parameter justification following the descriptions.

3.7 Ideal Voltage Source with BSS - Case 1a

The base case used in the electrical performance analysis is known as the ideal voltage source BSS design (Case 1a). Herein the battery storage system (BSS) is used to supply a load. Essential components are described for the base case below, with the same components referred back to in subsequent cases.

3.7.1 Model Layout

A schematic diagram of the Case 1a system is shown in Figure 3.12 to describe the flow of electricity and signals in the ideal voltage source BSS. This case aims to evaluate the feasibility and utility of the BSS when supplying a load. The system is greatly simplified since the constant voltage source supplies the converter, which in turn charges the battery. The battery is then used to supply the load.

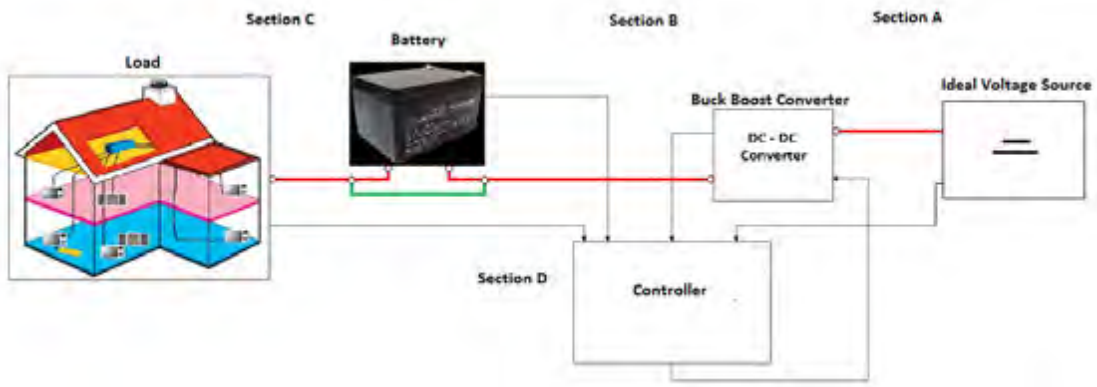

Figure 3.12 Electric and Signal Flow Schematic for Ideal Source BSS

Section A - In Section A the ideal voltage source directly feeds the constant voltage to the DC-DC converter.

Section B - Section B contains the DC-DC converter is employed to step the voltage up or down depending on the load demand. The allocated battery voltage is supplied by the converter, and the battery supplies the load. In this instance the battery is solely responsible for supplying the load but is indirectly sourced by the voltage bus.

Section C - Section C shows the transfer of the generated electricity from the battery to the load.

Section D – In Section D the feedback loop used for the load control is implemented. The schematic shows that all subsystems are reliant on the signal flow generated by the control block, which is responsible for energy management.

3.7.2 Load Profile Description

The load profile design needs to accurately demonstrate the dynamics of the selected simulated region for the feasibility study. The load also needs to be set strategically so as to facilitate an accurate RES electric performance analysis. The description of how both of these requirements are achieved is now shown.

a) Load Curvature

The load profile model is designed with the objective of accurately portraying the dynamics of remote area electricity demand. For the correct curve to be selected the demographic of remote areas was considered. Remote areas in South Africa are too far for utility grid connection, and so are often very far from other electrified communities. As a result the remote area community would reside, but also trade and work, in the enclosed region. Based on this consideration the load designed will need to show commercial and residential properties in an effective way, whilst still allowing for simple RES and storage device feasibility studies and electric performance analyses. A case study conducted in [126] considers the regional electricity demand in residential and commercial sectors for PV system deployment. Based on the analysis, the following combination of both residential and commercial load profiles are shown in Figure 3.13 below [126].

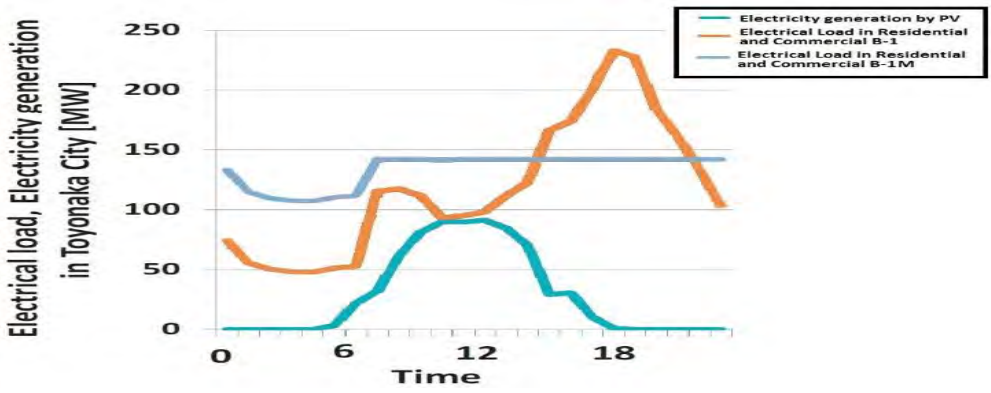

Figure 3.13 Scenario Analysis for Electrical Modelling of Commercial/Residential Load Profile [126]

Figure 3.13 contains a PV electricity curve in light blue, since the scenario analysis is based on RES deployment. Two differently weighted combinations of commercial-residential based electric load profiles are also presented in Figure 3.13 [126]. A combination of both commercial-residential load profile curves shown in Figure 3.13 was proposed as the new electric performance analysis load curve, to be used for simulation in Matlab and HOMER.

The curvature of the load profile designed in Figure 3.15 uses the orange and light blue curves in Figure 3.13 as a basis. In the initial hours the curve remains at a low power demand, similar to the orange and blue plots. The curve then undergoes a transitional phase which shows the residential electricity demand steadily increasing. After which the constant load remains at a maximum, showing the commercial profile curve, depicted in light blue, as higher than residential demand. The curve then transitions down to lower power demand values at a slower gradient. The slow gradient is used since the peak residential demand must still be modelled (orange curve) during this commercial power decrease (light blue curve). The load curve is then set back to the lower demand power value, to maintain continuity for late evening and morning hours. Based on the lack of evening transitions and constant maximum power, the commercial/residential load also allows for simplified solar panel profile implementation. This is due to the power generated by the PV which will have a direct effect on the success of the RES, in addition to the necessity of the storage devices being tested [117]. The wind speed profile has a uniform speed in comparison to solar irradiance, therefore its profile was not significant on the load profile[44].

b) Load Profile Scaling

The commercial/residential load curvature of Figure 3.15 has been described, but the magnitude of power demanded for the remote area use must still be considered. The load profile scale was based on the average component electricity contributions, seen in a study released in 2014 by South Africa's national energy utility.

Figure 3.14 Average Daily Component Power Consumption [127]

Based on Figure 3.14, the average local household consumes 6.2kWh of energy per day. When using a 25 hour day (to match simulation time) the average power demand is 0.248kW in South Africa. This figure can jump up to as high as 3kW for 2-9 minutes when using apparatus such as washing machines, water geysers or industrial electricity

contributions including large urns, and heating and cooling appliances etc. [127]. These power surges create a need for high power density provisions which facilitate the need for supercapacitors. Based on these values, the combined commercial-residential load generated in Matlab is shown in Figure 3.15.

c) Load Profile Modelling

The average commercial-residential load profile curve is generated in Matlab, by using a vector block with hourly unit inputs. Random rectangular pulses were included to model potential load fluctuations for the sake of evaluating the supercapacitor contribution in HBS mode, as well as to compensating for short term high power components. The resultant load profile is shown in Figure 3.15.

The objective of this performance analysis is to establish the feasibility of RES in remote areas. The figure average and peak parameters are therefore based on the average South African load profile data. Based on the scale used, a maximum demand of 1.6kW can effectively supply 7 average sized households or 15 basic households considering the remote area basis of the study [127].

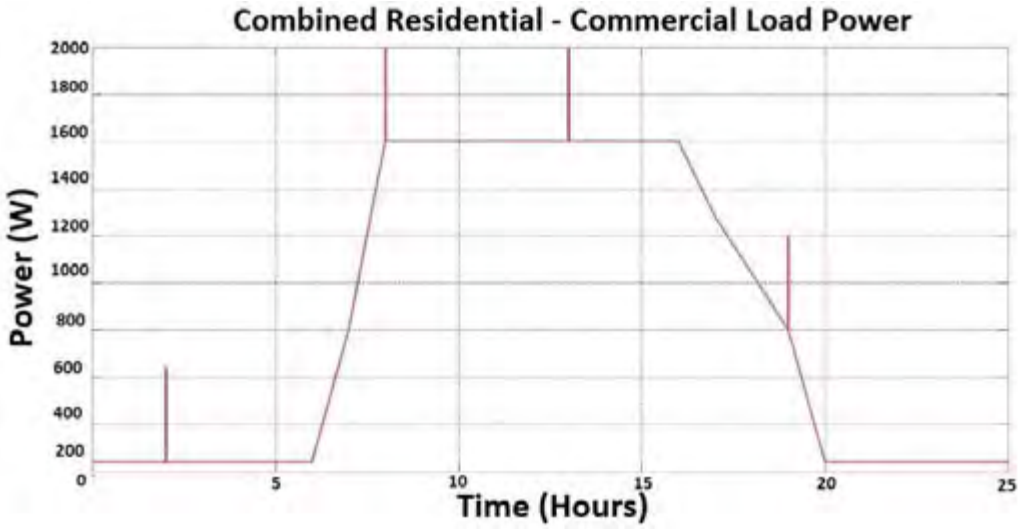

Figure 3.15 Load Profile modelled in Matlab [127], [128]

The load profile is measured over a span of 25 hours. A single supercapacitor charging is limited to 30 seconds, which makes the impulses seem relatively short compared to the total load demand. In most cases the impulse disturbances observed are not as short in time frame or as high in Watts, but the short term rectangular pulse can assess the storage systems under its potentially worst case conditions [51]. The load curvature, capacity and disturbance magnitudes have now been justified for modelling and are used for the duration of the electric performance analysis.

3.7.3 Battery Parameters

The same 18 Ah lead acid battery system is used in the BSS and HBS models which allows for a fair comparison. The complete parameter table can be found in capacity justification section 3.13. Based on the parameters entered into Matlab, the battery discharge curve is

generated and can be seen in Figure 3.16. Battery voltage terminals are connected to the DC-DC converter which regulates the voltage of the wind, solar or ideal supply used.

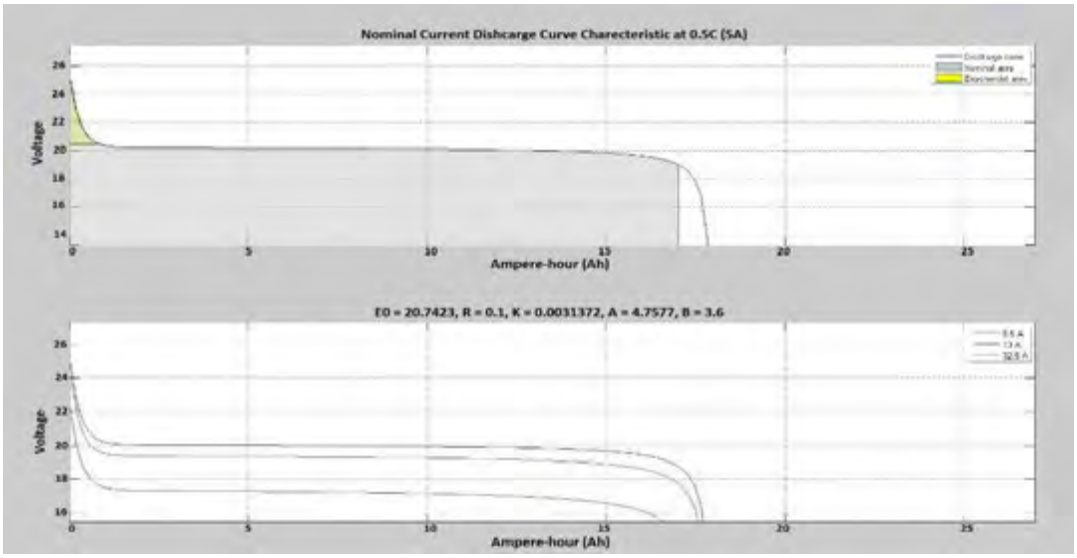

Figure 3.16 Battery Discharge Curve [109]

Unlike an ideal bus or ideal power source, a battery does not always maintain a fixed voltage since its parameters are non-linear. The blue trace in Figure 3.16 shows the battery discharging at 6.5 Amps. When the Amp-hour values are below 17 Ah the voltage remains relatively fixed; this is defined as the nominal area, which is ideal for discharge. The battery curves for different discharge currents are illustrated in red, blue and green in the bottom graph of Figure 3.16. When the current is higher, the voltage at the nominal area is reduced, batteries tend to discharge and charge using either constant current or constant voltage methods in sequence, this is the fastest way to charge them whilst protecting the battery.

3.7.4 Subsystem 2a – BSS Controller

Subsystem 2a represents the BSS control block or BSS controller used for battery storage energy management. The BSS controller contains 4 inputs and 2 outputs as seen in Table 3.5, and sends instructions based on the inputs illustrated in the table.

Table 3.5 Subsystem 2a BSS Input and Output Parameters

Input	Function	Output	Function
Load Profile 1	Load + Pulses	Output 1	Power tag
Load Profile 2	Solar + Pulses	Output 2	Battery signal
Load Profile 3	Pulses		
Load Profile 4	Solar / Wind		

The BSS controller inputs as shown in Table 3.5 have six signal connections as shown by the schematic of Figure 3.12, as well as the electric circuit diagram seen in Figure 3.17 below. The four inputs define the load and generated energy profiles. The load and RES generated energy profiles (Load Profile 1 and 2) are entered with and without their rectangular impulse disturbances. The independent rectangular disturbance impulses are separately sent into the load through Load Profile 3 with the ideal voltage, solar or wind

power generated equivalent signal sent via Load Profile 4. All four inputs are used in order to evaluate the signal disturbance rejection of the controllers used in subsystem 2a. After applying the controller algorithm, the required power and actual battery signal outputs are generated. The required power (Output 1) is used for profile comparison and Output 2 is sent to the DC-DC converter.

The subsystem shown in Figure 3.17 contains multiple switch signals whose statuses correspond to the 4 input conditions (refer to Table 3.5), and sends out the required battery signal and the filtered load demand to be used for performance measurements. The BSS control block manages to isolate the high frequency or high power signals which are identified as load disturbances. This is important in the hybrid storage cases where the average load is divided amongst the battery and supercapacitor. In the BSS case however, sole storage reliance is appointed to the battery, therefore, the highlighted blue block shows the combination of separated high and low power and frequency signals, which are both sent to the battery.

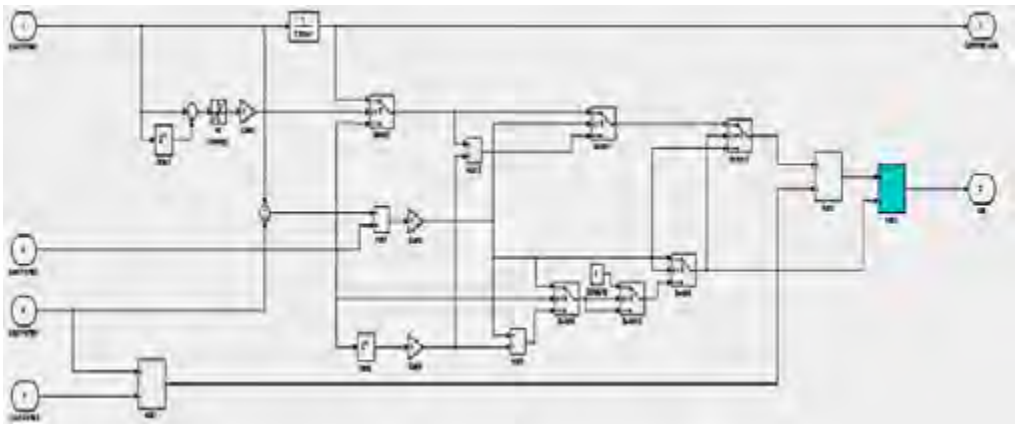

Figure 3.17 Subsystem 2a BSS Controller Block

Based on the inputs and outputs described in Table 3.5 and the circuit diagram in Figure 3.17, the BSS charging algorithm is illustrated in Table 3.6.

Table 3.6 Subsystem 2a Control Algorithm for BSS Controller

Condition	Additional Condition	Instruction	Additional Instruction
Solar/Wind> Load	None	Charge battery	Charge battery with excess energy
Load > Solar/Wind	None	Discharge battery	None
Solar/Wind > Load	Impulse fluctuation	Discharge battery	None
Load > Solar/Wind	Impulse fluctuation	Discharge battery	None

Table 3.6 uses the comparative switches to decide when the generated energy is above the load. The battery is charged in the event of excess energy being made available, but this value is still restricted in order to prevent overcharging. In addition to overcharge protection, the battery only charges with available energy, therefore the assigned additional instruction column in Table 3.6 states that the battery is charged with excess energy after the load is supplied. When comparing the filtered signal with the original, if an impulse is detected the battery will once again discharge, but in this case the converter will direct the

current to the load or supply based on the magnitude of the disturbance. This will in turn maintain system balance, but does add electrical strain onto the battery.

3.7.5 Subsystem 3a – Battery Buck-Boost Converter

The Battery buck-boost converter contains 4 voltage terminals and 2 signal inputs as seen in Table 3.7.

Table 3.7 Subsystem 3a Battery Converter Input and Output Parameters

Input	Function	Output	Function
V 1	+ Battery terminal	V 2	+ Solar / Wind terminal
V 3	- Battery terminal	V 4	- Solar / Wind terminal
Signal 1	PWM signals		
Signal 2	Battery signals		

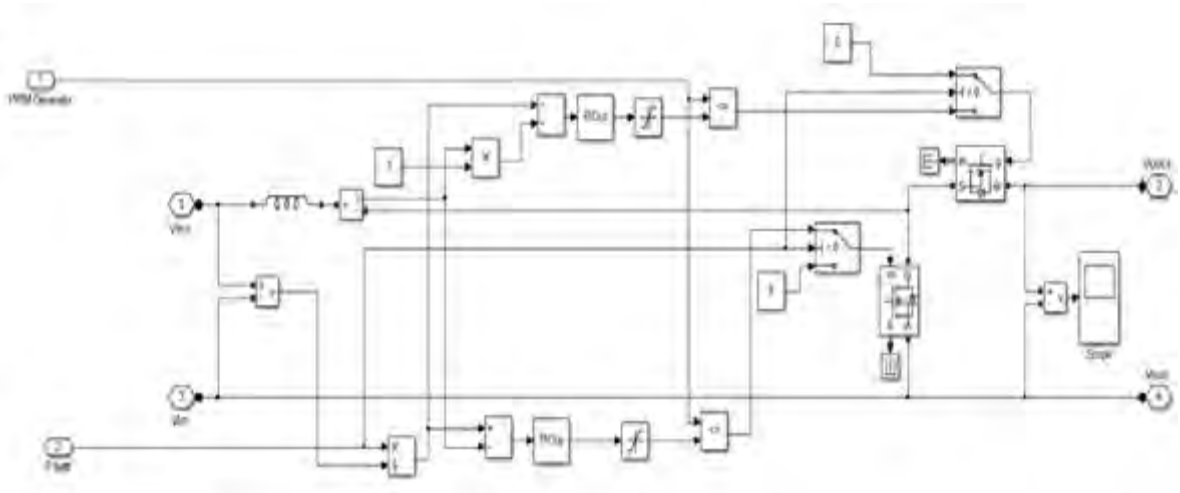

Figure 3.18 Buck-Boost Battery DC-DC Converter

The input electric terminals mentioned in Table 3.7 and illustrated in Figure 3.18, refer to the applied battery voltage. Signal 1 refers to the Pulse Width Modulation (PWM) signals used for generating a switching frequency for the converter, and Signal 2 is the controlled generation instruction signals sent from the controller known as subsystem 2a or 2b.

The buck-boost converter seen in Figure 3.18 is used for bidirectional power flow of the storage device and the supplied power. The converter is also responsible for scaling the voltage to an operable value; hence it serves as a protection system whilst implementing the requested control instructions sent by the control block subsystems.

Voltage is stepped by considering the (PWM) signals and battery signals sent from the controller block used. The resultant voltage is then used to either charge or discharge the battery. The system uses a Proportional Integral Differential (PID) controller, which restricts the current flowing through the series connected Metal Oxide Semiconducting Field Effect Transistor (MOSFET) when its gate is closed. Another PID controller is at the bottom of Figure 3.18, which regulates the power measured from the control block. This power is then divided by the voltage and a current is obtained. The current is then regulated through the PID and used to regulate the parallel MOSFET gate.

3.8 Ideal Voltage Source HBS - Case 1b

This section shows the introduction of the new storage device known as the HBS. In this case the battery and supercapacitor are employed as storage devices, with the same load and ideal voltage source used in Case 1a. Since the load and battery subsystems have already been explained, the supercapacitor and new HBS controller and converter systems are explained in this chapter.

3.8.1 Model Layout

The layout for the HBS model is now shown in the following schematic of Figure 3.19. This diagram has a more involved storage electricity flow since the load is now isolated. In this case high frequency and power variations are sent to the supercapacitor with the primary load being supplied by the battery.

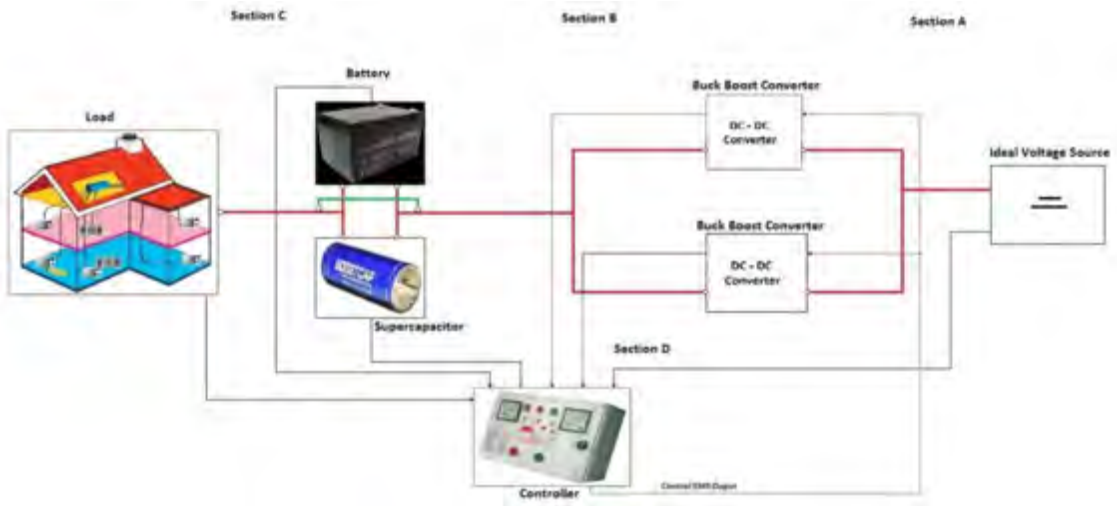

Figure 3.19 Electrical and Signal Flow Schematic for Ideal Source HBS

Section A – In Section A the ideal voltage source set at 100V, directly feeds the constant voltage to the DC-DC converters.

Section B – In Section B, the DC-DC converter is employed to step the voltage up or down depending on the load demand. The stepped voltage is sent to the supercapacitor or battery based on the controller instruction. In this instance two converters are used, one for the battery and the other for the supercapacitor. This is known as a semi active power electronic configuration [79]. It connects both storage devices in parallel, allowing them to contribute to the demand at different times. Both DC-DC converter systems are then connected to the controller.

Section C – In Section C the load is supplied by the battery and supercapacitor. The decision of load deployment is based on the controller instruction.

Section D – In this section the controller takes in the signals from the source, storage and load subsystems. Based on the load demand at the time, the controller will then instruct the converters and the designated storage device will supply the load.

3.8.2 Supercapacitor Parameters

The supercapacitor discharge curve based on the input parameters is now illustrated in Figure 3.20, which includes the capacity, voltage and current of the supercapacitor during a single discharge pulse.

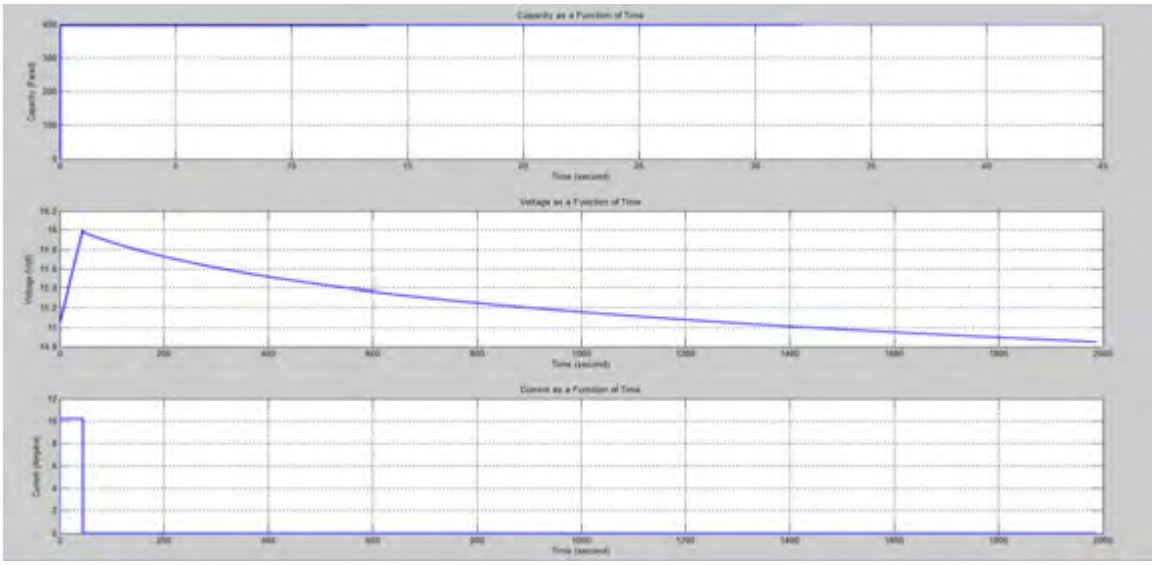

Figure 3.20 Supercapacitor Capacity, Voltage and Current as Functions of Time[109]

The supercapacitor has a 400 Farad capacity and a high power density which can be confirmed by the Rapidity at which is approaches peak voltage. The supercapacitor has a 2.1 milli-Ohm series resistance, a rated voltage of 16V with a surge voltage of 17V which can be seen by the voltage function in Figure 3.20. The peak current selected was set at 10 Amps. This gave the supercapacitor a potential power peak response of 1600VA. Based on the load and solar fluctuations designated and explained, the supercapacitor parameters were set to adequately supply these fluctuations whilst remaining economically sized. Further explanation into component sizing will be given in the parameter justification table.

The current plot shown in the lowermost graph of Figure 3.23 shows a rectangular pulse which discharges for 80 seconds. This is ideal in responding to the rectangular pulsed disturbances found in the load and supply.

3.8.3 Subsystem 2b – HBS Controller

Subsystem 2b is the subsystem which acts as the hybrid storage controller or HBS controller. Table 3.8 explains the 4 inputs and 3 outputs of this controller, which are also shown in Figure 3.21.

Table 3.8 Subsystem 2b HBS Input and Output Parameters

Input	Function	Output	Function
Load Profile 1	Load + Pulses	Output 1	Power required
Load Profile 2	Solar + Pulses	Output 2	Supercapacitor signal
Load Profile 3	Pulses	Output 3	Battery signal
Load Profile 4	Solar / Wind		

Table 3.8 contains the same inputs as the BSS controller shown in Table 3.6. However, an additional output signal is presented in subsystem 2b. The HBS controller isolates the output signals. The supercapacitor signal is now employed to distribute control instructions for high power and high frequency operations. The HBS control system separates the load and disturbance impulses in Load Profile 1 using a series of switches, controllers and hit crossing blocks. The isolated high frequency and high power disturbances are then sent to the supercapacitor, while the controlled average load energy required by the system is sent to the battery. This procedure is illustrated in Figure 3.21.

The circuit diagram of the designed HBS controller shown in Figure 3.21 works in the same manner as subsystem 2a for BSS controllers, but does not combine the controlled outputs. Switches and measuring blocks monitor the ramp and amplitude of the input signal and allocate loads to the battery or supercapacitor converters respectively.

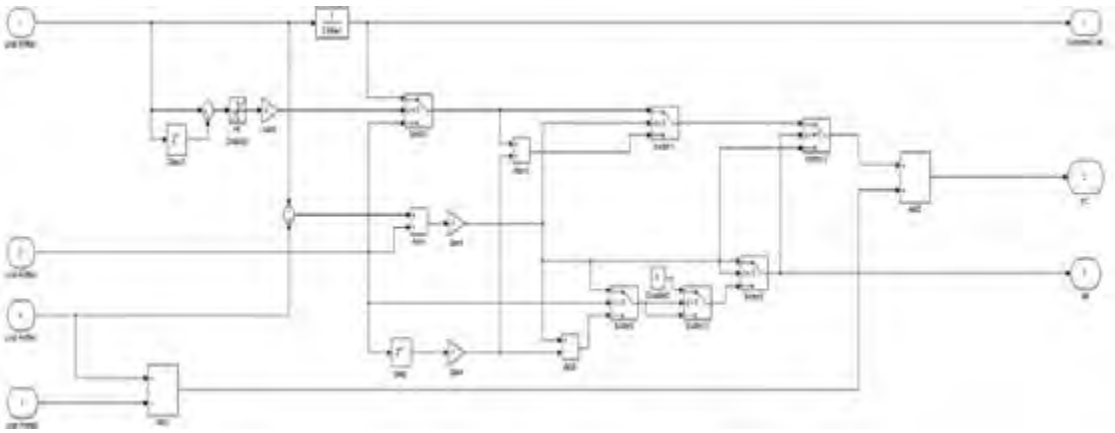

Figure 3.21 Subsystem 2b for HBS Controller Block

Table 3.9 now illustrates the control algorithm for HBS controllers implemented, based on the circuit and input and output values defined. The algorithm ensures that the load is always matched, and that the battery and supercapacitor recharges with the excess solar supply when possible.

Table 3.9 Subsystem 2b Control Algorithm for HBS Controller

Condition	Additional condition	Instruction	Additional Instruction
Solar or Wind > Load	None	Charge battery	Charge bat with excess energy
Load > Solar or Wind	None	Discharge battery	None
Solar or Wind > Load	Impulse fluctuation	Discharge SC	Recharge SC with excess energy
Load > Solar or Wind	Impulse fluctuation	Discharge SC	Do not recharge SC

Table 3.9 describes the charging algorithm followed for the HBS controller. The first column shows the initial condition, which is being assessed based on the comparisons of

ideal voltage source, solar or wind energy and the load demand. After the initial condition is established, the instruction to charge or discharge is sent out in the third column. The last column shows the additional instruction which limits the charge capacity to prevent shortages or over charging. The term 'excess energy' used here refers to the amount of energy which remains, based on the generation and load comparison.

The charging algorithm allows the RES to sustain autonomous supply without utility grid connection. The additional conditions in the algorithm ensure that only realistic magnitudes of recharging are considered. This is done with the series of switches used to set conditions. For instance, if excess energy is being generated by the solar panels, the controller will direct the excess energy to the battery for charging, but this charging will be limited to the excess energy generated only.

3.8.4 Subsystem 3b – Supercapacitor Buck-Boost Converter

A bidirectional buck-boost converter is implemented here with its parameters shown in Table 3.11 below. The circuit diagram for the supercapacitor converter and battery converter, known as subsystem 3a, are identical and can be found in Figure 3.21. The charge profile is determined by the controller so the converter simply uses the supercapacitor signals and PWM signals as in the previous system.

Table 3.10 Subsystem 3b Supercapacitor Input and Output Parameters

Input	Function	Output	Function
V 1	+ SC terminal	V 2	+ Solar / Wind terminal
V 3	- SC terminal	V 4	- Solar / Wind terminal
Signal 1	PWM signals		
Signal 2	SC signals		

Table 3.10 defines the input and output parameters considered in the DC-DC converter known as subsystem 3b. The inputs in this table are identical to the Table 3.7 used for subsystem 3a, with the supercapacitor simply replacing the battery terminals and signal inputs. In Table 3.10 the term SC refers to the supercapacitor.

A distinct difference between the battery converter and supercapacitor converter is the cost of components. The supercapacitor is primarily used for power quality enhancement and disturbance response which means it will operate for very short intervals. Since supercapacitors have a high power density and these disturbances observed are higher than the average load, the power ratings of MOSFETs, switches and inductors in subsystem 2 are increased. This makes subsystem 3b more expensive.

3. 9 Solar BSS - Case 2a

Since the majority of the components have been described in the base ideal cases, the RES resource modelling procedures are now explained in the remaining cases.

3.9.1 Model Layout

This schematic describes the flow of signals (in black) and electricity (in red), starting off with the solar rays and ending with electricity supplied to the remote area load. Each step is labelled by sections which are then described.

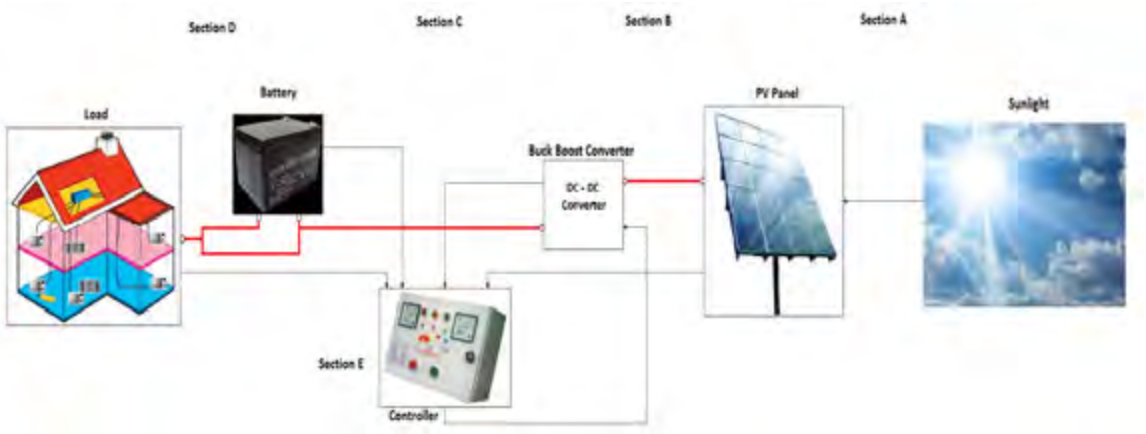

Figure 3.22 Electrical and Signal Flow Schematic for Solar BSS System

Section A - In Section A the solar irradiance is being absorbed by the PV panel and converted into electrical energy.

Section B - In Section B electricity generated by the PV panel is fed to the DC-DC converter (flow marked in red). In terms of signal flow the measured value of PV power generated is sent to the controller.

Section C - Section C shows the battery and DC-DC converter's communication with the controller. The battery, converter, PV panel bank and load all feed their recorded power values to the controller. The controller then establishes whether the load is adequately supplied by the PV panel, or whether the additional stored capacity is required using a charging algorithm. After the controller establishes the required energy a waveform signal, which allocates the required voltage, is fed back to the DC-DC converter for voltage control.

Section D - Section D indicates that the converter has now been instructed by the controller. The battery is either charged or the converted energy is sent directly to the load. In the event of a shortage during peak load demand, the necessary energy is acquired from the PV panel and the battery to maintain supply.

Section E - In Section E, the schematic shows the controller connections. All systems are reliant on the signal flow generated by the control block responsible for energy management. The output signal of the controller is sent to the converter. The converter implements the instructed output by stepping the PV panel voltage up or down. The bidirectional property of the converter means it can charge or discharge the battery, and therefore regulate the load and supply.

3.9.2 PV Energy Generation Modelling

a) Resource Modelling - Solar Irradiance Profile

The model parameters measure the irradiance input in $\frac{W}{m^2}$, hence, this is the unit of measurement for the solar vector specified. The values are generated in Matlab using a

vector input block of hourly irradiance values, collected from the NASA database and validated by Google Maps [128], [129].

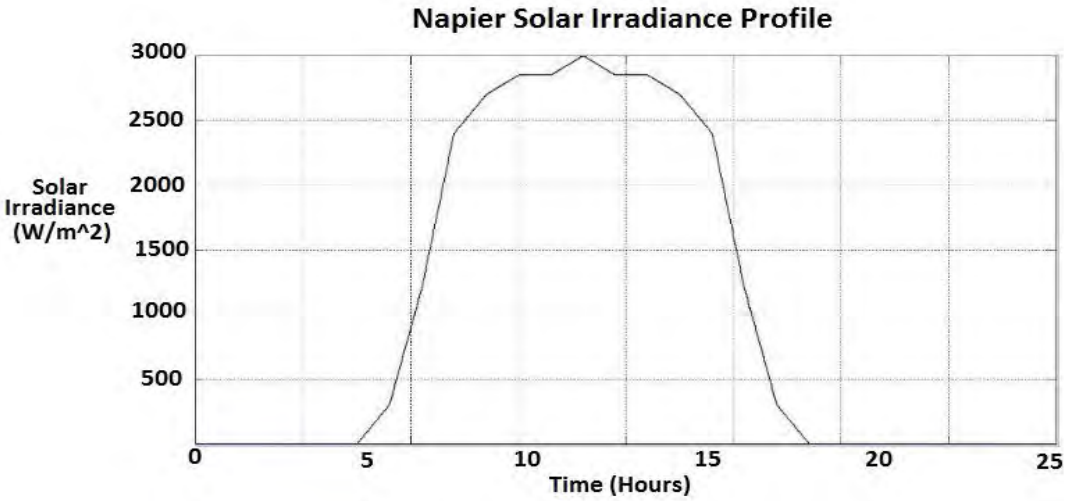

Figure 3.23 Solar Irradiance Profile

As mentioned in Chapter 2, in certain instances clouds will block the sunlight and can significantly reduce the solar supply. In other cases things could block the exposure from the solar panel to the sun. These disturbances can reduce the irradiance and cause additional fluctuations, emphasizing the need for storage in renewable energy systems [38], [39].

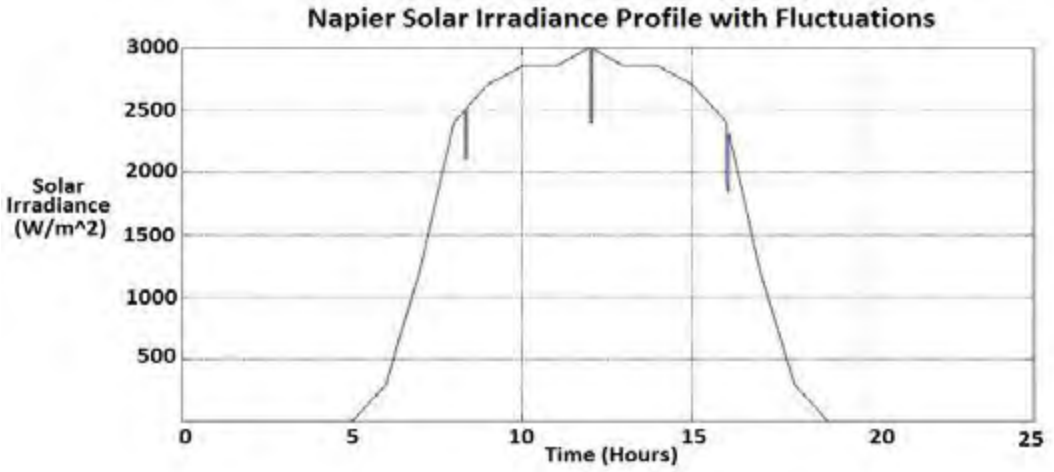

Figure 3.24 Solar Irradiance Profile with Estimated Supply Disruptions

Figure 3.24 models small scale disturbances with rectangular impulses, reducing the solar irradiance. The width of the impulse is kept between 30-60 seconds which reflects the average charge and discharge times of a single supercapacitor. It is possible to increase the time period of the PV disturbance. However, this would dilute the individual supercapacitors worst case storage contribution and performance evaluation, since a larger supercapacitor bank would need to implemented [130].

b) Solar Panel Bank Modelling - Subsystem 1

A set of 72 solar cells are used for a solar panel bank which makes up subsystem 3. The main input parameters of the solar cell are specified in Figure 3.25. The solar cell block measures the solar irradiance in W/m^2, and is therefore the unit of measurement used in the solar vector as well. This is important when comparing the power plots and solar irradiance supply in the results of Chapter 4. The temperature dependence and device temperature parameters are entered in Matlab as well.

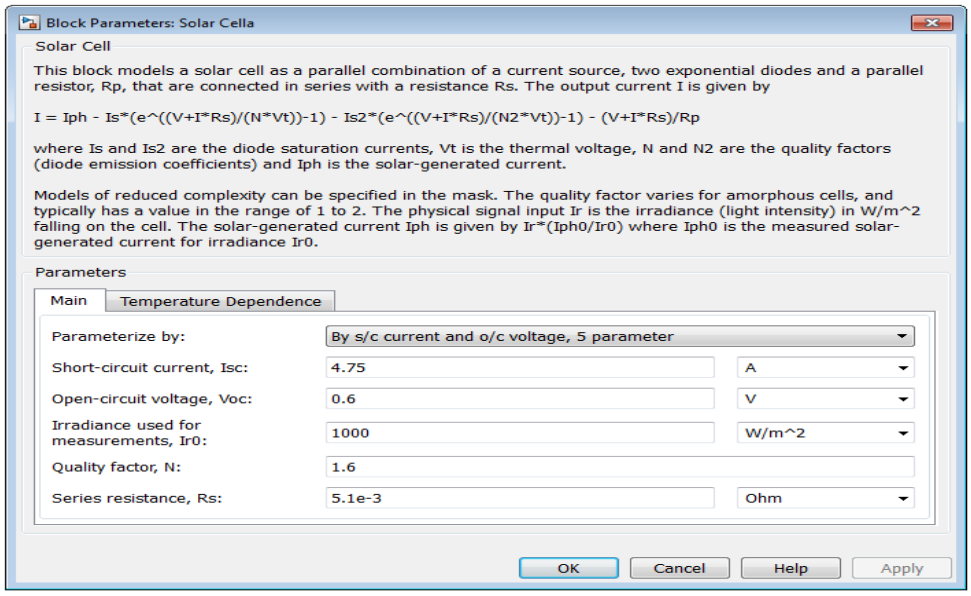

Figure 3.25 Solar Cell Main Parameters

The solar panels used here are imported from the SimScape block set. A solver configuration and a conversion tool are used in the subsystem block, in order to convert the SimScape library values to equivalent SimPowerSystems library values. The solar cell subsystem input and output values and their function descriptions are presented in Table 3.11 and in Figure 3.25.

Table 3.11 Solar Cell Block Input and Output Parameters

Input	Function	Output	Function
In 1	Irradiance vector	Out 1	Solar Signal
		Out 2	Solar & Impulse Signal
		Conn 1	+ Solar terminal
		Conn 2	- Solar terminal

Table 3.11 describes the input solar irradiance vector label, In 1. The electrical voltage terminals based on the solar energy generated are shown by Conn 1 and Conn 2, and can be seen in Figure 3.26 measured across the SimPowerSystems series resistor. The first output signal is used to illustrate the clear solar power generated with rejected noise, shown by the controller block in the figure. Lastly, Out 2 refers to the solar impulse with the included solar fluctuations, which are modelled by three rectangular impulses. Separate solar signal outputs are used in this subsystem, which allows for easier storage device deployment.

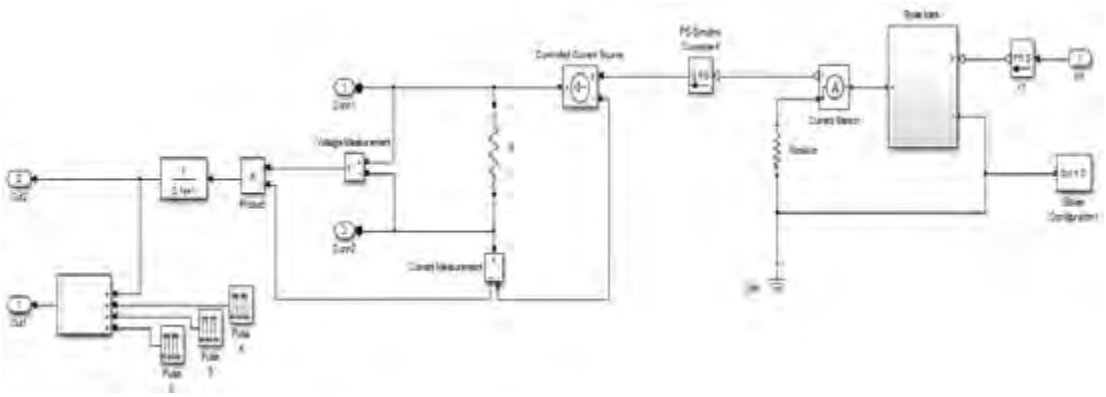

Figure 3.26 Subsystem 1 Solar Generation Overall Subsystem

The solar values undergo a ripple because of the conversion from SimScape to SimPowerSystems which required noisy passive resistors. A controller is used to smooth the solar bank power output signal. The configuration of the solar panel bank known as subsystem 1 is shown in Figure 3.26.

The solar panel bank comprises of multiple subsystems containing solar cells. The cells convert the solar irradiance signal into a current which is then measured and sent out to the controller, as well as applied onto the converter for interfacing with the storage devices. The multiple input subsystems which make up the solar panel bank is shown in Figure 3.27.

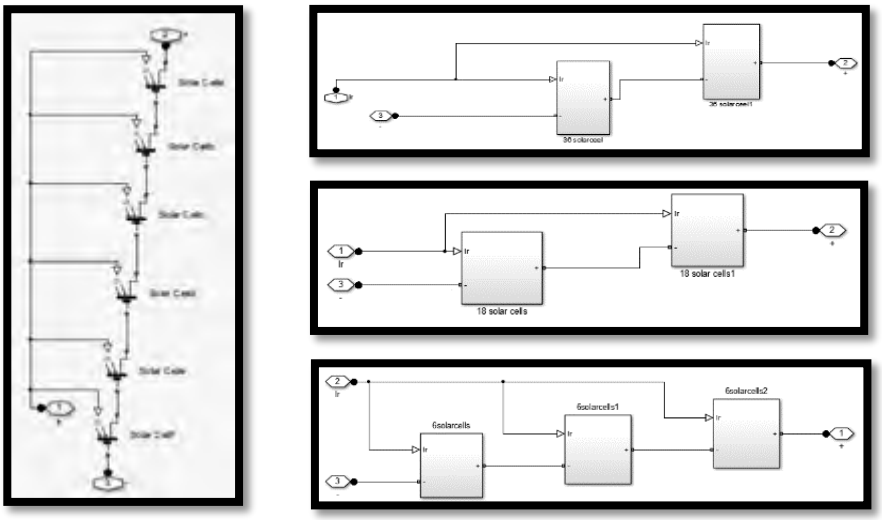

Figure 3.27 Solar Generation Internal Subsystems

3.9.3 Complete Solar BSS design in Matlab

Lastly the combinations of all subsystems described are shown in Figure 3.28. It closely matches the schematic shown initially in Figure 3.22, with included connection for system plots and interfacing.

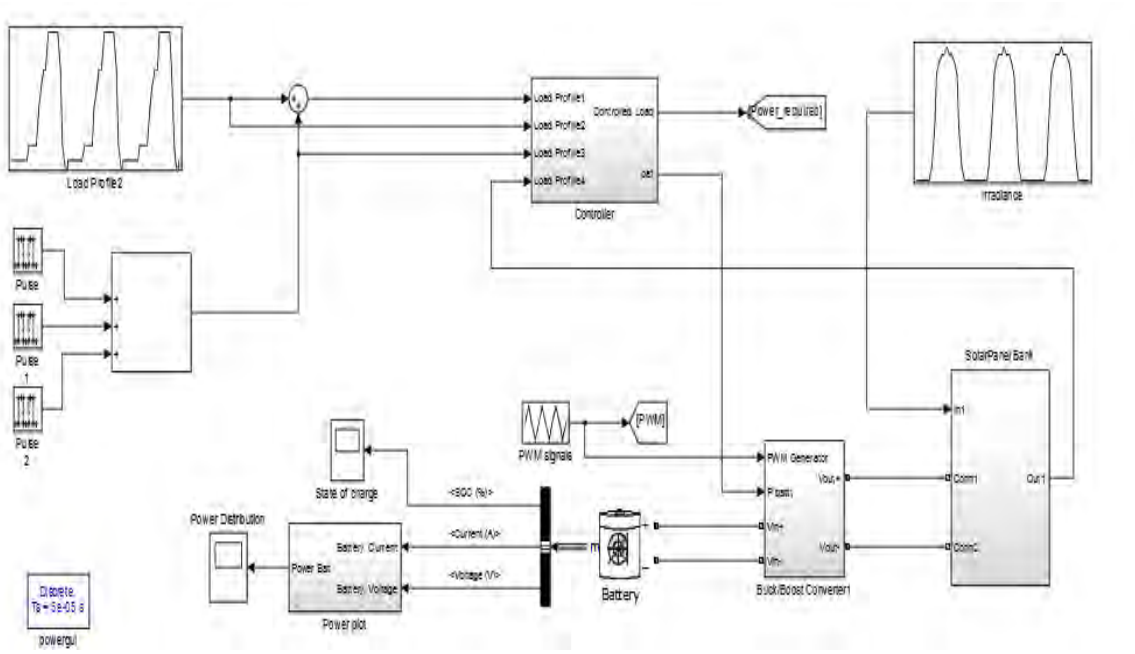

Figure 3.28 Complete Model for Battery Storage System (BSS)

The solar generation system receives the input irradiance and generates a voltage single which is stepped up or down by the DC-DC converter. Thereafter the converter refers to the control signal instruction and either charges or discharges the battery accordingly. Measurements at all of the described points are taken and used in the RES electrical performance analysis of Chapter 4. The subsequent cases will follow the same structure as Case 2a, with minor adjustments in supply and storage device which will be detailed for respective cases.

3.10 Solar HBS - Case 2b

The procedure of modelling the PV generation hybrid storage system of Case 2b is now explained. It follows a similar structure to the solar BSS as described in Section 3.9.1 with some modifications to the storage device, converter and controller used. It is worth noting that Case 2b uses the same battery converter and solar generation block as in Case 2a. The load and variations are the same as in Case 1a, described in section 3.7.2.

3.10.1 Model Layout

The flow diagram based on Case 2b is shown in Figure 3.29. The initial stage marked as Section A is the same as the PV BSS shown in Case 2a. The difference observed in Figure 3.29 is that the Solar HBS employs both the battery and supercapacitor storage devices, which in turn require different energy allocation, control and interfacing methods.

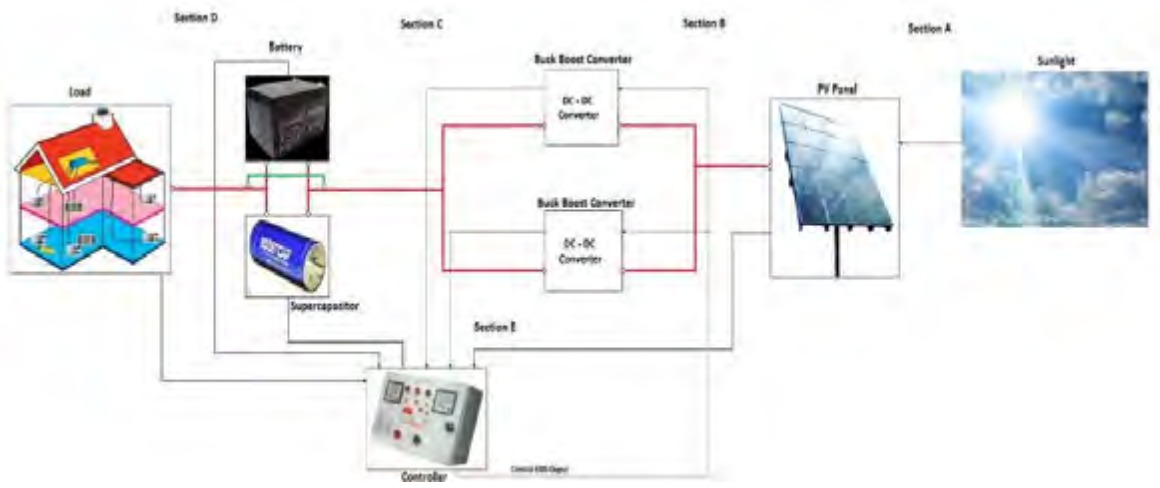

Figure 3.29 Electrical and Signal Flow Schematic for Solar HBS System

Section A - Section A is the same as that in the solar BSS in Figure 3.22, in section 3.9.1. Electricity flow is shown via red lines.

Section B - Section B is similar to Figure 3.22 for Case 2a but in this instance two converters are used, one for the battery and the other for the supercapacitor. The semi active DC-DC converter designed is maintained for battery and supercapacitor, as explained in section 3.8.1. However, in this section the ideal voltage source converter input is now replaced with the PV equivalent voltage generated.

Section C – Section C indicates that respective converters and storage devices both send output measured signals to the controller. The load and PV power generated is monitored here. The regulated voltage taken from the buck-boost converters, is sent to the storage devices.

Section D – Section D shows that the output power of the battery and supercapacitor is sent to the load when instructed by the controller. The averaged load is still supplied by the PV panels, directly after the DC-DC converter regulates the voltage.

Section E - Section E shows the control system behaviour. When the primary load is above the generated PV power then the battery will supply the load. If high frequency fluctuations occur then the supercapacitor will momentarily supply the load. This is decided based on the ramp and comparison blocks used in the control subsystem. Based on the control algorithm the controller will instruct the converters, and allocate power to either storage device or load.

3.10.2 Complete Solar HBS Circuit Diagram

The overall solar HBS system, with previously described interconnected subsystems, is shown in Figure 3.30. The power electronic converters of subsystem 3a and subsystem 3b are directly connected to the solar panel bank of subsystem 1.

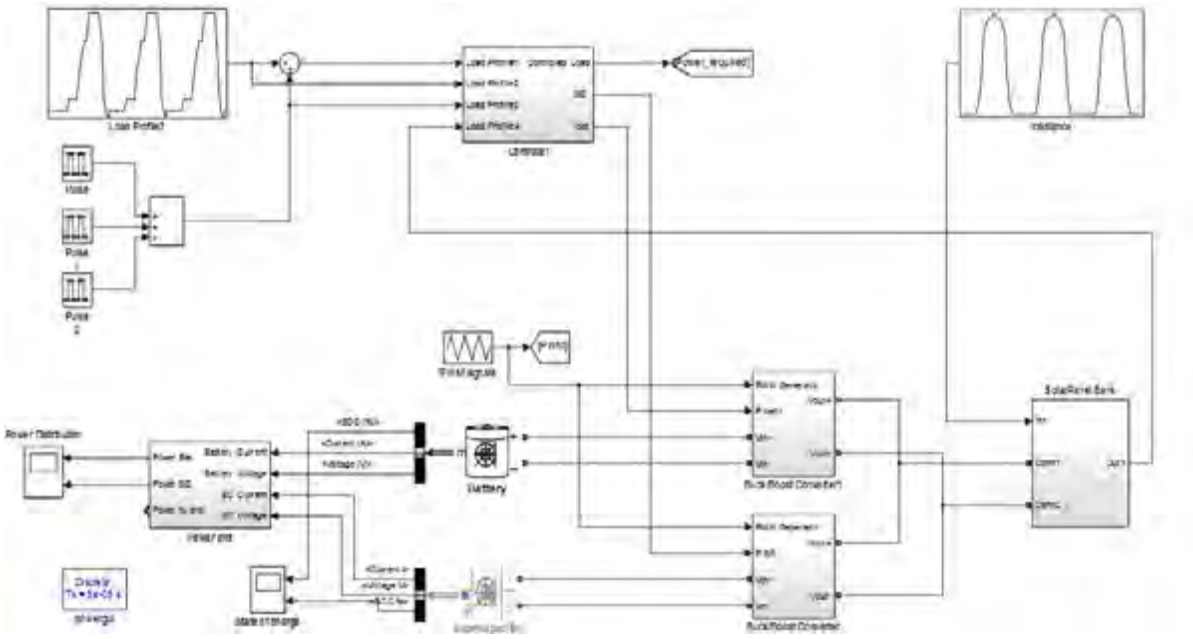

Figure 3.30 Complete Solar-HBS Matlab model

The entire system is automated and controlled and can therefore be tested by simply varying the input parameters of the load profile, disturbance blocks and irradiance vector. Figure 3.30 shows the combined solar-HBS model used in Case 2b but can be applied to Case 1b (ideal source - HBS) or Case 3b (wind-HBS) by simply replacing the PV subsystem.

3.11 Wind BSS - Case 3a

3.11.1 Model Layout

The schematic of the wind BSS is shown in Figure 3.31. All components in this system from Section B onwards are the same as the solar BSS. All components prior to Section C are used for absorbing, generating and converting wind energy.

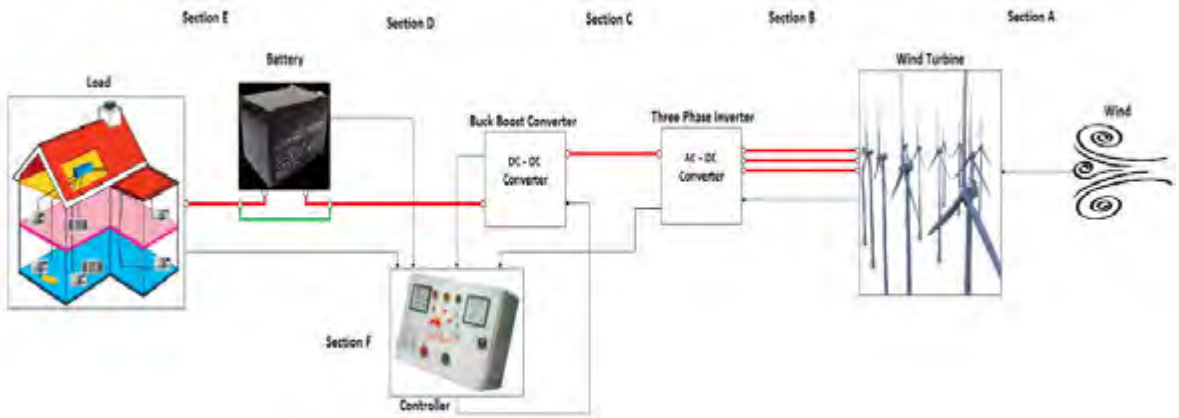

Figure 3.31 Electric and Signal Flow Schematic for Wind BSS System

Section A - The fundamental difference between the solar and wind RES, is seen in the first two sections. In this case, Section A represents the conversion of the wind gusts which drive the wind turbine, thereby generating electricity.

Section B - Generated wind energy is shown by the three red wires, because wind PMSG turbines use three phase generation. In this case the resultant three phase voltage must still be converted to DC for implementation in the DC controller. l.

Section C - Section C now has the converted DC power which can be driven into the buck-boost converter. Before this conversion the DC equivalent of the wind energy generated is fed into the controller. The controller instructs the DC-DC converter via a feedback loop, which distributes the flow of energy using the charge algorithm.

Section D - Same as in Solar BSS in Figure 3.22

Section E - Same as in Solar BSS in Figure 3.22

Section F - Section F operates in a similar manner to the Solar BSS and once again uses the DC-DC converter as the interface for load allocation and energy management. This is because it is much simpler to control DC signals than to use the three phase energy. Alpha Beta domain or state space operation would be required for three phase control and could show promising results, but is out of the scope of this study [86], [131].

3.11.2 Wind Power Generation System - Subsystem 4

a) Wind Resource Modelling

The wind speed data recordings are taken from the Wind Atlas of South Africa (WASA). The data acquisition and justification of this selected region will be explained in Chapter 5 [44]. Since the common practice for wind speed data acquisition is hourly measurements, the wind speed profile is modelled using an hourly vector block. This speed vector is used as an input to the PMSG demo used for simulation in Case 3a and Case 3b.

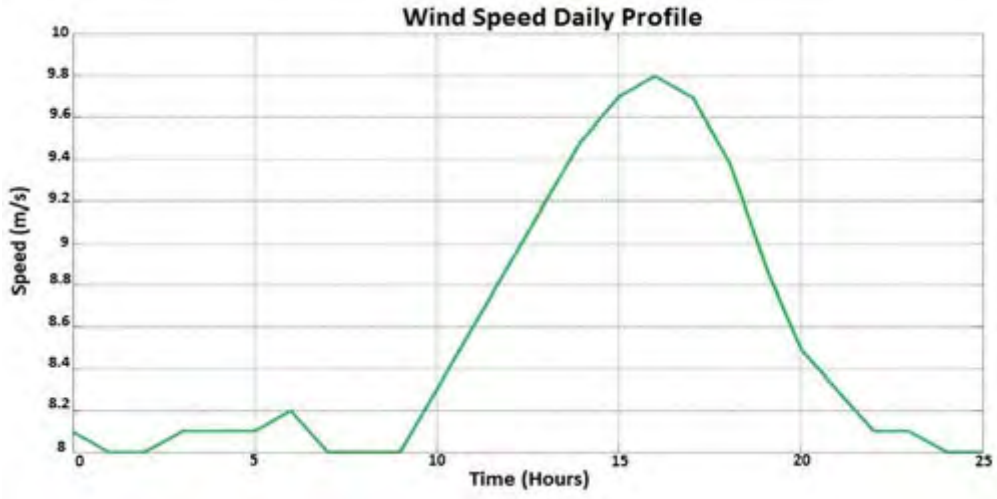

Figure 3.32 Napier Wind Speed Profile Modelled as Matlab Vector

The wind speed profile in Figure 3.32 does not show significant fluctuation when compared to the solar irradiance profile observed in Figure 3.23. A combination of resources could suggest a well distributed load levelling scheme.

b) Subsystem 4 – Wind Power Generation System

The wind energy generation system used was designed as an alternative energy source for RES testing. The PMSG wind turbine block is highlighted in red in Figure 3.31, and is taken from Matlab Simulink open source demo library [124]. The authorship, permission and demo licence is shown here [125]. The red PMSG block was then integrated using an AC-DC converter for DC voltage supply, and then interfaced with the storage devices. The wind system inputs are shown in Table 3.12. The wind speed profile mentioned earlier is illustrated by Signal 1 in the table.

Table 3.12 Wind Generation System Input and Output Parameters

Input	Function	Output	Function
Signal 1	Napier Wind Profile	Conn 1	Positive Voltage Terminal
		Conn 2	Negative Voltage Terminal
		PQ	Real & Reactive Power Signals

Table 3.12 describes the inputs and outputs used in System 4. The input Signal 1 is used to transfer the wind speed profile data generated by the unit vector block. The two output voltage terminals represent the DC equivalent wind PMSG voltage generated. This is of course taken from the universal bridge terminals, which convert the initial three phase voltage into the DC voltage values shown in Figure 3.33. The output PQ signal in Table 3.12 represents the equivalent active and reactive power signals which are used for supply and load comparisons. The wind generation PMSG block is connected with a three phase universal bridge interface, as is shown in Figure 3.33. The output of the PQ per unit terminal is multiplied by the rated Volt Ampere value, and the real and reactive power is de-multiplexed. The de-multiplexed output value is then used as a feeder signal for the energy management system. This allows for control of energy stored due to wind generation.

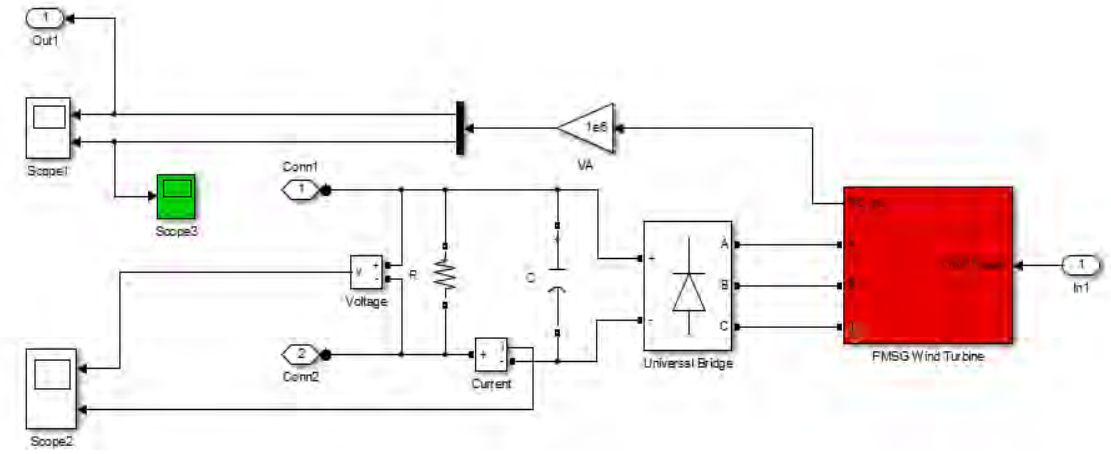

Figure 3.33 Wind Generation Subsystem

The amalgamation of described converter, load, controller and generation subsystems is then interfaced with either the HBS or BSS.

3.11.3 Complete Wind BSS

The wind-BSS uses the same electrical design as the solar-BSS (refer to Figure 3.28), after replacing the input power supply block, viz. subsystem 4 with subsystem 1. The complete

wind-BSS uses the BSS converter and controller described in section 3.7.4 and 3.7.5. Since the only difference between the cases is input power supplied, the same charge algorithm strategy is implemented (refer to Table 3.7), for uniform comparison amongst cases.

3.12 Wind HBS - Case 3b

3.12.1 Model Layout

The last schematic considered is the wind-HBS. Before Section C, Figure 3.34 shows the wind generation and energy conversion much like the wind-BSS in Figure 3.31. The schematic is the same as the solar HBS after Section C.

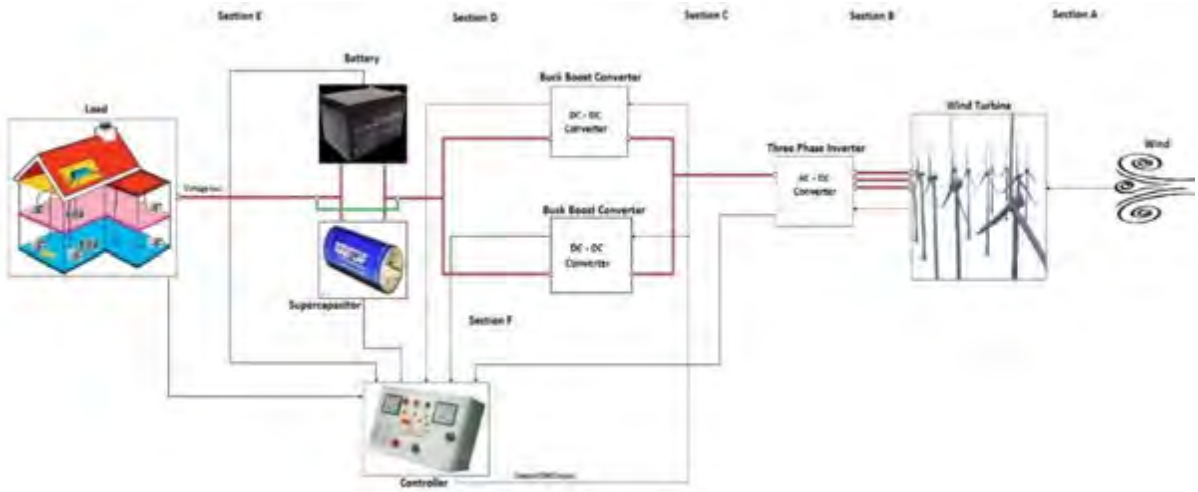

Figure 3.34 Wind HBS Schematic

Section A – The wind drive turbines used to generate three phase electricity.

Section B - Three phase voltage is inverted in to the DC equivalent.

Section C - The three phase power is fed into the supercapacitor and battery converter. The control output signal drives both converters, determining the state of the storage devices and load allocation. The converted DC wind energy value is sent to the controller. Minor fluctuations in wind energy may be distorted through the AC-DC inversion process, which can affect the system control. However, AC control is out of the scope of this study.

Section D - Same as solar HBS, refer to Figure 3.29

Section E - Same as solar HBS in Figure 3.29, but in this case the supercapacitor will be called upon more often due to high frequency disturbances being extra pertinent here.

Section F - This is the same as the solar-HBS, and once again the DC signal control was preferred for simplicity.

3.12.2 Complete Wind HBS

This system contains no new individual subsystems since HBS converters and storage devices have already been described and the wind generation section was defined for Case 3a. The electric circuit schematic is identical to Figure 3.30 with the subsystem 4 replacing subsystem 1.

3.13 Capacity Justification of all components

After considering the circuit diagrams and procedures followed for every case, a list of parameters is now presented in Table 3.13. It mentions the standard parameters used for every important component in the described simulation.

Table 3.13 Capacity Specification and Justification

Subsystem	Component	Parameter	Rating	Description
Solar Panel Bank - Subsystem 1	Single PV cell	Short Circuit Current	4.75 A	Current flowing when the cell is short circuited. The current rating is set to match the values of the standard PV panels. This represents a single cell in a bank of 72 cells tested.
		Open Circuit Voltage	0.6 V	Voltage measured across cell when not connected. When this value is multiplied with a high current and the series cell bank then the intended 2kW power rating is observed.
		Irradiance used	1000 W/m2	Irradiance needed for energy absorption. This value was left at default as it matches average panel characteristics.
		Quality Factor	1.6	This factor varies and is based on the amorphous cells used in the PV panel.
		Series Resistance	5.1mΩ	Internal resistance of the cell.
		Temp Exponent - Is	3	First order exponential increase, in the current from the initial diode as the temperature is increasing.
		Temp Exponent - Rs	0	First order exponential increase in the internal resistance as the temperature increases.
		Measurement Temp	25 oC	Temperature that parameters are measured at.
		Device Temp	25 oC	Temperature the device simulation took place at.
Wind Generation - Subsystem 4		Rated Voltage L-L	500 V	Rated Line to Line Voltage. PMSG considers collective WECS
		Rated Power	5 kVA	Rated Voltage Amperes of all turbines
		Rated Frequency	60Hz	Frequency of AC output power
		Time Constant	0.005	Increment of measurements taken in PMSG
	Universal Bridge	Snub Resistance	10000	The protective default resistance used for AC - DC converter
		Snub Capacitance	inf	When set to inf allows for resistive snubber
		On Resistance	1mΩ	Diode internal resistance
		On Inductance	0 H	Set to zero since the bridge is discretized for conversion
Battery Converter - Subsystem 2a	MOSFET	On Resistance	0.1 Ω	Internal Resistance
		Snub Resistance	100000 Ω	Snubber Protection Resistor
		Snub Capacitance	inf F	When set to inf system only uses a snubber resistor
		Diode Voltage	0V	Forward voltage of the internal diode
	Inductor	Inductance	1mH	Series inductor used to regulate the input voltage and feeds the current detection controller
	PWM Generator	Triangular Wave	Amp - 1 Freq - 1kHz	Triangular wave used in PWM generation to set switching frequency of the DC-DC converter in both converters
Supercapacitor Converter - Subsystem 2b	MOSFET	On Resistance	0.1 Ω	Internal Resistance
		Snub Resistance	1000000 Ω	Snubber protection Resistor increased since supercapacitor is supplying varying secondary load
		Snub Capacitance	inf F	When set to inf system only uses a snubber resistor
		Diode Voltage	0V	forward voltage of the internal diode
	Inductor	Inductance	1mH	Same size inductance as previous converter but the component would be more expensive due to high power ratings required for supercapacitor conversion
	PWM Generator	Triangular Wave	Amp - 1 Freq - 1kHz	Same generator signal fed into both converters

Controller - Subsystem 1 a/b	Controller	First Order Controller	1 / (0.99s + 1)	Used to smoothen out initial load and reduce potential fluctuations. Then compared to original signal and if large loads are reduced, is sent to battery or supercapacitor
	Hit Crossing	Offset of Hit Crossing	100	This component compares two signals. If a value larger than the offset is observed, it sends out a logic 1 otherwise a 0
	Switch	N/A	N/A	The switch is fed by the offset value. The switch is used to allocate the load to the battery or supercapacitor system. Other switches are used to monitor the controlled signals for analysis but is not essential to the controller system
BSS - System 2 **Also used in HBS**	Battery	Nominal Voltage	20V	Represents the end of the linear zone of the discharge curve. The voltage until the battery nears the end of its capacity.
		Rated Capacity	15Ah	This represents the minimum effective capacity of the battery which can be used reliably
		Initial State of Charge	70%	The initial condition set, determining how full the battery is. The parameter was set at 70 per cent, as it lays within the optimised SOC region [118]
		Maximum Capacity	26.0417Ah	This value is different to the rated capacity as it represents the max capacity seen during a discontinuity. This can be essential to high power fluctuations but only represents 105% of the rated capacity which is not much higher.
		Fully Charged Voltage	5A	Should not be confused with no load voltage. No load is the voltage across terminals when the battery is not connected. The fully charged voltage represents the reading taken at full voltage, given a discharge current.
		Nominal Discharge	5A	This is based on the nominal discharge curve which will show a current, which encircles the best charging region
		Internal Resistance (IR)	0.02Ω	IR remains fixed regardless of current and usually represents 1% of the nominal power. Due to its small influence, the related temperature effect is neglected
		Capacity	7.7569Ah	This represent the capacity of the bat at nominal voltage
		Exponential Zone	23.046 V 0.0833Ah	Represents the exponential zone of the battery discharge curve, which can be configured to create a high initial energy surge for fast absorption rate
HBS - System 1	Supercapacitor	Rated Capacitance	400F	Represents the nominal capacitance in Farad
		Rated Voltage	16V	Minimum voltage value used by supercapacitor
		Surge Voltage	23V	Corresponds to the supercapacitor voltage when an internal electrolyte becomes gas. This means it is the maximum voltage which can be found in the SC. By varying the amount of capacitors used in series, this value largely increases creating a high density power bank.
		Initial Voltage	15V	Represents the initial voltage and is highly reflective of state of charge. It should therefore be maintained at an operable region for fast recharging and discharging
		Leakage Current	5.2mA	This value is the supercapacitors biggest weakness. The milli-Amp region is not big in this simulation since a short timescale is used for testing, but this value can be highly influential in large scale simulation when load scaling and time shifting become a factor
		Operating Temp	25 oC	Specified temperature the supercapacitor is operating on. In this case it matches the battery temperature
		Equivalent Series DC Resistance	2.1mΩ	Minor internal resistance losses since the supercapacitor is one of the most efficient storage systems

3.14 Conclusion

The importance of storage for autonomous RES storage has been well established in this thesis. Battery and hybrid storage are important keys to unlocking the full extraction of South Africa's resources for autonomous generation in remote areas.

Proprieties which favour the hybrid battery supercapacitor storage system (HBS), are its complimentary characteristics between supercapacitor and battery. In order to effectively model the RES in isolation many storage, supply and disturbance factors had to be considered. A powerful and diverse simulation tool was required, and so the Matlab Simulink software was selected. This software has the capacity to integrate storage device mathematical modelling and renewable energy technology as well as power electronic sources. The SimPowerSystems and SimScape toolbox were used to integrate the solar cell blocks, converter system, wind generation tools, control operators, modelled loads and storage devices.

The electrical simulation aims to establish the possibility and effectiveness of operates RES without connection from the grid using the resource profiles generated in South Africa. The comparison of all RES and storage combinations are then compared and analysed amongst cases. The electrical performance of the supercapacitor specifically, will further validate assumptions made in the subsequent economic study chapters. This will present the feasibility of autonomous operation through the use of storage in addition to determining what the ideal storage device per case would be.

4. Chapter 4 - Results for Electrical Performance Analysis

Chapter 4 presents the results of the electrical performance analysis described in Chapter 3. The results section of this chapter is divided in to three sets of case studies 1, 2 and 3. The three case studies each consist of a different input energy source namely, an ideal voltage source for Case 1, solar PV panel for Case 2 and wind turbine for Case 3. Each case consists of two different storage device categories, namely for Case 1, battery storage system (BSS) as Case 1a and hybrid battery supercapacitor storage (HBS) as Case 1b. For each case's response of both BSS and HBS to the varying load and supply inputs are observed and compared.

The objective of this electrical simulation is to gain insight into the performance of RES using BSS and HBS storage instead of connection with the utility grid. It attempts to evaluate the accuracy and success of using storage devices and varying renewable energy sources to provide islanded power supply to remote areas. The power systems modelled are all evaluated under the following criteria per case:

- The accuracy of how well the combined power supply (renewable supply and storage) match the load power demand in the system, is assessed;
- Security of the power supplied is evaluated by measuring the average difference between supplied power and load;
- Based on the average power difference and average load the efficiency of the system in terms of meeting load demands, is assessed;
- Lifespan benefits of using a supercapacitor for high power buffering protection of the battery in the HBS is evaluated by considering the battery SOC results.

These criteria mentioned above are expected to provide insight on the electric performance of the three remote area power supply cases.

4.1 Case 1: Ideal Voltage Source

Case 1 uses an ideal voltage input source for the electrical performance analysis of the BSS and HBS devices. The objective of the electrical performance analysis is to establish the feasibility of remote area islanded RES deployment by using battery and hybrid storage devices as secondary supply alternatives. However, this objective means that the remote area loads and renewable power generated locally, are both varying parameters in the electrical performance simulation. In order to evaluate the remote area load provision and storage devices performance in a simplified initial manner, the ideal voltage source base case is proposed. In this case the variation in supplied voltage through renewable energy input sources is replaced with a constant ideal voltage input source. Here the ideal voltage source maintains a constant voltage supply at the storage device terminals via a DC-DC converter. The storage devices are then charged and discharged based on an algorithm with the aim of effectively supplying the load. The use of a constant input voltage in Case 1 simplifies the initial charging algorithm mentioned.

Case 1 can be understood as a renewable energy resource being replaced by a constant voltage bus. Since a constant input voltage needs to be manipulated in order to supply a varying load voltage, the power electronic converter; controller based charging algorithm and

storage devices employed will still be assessed. Furthermore, by removing the variation in supply, a clear comparison between HBS and BSS can be made in this case. These considerations make the ideal voltage source ideal as a base case for electrical performance analysis.

The total power and efficiency of power supplied by the storage devices will be assessed in this case. Load fluctuation response and storage lifespan potential is also presented in the set of results shown in section 4.1.

4.1.1 Basic Operation of Case 1 Simulation

a) Load Demand Details

The ideal voltage source is used to evaluate the electrical performance of a storage device under constant voltage supply input conditions. The load described in section 3.7.2 is simulated in Matlab, and shown in Figure 4.1. Section 4.1 presents both the BSS and HBS storage device tests with their schematic operation being described in section 3.8.1 and 3.9.1 respectively in Chapter 3. The parameters of the load used for the simulation is shown in Table 4.1 below.

Table 4.1 Load Parameters for Electrical Performance Analysis

Simulation Parameter	Magnitude	Unit
Simulation Start time	0.0	Hours
Simulation End time	25.0	Hours
Average load value	848	Watts
Minimum average load	240	Watts
Maximum average load	1600	Watts

In this case, the BSS and HBS are implemented to supply the varying load demand, while a constant input voltage is maintained. Firstly, the load power curve is shown in the red axis in Figure 4.1. In this load profile the daily curve for the 25-hour simulation is shown with four 400W disturbance impulses included. The first six hours of simulation show the load at a relatively low 240W; this represents the off-peak morning hours of operation. After which a steady increase in power is seen from six to eight hours. This represents the beginning of the average commercial load power reaching its maximum. From eight to 16 hours the load remains at the maximum of 1.6 kW while undergoing two 400W peak disturbances at eight and 13.5 hours respectively. The load steadily declines from 16 - 20 hours while experiencing a final 400W disturbance. The last remaining five hours of the load power profile is then fixed at 300W.

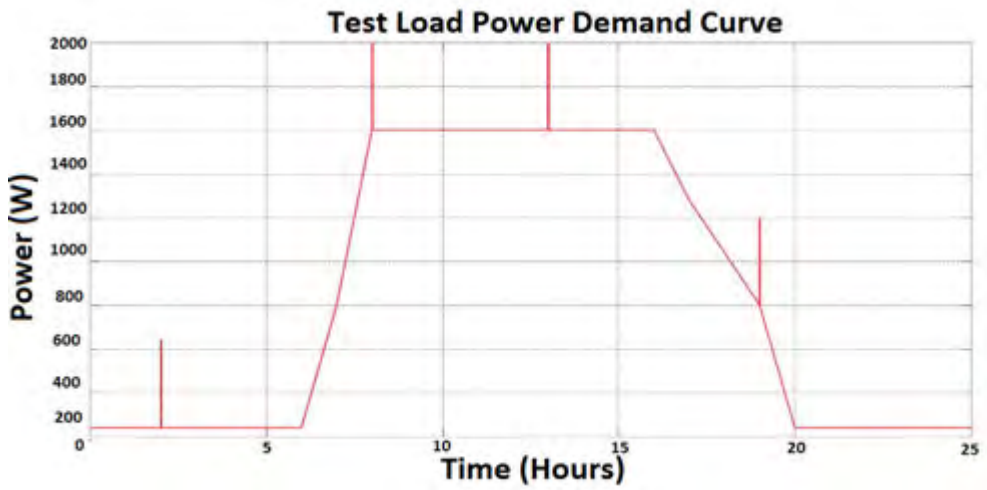

Figure 4.1 Load Profile for Electrical performance Analysis

The load demand shown above is used as the benchmark requirement for all cases being electrically evaluated. The load following and performance efficiency of the RES with storage device is dependent on the load provisions made in the regions described in Table 4.2.

Table 4.2 Load Profile Regions

Region	Load Magnitude	Power	Time Zone
1	Constant Low	300 W	20 - 6 hours
2	Increasing Load	300 - 1600 W	6 - 8 hours
3	Constant Maximum	1600 W	8 - 16 hours
4	Decreasing Load	1600 - 300 W	16 - 20 hours
5	Peak Power Fluctuation	Load + 400 W	2.1 , 8.33, 13.5, 19.8 hours

Table 4.2 shows the different transitional regions which describe the load profile. The load following, or power supply response of the storage devices in supplying the varying demand, is used to evaluate the electrical performance and feasibility of RES, with storage in remote areas where such load variations are prominent.

b) Discharge Cycle and Disturbance Rejection

In order to understand the charge and discharge cycles of the storage device for the single day system operation, load disturbances are superimposed on the load profile of Table 4.2. The load disturbance parameters are described in Table 4.3.

Table 4.3 Load Disturbance Parameters for All Cases

Sim Parameter	Magnitude	Unit
Disturbance Width	60	Seconds
Disturbance Amplitude	700	Watts
Disturbance Times	2.1 , 8.33, 13.5 , 19.8	Hours

In Case 1, the storage device discharge cycle is simplified as it only needs to consider variations in the load profile of Figure 4.1, with no variations being attributed to the constant input ideal voltage supply source. In regions 1 to 4 of Table 4.2, the load disturbances seen in Table 4.3 present another challenge for the charging algorithm. For Case 1a, BSS discharges based on the average load in Table 4.1, and the load disturbance in Table 4.3. The HBS in Case 1b however, uses the battery to supply the load described in Table 4.1 with the supercapacitor discharging the disturbances described in Table 4.3. Storage discharge curves are determined using the control systems and converters explained in sections 3.7.4 and 3.7.5 for the BSS and in sections 3.8.3 and 3.8.4 for the HBS, all sections being in Chapter 3.

c) Electrical Performance Evaluation Criteria

The load which is tested contains average and large scale fluctuations unlike the constant voltage source. Based on the described load the electrical performance falls under the following criteria:

1. Load Matching

   This evaluates how accurate the power allocated by the charging algorithm and consequently supplied by the storage device are in matching the load power demand.

2. Security of Power Supplied and Storage Device Supply Efficiency

The unmet load capacity is evaluated through a power difference calculation. It gives an indication as to how secure the power supply is. The average power difference is found by subtracting the average load demand from average output power supplied by the system. If a positive power difference remains, the average power supplied will be higher than the average load demand. A positive power difference is a good indication of security of power supplied by the system. If the power difference is negative, the power supplied will be less than the average load demand, which means that the power security of the system must be improved to some extent.

Based on the average power difference and the average load demand shown in Table 4.1, the average BSS supply efficiency can be calculated. The supplied efficiency refers to the percentage of load demand capacity which has been met. This is found by adding the (often a negative magnitude) power difference value from the actual average load demand. Based on the remaining power supplied, this numerator is divided by the average load demand to find the ratio of supplied load power and load demand. This ratio is shown in Equation 4.2 and refers to the efficiency of load demand being met i.e. supplied load efficiency.

Case 1 uses an ideal voltage source which means no input voltage supply fluctuations can affect the input energy source efficiency. Since the input energy source is ideal, the anticipated losses can only be due to the converters, controller and storage devices used. According to previous power electronic literature, an ideal converter efficiency is between 96 - 97 % [132], [133]. Review of recent lead acid battery discharge efficiency studies show that the battery efficiency can vary from 60 to 80% with the supercapacitor showing an efficiency of between 80 to 95% [13], [54], [59], [74], [134], [135]. The supercapacitor is not used as often but it is expected to slightly improve the system efficiency in the HBS. Based on the researched efficiency values the ideal system efficiency is set at 85 - 95% for the electrical performance evaluation. This efficiency value means that the total load is not constantly met but ways to improve system efficiency can be recommended after reviewing the results.

3. Storage Device Lifespan Extension

The major weakness found in lead acid batteries is their limited lifespan of 3-12 years. This short lifespan is due to the low cycle life of the battery which is measured at less than 1500 cycles. In addition, they are susceptible to lifespan degradation as a result of frequent shallow discharge cycles [56], [65]–[67]. It has been mentioned in the literature review that using a supercapacitor with a battery in the HBS, can extend the lifespan of the battery by protecting it from shallow and excessively deep discharge cycles [136]. The rectangular impulses applied to the load in this study are a prime example of how deep discharge cycles which are experienced in the BSS battery and avoided in the HBS battery because of the supercapacitor.

The electrical performance analysis is based on a 25 hour simulation in Matlab. For the battery to reach failure, a 3 - 12 year simulation of the battery will need to take place but this is not computationally possible. Due to the importance of battery lifespan, its properties in both storage methods need to be evaluated in an alternative way. The battery state of charge (SOC) when connected in HBS and BSS modes as proposed in section 3.5.2 of Chapter 3 is therefore used as an indicator of battery lifespan through extrapolation methods.

The SOC difference is based on the battery protection of deep discharge cycles due to the load disturbances (secondary load) mentioned in Table 4.3. Without a supercapacitor, the BSS battery will supply the additional secondary load on its own. SOC of each battery is measured during the simulation and average values are taken and subtracted in Microsoft Excel to find the SOC difference amongst BSS and HBS. Since the BSS will be supplying an

additional load its average SOC will be lower than that of the HBS. This average reduction accumulates onto the BSS for a certain time period until it reaches failure to supply at under 25% SOC [119], [136]. This time frame will indicate how long the HBS battery is protected hence its potential lifespan extension due to supercapacitor addition.

4.1.2 Results for Case 1: Load Matching

The ideal voltage source directly feeds the DC-DC converter(s) with 100 Volts. One converter is directly coupled at the battery terminal in the BSS (refer to section 3.7.5) and two converters are coupled in the HBS at the battery and supercapacitor terminals (refer to section 3.8.4) respectively. The equivalent ideal voltage signal is sent to the controller as one of the four controller inputs used which will determine how the load is matched.

The converter(s), is employed to step the voltage up or down based on the control charging and discharging algorithm. The controller has an equivalent signal input for the load, storage device, and converter readings. These inputs are all implemented in the charging algorithm for storage devices. The controller will implement the charging algorithm, and send the resultant instruction to the DC - DC converter(s) as its output signal (refer sections 3.7.4 3.8.3). The DC-DC converter will adjust the voltages sent to each storage device. Based on the converter voltage levels, each storage device will charge or discharge accordingly. The combined output power of the storage device(s) due to their discharge and charge profiles aim to perfectly match the load profile in Figure 4.1.

The BSS and HBS output power generated based on the charging algorithm and storage device implementation of the algorithm is shown in Figure 4.2 and Figure 4.3. The simulation takes place over 25 hours and attempts to effectively reflect the commercial - residential load design with the black BSS curve in Figure 4.2 and blue HBS curve in Figure 4.3.

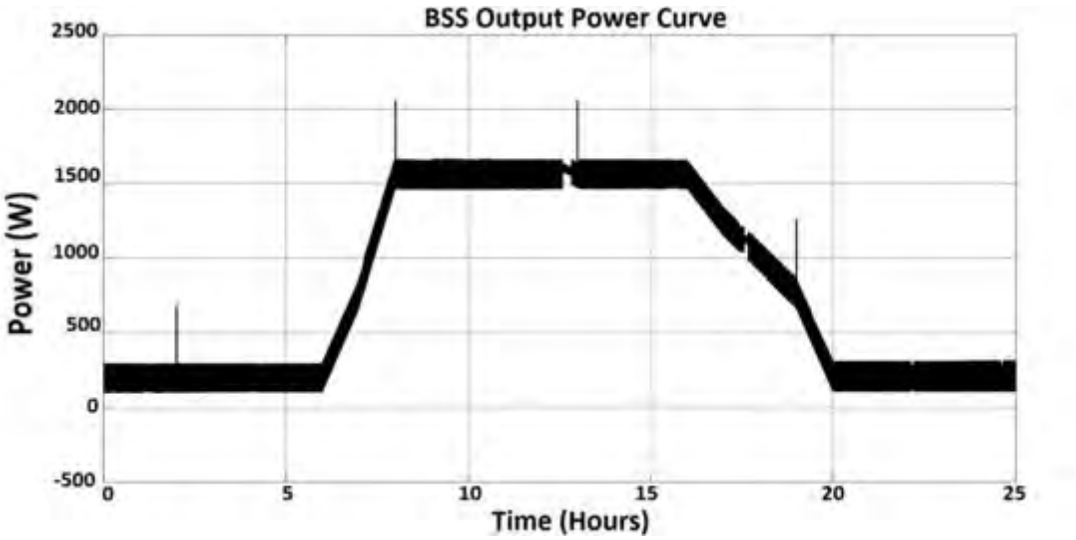

Figure 4.2 Power Supplied by BSS (Case 1a)

It is to be noted that in Figure 4.2 the BSS battery is the sole power supplier but in Figure 4.3 the power profile is a combination of the power generated by the battery and supercapacitor.

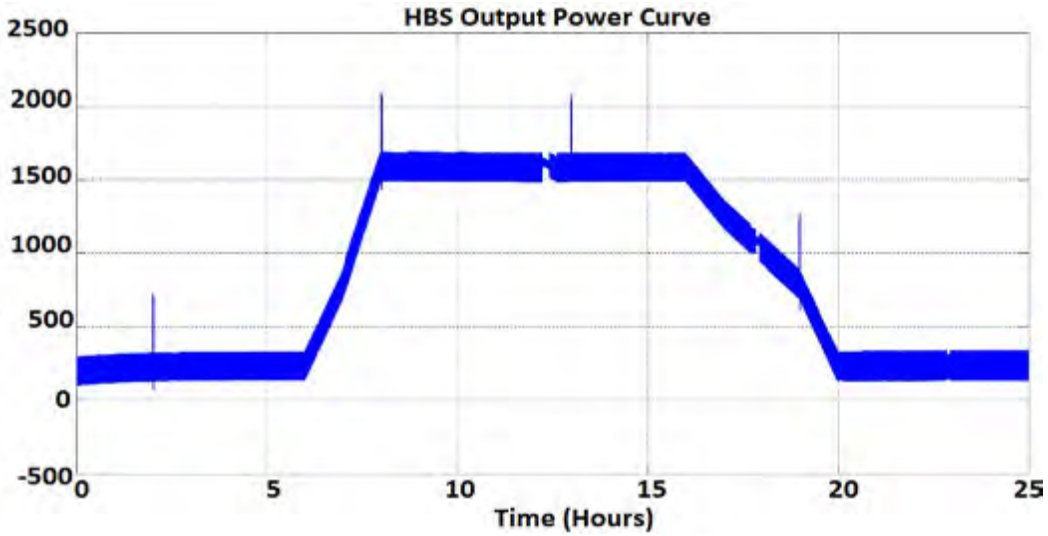

Figure 4.3 Power Supplied by HBS (Case 1b)

In order to compare the load matching or load following performance of BSS and HBS, output power profiles, the load profiles are plotted on the same set of axes in Figure 4.4. The load matching comparison on the same axes will allow for easy evaluation of HBS and BSS control charge algorithm instructions and system implementation of those instructions. In Figure 4.4, the blue curve represents the HBS power output, the black the BSS power output, and the green curve represents the load.

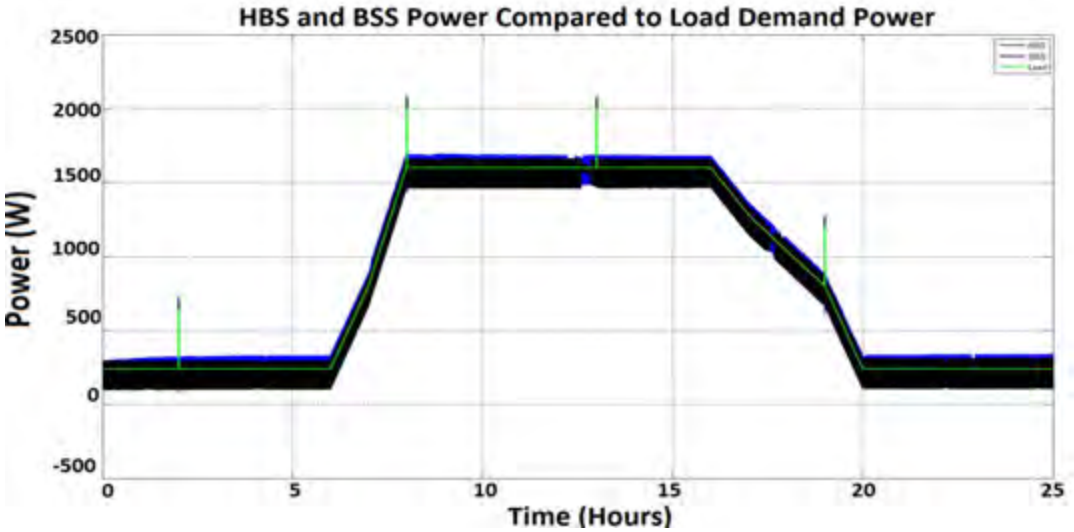

Figure 4.4 Comparison of load matching of BSS and HBS for the same load profile (Case 1)

With reference to Table 4.2, the load matching in the first region shows that both storage devices provide sufficient supply but their output profiles contain large power variations due to voltage switching which takes place in the DC-DC converter. In the increasing and decreasing power regions the storage devices show a slightly constrained power ripple with both BSS and HBS output accurately matching the load. It is worth noting that at 13 hours and 17 hours the black BSS curve does show a power reduction yet manages to maintain load supply. The HBS does exhibit less power dips in supply when compared to the BSS.

While considering the disturbance fluctuations designated at region 5 of Table 4.2, the BSS and HBS show different results. In Figure 4.4 disturbances are applied onto the load at four

different times indicated by the narrow green rectangular pulses. The first disturbance response shown in Figure 4.4 is now shown more closely in Figure 4.5.

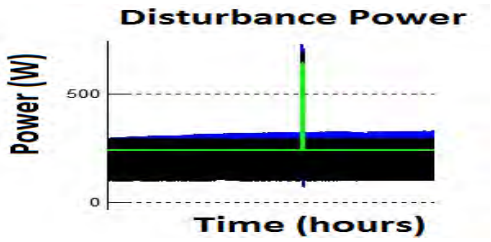

Figure 4.5 Zoomed in View of Response of BSS and HBS to Load Power Disturbance (Case 1)

The colour scheme remains the same in Figure 4.5 with the load shown in green, the BSS power output presented in black, and the HBS output indicated in blue. The rectangular pulse in Figure 4.5 clearly shows that the HBS maintains the highest power response for load power fluctuations. This high power response in the HBS is due to the redistribution of the load. The HBS allocates the average load demand to the battery with high power load variations being allocated to the supercapacitor. This is now validated by the supercapacitor power response to load fluctuations in Figure 4.6.

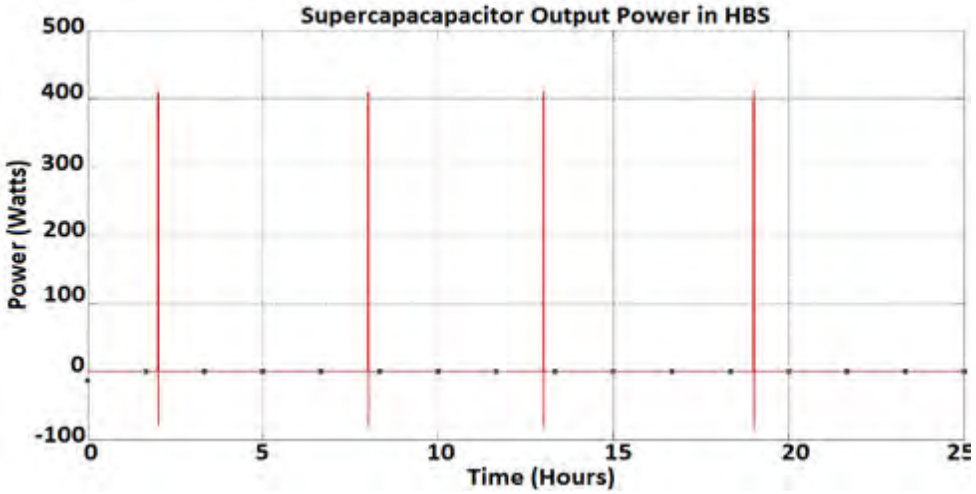

Figure 4.6 Power Output from Supercapacitor in HBS

Figure 4.6 shows that the supercapacitor effectively responds to the four disturbances mentioned in Table 4.2. The negative rectangular pulses shown in Figure 4.6 represent recharging of the supercapacitor. As mentioned in the recharging algorithm of section 3.8.3, recharging of the supercapacitor is restricted in order to maintain sufficient power supply. The ideal source-HBS supercapacitor result in Figure 4.6 shows the effectively implemented recharge restriction which ensures that there will not be any deficit in the energy supply to the load. Based on the power output responses of BSS and HBS in Figures 4.2 - 4.5 the following important observations are made:

- The HBS and BSS storage methods both adequately supply the average load through the use of the 18AH lead acid battery.
- A 100V constant ideal voltage source is used to supply the converters which effectively step the voltage up or down based on the charge algorithm instructions.
- Both BSS controller and HBS controller accurately instruct the storage devices to provide the necessary power during load power transitions.

- BSS shows slight discharge power shortages for load fluctuations responses at 13.5 and 17 hours due to the battery's low power density. This means that the power curve does not fully match the load during abrupt and rapid changes in power.
- The HBS battery does not respond to fluctuations since the supercapacitor discharge during high power density variations, thereby reducing the strain of rapid discharge on the battery.
- The HBS shows a higher power density when considering the zoomed in disturbance of Figure 4.5, since the additional supercapacitor used here is deployed to supply high power load fluctuations.
- The supercapacitor response in Figure 4.6 shows that the HBS charging algorithm successfully redistributes the high power load demands to the supercapacitor.
- The charging algorithm for HBS also allows for storage recharging but only after ensuring uninterrupted and adequate power supply to the load.

4.1.3 Results for Case 1: Security and Efficiency of Power Supplied

In this section, the security and efficiency of power supplied by the storage device is evaluated for Case 1. Security of power supplied is defined by the power difference measured by subtracting load from the supplied power. The power difference for Case 1 is displayed in Figure 4.7 for the BSS and Figure 4.8 for the HBS. Based on the power shortage figures, the average power difference is calculated using the average function in Microsoft Excel. After the average power difference is found, the efficiency of the supplied load is calculated. The efficiency considers the converter, controller and storage device losses in the output power curve.

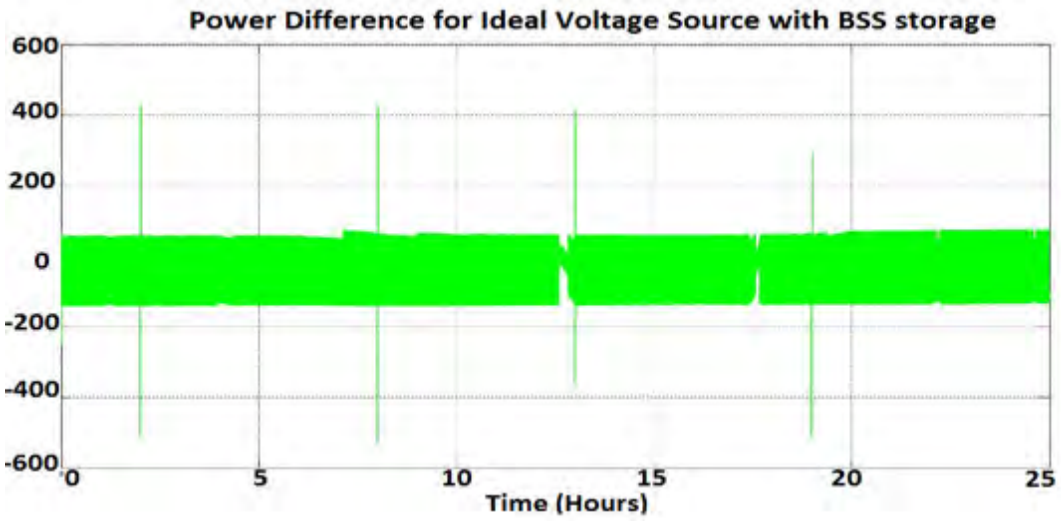

Figure 4.7 Difference between BSS Power Output and Load (Case 1a)

The power difference curve used in Figure 4.7 is calculated using the BSS power difference equation seen below:

$$P(t)_{BSS\ Power\ Difference} = P(t)_{Battery} - P(t)_{Load} \quad (4.1)$$

If the power difference is positive, it means that on average an excess power is supplied to the load, and if negative the average power supplied is lower than the average demand. Figure 4.7 shows power values which range from roughly 60W to -130W. This high power

ripple is due to the increased reliance on the battery during discharge. It is also increased by the switching losses taking place in the DC-DC converter. The power difference average calculated in Microsoft Excel is -50.23W, and can be validated by looking at centre of the trace in Figure 4.7. This means that Case 1a shows an average 50W shortage of power supplied to the 1.6kW rated load. Based on the average power difference and the average load demand shown in Table 4.1, average BSS supply efficiency can be calculated as follows:

$$Efficiency = \frac{P(t)_{\,Average\ Load} + P(t)_{\,BSS\ Shortage}}{P(t)_{\,Average\ Load}} \tag{4.2}$$

The efficiency of supplied power (in this case by the storage device) is given by Equation 4.2 using the power difference found in Equation 4.1. The average load value of 848W is taken from the load description in Table 4.1 and is used to calculate the efficiency of power supply. Overall supply efficiency for the BSS is 94.28%. Based on the electrical performance criteria established in section 4.4.1c the BSS power supply efficiency lies in the satisfactory region of 85 - 95%.

The power supply security and efficiency are now evaluated for the HBS, with important calculation distinctions and result improvements. The HBS power difference curve is shown in Figure 4.8 below, and calculated using Equation 4.3.

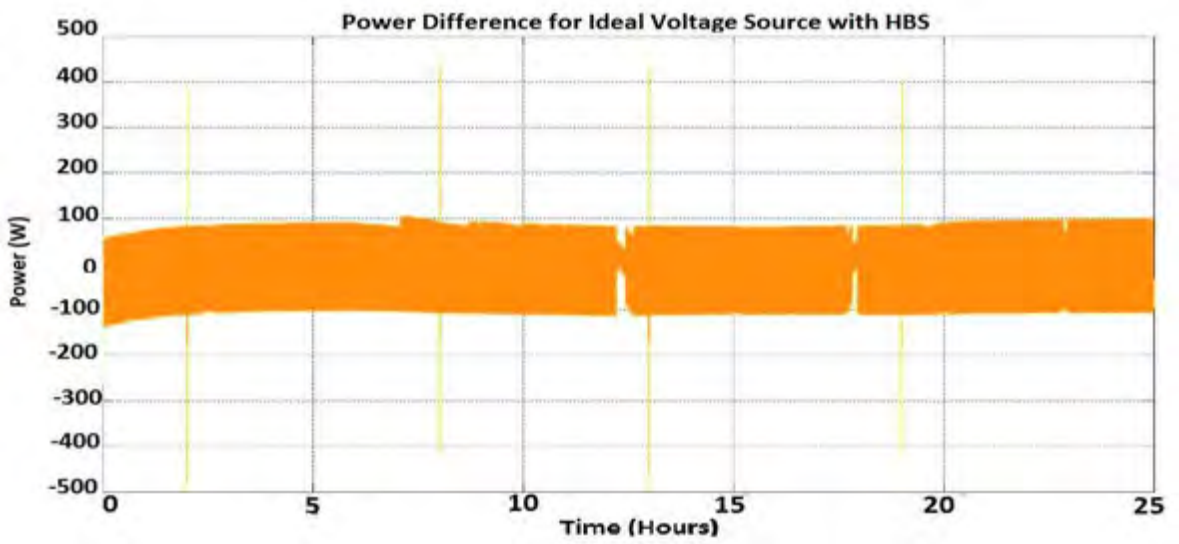

Figure 4.8 Difference between HBS Power Output and Load (Case 1b)

$$P(t)_{\,HBS\ Power\ Difference} = P(t)_{\,Battery} + P(t)_{\,Supercapacitor} - P(t)_{\,Load} \tag{4.3}$$

The key difference between Equation 4.1 and Equation 4.3 is the inclusion of supercapacitor power supply. The battery power in both storage schemes will be different as well since the load is allocated amongst two storage devices. In this case (Case 1b), the power difference stays within the region of 80W to -115W. The equation for calculating HBS supply efficiency is shown in Equation 4.4.

$$Efficiency = \frac{P(t)_{\,Average\ Load} - P(t)_{\,HBS\ Shortage}}{P(t)_{\,Average\ Load}} = \frac{848 - 42.6}{848} = -42.6W \tag{4.4}$$

Through Microsoft Excel the average power difference for HBS is calculated to be -42.6W for the 1.6kW rated load. Using the average load power of 848W the HBS supply efficiency of 94.98% is calculated using Equation 4.4. This efficiency of HBS power supply is slightly better than the BSS.

As mentioned in section 3.5.3, part II of Chapter 3, the software employed has computational limits when simulating the electrical model. Since a discrete sample time was implemented in the system, some the control responses required discrete controller blocks (refer to subsystems 2a and 2b in Chapter 3). These discrete control blocks cause a delay when feeding back the recorded power response in the simulation. The power difference block subtracted the supplied and load power the delay between power curves was seen in Figure 4.7. The high power rectangular impulses seen in Figure 4.7 for BSS and Figure 4.8 for HBS occur as a result of this time delay error. It should not be considered when measuring the effectiveness of storage device in this case [109]. This error is confirmed by the matched load curve in Figure 4.4, which shows that both storage systems accurately respond to the short term load disturbances in time. The storage power supply security and efficiency results are now interpreted in terms of electrical performance.

- Firstly, for both BSS and HBS an average ripple power is observed in their outputs due to the high switching frequency of the converter in constantly stepping the voltage up or down based on the charging algorithm.
- The power shortages observed are measured at -50.23W on average for the BSS curve and -42.6W for the HBS curve. This shortage in supply means that some load demand will need to be restricted at times of peak demand but majority of the priority average load is be supplied.
- The power security is increased when using the HBS (as compared to the BSS) since the strain on the battery during discharge is reduced through supercapacitor addition. This means the average power discharged by the HBS battery to the load will contain smaller ripples and can reach higher values when necessary.
- Furthermore, the efficiency of HBS power supply improves with respect to BSS as shown in Table 4.4 below:

Table 4.4 Power Supply Efficiency in HBS and BSS

Efficiency	Magnitude
BSS	94.08%
HBS	94.98 %
HBS % Increase	0.90 %

- Since the systems are tested on a small scale load, the voltage ripple error observed in the DC-DC converter can be alleviated by including a shunt capacitor in parallel with the output voltage before supplying the battery.
- However, this would result in additional capital cost which should be evaluated before implementation.
- In spite of output power ripple and minor reductions of power security with the power supply shortages, the electrical performance both storage systems are able to maintain a maximum power supply efficiency of over 94%, which is better than anticipated
- However, only 100% supply efficiency will maintain the load completely. This means that the storage device sizes could be increased, the power ripple could be

reduced through a supercapacitor, or an additional storage device can be included to maintain conditions supply in Case 1.

4.1.4 Storage Device Lifespan Extension

In section 4.1.4 the state of charge of each battery used is evaluated. The BSS uses the battery as the sole output power supply source. This means that it is responsible for responding to the average load in addition to the power fluctuations known as the secondary load. Through secondary load supply, the BSS battery is forced to undergo deep discharge cycles. However, HBS battery is protected from the secondary load responses thus shows an improve discharge profile compared to the BSS. The reduction of deep discharge response requirements results in a longer lasting battery which can be seen by an increased SOC. By comparing the SOC of both batteries for the duration of the 25-hour simulation the lifespan improvements of using HBS can be evaluated in the electrical performance analysis. From this SOC difference long-term lifespan improvements can be extrapolated. SOC plots which are generated in Figure 4.9 show the HBS battery SOC in black, and BSS battery SOC in blue. The SOC determines the amount of battery capacity variation for the duration of the simulation. It will increase when the battery is charging and decrease upon discharge.

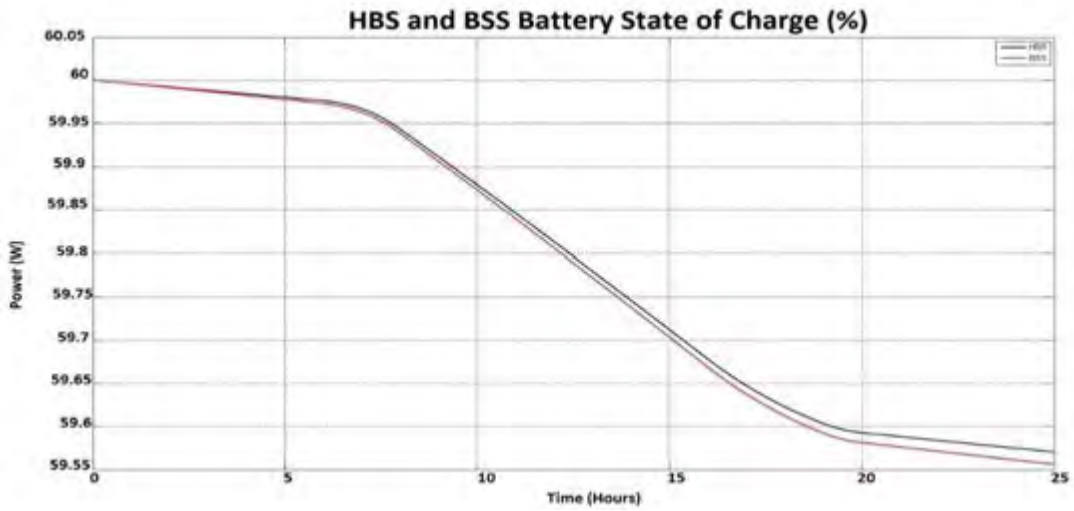

Figure 4.9 Comparison of SOC for Battery in BSS and HBS (Case 1)

SOC difference between batteries can serve as an indication of which battery will potentially last longer based on the discharge profile. In Figure 4.9, the HBS battery SOC plot in black shows a slightly higher SOC (about 0.02% higher) throughout the 25-hour simulation.

The SOC difference seen between the two batteries is now evaluated in the long term. Using the lead acid lifespan region of 3-12 years based on the collection of storage device literature reviewed an equivalent lifespan extension prediction table can be seen. The reduction in SOC due to the secondary load is accumulated per year in Table 4.5. Table 4.5 assumes that the secondary load is constant every day and neglects the primary load contribution since this is supplied by the battery in both storage strategies hence its contribution is cancelled out.

In Table 4.5 the contribution of deep discharge pulses is evaluated over a longer time frame. It compares the SOC that the BSS battery is losing by not using a supercapacitor thus only the secondary load SOC reduction is measured. The result in Table 4.5 shows that if both

HBS and BSS batteries supplied the same average load which does not affect their SOC, the secondary load SOC reduction in the BSS can cause it to reach failure five years before the HBS battery. Lead acid batteries are not recommended to operate under 40% SOC and will fail to operate once they reach an SOC of 25% [65], [98], [103], [119]. The extrapolated improvements of the HBS battery (due to the secondary load alleviation) compared to the BSS battery in terms of lifespan is now shown.

Table 4.5 Battery Lifespan Extrapolation

Time Frame	SOC reduction	BSS SOC	Battery Life
1 day	0.02 %	59.55 %	Running
1 month	0.60 %	58.95 %	Running
1 year	7.30 %	52.25 %	Running
2 year	14.60 %	44.95 %	Running
3 year	21.90 %	39.65 %	Barely Operable
4 year	29.20 %	30.35 %	Barely Operable
5 year	36.50 %	23.05 %	Failure

Table 4.5 shows that the supercapacitor addition in the HBS can extend its battery lifespan by at least 4 years before reaching failure. Based on the comparison of the SOC plots, the following observations are made:

- The HBS battery maintains a slightly higher SOC since the battery is discharged at a lower load only while the supercapacitor responds to secondary load disturbances
- Based on Figure 4.9 and Table 4.5, it can be concluded that the HBS battery will last slightly longer than the BSS battery as it does not undergo deep discharge cycles.
- The result in Figure 4.9 supports adding supercapacitors in RES with HBS due to frequent supply and load fluctuations experienced in these generation schemes.
- In Case 1, the load fluctuations are limited to four instances for supercapacitor evaluation but its contribution can be made more significant if additional disturbances were added to the load profile in Figure 4.1.
- The 0.02% increase is understandable since the simulation considers very short width rectangular disturbances.
- Additional disturbances, or longer periods of power disturbances would result in an increased SOC difference between BSS and HBS.
- The SOC variation is limited in both cases since the battery is largely oversized but the difference between HBS and BSS is still clear.
- If 0.02% SOC was accumulated onto the BSS battery, it would reach failure five years earlier than the HBS battery.
- The early BSS failure after five years does make conceptual sense, since the average lifespan of the lead acid battery ranges between 3 - 12 years.

4.2 Case 2: Solar PV Panel Generation Source

Case 2 considers a solar Photo Voltaic (PV) panel generation system tested with BSS (Case 2a) and HBS (Case 2b) storage. In Case 1 the objective was to establish the performance of the storage devices whilst simplifying input supply by using a constant ideal voltage source. Case 2 evaluates the storage devices in a more realistic way by considering intermittency of solar PV generation.

Solar PV brings forth changes in the electric charging profile in terms of the system control, converter operation, battery and supercapacitor operation when supplying the residential - commercial load. The controllers implemented must align with a varying supply and load by employing charge algorithms. This takes place by evaluating the input PV power generated, and then isolating potential noise. Storage devices must distinguish between PV power, resistive noise and intended supply disturbances which are included to model solar fluctuations such as shading and cloud cover mentioned in the PV generation factors of section 2.3.1 of Chapter 2, and modelled in section 3.9.2 of Chapter 3. The isolated primary (average) and secondary (rectangular pulse fluctuations) loads and supply power signals are distinguished using signal evaluation blocks in the controller. Once the supply and load signals and their accompanying disturbances are isolated, they are used as inputs to the charge algorithm. The charge algorithm decides how much power will be supplied by the PV panels and storage devices in combination to meet the load. Afterwards, the charge algorithm signal instructs the DC-DC converter(s) to accordingly regulate the voltage for storage device input. Based on the regulated voltage, the battery and supercapacitor are charged and discharged. The combination of generated PV power and storage device power is then supplied to the load.

By including additional variations in PV supply and the combination of storage and solar power for generation, Case 2 allows for a more realistic electrical performance analysis of not only storage but the solar RES collectively. The Case 2 results are presented in a similar format as Case 1 starting with the description of the basic operation of the simulation, and followed by different sets of results and their interpretation.

4.2.1 Basic Operation of Case 2 Simulation

a) Load Demand Details

The load demand details are the same as Case 1 (refer to section 4.1.1a).

b) Solar Power Generation Details

Solar PV panel generation details in this section are described based on the Matlab model which incorporates PV panel bank and solar irradiance profile explained in Chapter 3. The solar irradiance modelling data is shown in Table 4.6 below.

Table 4.6 Solar Irradiance Parameters for Electrical Performance Analysis

Simulation Parameter	Magnitude	Unit
Simulation Start time	0.0	Hours
Simulation End time	25.0	Hours
Average Solar Irradiance	876	W/m^2
Minimum Solar Irradiance	0	W/m^2
Maximum Solar Irradiance	3000	W/m^2

Based on the solar irradiance value recorded, a current is generated in the PV cell through a resistor [109]. The equivalent voltage is found across a 1 Ohm resistor used to convert

parameters across Simulink and SimScape block sets. The resultant solar power generation profile is shown in Figure 4.10.

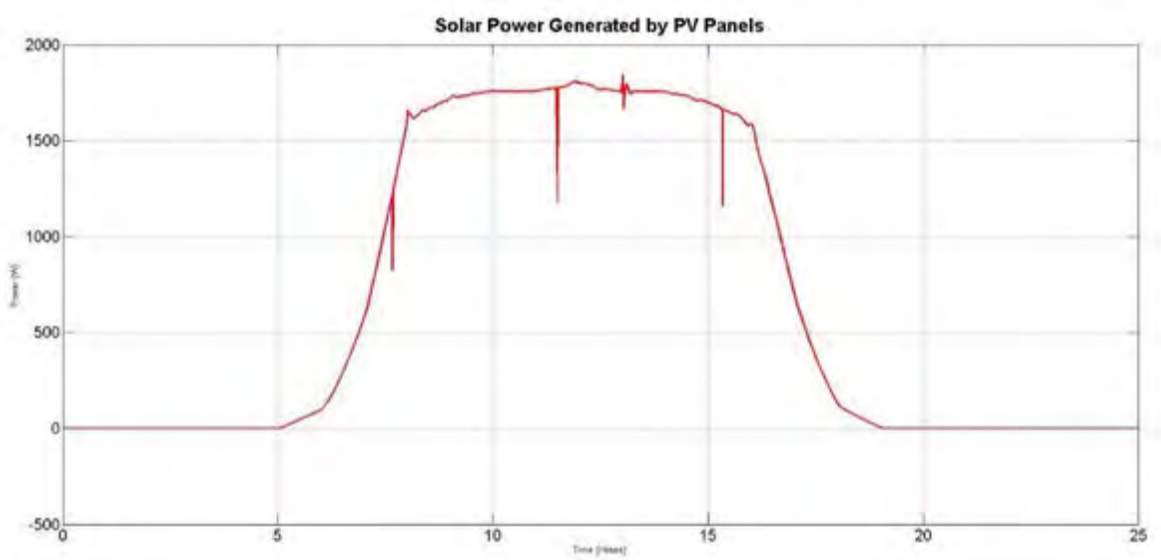

Figure 4.10 Solar Power Generated after Elimination of Resistive Noise

Based on Figure 4.10, the power generated in Case 2 is substantially different to the constant ideal voltage source of Case 1. No power is generated by the PV panels during late evening and morning hours. A progressive increase in power is seen after 5 hours, which roughly matches the commercial-residential load demand. At low generation hours of night time, the load is reduced which is ideal for the PV power profile. The off-peak generation problem is minimised but will still require alternative power supply. Storage devices are especially employed during the evening and descending hours of 16 - 20, when the load is high and the solar power begins to decline. Lastly, the storage devices are also required to supply the system during load disturbances (which result in high power spikes) or supply fluctuations (which are seen as generated power dips) as seen in Figure 4.1 and Figure 4.10.

The solar power generated has a more rounded curvature compared to the solar irradiance vector generated in Figure 3.24. This makes sense since the solar panel I-V generation curves are non-linear, thus will not directly reflect the solar irradiance values seen in Figure 3.24. The result in Figure 4.10 shows that, the controller model proposed improvements in section 3.5.2 has successfully filtered out fluctuating solar generation and resistive noise. This result simplifies simulation operation, results analysis and charge algorithms applied. Discharge cycle and disturbance response functions are now discussed.

c) Discharge Cycle and Disturbance Rejection

The PV charging algorithm considers the irregular load profile shown in Figure 4.1 and the fluctuating solar power generated by PV panels in Figure 4.10. The discharge profile in Case 2 determines the system efficiency and effective absorption of power. This is because the solar power generated exceeds the load required between the hours of 8 and 16 which is a substantial portion of the day. Effective energy absorption will reduce the wastage of excess solar energy, by properly scheduling the charging of storage during these hours.

Solar power generated is susceptible to reductions as discussed in section 2.3.1 of Chapter 2, due to shading, cloud cover and natural disturbances. The parameters of these disturbances as used in this study are listed in Table 4.7.

Table 4.7 Solar PV Generation Disturbance Parameters for Electrical Performance Analysis

Simulation Parameter		Magnitude	Unit
Fluctuation Width	Fluctuation 1, 2, 3	60	Seconds
Fluctuation Amplitude	Fluctuation 1	-400	Watts
	Fluctuation 2	-600	Watts
	Fluctuation 3	-500	Watts
Fluctuation Times	Fluctuation 1	7.986	Hours
	Fluctuation 2	11.97	Hours
	Fluctuation 3	15.97	Hours

Sudden disturbances in solar PV generation described in Table 4.7, are represented as sharp rectangular dips in solar power generation profile of Figure 4.10. Storage devices must provide fast discharge responses and re-stabilisation of the system at the times mentioned to cater for such power supply dips. The same justification can be made for the sharply rising rectangular pulses or spikes in the load profile which represent sudden load fluctuations (refer to section 4.1.1). Both supply and load disturbances are used to evaluate the effectiveness of using supercapacitor in the storage device. They also serve as means of testing the maximum BSS capabilities.

d) Electrical Performance Evaluation Criteria

The electrical performance of the solar PV RES using BSS and HBS devices, is evaluated under the same categories as Case 1 with additional observations included.

1. Load Matching

In Case 2, solar PV panel acts as the input voltage source and its generation is dependent on the available solar rays. Here, the load and supply must be aligned through storage, converters and the charging algorithm mentioned, in order to maintain an accurate power supply which would match the load profile. In this case, solar PV acts as the primary power supply source which means that PV power generated is used to supply the load and any energy deficit will be compensated for by the storage devices. Any excess solar energy from PV will be used to charge the storage devices accordingly. Matching the load under these conditions are far more challenging in terms of control algorithms described in section 3.7.4 for BSS and section 3.8.3 for HBS.

2. Security of Power Supplied and Total Supply Efficiency

Power security is expected to change substantially in Case 2 because of the load demand and solar power variations. In Case 2 the efficiency of the total system will be influenced by solar panel losses in addition to the component losses as included in Case 1.

Based on variations in solar power associated with irradiance conversion through polycrystalline PV panels, shading and dust build up, the ideal efficiency region is adjusted. A recent study conducted in [137], showed that for PV panels, electrical conversion efficiency can be reduced by up to 30% due to extreme shading and dust build up [137]. For this simulation variations of up to 10% is considered reasonable due to better environmental conditions which can cause fluctuations as shown in [40]. For Case 1, ideal efficiency for the RES with storage devices was set at 85 - 95% considering an ideal supply source. The ideal

efficiency intervals for Case 2 is however set in the range of 75 - 95% in order to compensate for PV power losses. It is important to note that the efficiency considered, is a reflection of the power supplied to fully meet the load. The ideal supply efficiency should be 100% for uninterrupted power supply. By evaluating the supply efficiency, recommendations on how to improve the system and therefore obtain 100% load supply can be made for all cases.

3. Storage Device Lifespan Extension

The lifespan extension of the HBS battery is evaluated by comparing the battery SOC in HBS and BSS for the reasons already explained in section 4.1.1. The battery SOC curve in Case 2 will follow a different trajectory to Case 1 since here it is used as a secondary power supply to the load. The battery discharges and charges depending on solar PV generation capacity and as guided by the controller. The difference between HBS and BSS battery SOC throughout this trajectory (and potentially after) determines the extent of potential lifespan improvement when using an HBS.

4.2.2 Results for Case 2: Load Matching

The load matching capability of the solar RES with BSS and HBS is evaluated in this section. In this case the total load (Figure 4.1) is supplied by the combination of power generated by PV (Figure 4.10) and the BSS battery. The BSS controller ensures that discharging and charging of the battery is based on the solar power availability. The BSS power curve is shown in Figure 4.11 below.

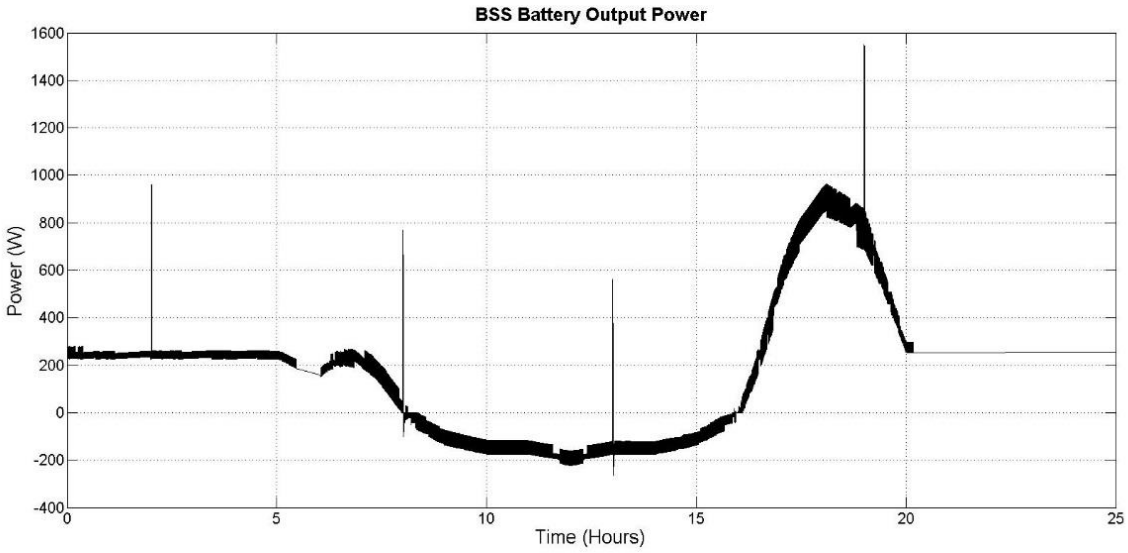

Figure 4.11 BSS battery Output Power Case 2a

The power delivered and absorbed by the BSS battery used in solar RES shows a substantial difference from Case 1a. The power dissipated is at 300W for the first five hours, after which it begins to decline and reaches negative values from 5.2 to 16.5 hours. This region represents the charging of the battery since solar power generated at this time is at its maximum as confirmed in Figure 4.10.

The sudden decline in solar power, can be seen between 16 to 20 hours in Figure 4.11. Additional storage power supply is necessary to maintain the residential peak power demanded by the load. The power generated by the BSS in Figure 4.11 shows an increase in power between 17 to 20 hours in order to compensate for solar power decline (in Figure 4.10) and supply the load demand during that time (in Figure 4.1). The BSS charging

algorithm successfully identifies low frequency fluctuations in solar power as seen in the evening a morning hours, from 16 to 5 hours in Figure 4.11 but filters out high frequency solar fluctuations to protect the BSS battery. The BSS battery has successfully supplied load disturbances because of charge algorithm restrictions, but does not respond to high power solar fluctuations.

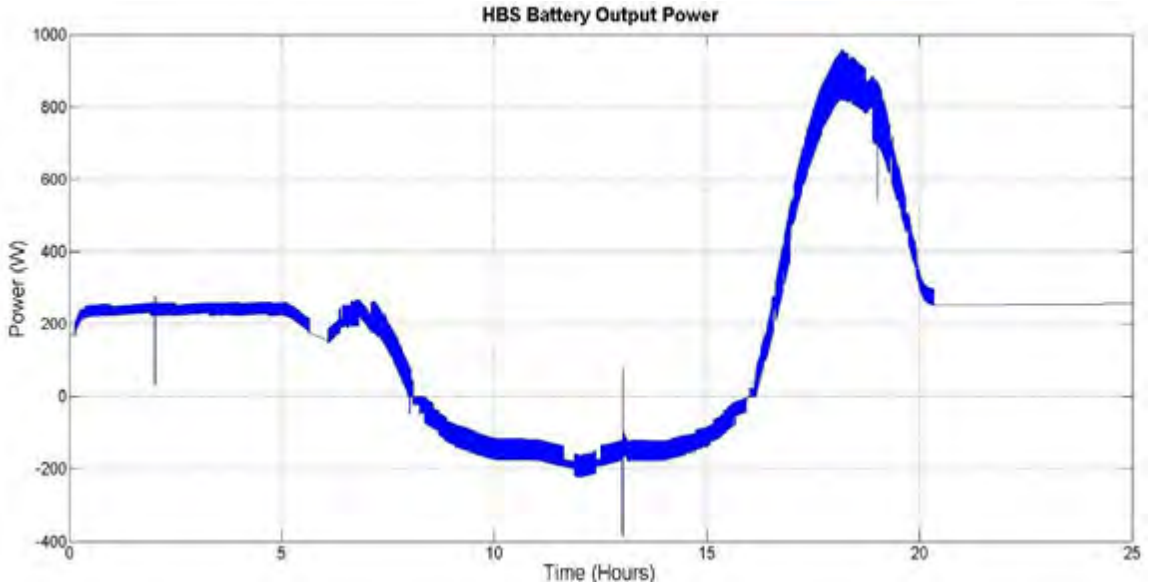

Figure 4.12 HBS battery Output Power for Case 2b

Figure 4.12 shows only the battery output power in Case 2b. This should not be confused with the total storage power which includes both the supercapacitor and battery for the solar RES with HBS. The battery power output in Figure 4.12 has a few minor differences when compared to the BSS in Figure 4.11. The HBS battery does not supply rectangular load pulses or respond to solar disturbances as they are allocated to the supercapacitor. Apart from the power impulse errors seen at 13.5 hours and attributed to a DC-DC converter error, the battery does not show any disturbance rejection discharges. Out of the seven rectangular impulse disturbances (three for solar and four for load) observed; only one error at 13.5 hours was found. The control charging algorithm and converter implementation is therefore deemed successful for the most part of the simulation.

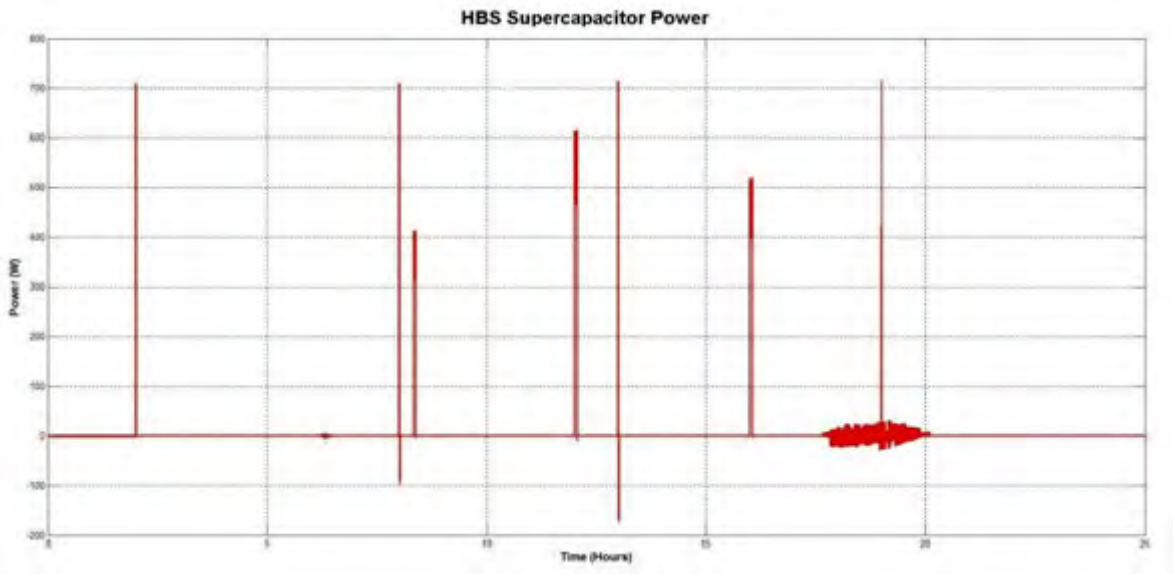

Figure 4.13 Solar-HBS Supercapacitor Power for Case 2b

Figure 4.13 shows the supercapacitor response to rectangular pulses representing both solar power dips and load demand peaks. The average load signal is successfully removed from the scope of supply of the supercapacitor. This means HBS discharge algorithm instruction and implementation is adequate in Case 2b (refer to section 3.8.4 for HBS charge algorithm).

The combined power supplied by the solar-HBS and solar-BSS is evaluated in terms of load matching, where the load is supplied by the combined generation capacity of the PV and the storage devices. For Case 2a, combined output power of solar PV and BSS is assessed in Figure 4.14.

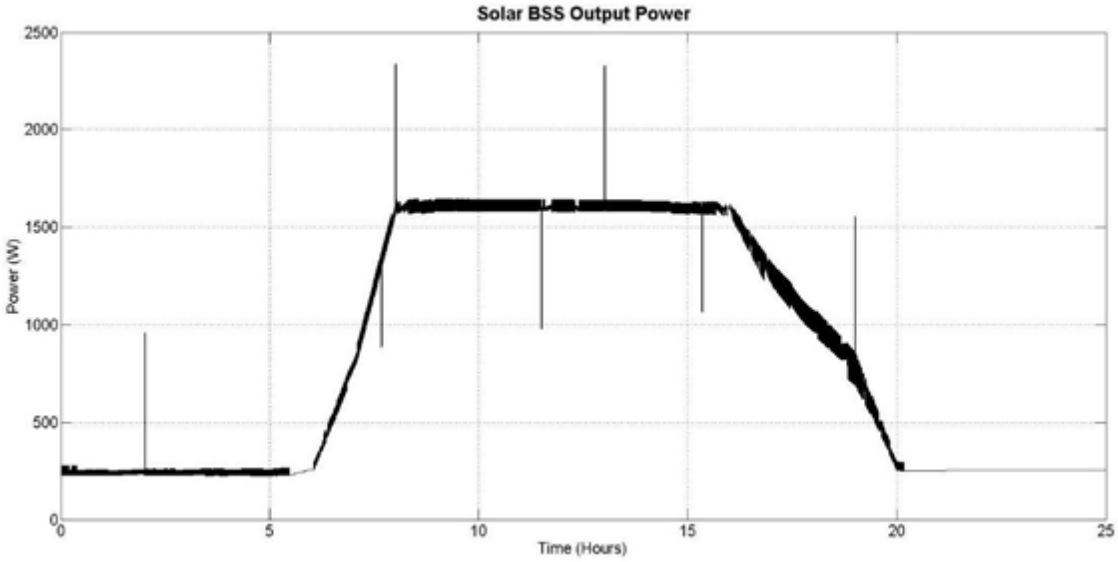

Figure 4.14 Combined Output Power of Solar PV and BSS (Case 2a)

Figure 4.14 shows that the combined output power of the solar panels and BSS does match the load profile described in Figure 4.1 for most of the simulation. Successful load matching is attributed to the efficient application of the control charging algorithm mentioned in section 3.8.3 as well as the model improvements proposed in section 3.5.2 of Chapter 3. The charging algorithm effectively tracked the solar power generated and load variations; it then instructed the DC-DC converter which regulated the battery voltage accordingly. This allowed the storage device to absorb excess solar energy at times of low power demand, therefore maximising the solar power usage. The BSS employed compensated for solar power shortages and increases in load demand by discharging when instructed. Model improvements led to minimal noise while comparing the total power signal to the actual solar power signal. This is because a first order control has been used to reject disturbances and therefore to separate high frequency disturbances and noise when necessary. All these improvements are especially for performance analysis of a stand-alone solar RES with BSS where there is no grid-connection to compensate for deficit in generation.

The BSS control system successfully detected load disturbances which allowed the battery to provide high power discharge pulses at the times described in Table 4.3. Unfortunately, the BSS control system failed to detect the solar supply fluctuations described in Table 4.7. This resulted in failure to compensate for the power dips in supply which are clearly visible in Figure 4.14. Further assessment of this profile will be conducted after the solar-HBS response has been presented in Figure 4.15 below.

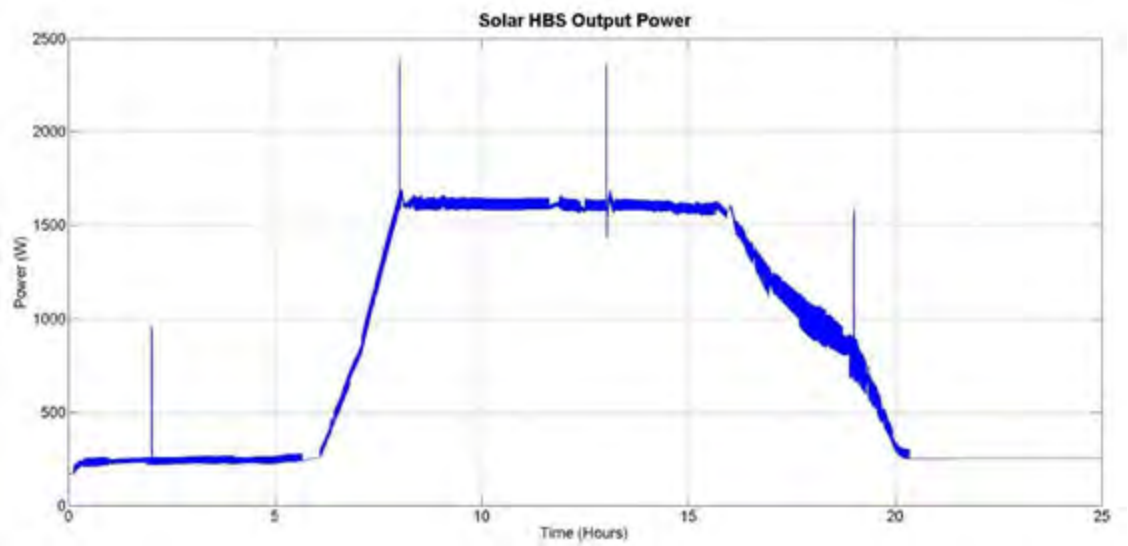

Figure 4.15 Combined Power Output of Solar PV and HBS Battery and Supercapacitor (Case 2b)

The combined output power supplied by solar PV and HBS storage is shown in Figure 4.15 for assessing load matching. The HBS uses two DC-DC converters because of the supercapacitor inclusion. This results in larger switching losses when compared to the BSS model. Despite the noisy switching losses, output power of solar-HBS completely matches the primary (average load) and secondary (disturbances) load demands. When comparing Figure 4.14 and Figure 4.15 it is clear that the HBS exhibits a better response than the BSS in terms of solar power disturbances. At roughly 8, 12 and 15.2 hours the solar BSS suffers from solar power dips which are not compensated for by storage. These power dips are not visible in the solar-HBS power because HBS charging algorithm successfully detected solar power shortages (at 8, 12 and 15.2 hours) and instructed the supercapacitor to compensate for them through fast power discharge This is resulted in a more balanced solar-HBS power profile which matches the load demand accurately.

The BSS compensates for load demand increases through battery discharge. The HBS supercapacitor compensates for load demand increases as well as solar power decreases which results in a much better load matching. This observation is made clear in Figure 4.16 which shows the output power profiles for the HBS, BSS and load demand on the same axes.

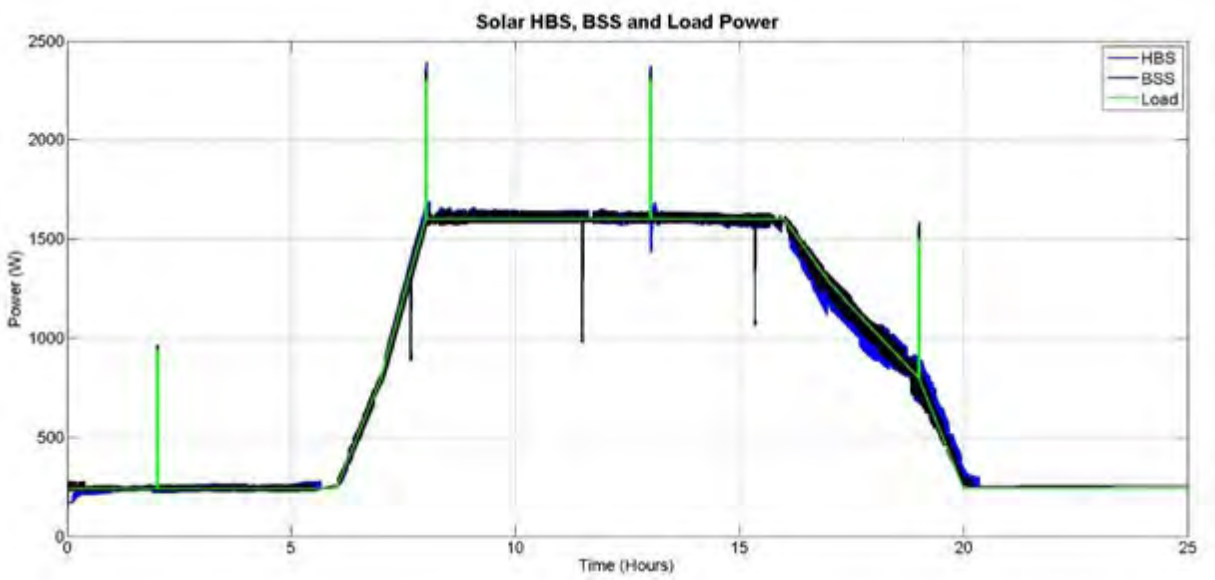

Figure 4.16 Solar-HBS, BSS and Load Power Comparison

Figure 4.16 shows total output power profile for the solar PV with BSS (Case 2a) and solar PV with HBS (Case 2b) with the load profile all plotted on the same axis with the colour code shown in the same figure. It is clear both systems successfully supply the average load in spite of switching losses and ripples.

The inability of the BSS in compensating for the power dips (caused by disturbances in solar power generation) is highlighted in Figure 4.16 at 8, 13.5 and 15.4 hours. The HBS supercapacitor compensated for these dangerous power dips at the expense of minor ripples shown between 16 to 20 hours but slight ripples are well worth the uninterrupted power supply and protection of components provided by the HBS.

Interpretation of Results

- PV power supply varies with the irradiance profile and is incapable of supplying the load on its own for the entire day.
- PV panels suffer from abrupt power dips caused by shading and cloud cover for the duration of the simulation. This must be compensated for in order to match the load effectively.
- Solar power generated is used to successfully charge the battery in the HBS and BSS through the charge algorithms presented in sections 3.7.4 and 3.8.3.
- The supercapacitor is successfully recharged but only for load fluctuations and not solar power disturbances. This is an observed limitation in the charge algorithm.
- Based on the solar-HBS and solar-BSS performance the key load matching criteria of both systems are tabulated below:

Table 4.8 Solar-HBS and Solar-BSS load matching performance

Load Matching Criteria	Case 2a - Solar-BSS	Case 2b - Solar-HBS
Average Load Supply	Yes	Yes
Load Fluctuations Peak Supply	Yes	Yes
Solar Disturbances Compensation	No	Yes

- Both solar-HBS and solar-BSS successfully supplied the average load demand which necessary for the duration of the simulation.

- The solar-HBS responded to all power peaks and dips observed which protects customer compost better than the BSS.

4.2.3 Results for Case 2: Security and Efficiency of Power Supplied

Security of power supply for Case 2 is presented in this section by evaluating the difference between the supplied power and load demand. This is followed by calculation of supply efficiency for both solar-BSS and solar-HBS as done in Case 1.

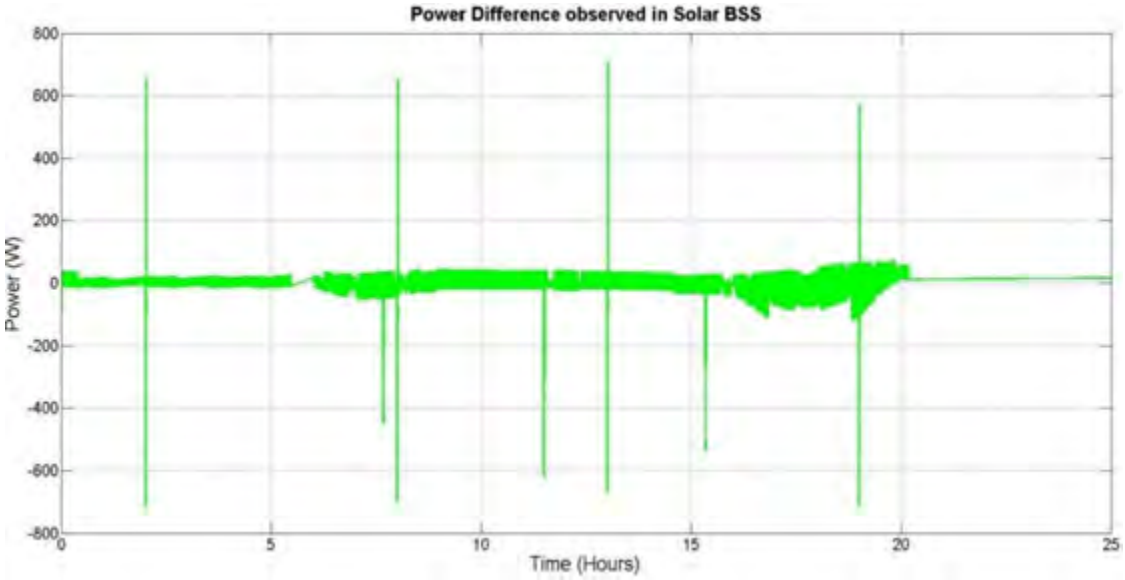

Figure 4.17 Difference between Solar-BSS Power Output and Load (Case 2a)

Figure 4.17 plots the difference between solar-BSS power output and the load demand according to Equation 4.5.

$$P(t)_{BSS\ Power\ Difference} = P(t)_{PV\ Panels} + P(t)_{Battery} - P(t)_{Load} \quad (4.5)$$

Figure 4.17 shows a small power ripple of between -20W to 15W. The difference in power due to solar power dips neglected by the BSS battery is included in Equations 4.6 - 4.8. As mentioned in the load matching results for Case 2a, the BSS fails to fully compensate for solar power disturbances. An additional solar disturbance power difference term is included in Equations 4.6 and 4.7 due to this.

$$E(t)_{Solar\ Dist} = [P(t)_{Disturbance\ 1} + P(t)_{Disturbance\ 2} + P(t)_{Disturbance\ 3}] \times T_{all\ dist} \quad (4.6)$$

$$= [-500 - 400 - 600] \times {}^{3}/_{60} = -75\ Wh$$

$$P(t)_{Disturbance\ difference} = \frac{E(t)_{Solar\ Disturbance}}{25\ hours} = -75/25 = -3\ W \quad (4.7)$$

The total power difference is now found by combining the solar disturbance and average load power differences measured in Equation 4.8.

$$P(t)_{Solar\ BSS\ Ave\ Difference} = P(t)_{Disturbances\ difference} + P(t)_{Average\ difference} \quad (4.8)$$

$$P(t)_{Solar\ BSS\ Ave\ Difference} = -3 - 3.48 = -6.48W$$

Despite the additional solar disturbance power difference, Case 2a showed an average total power difference of only -6.48W. The power security for the solar-HBS is now shown below:

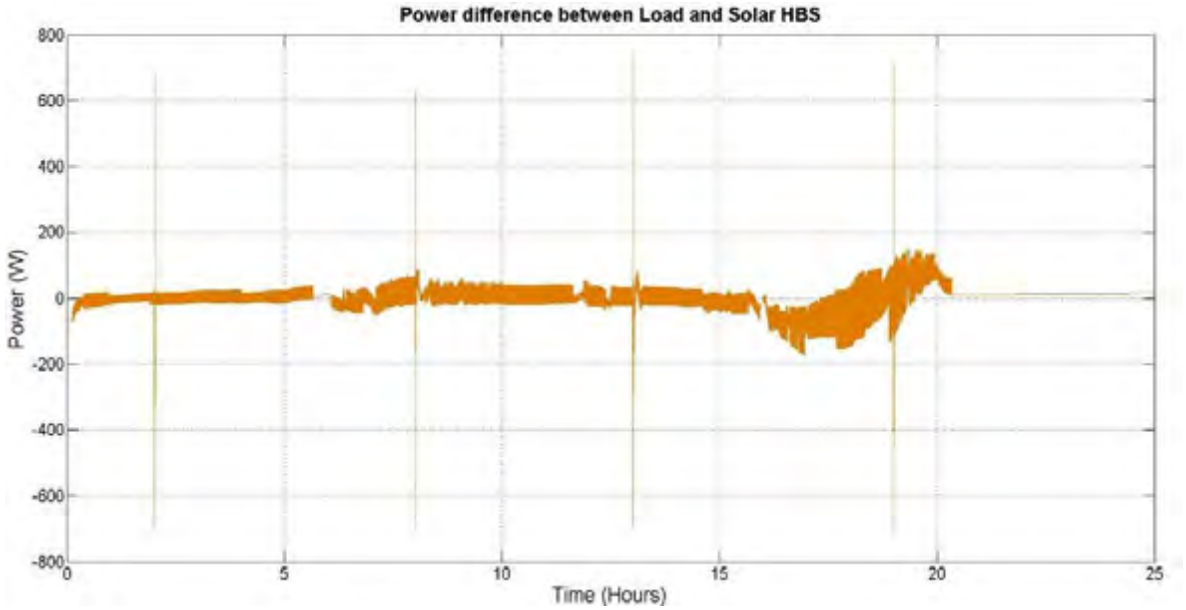

Figure 4.18 Power difference observed between the load and Solar-HBS

Solar-HBS power difference is calculated using the same method as Case 1b. Case 2b shows an average power difference of only -3.12W. This is very low which means the solar-HBS has a high power security. Based on the power differences calculated the supplied efficiency results are shown in Table 4.9 below.

Table 4.9 Power Supply Efficiency in Solar-HBS and BSS

Efficiency	Magnitude
BSS	99.24%
HBS	99.63%
HBS Percentage Increase	0.39 %

Solar-HBS shows an efficiency increase of 0.39% in Case 2. Both systems yield a supplied load efficiency of over 99% which surpassed the predicted 75 - 95% efficiency region. Case 2 shows impressive supplied load efficiency despite increased supply variations compared to the ideal Case 1. However, the system results still need to be improved through a more accurate storage device to reduce the ripple found and fully supply the load resulting in 100% efficiency.

- Case 2 simulated a more realistic test of power security by evaluating the difference in PV panel power supplied instead of a constant voltage source.
- Since PV power supply and load demand were both varying, the power security was expected to be lower in Case 2 compared to the ideal supply based Case 1.
- The power security was improved in Case 2 compared to Case 1, with the power difference curves showing smaller ripple bands with higher average amplitudes.
- The solar-HBS and BSS both recorded efficiencies of above 99% which is well above the accepted minimal region of 75% but should still be improved for uninterrupted power supply in the islanded RES.

- When PV panels and storage devices are responsible for supply, the power electronic DC-DC converter used, generates lower ripples since the storage devices are called upon (for discharge) less, this improves power security.
- An important result seen in Figures 4.17 and 4.18 is the effectiveness of charge algorithm instructions by the controller as well as the implementation by the converter and storage devices.
- Charge algorithm successfully allowed storage devices to be recharged by excess PV panel energy thus reducing wasted energy and maximising PV panel penetration to supplying the load and storage devices when possible.
- Storage devices are successfully compensated for the PV power during low irradiance availability which maintained electricity supply in the evening and morning hours.
- More importantly in terms of power security, the storage devices (battery and supercapacitor) recharge values were restricted to excess PV power only. Storage devices recharge was restricted to excess energy available. This restriction maintained the high power security of the solar-HBS and solar-BSS while minimising wasted energy.
- The observed performance of the Solar RES shows that islanded generation is indeed feasible in SA in terms of effectively matching the load with adequate security of power without connection from with the utility grid

4.2.4 Storage Device Lifespan Extension

Lifespan extension properties of the HBS are evaluated by comparing HBS and BSS battery SOC for the duration of the Case 2 simulation. The batteries initial SOC was set at 70% in Case 2. The SOC comparison of batteries is shown in Figure 4.19 below.

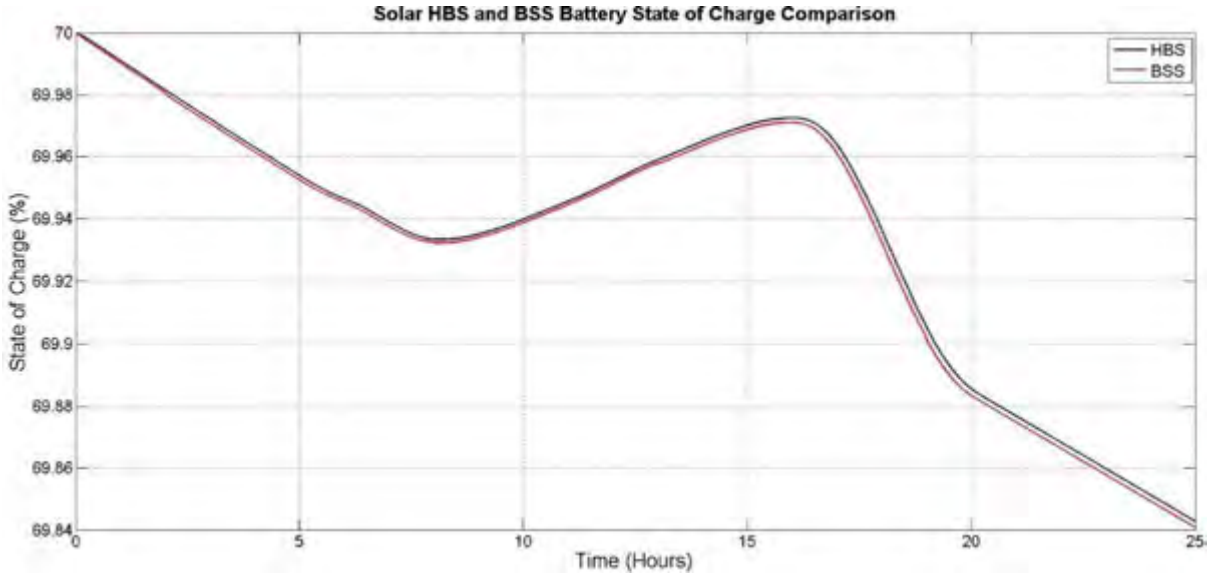

Figure 4.19 Solar-HBS and BSS Battery State of Charge Comparison

The first observation made for Figure 4.19 is fluctuation in the battery SOC curve. The battery is discharging in initial hours then recharging during times of excess solar power generation. The Average SOC for HBS battery is almost 0.01% higher than the BSS battery. The percentage difference in Case 1 is approximately 0.02% which is twice as much as Case 2.

In Table 4.5, Case 1 predicted that the BSS battery will reach failure due to the additional load after five years of secondary load supply. Using the same rate for Case 2 would mean the Case 2a BSS battery would reach failure in roughly eight to nine years [65], [98], [103], [119]. This value will be calculated in more detail during the case comparison in section 4.4.

The Case 2 percentage SOC difference between HBS and BSS is lower than in Case 1. This is because the supercapacitor power contribution in the Case 2a HBS progressively builds up over time when contributing to the battery cycle life. By using the storage devices less the SOC difference builds up slower. This is confirmed in Figure 4.19, after 13 hours the gap between SOC curves begins to grow due to the increase in load and supply variations. This result means the HBS contribution is more substantial in Case 1 than in Case 2.

- Case 2 uses storage devices as a secondary generation source which is reflected by the SOC curve in Figure 4.19.
- Battery SOC is decreased initially since it is being discharged to compensate for a lack of sunlight (and therefore PV power) in the morning operation hours.
- Battery SOC is increased during peak generation times since the PV panels charge the batteries with excess energy generated.
- Storage devices facilitate better utilization of solar energy by ensuring excess PV energy is not wasted. This is confirmed by increases in SOC seen in the middle of Figure 4.19.
- PV panels are incapable of maintaining supply without storage unless tremendously oversized or without utility grid connection which is not always possible.
- SOC difference of HBS and BSS batteries is reduced to 0.01% in Case 2 as storage devices are used less often than in Case 1.
- BSS battery is used less and therefore reaches failure only after nine years of secondary load responses as explained in section 4.2.1.
- The percentage SOC difference between HBS and BSS would increase if the BSS battery responded to the solar power dips as intended.
- Smaller storage devices are recommended for a clear SOC comparisons in future work.

4.3 Case 3: Wind Energy Conversion System with PMSG

The results for Case 3 involving the wind energy conversion system (WECS) and storage are presented in this section. In this case the WECS operates using a Permanent Magnet Synchronous Generator (PMSG) and is modelled with a BSS (Case 3a) and a HBS (Case 3b). The layout of results and its interpretation will follow the same format as the previous cases considered.

4.3.1 Basic Operation of Case 3 Simulation

a) Load Demand Details

The load demand details for this case remains the same (refer to section 4.1.1).

b) Wind Turbine Power Supply

The WECS is modelled in Matlab and uses data collected from WASA to provide accurate local wind speed input data [44]. The wind speed profile generated is used to drive the WECS which then converts the AC power generated into a DC equivalent through a 3-phase inverter. The equivalent DC power generated by the WECS is shown in Figure 4.20 to supply the DC load power demand.

After two hours, the WECS reaches its maximum power of 1280W then steadily declines to an average power of 1200W in Figure 4.20. The system generates a relatively constant power compared to the solar profile but does require additional storage compensation to meet peak load demand, load disturbances and fluctuations and load supply during WECS start-up phase.

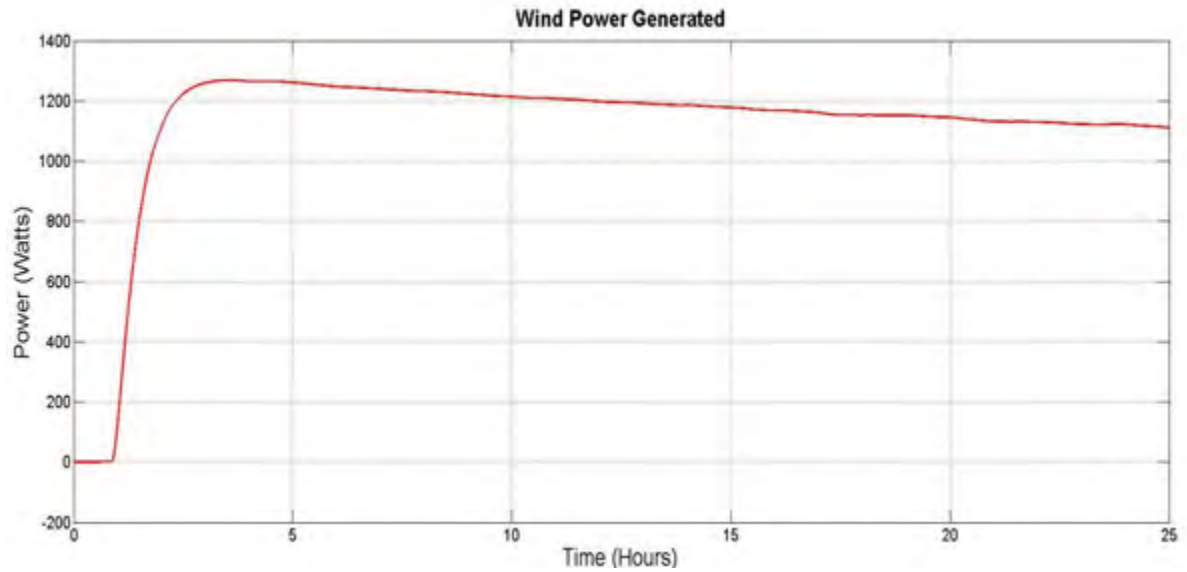

Figure 4.20 Wind PMSG Output Power Generated

c) Discharge Cycle and Disturbance Rejection

Case 3 includes the same load power disturbances seen in previous cases and subsequently requires storage device discharge in order to effectively meet the load demand. The fundamental difference in Case 3 is that the WECS generates AC power, which poses potential computational problems when using the DC equivalent control charging algorithm. The charging algorithm makes use of the DC converted wind power value as its supply input (Figure 4.20) but this method may overlook the contribution of reactive power imbalances.

The effectiveness of the designed charging and control algorithm mentioned in section 3.8.3 and 3.9.4 are evaluated based on the control power instructions to storage devices, the implemented storage devices output power and the total power supplied.

d) Electrical Performance Evaluation Criteria

1. Load Matching

Case 3 shows a relatively constant WECS power profile in Figure 4.20. In Case 2 the solar power made use of storage devices at low irradiance hours of the morning and evenings but provided excess solar energy during the daytime. The WECS has a converse load matching challenge since the storage devices are now mostly employed during daytime hours. This is when the wind power supply (of an average 1200W) is below the peak 1600W load demand. In both cases the storage devices are essential to matching the load demand. Load matching accuracy is evaluated using the same procedure as Case 2 (refer to section 4.2.1 -part d).

2. Security of Power Supplied and Total Supply Efficiency

Results for security and efficient of overall supply from wind RES with storage are evaluated by following the same procedure used in Case 2 (refer to section 4.2.1 part d)

3. Storage Device Lifespan Extension

Lifespan extension and SOC evaluation follows the same procedure as Case 2 (refer to section 4.2.1). Battery discharge for the WECS follows a different SOC curve to the Case 2 but the average difference in SOC is still being used to observe lifespan extension changes.

4.3.2 Results for Case 3: Load Matching

The load matching properties for the wind BSS and HBS are now compared in this section. The output power from BSS battery while it is supplying the load (discharging) and absorbing excess energy (charging) is shown in Figure 4.21. In Case 3a the load supply compensation refers to when the BSS battery is used to discharge in order to meet the load demand at times of low wind power generation. On the contrary, excess energy absorption for BSS refers to when the BSS battery is charged by absorbing excess wind energy generated after the load power demand is met.

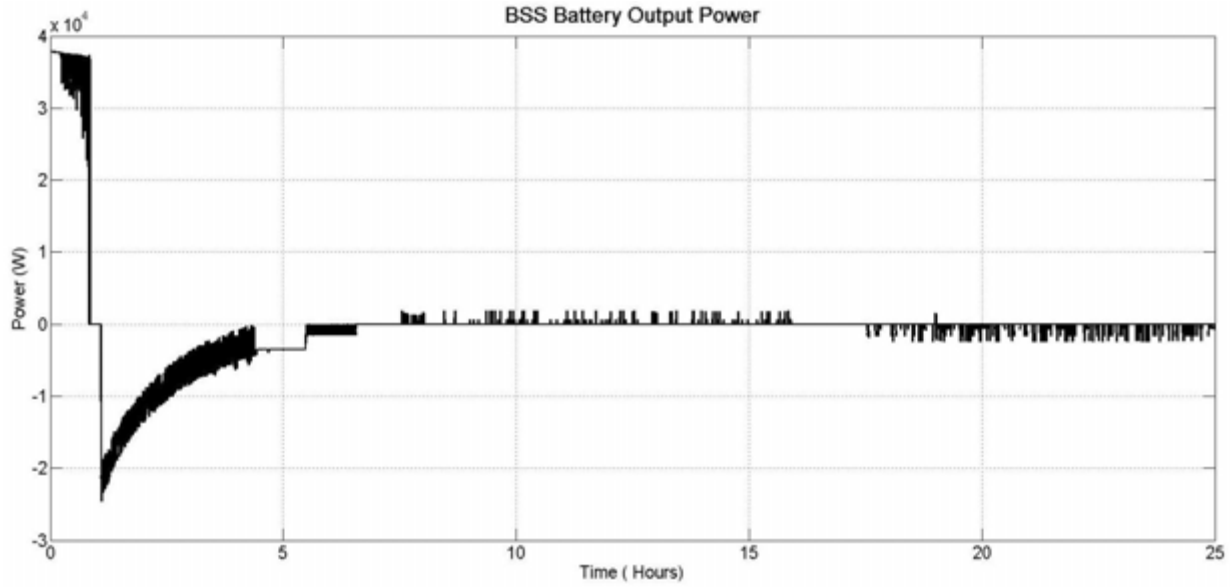

Figure 4.21 BSS Battery Power Output (Case 3a)

During the initial WECS start-up phase seen in Figure 4.21, the BSS battery attempts to supply the load power but unfortunately discharges at a dangerously high value of almost 40kW. This error is due to the DC control charge algorithm which fails to effectively restrict the initial battery discharge value. The Hysteresis block used in the algorithm does not detect the large reactive power deficit when using DC power values hence the battery discharges this 40kW excess power error when only 240W is demanded by the load at this time. This error takes place in the first hour of the storage profile but the system only manages to recover two and a half hours later at roughly 3.5 hours. From four hours onwards the load is once again met by the supplied power.

The battery discharge error compromises the power stability of the wind-BSS in Case 3a. Power stability, refers to an electrical power system's ability of regaining state of operating equilibrium after being subjected to a physical disturbance so that most of the system parameters can remain bounded and operable [138]. Fortunately, the DC charge algorithm successfully instructs the BSS battery once the system has recovered from the initial discharge error (after four hours). Once the WECS power generated reaches its settled maximum value of 1200W (at six hours), the BSS can successfully discharge as instructed by the DC algorithm.

After six hours of simulation, the BSS battery shows minor switching losses which can be seen by the fluctuating battery power in Figure 4.21. This is due to switching losses uncovered by the DC-DC converter. Despite these losses, the average battery power after six hours still roughly matches the required load power needed to ensure load matching. The HBS battery performance is now shown in Figure 4.22 followed by the HBS supercapacitor power profile in Figure 4.23.

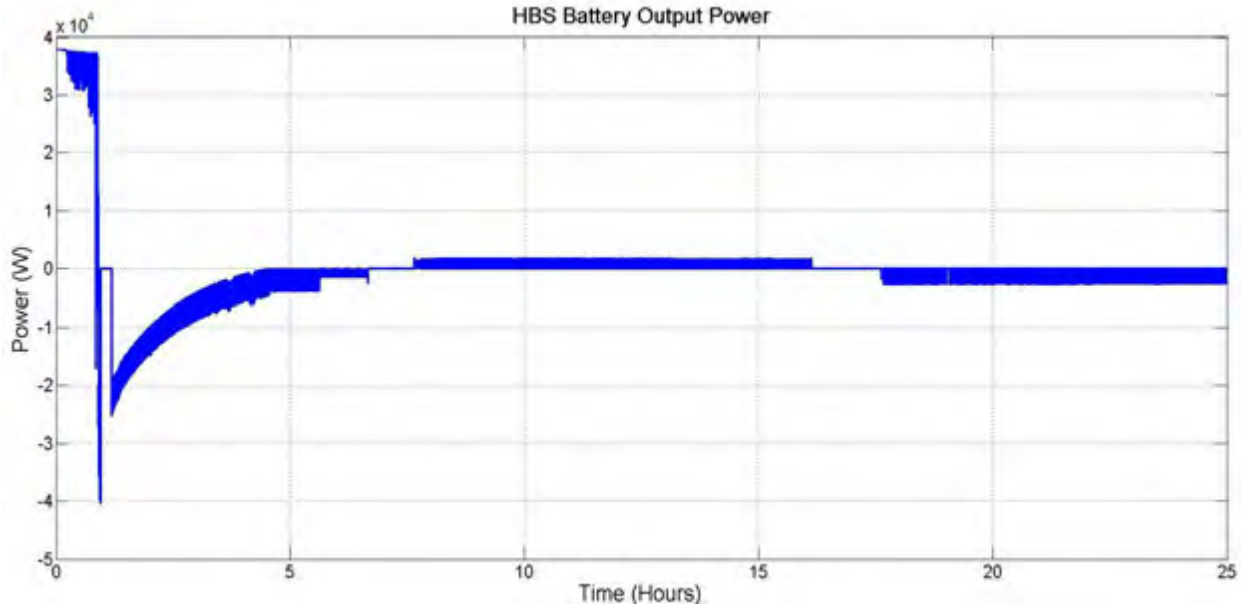

Figure 4.22 HBS Battery Power Output (Case 3b)

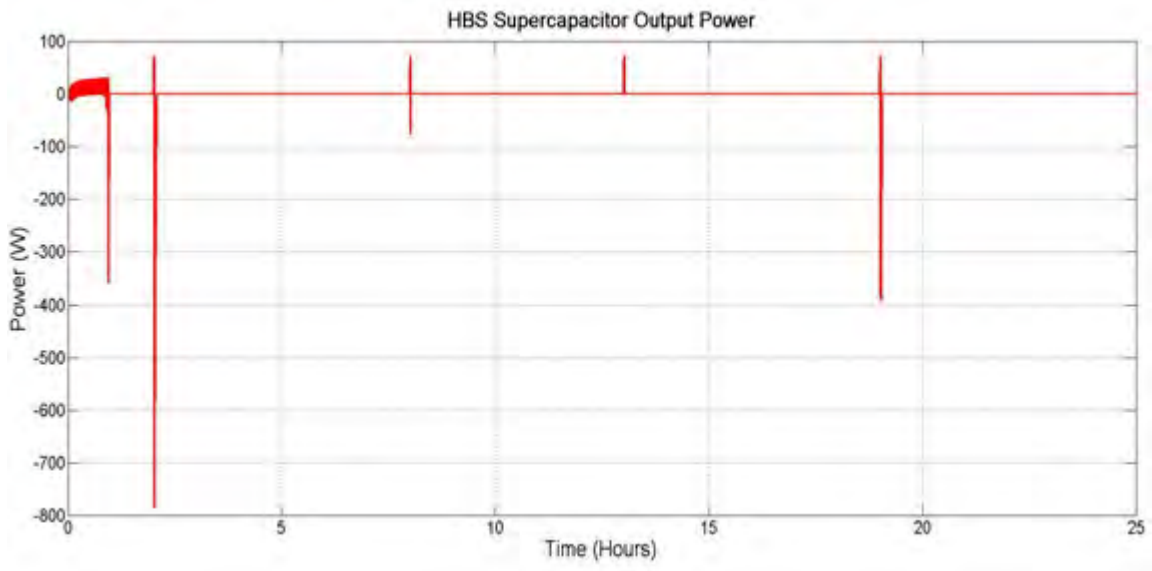

Figure 4.23 HBS Supercapacitor Power Output (Case 3b)

HBS battery power output seen in Figure 4.22 contains the initial battery discharge error in its power supply curve. This is due to the DC charging strategy used in the HBS design. In Figure 4.23, the supercapacitor power output curve exhibits accurate charge and discharge responses to majority of the load disturbances experienced in Figure 4.1. The supercapacitor power profile shows that the initial load was supplied to the supercapacitor for the first two hours in Figure 4.23 (during WECS start-up). The load was then successfully matched by the HBS supercapacitor in this initial stage but the HBS battery still showed the same high power 40kW dangerous discharge error in Figure 4.22 as in the BSS power profile. This HBS battery discharge error then compromises the HBS supercapacitor disturbance response at three hours in Figure 4.23 by absorbing too much power during its recharging phase. Power stability of the system is once again comprised but manages to settle after 6 hours in the wind-HBS Case 3b. The WECS supply is constant in terms of its DC equivalent power generated by six hours. After six hours the power stability is reached in both cases but the wind-HBS shows a more consistent discharge profile compared to the BSS in Figure 4.21.

Each WECS case has shortcomings in terms of load matching during WECS start-up. Overall performance of both systems is now compared by showing the load power demand, wind-HBS total power supplied and wind-BSS total power supplied on the same axes in Figure 4.24.

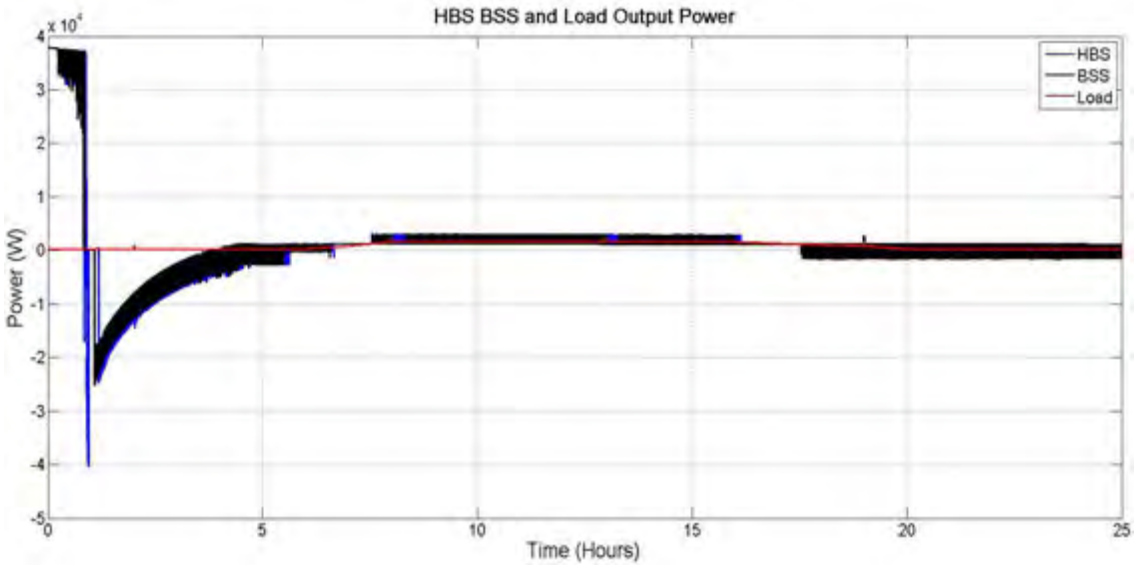

Figure 4.24 Wind-HBS, Wind-BSS and Load Power for load matching of Cases 3a and 3b

The combination of the WECS power, HBS supercapacitor and HBS battery power is shown in Figure 4.24 in order to present the load matching performance result of the wind-HBS plotted in blue. The combined WECS power and BSS battery power is shown in black for the same load matching performance evaluation on the same axes.

Figure 4.24 confirms the initial power stability errors seen in both WECS storage designs used in Case 3. The result shows that the wind-HBS and wind-BSS successfully supply the required load demand once the WECS constant power phase is reached at six hours. Both storage systems fall victim to switching losses due the AC-DC WECS rectifier and the DC-DC storage devices converters used. The HBS is a more consistent (does not fall to zero as often) supply which can be seen by the blue background points at 8, 13 and 16 hours in Figure 4.24. In general, Case 3a and Case 3b both fail to match the load in the start-up phase and roughly matches the load in the constant WECS power phase (after seven hours of simulation). The constant power phase (of 6-25 hours) is still operable since the supplied power is above load demand, but the accuracy of power supplied remains low because of the DC charging algorithm which is applied onto the AC WECS generating system. The following observations are made based on the results considered in Figure 4.21-4.24.

- The wind PMSG power supplied progressively increases to reach a constant 1200W. This is an ideal value for load matching assessment since the load is at 1600W at maximum meaning the storage devices contribution are essential to maintain supply.
- BSS battery successfully responds to load fluctuations but does exhibit a large power spike during the initial WECS start-up phase.
- BSS is responsible for load and supply start-up disturbances in Case 3a, while the supercapacitor responds to these disturbances in the wind-HBS of Case 3b. This shows the successful isolation of the average load demand in the wind-HBS.
- Failure to comply with the charge algorithm is due to oversized storage devices and a lack of protection considerations being implemented in the DC charge algorithm.
- Reactive power effects are not seen by the DC charging algorithm for Cases 3a and 3b [139]–[141]. This result in storage device discharge errors in the start-up phase (first seven hours) and the positive battery discharge phase (between 8-16 hours).

- HBS battery delivers the same initial discharge error seen in the BSS battery discharge profile. A different charging algorithm in section 3.9.4 is used in the wind-HBS but still makes use of an equivalent DC WECS power value for its input signal.
- HBS supercapacitor successfully responds to all load fluctuations once power stability has been established. This means that the DC charging algorithm is more successful once the WECS power becomes constant.
- Wind-HBS shows a more regulated power supply compared to the wind-BSS as confirmed by Figure 4.24.
- Both WECS supply adequate power after stabilisation but the load is still not accurately matched in either case. This is because of the inferior DC charging algorithm. By using the DC charge algorithm the system includes additional DC-DC converters for storage device interfacing after the AC-DC WECS rectification takes place. This means the current ripple found in the AC-DC WECS is amplified in the DC-DC converter. Resulting in switching losses by the storage device as the power jumps from its maximum point to zero as seen in Figure 4.24.
- A 3-phase AC charging algorithm is suggested for future designs which will consider the reactive and active power contributions from the WECS.

4.3.3 Results for Case 3: Security and Efficiency of Power Supplied

The power security and efficiency of the wind-BSS and wind-HBS are now evaluated following the same procedure as Case 2. The power difference for the wind-BSS and wind-HBS is now presented in Figure 4.25 and Figure 4.26 below.

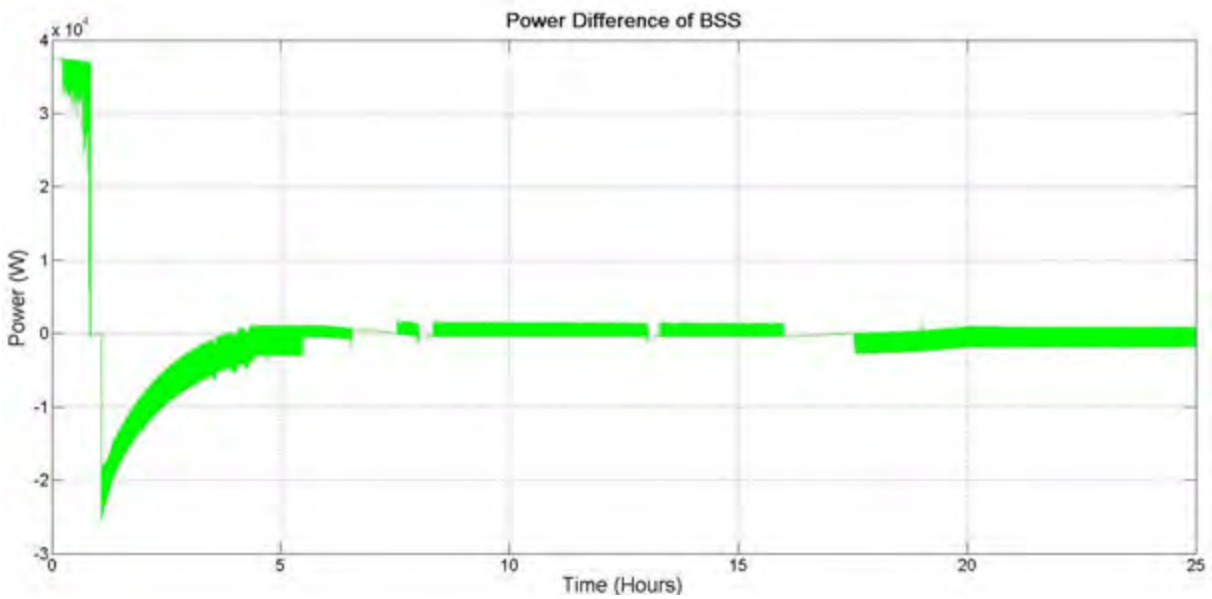

Figure 4.25 Wind BSS Supply Power Difference Compared to the Load for Case 3a

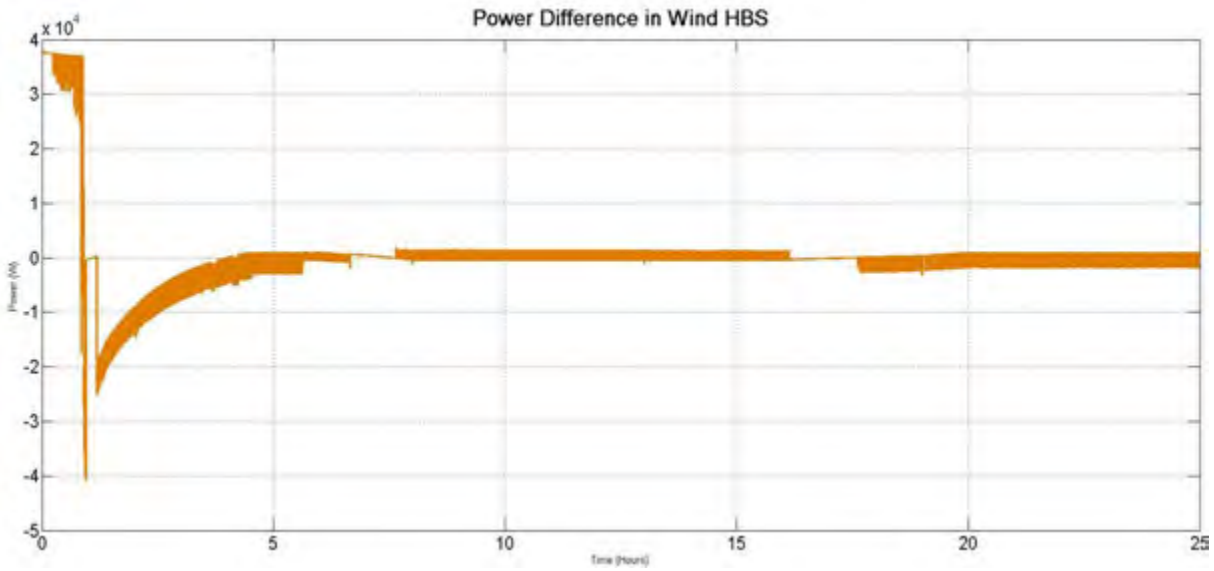

Figure 4.26 Wind HBS Supply Power Difference Compared to the Load for Case 3b

The power difference average values were calculated in Microsoft Excel based on Equations 4.4 and 4.5. The new power difference equations for Cases 3a and 3b are now given below:

$$P(t)_{BSS\ Power\ Difference} = P(t)_{WECS} + P(t)_{Battery} - P(t)_{Load} \quad (4.9)$$

$$P(t)_{HBS\ Power\ Difference} = P(t)_{WECS} + P(t)_{Battery} + P(t)_{SC} - P(t)_{Load} \quad (4.10)$$

Since the initial discharge error by the HBS and BSS battery sets the power security average value out of proportion, the average power security was calculated once the system reached power stability. This calculation took place for the period of 6-25 hours. Average power security values found are now shown in Table 4.10 below:

Table 4.10 Average Power Difference for Case 3a and Case 3b Wind RES with storage

Power Difference	Time Period	Average Load Power	Case 3a - Wind BSS	Case 3b - Wind HBS
Unstable Region	0 - 6 Hours	240 W	22.88 W	32.95 W
Full Sim Region	0 - 25 Hours	**848 W**	**-101.82 W**	**-92.83 W**
Stable Power Region	6 - 25 Hours	**1040 W**	**-204.09 W**	**-202.62 W**

Table 4.10 confirms the inaccuracy of the full simulation region based on the power difference average values found. When calculating the average power difference over the entire simulation region the power supplied is subtracted from the load demand. By including the battery discharge error of 40kW for a full hour, the power supply value increases excessively. The increased power supply value results in an inaccurate increased power difference value which makes the system look more secure than it actually is. The new power difference value is therefore measured over the stable region using a new average load value and results in a power difference value which more accurately represents the designed WECS capabilities. The more reliable results showed a power difference of 204.9W for Case 3a and 202.62W for Case 3b. These values are much higher than in the previous cases. It is worth noting that the average load for this interval will change and therefor contribute to the

higher power differences measured. The new power difference values are then used to calculate the supplied load efficiency using Equation 4.2 for the wind-BSS and Equation 4.3 for the wind-HBS. For a more clear evaluation of the system the respective power supply efficiency values of the Case 3a and Case 3b systems are now shown in Table 4.11.

Table 4.11 Wind RES supply Efficiency of Case 3a and Case3b

Efficiency	Time Period	Case 3a - Wind BSS	Case 3b - Wind HBS
Unstable Region	0 - 6 Hours	109.54%	113.73 %
Full Simulation Region	0 - 25 Hours	87.37 %	88.49 %
Stable Power Region	6 - 25 Hours	80.37 %	80.52 %

Table 4.11 shows the efficiency of power supplied in Case 3a and 3b, based on the average load demand and power difference values of each region tested. The full region shows an 87-88% efficiency value but when the accurate stable power region is calculated, the power supply efficiency values is reduced to 80%. Efficiency results show that the WECS has a substantial deficit in supplied power because of the increase in switching losses since additional AC-DC converters are used for wind power rectification as well as the implementation of the DC charging algorithm despite its reactive power measuring limitations. Based on the power difference and power supply efficiency results obtained the following results observations are made:

- The battery discharge error initially found has led to a disproportioned power security measurement value. The unstable power region shows power differences which are not practical based on the current simulation as seen in Table 4.10. As a result, power difference was measured across the stable power region to find a more accurate power security measurement. Within the stable power region the wind BSS showed a 204W power difference and the wind HBS showed a 202W difference in supply and load demand
- The contribution of the wind-HBS supercapacitor is seen through a 2W power difference increase. This is similar to the 3W increase seen in solar-HBS Case 2b
- Using the power difference value mentioned and the load average value, the security of power supplied for the full simulation is calculated with Equation 4.9
- The efficiency was calculated across the stable power region (6-25 hours) as the unstable region (0-6 hours) showed efficiency readings of over 100% in Table 4.11
- A new supply region meant the average load value was increased 848W to 1040W in the stable power region
- This provided some explanation as to why the power difference was so much higher in Case 3 than in previous cases
- System load supply efficiency of HBS and BSS is roughly 80% each in the stable power region which is much lower than Case 1 and 2
- Case 3 suffers in terms of power security because of the simplified DC charge algorithm used. Storage device power curves roughly match the required power during the stable regions but still contain far too many fluctuations as seen by the power dips to zero in Figure 4.24
- Since the DC control algorithm could not accurately track the storage device power required, the battery voltages fluctuated constantly and resulted in the converter often switching storage devices on and off

- This constant switching is because of the sinusoidal current which is still apparent in the WECS power supply despite the use of the three phase rectifier. This is due to the current ripple which is still observed after conversion. This problem can be mitigated by increasing the switching frequency, including a shunt DC capacitor
- The storage devices fall victim to high switching losses which results in a lower average discharge power output value. This brings forth an increased power difference value since supplied power is reduced
- A more applicable three phase charging algorithm is recommended for WECS simulation. This will reduce the need for an additional DC-DC voltage converter since the controller will be based on the rectifier already implemented
- The three phase charge method will also reduce the power dips to zero observed by reducing power ripple
- A new charging algorithm will also allow for more advanced storage interfacing such as the infection of active power during fluctuations in supply when reactive power is observed
- This system may be more applicable to AC loads but can implemented in the current simulation as well
- The power dips observed were substantially reduced by load allocation in the wind-HBS but it can the removal of the seconds DC-DC converter and a more specified control algorithm will still result in improvements in Case 3b
- In addition, the AC - DC rectifier used for WECS power must reduce the current ripple found which can minimise storage and converter switching losses.
- Protection circuits and a more accurate power limiting strategy should be used for the battery to prevent excessive discharge errors

4.3.4 Storage Device Lifespan Extension

The lifespan extension of the battery in wind-BSS and wind-HBS systems in Case 3 are once again evaluated using the SOC performance of the batteries. Figure 4.27 shows the SOC curves of the BSS and HBS over the entire simulation.

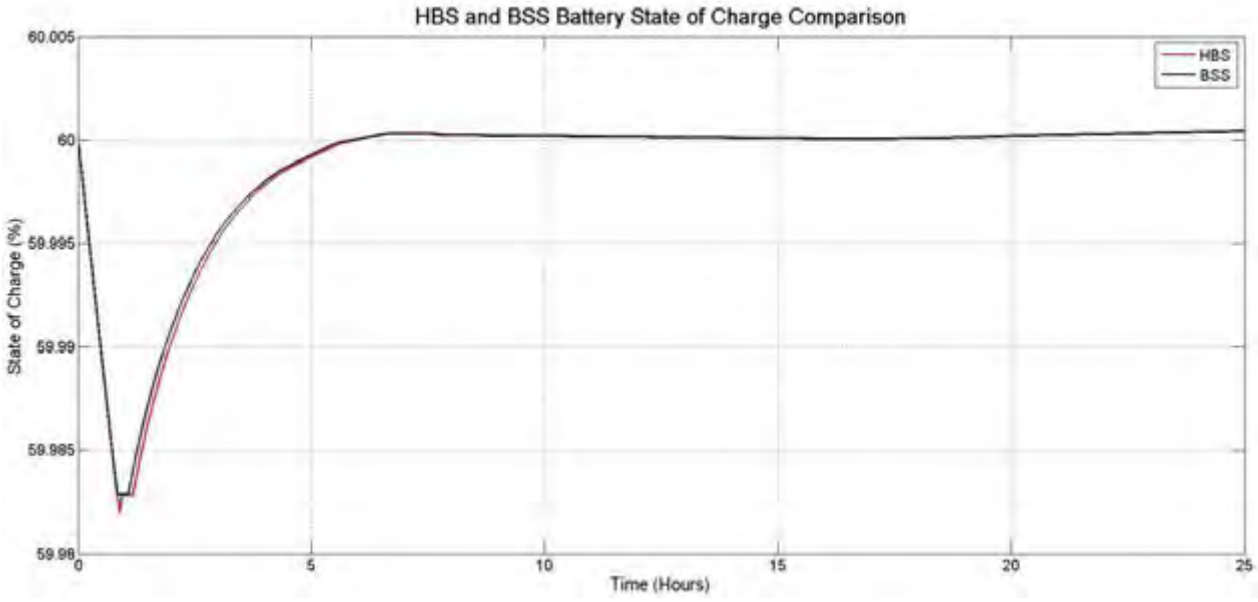

Figure 4.27 HBS and BSS Battery State of Charge Comparison for Wind PMSG in Case 3

Figure 4.27 clearly illustrates the significance of the initial battery discharge error pulse observed. The batteries were protected from damage during the dangerous discharge error because they were oversized to a large extent. Oversized batteries meant that a large discharge did not cause a major dip in SOC known as a deep discharge cycle. Batteries were oversized to allow for disturbance responses in the BSS when no supercapacitor is available. If a smaller battery was used then they would break down after frequent deep discharging [72], [142]. The lifespan extension comparison is not clearly seen in Figure 4.27 since the scale on the Y axis is too large to seen any visible changes. The battery SOC difference between HBS and BSS is now presented clearly in simulation run from 6 - 25 hours.

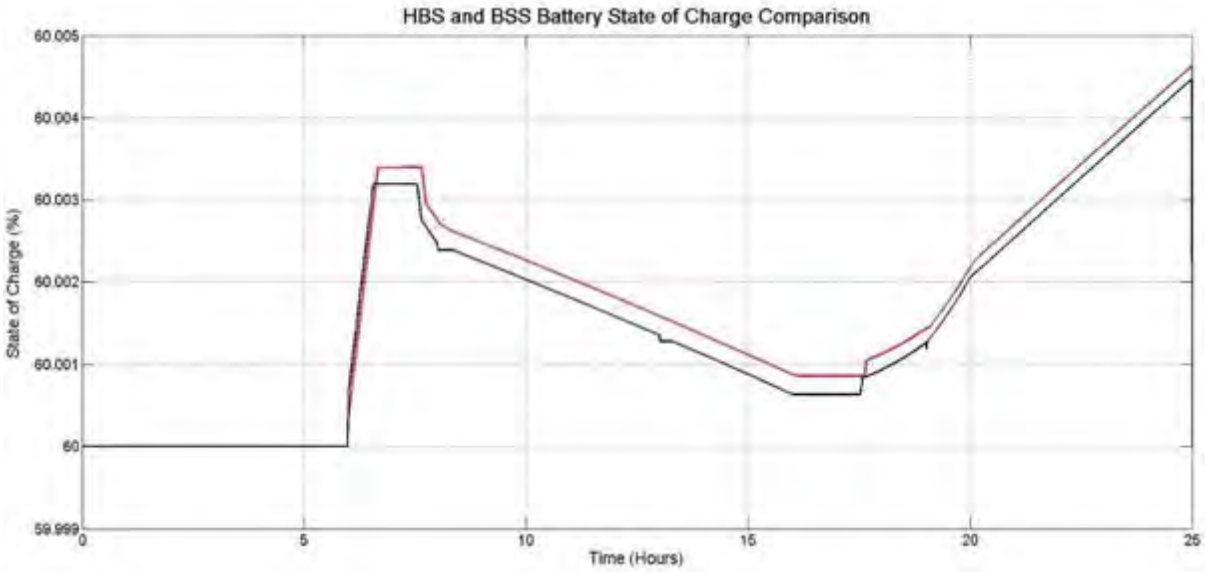

Figure 4.28 HBS and BSS State of Charge Comparison

The SOC comparison of the batteries shows that the HBS does yield an SOC improvement during the Case 3 simulation. The difference between BSS and HBS battery SOC characteristics is approximately 0.001%. Based on these results the SOC differences for all cases are presented in Table 4.12 with the accompanied lifespan extrapolation calculations. The same method used in Table 4.5 Case 1 is applied to Case 2 and Case 3.

Table 4.12 Evaluation of BSS battery lifespan when supply load disturbances without assistance

Case 2 and Case 3 Evaluation of BSS battery Life				
Time Frame	Secondary Load SOC losses	HBS battery SOC	BSS battery SOC	BSS battery Life
1 day	0.01%	59.55 %	59.54%	Running
1 month	0.30%	59.55 %	59.25%	Running
1 year	3.65%	59.55 %	55.90%	Running
2 year	7.30%	59.55 %	52.25%	Running
3 year	10.95%	59.55 %	48.60%	Running
4 year	14.60%	59.55 %	44.95%	Running
5 year	18.25%	59.55 %	41.30%	Running
6 year	21.90%	59.55 %	37.65%	Barely Operable
7 year	25.55%	59.55 %	34.00%	Barely Operable
8 year	29.20%	59.55 %	30.35%	Barely Operable
9 year	32.85%	59.55 %	26.70%	Failure

Table 4.12 shows an interesting observation which extrapolates the anticipated battery deterioration undergone. The table shows that Case 2 and Case 3 have the same SOC

difference with Case 1 still showing the most significant difference between HBS SOC and BSS SOC for the 25-hour simulation. The result shows that the BSS battery will reach failure after 9 years if only supplying the secondary load (otherwise allocated to the supercapacitor in HBS operation modes of Case 2b and Case 3b). This result applies to Case 2a and Case 3a but in Case 1a the BSS deteriorates after five years of secondary load supply. Case 1 is more reliant on storage devices since no primary generation source was used to supply the load, the battery would thus deplete at a faster rate.

- Despite a 40kW large discharge error the battery SOC for both cases only varied by 2%. This means that both batteries were protected from permanent damage because they were oversized and therefore large enough to withstand large unexpected discharges.
- HBS battery SOC was slightly improved when compared to the BSS average SOC.
- The SOC difference seen between HBS and BSS showed a 0.001% increase in HBS battery SOC for a single day.
- After extrapolation of SOC results (in Table 4.12), it is discovered that the wind-BSS battery is projected to reach failure after 9 years when supplying the secondary load.
- The use of a supercapacitor in this case can reduce the high peak secondary power demand thereby extending battery lifespan in the long term.
- BSS battery reaches failure at a faster rate in Case 1 since the battery is used more often. As a result the supercapacitor contribution is more substantial in this case.
- Based on this observation one can deduce that the SOC difference will increase when the supercapacitor is used to buffer the battery more frequently.
- This means that when more disturbances are sent to the supercapacitor the HBS battery lifespan is extended further.
- An increase in supercapacitor contributions and a smaller battery is recommended for future testing in order to check whether the battery lifespan improvements more.

4.4 Overall Electrical performance Analysis

The overall summary electrical performance results are now presented by comparing all cases under the criteria of load matching, power security and supply efficiency and lastly the battery lifespan improvements.

4.4.1 Load Matching Performance

Despite the similarities of each system, the load matching accuracy varies across all cases. The ideal Case 1 used a constant voltage source for power supply which resulted in an increased reliance on storage. In Case 1 the storage devices were charged with the ideal source and are then used to solely supply the load power. In Case 2 the solar RES provided a varying input power based on the solar irradiance penetration onto the PV panels. Case 2 used storage devices as an alternative supply source responsible for maintaining load supply, power security and system stability. Case 3 with the wind RES uses a wind speed profile as an energy resource. The WECS discharged 1200W for most of its on time; this meant that the storage devices were required at times of high load demand and during wind turbine start-up. The fundamental provisions of each cases storage and supply sources have been mentioned. A more detailed look into the load matching criteria for all cases is now presented in Table 4.13.

Table 4.13 Load Matching Evaluation

Load Matching Criteria	Case 1		Case 2		Case 3	
	BSS	HBS	BSS	HBS	BSS	HBS
Input Power Disturbance Response	N/A	N/A	Partial	Yes	Yes	Yes
Supply Shortage Compensation	Yes	Yes	Yes	Yes	Yes	Yes
Excess Energy Absorption	N/A	N/A	Yes	Yes	Partial	Partial
Primary (Average) Load Matching	Yes	Yes	Yes	Yes	Partial	Partial
Secondary (Impulses) Load Matching	Partial	Yes	Partial	Yes	Partial	Yes

In Case 1 the shortages in supplied power were compensated through storage device discharge. Primary load matching was achieved at the cost of wide power ripples because the battery remained on. Case 1 showed impressive load matching properties but did come at the expense of storage device errors and exhaustion in terms of lifespan and power security.

Case 2 showed the best load matching performance as compared to all other cases in this study. Case 2b successfully made provisions for all load matching criteria mentioned in Table 4.13. The result surpassed the ideal examples of Case 1. This is because the load was judiciously allocated to PV supply and storage device. By using the PV panels as the primary source the storage devices ripple was reduced which increased load power security and improved load matching. The HBS battery and supercapacitor were effectively combined and responded to all impulses and average load demands. The BSS managed to supply the impulses to the best of its ability but fell victim to power density restrictions by less than 5 Watts. Regardless of this 5 Watt deficit in BSS both the solar-HBS and solar-BSS are deemed best suited for load matching.

The WECS fails to accurately respond to load demands for the first 6 hours of operation. In the first hour the batteries used discharge dangerously and after that the systems attempts to recover from the large power spike. The system manages to recover by 3.5 hours and the load demand is met from four hours onwards. By six hours the WECS power generated reached its maximum value and the systems power is stable. After six hours the storage devices can accurately discharge (load response) and charge (excess energy) as instructed.

The DC charge algorithm is only effective once the supplied power is at a settled value. During the stabilised power region the storage device provisions are still limited and can dip to zero during discharge. This is because the storage devices used are connected to a DC-DC converter which is then coupled with the AC-DC WECS rectifier. This design is redundant and increases MOSFET switching losses. Furthermore, the rectified WECS supply contains a ripple current which then causes the power to dip to zero in the storage device outputs. Due to the delayed system stabilisation and ripples in storage device power, Case 3 is classified with partial energy absorptions and load response as stated in Table 4.13.

4.4.2 Power Security and System Efficiency

Power supply security and efficiency have been evaluated for all cases and a comparison of the same is presented here in Table 4.14.

Table 4.14 Power Difference between Total Supply and Load Demand and Resultant System Efficiency

		Average Load	Power Difference	System Efficiency
Case 1	BSS	848 W	-50.23 W	94.08 %
	HBS	848 W	-42.6 W	94.98 %
Case 2	BSS	848 W	-6.48 W	99.24 %
	HBS	848 W	-3.12 W	99.63 %
Case 3	BSS	1040 W	-204.09 W	80.37 %
	HBS	1040 W	-202.62 W	80.52 %

The results of Table 4.14 show that supply efficiency for BSS and HBS under Case 1 are at 94% and 95% respectively. The 1% increase in power supply efficiency is attributed to the supercapacitors fast discharge response to load disturbances. In Case 1, 5% of the load is not met due to the power ripple mentioned earlier caused by heavy reliance on storage devices. As a result the system would need to increase its input supply source or make use of more efficient batteries.

Case 2 shows the most impressive power difference values with an average of only 6.48W and 3.12W difference in the BSS and HBS cases. A lower power difference than Cases 1 and 3 is achieved in spite of solar PV generation resource fluctuations caused by irradiance variation and shading effects. In Case 2 the load is effectively distributed through storage devices and PV panel integration therefore minimal power ripple is observed. This means that the power difference is reduced and as a result supplied efficiency is 99%. Minor improvements must still be made to improve the efficiency of the batteries in order to ensure that the load is fully met. Since all cases considered are islanded, the power efficiency supply needs to be at theoretically 100% constantly to maintain electricity customers.

The same success in security and efficiency of supply is not apparent in the WECS case. The inadequate charging algorithm caused large fluctuations in storage supply takes place. The charge algorithm used is designed for implementation through a DC-DC converter. However, the WECS used requires a three phase AC-DC rectifier. As a result the charge algorithm was merely applied onto the DC-DC converter after WECS power rectification took place. This resulted in jumps in power since the rectified input was not perfectly smooth (DC). As a result the controller instructing the converter to charge or discharge the storage devices caused many jumps to zero in the storage device power. This resulted in power losses and an unmet load, more specifically in the wind-BSS as seen in Figure 4.24.

Storage device power provision was essential to maintaining supply since the maximum WECS power is only 1200W. As a result, only 80% of the average was met in Case 3. By increasing the WECS power generated the load capacity may be met but this solution

increases excess power generation and still cannot guarantee an operable system. A larger WECS power will still require storage devices to absorb excess energy. The root cause of the Case 3 failure must be dealt with in the form of an improved charging algorithm tailored to three-phase AC generation. This will allow for components savings since the DC-DC converters can be removed if the system was directly charged through a three phase conversion. By improving the charge algorithm and power limiting components this system will manage to accurately meet load demand through storage and supply integration.

4.4.3 Lifespan Evaluation and State of Charge Monitoring

The lifespan of the batteries employed are now evaluated per case by comparing the HBS and BSS battery SOC in every case. Once the average SOC difference between storage designs is established the results of the projected BSS degradation due to its extra load is found. This shows the lifespan benefits of using HBS as shown in Table 4.15 below.

Table 4.15 BSS Battery Lifespan Failure Point Due to Disturbance Responses

	HBS battery SOC	BSS battery SOC	Accumulated SOC losses	Ave SOC % Diff	BSS Failure point
Case 1	59.55 %	23.05 %	36.50 %	0.02 %	5 years
Case 2	59.55 %	26.70 %	32.85 %	0.01 %	9 years
Case 3	59.55 %	26.70 %	32.85 %	0.01 %	9 years

The battery lifespan measured in all cases was extended through the use of the supercapacitor. By conducting the extrapolation in Table 4.12 the expected battery SOC lost due to secondary load fluctuations in the BSS was calculated. The system showed that According to the results of Table 4.16 Case 1 shows the largest SOC difference between HBS and BSS. The BSS Case 1 battery is depleted in 5 years due to load fluctuations while the solar PV and WECS cases take approximately 9 years each. The increased reliance on storage devices in Case 1 means that the battery can benefit more from the buffering and high power discharge features of the supercapacitor used. In solar Case 2 and wind Case 3 the RES are used as the primary supplier therefore the storage is not scaled upon as frequently and would last longer.

Based on the summary in Table 4.16 the supercapacitor addition can bring about an extended battery lifespan in the long-term. The electrical performance analysis could potentially increase the focus on disturbance rejection and fluctuation response for a more effective supercapacitor contribution assessment. If smaller batteries were used the variation in SOC would also be more substantial which would make the extrapolation of battery lifespan clearer. The simulation could also make use of a smaller sample time if wider disturbances were used, this would result in less computations and therefore long simulation in Matlab. The results clearly show the potential for HBS lifespan extension of batteries but can be improved by applying the mentioned recommendations to future work.

5. Chapter 5 - Research Methodology for Economic Feasibility Analysis

Economic Feasibility Study Methodology

Chapter 5 explains the modelling procedure followed for the economic feasibility study. This chapter begins with the location selection and data acquisition methods used, as this is important for establishing the target region of deployment, and the need for RES in remote areas. This is followed by the development and explanations of how the case studies selected were laid out. Storage device and different energy sources are observed and compared through the simulation results. Technical explanations on modelling components and resources in the HOMER software are also presented.

5.1 Location Selection and Data Acquisition

The feasibility study for the remote area RES required a location with promising resources and no connection to the utility grid. South Africa was selected after uncovering its large potential for RES deployment in the literature review of Chapter 2 [143], [144]. The country has a wealth of solar and wind resource with easily obtainable topographic and geographic resource information [44], [117], [145], [146]. The city of Napier in the Western Cape province of South Africa was selected because of its high wind speeds and large unoccupied areas seen near informal settlements.

5.1.1 Un-electrified Areas

A study completed with the aim of providing communal electricity to rural areas in South Africa has shown that a major part of the Eastern Cape is un-electrified [9]. However, it is difficult to obtain resource data for this region in terms of wind speed, solar irradiance, land terrain, etc. Due to the close proximity of the current place of study (University of Cape Town), and easily available resource data, an alternative un-electrified area in the Western Cape was selected. Un-electrified regions in the Eastern Cape and Western Cape are encircled by green rectangles in Figure 5.1 below [9].

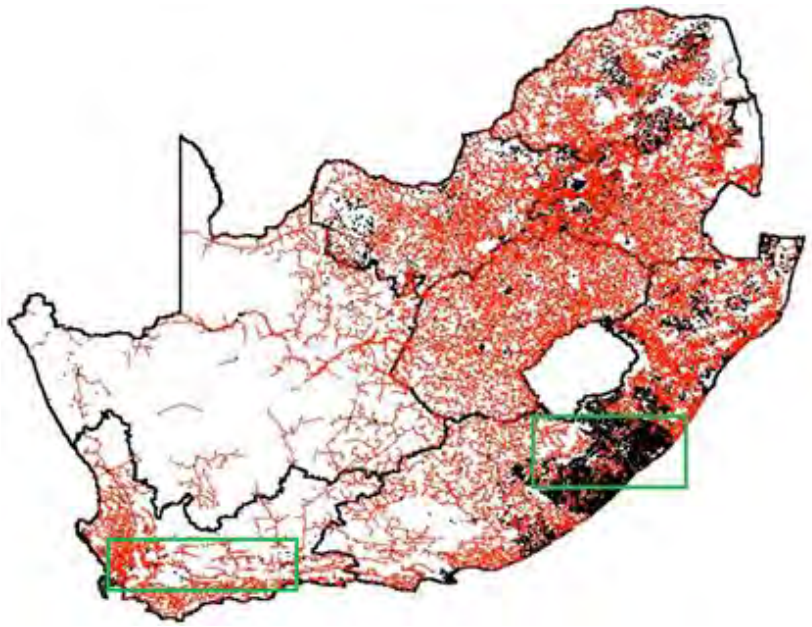

Figure 5.1 Areas in South Africa without electricity access [9]

For this study on economic feasibility of RES, Napier in Western Cape was selected. Napier is only 166km from the University of Cape Town (UCT). Their close proximity makes this study more feasible for future implementation and research at UCT [146]. The data collected justify this location and the properties of this region are now explained.

5.1.2 Population Density

Bird's eye view images of Napier were found by entering the coordinates of (34°61'S, 19°69'E) in Google Maps. It shows an informal cluster of houses (in blue) directly opposite a clear unoccupied field (in green) which has the potential for RES deployment as seen in Figures 5.2 and 5.3. After this different criteria for validating this area were considered with the Solar GIS, NASA and WASA databases [44], [117], [145], [146].

Figure 5.2 Zoomed in Rural Population and unoccupied land in Napier [146]

After using the street view function on Google Maps Figure 5.2 was expanded and a clearer view of the informal settlement was obtained as seen in Figure 5.3. Evidently, no transmission lines are connected to the informal settlements in this area [147]. Based on location and resources, this region shows ideal conditions for RES deployment which could be potentially cheaper than extending the utility grid in this area.

Figure 5.3 Informal settlement in Napier zoomed in image [147]

5.1.3 Landscape of Napier

In order to deploy solar or wind RES, the landscape of the area must be considered in the feasibility analysis. Solar GIS software uses the following index for comparing landscapes as seen in Figure 5.4.

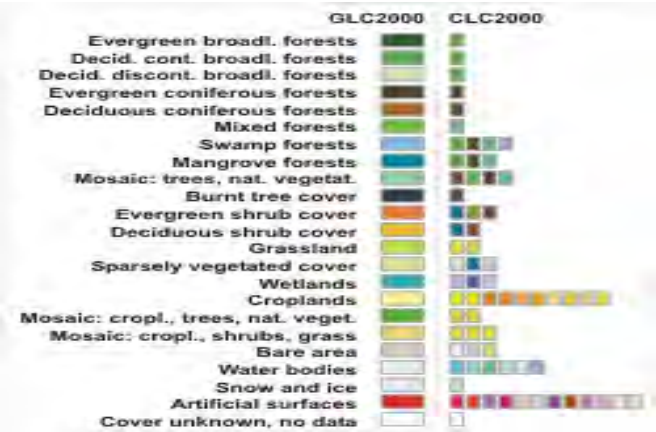

Figure 5.4 Solar GIS Landscape labels [145]

Using the index of Figure 5.4 the landscape is now shown in Figure 5.5 as the region inside the black rectangle.

Figure 5.5 Napier Landscape [145]

Based on the green, yellow and orange shades of marked regions in Figure 5.5, it is clear that Napier's landscape comprises predominantly of deciduous (dying) shrub cover and grasslands. This is an ideal landscape for deploying RES since no major reform is required. Deciduous plants could also indicate that an excess of sunlight is available in the marked region. The area is not densely populated which allows wider open spaces for wind to travel without any hindrance, and can also reduce user complaints of wind turbines in terms of visual and sound pollution.

5.1.4 Terrain of land

The terrain of the land can affect wind speeds and availability of the solar irradiance when deploying PV panels or wind turbines. The Western Cape has a wealth of mountainous land which can disrupt resource availability as well. Due to these factors the terrain of the selected region is shown in Figure 5.7 with its elevation scale in Figure 5.6.

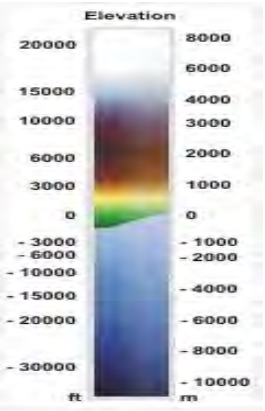

Figure 5.6 Elevation Scale of Area Terrain [145]

Figure 5.7 Terrain Comparison of Napier and Surrounding Areas [145]

The Napier area is located at an altitude of 105m with a slope inclination of 3.3 degrees and a slope azimuth of 329 degrees from the North West. Figure 5.7 shows that the selected region is on solid level ground without any excessively high elevations due to mountainous land or high hills. This makes the considered area more accessible by road [145].

5.1.5 Solar Irradiance Annual Profile

Solar irradiance exposure in the selected region is shown in Figure 5.8.

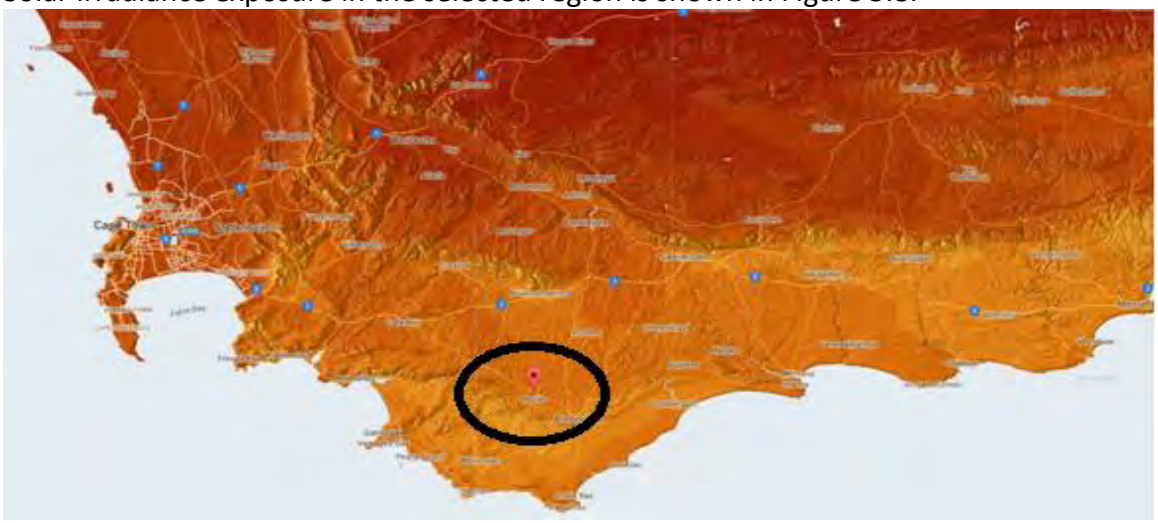

Figure 5.8 Solar Irradiance plot of Western Cape Region [145]

Solar irradiance is indicated by the saturation of colour in Figure 5.8. The encircled Napier area shows an orange-yellow colour which indicates slightly below average solar irradiance access compared to the rest of the Western Cape. However, Figure 5.5 and Figure 5.7 confirmed a favourable terrain and landscape for the considered area. The annual solar irradiance profile of the considered region is tabulated below in Table 5.1.

Table 5.1 Napier Western Cape Clearness Index and Solar Radiation Profile [117]

Month	Solar Irradiance ($kWh/m_2/d$)
January	7.620

February	6.710
March	5.450
April	4.010
May	2.940
June	2.470
July	2.700
August	3.480
September	4.650
October	6.070
November	7.250
December	7.720
Scaled Average	5.081

An annual irradiance profile is required for simulation study using HOMER software for the 20-year span. Using the NASA website, a solar irradiance profile in the Western Cape was found after entering the coordinates, (34°61'S, 19°69'E) [117]. An average daily irradiance exposure of 5.081kWh/m_2 was found based on the NASA database.

5.1.6 Annual Wind Speed Profile

The Google wind map generator was used to evaluate wind speeds available in South Africa. The wind speed scale is shown in Figure 5.9 and the local wind speeds are shown in Figure 5.10. The selected region is marked with a black rectangle in Figure 5.10 to show its wind speed relative to the rest of the country [146], [148].

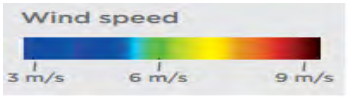

Figure 5.9 Wind Speed Colour Measurement Scale [145]

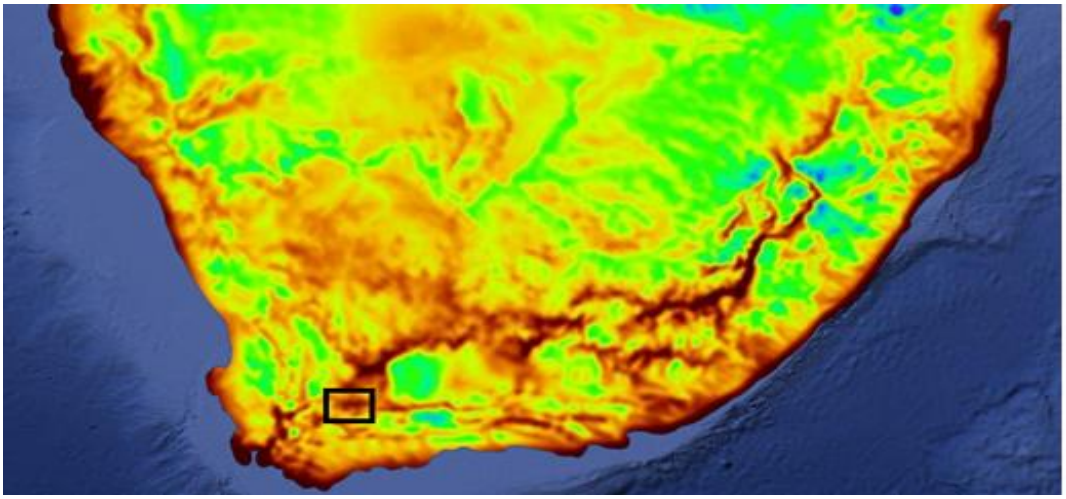

Figure 5.10 South Africa Wind with Marked Napier Region [145], [148]

The colour code of the region marked in Figure 5.10 shows that it has a strong wind reserve compared to the rest of the country which means that it also has high wind-based RES deployment potential.

The techno-economic study conducted in HOMER needed a reliable annual wind speed profile. Hence, the most recent WASA observational report published in April 2014 based on

the 2013 wind speed profile was selected for wind resource modelling [44]. The annual wind speed profile is now shown in Table 5.2 below.

Table 5.2 Recorded Wind Speeds in Napier - WASA observational report for April 2014 [44]

Hour	Jan	Feb	Mar	Apr	May	Jun	Jul	Aug	Sep	Oct	Nov	Dec	Year
0	8.3	7.6	7.9	7.9	7.0	8.4	7.8	8.3	8.7	8.4	7.8	9.0	8.1
1	8.2	7.6	7.8	7.9	7.2	8.4	7.8	7.9	8.7	8.2	7.8	8.8	8.0
2	7.9	7.5	7.6	8.1	7.0	8.7	7.9	7.6	8.6	8.1	7.7	9.0	8.0
3	7.9	7.6	7.6	8.3	7.3	8.5	8.0	7.7	8.7	8.3	8.0	9.1	8.1
4	8.1	7.5	7.6	8.3	7.5	8.5	7.8	7.5	8.6	8.6	8.1	9.0	8.1
5	8.1	7.6	7.5	8.3	7.6	8.5	7.7	8.0	8.6	8.4	8.0	9.0	8.1
6	7.9	7.8	7.5	8.4	7.7	8.6	7.7	8.2	8.7	8.6	8.0	9.0	8.2
7	7.7	7.3	7.7	8.3	7.6	8.7	7.6	8.2	8.4	8.3	7.7	8.8	8.0
8	7.8	7.0	7.5	8.4	7.1	8.1	7.7	8.4	8.1	8.3	8.0	9.2	8.0
9	8.2	7.3	7.9	8.0	6.8	8.1	7.6	8.2	8.1	8.8	8.1	9.4	8.0
10	8.6	7.6	8.1	8.4	6.7	8.0	7.3	8.3	9.0	9.1	8.5	9.8	8.3
11	9.0	7.8	8.5	8.5	7.2	8.2	7.5	8.6	9.1	9.4	8.8	10.2	8.6
12	9.5	8.4	8.7	8.7	7.3	8.6	7.7	9.0	9.4	9.7	9.0	10.3	8.9
13	9.9	8.9	8.8	8.9	7.3	8.9	8.3	9.2	9.5	10.1	9.5	10.8	9.2
14	10.0	9.2	9.5	9.2	7.6	8.7	8.4	9.6	10.0	10.7	10.0	11.3	9.5
15	10.5	9.7	9.6	9.6	7.7	9.0	8.3	9.3	10.2	10.8	10.4	11.5	9.7
16	10.6	9.7	10.0	9.5	7.6	8.9	8.1	9.5	10.2	11.0	10.6	11.7	9.8
17	10.6	9.7	10.0	9.6	7.3	8.5	7.9	9.3	10.1	10.8	10.6	11.5	9.7
18	10.3	9.5	9.7	9.2	7.4	8.7	7.6	8.8	9.5	10.5	10.1	11.1	9.4
19	9.9	8.9	9.0	8.6	7.2	8.5	7.8	8.5	9.1	9.7	9.3	10.5	8.9
20	9.2	8.4	8.5	8.2	6.8	8.2	7.8	8.2	9.0	9.1	8.8	9.9	8.5
21	8.9	7.9	8.3	8.1	6.9	8.1	7.7	8.2	8.5	8.8	8.2	9.4	8.3
22	8.4	7.8	8.1	7.9	6.8	7.9	7.8	7.9	8.4	8.6	8.0	9.3	8.1
23	8.6	7.8	7.8	8.1	6.7	8.0	7.8	8.3	8.7	8.6	8.1	9.1	8.1
Ave	8.9	8.2	8.4	8.5	7.2	8.5	7.8	8.4	9.0	9.2	8.7	9.9	8.6

Table 5.2 shows the average hourly wind speeds recorded for every month of 2013. The average annual hourly profile is seen in the blue column and has been used directly in HOMER simulation. Table 5.2 indicates that the wind speeds generally lie in a range of 8 - 9.7 m/s with the highest speeds recorded between 15 and 19 hours. This implies that high wind speeds during these hours are ideal for responding to the peak demand. In addition, the peak wind speeds obtained from WASA are seen to complement solar irradiance profile, which reduces after 17 hours as seen from NASA Solar GIS database. This will facilitate the hybridization of solar and wind resources in this region [44], [117].

5.2 Development of Case Studies

5.2.1 Need for an Economic Study

Storage devices are a mandatory requirement for maintaining energy security and power stability of a renewable energy systems. The electrical implications and provisos of storage is gradually becoming a well-researched area. However, a small fraction of large scale storage device research is allocated to the actual economic feasibility of a RES and storage from an engineering perspective [3]. Engineers tend to focus on the efficiency and outcomes or proof of significance in a system without considering whether this innovation is economically viable at the same time. As a result, multiple research papers related to HBS storage recommended a techno-economic study on this system to evaluate its feasibility of implementation in practical cases [58], [82], [87]. Based on the observed recommendation a techno-economic feasibility study is modelled in the HOMER v2.81 software package. HOMER is the world's leading microgrid software and extends to analysing large scale energy generation systems [128]. The software allows for multiple storage devices, renewable sources, power generation technology and loads to be used [13]. A basic illustration on the software's operation modes are shown in Figure 5.11.

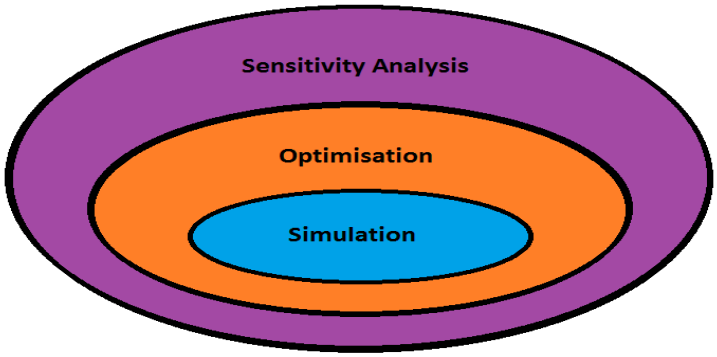

Figure 5.11 HOMER Software Model Architecture

HOMER primarily conducts multiple electrical and economic simulations, and compare their results to reach an optimum solution leading to system cost minimization subject to meeting the system objective such as supplying the load demand at all times. The software also performs a sensitivity analysis which involves multiple optimisation processes with a single variable assuming different values. Both these techniques are ideal for the present feasibility study which aims to compare multiple RES and storage device combinations at different load demands. Each combination of resources will be grouped in the form of a specific case study as described in the following section.

5.2.2 Layout of Case Studies

The techno-economic feasibility study presented in this chapter consists of six cases which vary in terms of energy generation resources and storage devices. Each case is optimised at different average load values which are selected as the variables for sensitivity study. Based on the set of sensitivity study results for each case, an overall comparison can be made which will determine the ideal remote area RES system configuration in terms of components, suitable for Napier in Western Cape. The layout of case studies is shown in Table 5.3

Table 5.3 HOMER Simulation Case Study Load Allocation Table

Case	Energy Source	Storage	Average Load Demand Range
Case 1a	Solar	BSS	1 - 7 in 0.5MWh/d increments
Case 1b	Solar	HBS	1 - 7 in 0.5MWh/d increments
Case 2a	Wind	BSS	1 - 7 in 0.5MWh/d increments
Case 2b	Wind	HBS	1 - 7 in 0.5MWh/d increments
Case 3a	Solar & Wind	BSS	1 - 2.5 - 5 - 7.5 - 10 MWh/d
Case 3b	Solar & Wind	HBS	1 - 2.5 - 5 - 7.5 - 10 MWh/d

Table 5.3 shows how the economic feasibility study is divided into cases based on the energy source and storage device used. Case 1a uses a solar PV panel for power generation and a BSS as its storage. Case 1b also uses the PV panels but employs an HBS. Case 2a uses a wind-BSS while Case 2b employs a wind-HBS design.

The first four cases (1a, 1b, 2a and 2b) have the same sensitivity variable test range. The selected sensitivity variable is the average load demand which starts at 1MWh/d and progressively increases by 0.5MWh/d until 7MWh/d is reached. This means each of the first four cases conduct 14 different optimisations.

In Case 3 the hybrid renewable energy system is used by combining solar PV panels and WECS. Case 3a thus is a wind-solar hybrid renewable energy system with BSS and Case 3b the same but with an HBS. The combination of solar and wind greatly increases the amount of data which must be simulated for every optimisation and sensitivity analysis and consequently increases the computation time. Hence, only five optimisation studies were conducted for each of Case 3a and Case 3b with five specific average load values as indicated in Table 5.3. Case 3 uses a sensitivity range of 1MWh/d - 10MWh/d because of the increased generation capacity available by combining solar PV and WECS.

In order to compare the influences of HBS and BSS on each RES, the battery size has been kept fixed across all cases. The battery capacity is tested up until battery failure is reached at a certain average load demand. The point at which the battery reaches failure is compared for each BSS and HBS combination. If the equal sized HBS battery can supply a larger load than the BSS battery, then it can be concluded the supercapacitor enhances the battery as well as overall storage capacity.

a) Solar PV Generation - Case 1a and Case 1b

Case 1a and 1b differ in storage type but the rest of the system configuration remains identical. Case 1 (both Case 1a and 1b) models an isolated solar PV RES in HOMER which can supply a remote area load in Western Cape. Solar resource is modelled using the Western Cape solar irradiance profile. The HOMER system configuration for Case 1 is shown in Figure 5.12.

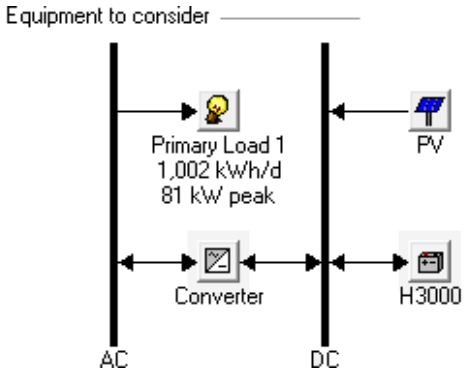

Figure 5.12 HOMER system configuration for Case 1a and Case 1b

Figure 5.12 shows that an AC load is supplied in accordance with local South African transmission regulations [31], [149]. However, the PV panels and the storage devices operate under DC conditions. This means a converter is required in order to interface the DC solar PV panels and DC storage devices (BSS or HBS) with the AC load. Since the storage devices and PV panels are both DC, the PV panel can directly charge the battery with DC power. This means the converter is used in inverter mode (DC-AC) to convert the PV or storage device output energy in order to supply the AC load.

b) Wind Generation - Case 2a and Case 2b

Cases 2a and 2b deal with the simulation and analysis of isolated wind-BSS and wind-HBS systems RESs in HOMER. The system configurations for Cases 2a and 2b are slightly different to Case 1 (refer to Figure 5.12) because the WECS is used generate three phase AC power. Figure 5.13 shows the HOMER system configuration for Cases 2a and 2b.

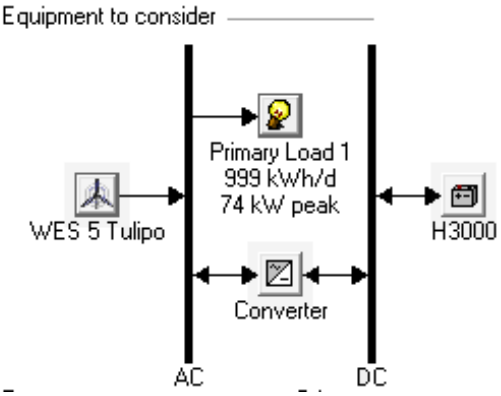

Figure 5.13 HOMER system configuration for Case 2a and Case 2b

In Case 2, the WECS and load operate at AC which means power can be directly supplied to the primary load from the WECS. Because of the direct connection majority of the load power demanded will not suffer from converter switching losses. The converter is still required for charging the storage device via the WECS and discharging it to the load as and when needed.

c) Hybrid Renewable Energy System - Case 3a and Case 3b

Cases 3a and 3b use the combination of wind and solar energy to create a Hybrid RES. The combination of solar and wind resources increases the generation capacity and facilitates generation of both AC and DC power in one isolated system. Case 3a involves a hybrid RES

with BSS while Case 3b uses a hybrid RES with HBS storage. HOMER optimisation software determines what renewable resource is going to be applied as the primary and secondary power supply and thus a ratio of wind turbines to PV panels purchased. This will depend on the load demand, storage device used (BSS or HBS) and the cost of energy. System configuration for Case 3 is shown in Figure 5.14.

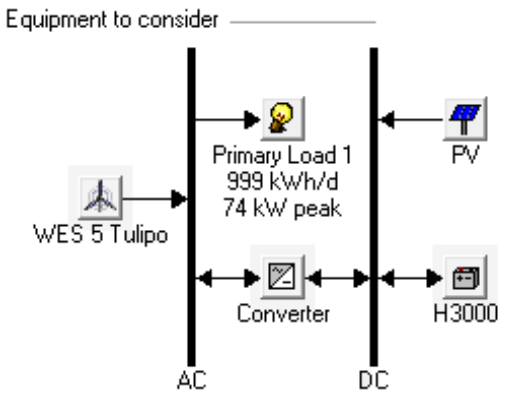

Figure 5.14 HOMER system configuration for Case 3a and Case 3b

Figure 5.14 shows that the PV panels are connected to the DC bus which allows easy charging of the DC battery. The WECS is connected to the AC bus, providing a direct supply to the AC load. The benefit of direct AC generation will count in favour of the WECS when selecting a primary generation source in Case 3. Figure 5.14 shows that Case 3 provides the benefits of both direct interfacing of the storage device and proximity of the AC load to the source of generation. Important assumptions made in the feasibility study are explained and justified in the following section.

5.2.3 Economic Assumptions & Constraints

The techno-economic feasibility study aims to find an economically viable configuration for a RES for a remote area based on a comparison of different renewable energy generation system and storage device combinations. For a more realistic comparison, the potential modelling problems have been identified in this section and the modelling constraints, assumptions and solutions relevant to simulation of the case studies in HOMER, are discussed.

a) Cost of Land

One problem faced is that HOMER software does not directly consider the price of land used for installation of an RES but the software does have a fixed capital cost tab which can be used to bring in the cost of land during the simulation. This solution would work for a single optimisation but the current feasibility study conducts multiple optimisations for a better comparison of cases. This comparison takes place by increasing the required load capacity through a sensitivity analysis. Naturally an increased load will require more land for energy generation. Using a fixed land cost is therefore not applicable for such studies.

The alternative solution is to simply include a progressive cost of land factor in the fixed cost. The progressive cost of land for each simulation is therefore included in the price of wind turbines and/or PV panels used. A linear pricing profile is used to define wind turbines and solar panel costs. This removes the potential for any bulk purchase savings. The additional cost incurred by removing bulk savings is used to model the cost of land for every wind turbine and PV panel purchased.

b) Solar Panel Switching Losses

Minor losses observed while interfacing the converter with the solar panel cannot be accurately monitored.

HOMER cannot model dynamic electrical properties but for the simulation a default error percentage based on the converters electrical characteristics is included in order to model switching losses [129]. This is done by considering the efficiency with which the converter converts AC-DC or vice versa. The software also measures the capacity relative to the inverter as HOMER assumes that most solid-state converters are less efficient at lower loads because of standing losses.

c) Environmental Impacts

Despite the obvious environmental benefits of renewable energy, it does include some negative effects which can be quantified as follows:

1. The land used for solar panels and wind turbine deployment is often excavated and levelled out.
2. A problem relevant to remote areas in South Africa is that the purchased land may be occupied by informal settlers.
3. Visual and noise pollution (e.g. by wind turbines), and potential disruption of the ecosystem (e.g. harm to bird life by wind turbines) may be caused by installation of renewable energy systems [12], [150].

As a solution, the landscape and data acquisition study conducted in section 5.1.1 ensured that a desolate area was selected for RES deployment. A low noise emission wind turbine was selected to prevent residential complaints.

In the instances where the land required for RES deployment is privately owned, a tender offer needs to be made. The company responsible for the RES deployment must come to an agreement with the land owners or must make a broad public offer to purchase majority of the owner companies' shares. The cost of this tender acquisition is built into the fixed capital cost mentioned in section 5.2.3a. Cost of land preparation/excavation is also built into the price of generation components. Thus, the PV panel and wind turbine capacity will determine the amount of land purchased and excavated if need be.

d) Power fluctuations and Operating Reserve

HOMER cannot model dynamic power fluctuations often seen in RES [128], [129], [151]. Dynamic power response modelling is integral to the comparison of HBS and BSS storage devices. In this simulation, power fluctuations in RES are generally compensated by increasing the operating reserve requirement or by including a high power density storage device. The operating reserves used in the BSS simulations are set at 50% for the WECS and 25% for PV panels. These operating reserve values were validated based on the general consensus of previous HOMER simulation based literature [35], [52], [53], [57], [152]–[158]. The use of operating reserve to achieve high power density response was also confirmed by the HOMER manual and knowledgebase [128], [159].

e) Lack of Supercapacitor Model in HOMER

A supercapacitor model is not readily available in HOMER. Hence the following solutions were employed here:

1. Design a Matlab model displaying the technical operation and validation of the supercapacitor addition and its improvements on power quality and load response. This is already reported in Chapters 3 and 4.

2. Adjust the operating reserve for load and renewable source capacity in BSS models, as suggested in section 5.2.3d and implemented in other published HOMER simulation works. [35], [52], [53], [57], [152]–[158], [160]
3. Reduce the operating reserve requirements for the HBS cases (1b,2b,3b) since the supercapacitor is included to respond to resource and load fluctuations.
4. Compensate for supercapacitor cost by including its initial capital cost in the battery model cost parameters for HBS simulations.

5.3 HOMER Modelling and Simulation Procedure

Selection of input parameters and modelling system component, renewable resource and storage device in HOMER are described in this section.

5.3.1 Modelling Energy Resources

Before the actual energy generation components are defined the renewable energy resources described in section 5.1 are modelled in HOMER.

a) Solar Resources

The solar resources modelled in HOMER are based on the same profile used in the Matlab simulation but now span across a 25-year period instead of a single day. The annual solar irradiance profile is obtained from the NASA online database by entering the following geographical coordinates (34°61'S, 19°69'E) [117]. The equivalent monthly clearness index is then calculated in HOMER. Clearness index and solar irradiance values for Napier are shown in Table 5.4.

Table 5.4 Clearness Index and Solar Irradiance Profile for Napier

Month	Clearness Index	Irradiance (kWh/m^2/d)
January	0.635	7.620
February	0.619	6.710
March	0.604	5.450
April	0.582	4.010
May	0.568	2.940
June	0.562	2.470
July	0.570	2.700
August	0.567	3.480
September	0.570	4.650
October	0.596	6.070
November	0.622	7.250
December	0.628	7.720
Scaled Ave	0.602	5.081

The parameters in Table 5.4 match the area defined in section 5.1. The average solar irradiance value for each month is defined and varies based on seasonal changes. HOMER uses a single annual solar profile to calculate equivalent values for the rest of the 20-year period for simulation.

b) Wind Resources

The wind speed profile modelled in HOMER is similar to the one used for Matlab simulation but is now extended over a 20-year period as well. Wind speed measurement

parameters have a significant influence on the integrity of the recorded data. The measurement parameters used by WASA are defined in Table 5.5.

Table 5.5 Wind Measurement Parameters of WASA

Name	Symbol	Value
Data Recovery Rate	***R***	98.6 %
Measurement Height	***h***	62 m
Weibull Parameter	***A***	9.7 m/s
Weibull Parameter	***k***	2.21
Weibull Wind Speed	***U***	8.63 m/s

The parameters in Table 5.5 are directly entered into the HOMER through the wind resources tab. The data recovery rate of 98.6% allows for very accurate wind speeds. Since the wind speeds recorded can be volatile, the Weibull distribution statistical method is applied to the wind speed profile.

The directions of the collected wind are divided into 12 sectors of 30° each with the angular axis of course made up of 0°-360 ° clockwise. The total distribution of observed wind speeds are processed and fit into a histogram. This histogram is fitted with a Weibull distribution function for each sector. From this the emergent distribution of the measured data is found by adding all 12 sectors with the units in ms^{-1} along the x axis and [% per ms^{-1}] along the y-axis. Through this collection and distribution method, the wind speeds recorded will factor in the height, speed and recovery rate of wind measured, resulting in the accurate profile shown below.

Table 5.6 Monthly Wind Speed

Month	Wind Speed (m/s)
January	*8.7*
February	*8.2*
March	*9.3*
April	*7.6*
May	*7.0*
June	*8.7*
July	*8.4*
August	*8.9*
September	*9.2*
October	*8.3*
November	*9.3*
December	*9.6*
Yearly Average	***8.6***

The Weibull distributed average wind speed of 8.63 m/s mentioned in Table 5.5, closely matches the speed listed in Table 5.6 and is only 0.03m/s lower than the annual average speed recorded. These wind speed are directly entered into the HOMER resources tab.

5.3.2 Modelling Solar PV panel

The polycrystalline Suntech STP210-18/Ud PV panel is selected due to its superior performance to cost ratio when compared to the Monocrystalline alternative [161]. The panel was also used in existing HOMER-based studies and allowed for a baseline comparison

and easy modelling in the software [52]. The PV panel data sheet can be found in Appendix A. The electrical parameters used to model this PV panel in HOMER are shown in Table 5.7.

Table 5.7 Electrical parameters for Solar Panel for HOMER Simulation

Input Parameter	Magnitude	Units
Maximum Power	210	Watts
Operating Voltage	26.4	Volts
Output current type	DC	Amps
Dimensions	1482 x 992 x 35	mm
No. of solar cells	54 (6 x 9)	156 x 156 mm
Slope	22.3	Degree
Derating factor	80	%
PV Capacity Search Space	250 - 8000	kW in 250 increments

The PV panel has a rated power of 210W when operating at 26.4V which is acceptable, given its physical dimensions (refer to Appendix A) [161]. The PV panel search space determines the options for panel selection. In this case, HOMER considers 32 different panel combinations ranging from 250kW - 8MW. This large search space allows for accurate sizing of components but increases computation time significantly. The panel selection is not limited to the electrical demands of the system. The economic or cost parameters used for this panel modelling in HOMER are listed in Table 5.8.

Table 5.8 Economic HOMER Inputs for PV Panel

Input Cost Parameter	Magnitude	Units
Capital	2000	$
Replacement	2000	$
O & M	0	$ /year
Lifetime	25	Years

In order to generate 1kW worth of PV power, roughly 20 panels must be purchased (depending on the operating reserve and capacity factor used). Table 5.8 refers to the price of 1kW worth of PV panels (which costs $2000). When this price is scaled down the PV panels yield a ratio $2 capital per Watt of power. This is higher than the average price per Watt but does include the cost of land and the cost component related to environmental impacts of the system (refer to section 5.2.3). The electrical parameters entered are considered along with the cost parameters while selecting the required PV capacity.

5.3.3 Modelling the Wind Turbine

The WES5 Tulipo wind turbine is selected because of its low component cost, market popularity, high efficiency and low noise generation properties [162]. The turbine has been modelled in previous HOMER simulations which allowed for a baseline performance comparison [153]. It is also available as a default wind turbine in HOMER software which means it does not have to be specifically built in the software database. Accuracy of the HOMER model is demonstrated through a comparison presented in the Appendix B and its electrical parameters are shown in Table 5.9.

Table 5.9 Electrical Parameters for WES5 Tulipo

Input Parameter	Magnitude	Units
Maximum Power	2500	Watts
Hub height	25	m
Number of blades	3	Blades
Rotor diameter	5	m
Survival Wind Speed	59.5	m/s
Nominal Wind Speed	9	m/s
Noise emission	35dB	at 9m/s
Quantity	250 - 6000	in 250 increments

This wind turbine shows a maximum power of 2.5kW per turbine with a nominal wind speed of 9m/s. The hub is 25m which poses a slight disadvantage since wind speeds are measured at a height of 62m (refer to Table 5.5). Hence, the wind speeds which penetrate the turbine blade might be lower than the measured speeds. A low 35dB noise emission is found at a nominal speed. A single wind turbine cluster is made up of 250 turbines. The modelling search space contains 24 different combinations of clusters, resulting in a search space of 250 - 6000 wind turbines. The large wind turbine search space enforces accurate components sizing. The cost parameters of the turbine are listed in Table 5.10 below.

Table 5.10 Cost Parameters for WES5 Tulipo

Cost Parameters	Magnitude	Units
Capital	5000	$
Replacement	4000	$
O & M	50	$ / year
Lifetime	15	Years

Capital cost for a 2.5kW single turbine is $5000 and it can be replaced at $4000. Amounting to an initial capital to power purchase ratio of $2 per Watt, which is the same ratio as the PV panels used. Unlike PV panels, wind turbines can be replaced at a lower cost but they do require more maintenance at a cost of $50 per year [153], [155]. The lifetime of the wind turbine is only 15 years which means it will definitely be replaced during the 20-year period covered in simulation.

5.3.4 Modelling the Converter

A converter is essential to the architecture of these RESs since the battery used in all cases operates at DC while an AC load needs to be supplied at the same time. The AC-DC bidirectional converter is modelled here based on the design seen in [153]. The component parameters are specified in Tables 5.11 and 5.12 as well as Figure 5.18 which shows the HOMER input block.

The converter is used to interface the storage devices, power generated and load demand thus it must be rated at a capacity which can cater to all systems. The search space includes 32 different converter ratings ranging from 100kW - 5MW. The cost parameters of the converter are defined in Table 5.12.

Table 5.11 Technical Input Parameters for Converter

Input Parameter	Magnitude	Units
Power	1	kW
Inverter efficiency	98.5	%
Rectifier efficiency	97	%
Search Space of Converter Capacity	100– 2000	100 increments
	2000 – 5000	250 increments

Table 5.12 Economic Inputs for Converter

Cost Parameter	Magnitude	Units
Lifetime	25	Years
Capital	400	$ / kW
Replacement	250	$ / kW
O & M	1	$ / kW

The converter power rating will be varied in the simulation in terms of the operating reserve of the RES, converter energy throughput and replacement time. Since the HBS contains lower fluctuations and requires a lower operating reserve it is expected that a smaller size converter can be selected in this instance. A smaller converter will result in cost differences but these differences will be rather minor as compared to the overall cost.

5.3.5 Modelling the Load

The selected load profile is based on the same commercial-residential curve defined in section 3.7.2 of Chapter 3. However, for HOMER simulation, the load spans across an entire year and contains no impulse disturbances which were included for electrical performance analysis and shown in Figure 3.15. It must be noted that the electrical performance analysis of Chapter 3 involves modelling technical impacts while Chapter 5 is aimed at establishing techno-economic feasibility of the RES. Special care must be taken in accurately defining the load since it is used as the sole sensitivity variable in the feasibility study. The average magnitude of the load will be varied from 1MWh/d to a maximum of 10MWh/d.

a) Daily Trace Design

The daily trace design uses hourly load values which are manually entered into HOMER. Once the daily trace is defined, the latitude and longitude coordinates of RES deployment are specified in the software, and used to calculate the equivalent annual load profile (as well as solar and wind resource generation profiles) based on seasonal changes in demand. Load details are defined in the primary load input window shown in Figure 5.15.

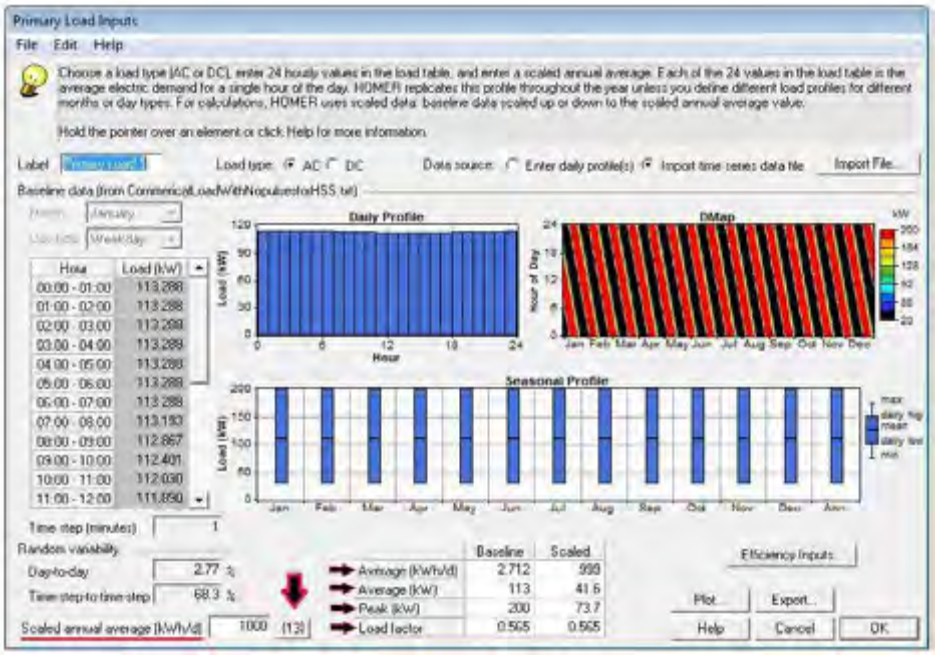

Figure 5.15 Primary Load input window in HOMER

The peak demand, average power demand, average energy demand and load factors are all implicitly varied during the sensitivity analysis by using the scaled annual average energy as a sensitivity variable. The scaled annual average value underlined in the bottom left tab of Figure 5.15 is used to specify the various average load magnitudes. Seasonal demand variations are noticeably illustrated as the load demand increases during South Africa's autumn and winter seasons. The D-Map represents the capacity of the load in terms of colours. It is shown to be predominantly red, which means the load is at maximum demand for most of the simulation period.

b) Load Plots and Modelling

Based on the data entered into the daily trace design block shown in Figure 5.15 the relevant load curves are now generated in this section. The weekly load profile is now shown in Figure 5.16.

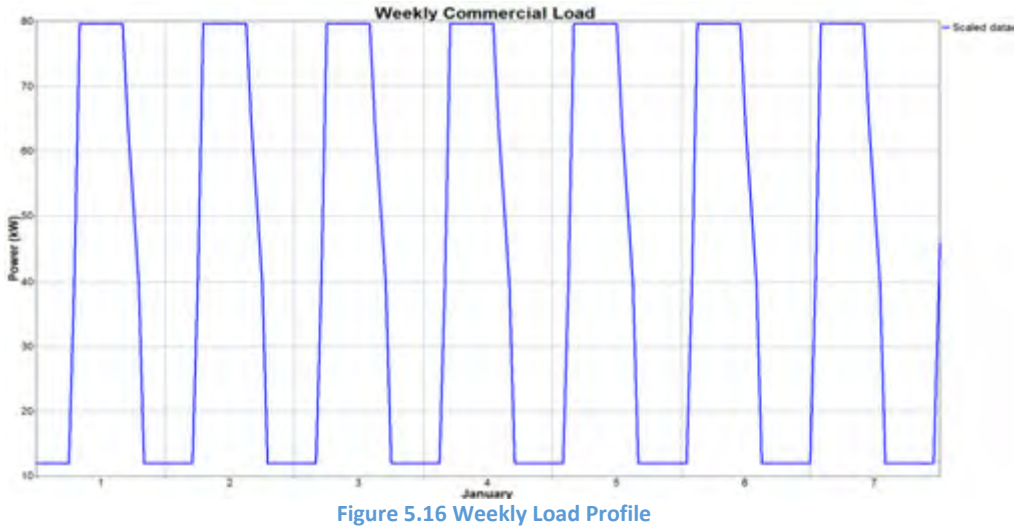

Figure 5.16 Weekly Load Profile

The profile seen in Figure 5.16 matches the load defined for Matlab simulation of electrical performance analysis presented in Figure 3.15, in terms of its power curvature. The curve differs average magnitude and the high power disturbances are removed in Figure 5.16 compared to the Matlab load. This is because the supercapacitor contribution has been modelled indirectly through operating reserve provisions which will be described later. The last factor which must be acknowledged is that this feasibility study models an AC load instead of DC demand; hence the amplitude and not the actual sinusoidal power profile is described in Figure 5.16. The electrical study was predominantly based on controlled design and provisions of the battery and supercapacitor in terms of load matching, power security and system efficiency. The feasibility study is more concerned with the economic impact of islanded RES supply. As a result the more common AC load is used in the economic feasibility study.

5.3.6 Modelling the BSS

The Hoppecke 24 OPzS 3000 lead acid battery is selected for modelling because of its impressive power to energy density ratio which is still at a respectable cost per kilowatt [163]. Based on the comparative literature review conducted in Chapter 2, the lead acid battery is ideal for RES storage and pairing with supercapacitors because of its low cost and limited SOC range [89], [135]. The electrical and cost parameters of the battery are now summarised below.

a) Input Parameters

The Hoppecke battery is a default battery option in HOMER, meaning details such as capacity, charge rate and discharge plot are already defined in the HOMER database. However, some parameters must be entered manually entered based on the component data sheet which can be seen in Table 5.13. These parameters were found after consulting the Hoppecke data sheet and other research literature which use the same battery for RES modelling in HOMER [52], [163].

Table 5.13 Electrical battery input parameters for HOMER

Input Parameter	Magnitude	Units
Bus Voltage	300	Volts
Initial state of charge	100	%
Search space	1248	batteries
	20000	batteries

An important observation seen in Table 5.13 is the search space restriction to two sizes. The two battery sizes are one of an accurately sized battery bank and the second being an intentionally oversized battery. The oversized battery is set to 20 000 batteries which will never be economical for supply. If the optimisation uses the oversized battery it will be so, solely because the accurate battery reaches failure and cannot supply the load. The load sensitivity value at which the battery reaches failure will be compared across all cases considered. The comparison of sensitivity load will establish whether the HBS can maximise the battery potential by allowing it to supply larger loads than when used in a BSS. If the supercapacitor can compensate for infrequent fluctuations then they a smaller battery can be used for the same application or the same size battery can be used for larger applications. The cost parameters of the selected battery are shown in Table 5.14 below.

Table 5.14 Economic Battery input parameters [52]

Input Parameter	Magnitude	Units
Capital	1644	$
Replacement	300	$
O & M	100	$/year
Rated Lifespan	20	years

Table 5.14 shows the economic parameters for a single battery but obviously a combination of batteries will be used to establish the 300V DC bus required. The battery used is relatively expensive but does last a long time and is cheap to replace. Prices were validated by other simulations as well as data sheets for the battery [155].

b) Hoppecke Battery Model Details

The selected battery was available as a default example in the HOMER battery database. The Hoppecke model was configured by the HOMER software developer and previously tested in other literature [89], [128], [163]. The electrical parameters specified by the software are now shown in Table 5.15.

Table 5.15 Electrical input parameters for Hoppecke battery [163]

Input Parameter	Magnitude	Units
Nominal Capacity	3000	Ah
Nominal Voltage	2	V
Round trip efficiency	86	%
Min state of charge	30	%
Lifetime throughput	10,196	kWh
Suggested value	10,241	kWh
Max charge rate	1	A/Ah
Max charge current	610	A
Maximum capacity	3,575	Ah
Capacity ratio	0.315	/
Rate constant, k	1.24	1/hour

The battery shows a roundtrip (energy lost due to storage) efficiency of 86% with a minimum state of charge of 30%. This means that 86% of the energy used to charge the battery will be dissipated during discharge, when operating in the effective SOC region. The parameters of Table 5.15 agree with the average lead acid battery specifications mentioned in the literature review of Chapter 2 [41], [107], [108]. A single battery has an estimated throughput of 10196kWh which results in a 20-year lifespan specified in Table 5.14. This can be reduced if the throughput value is reached first.

The capacity curve shown in Figure 5.218 shows the amount of energy that can be extracted from a fully charged battery. The battery capacity (Ah) depends on the rate at which energy is extracted from it. The higher the discharge current (A), the lower the capacity [129].

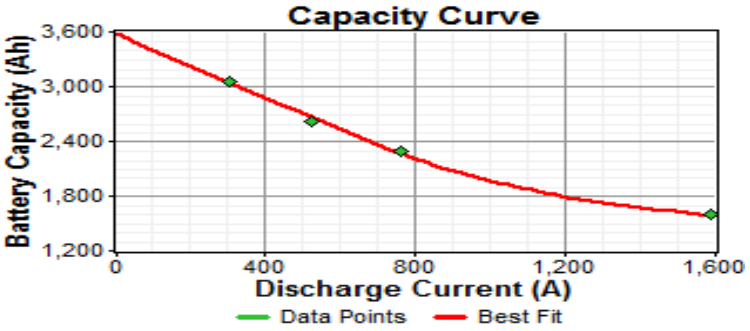

Figure 5.17 Battery capacity curve related to the discharge current

In addition to energy throughput, the cycles to failure will also determine the lifespan of the battery. Recent battery studies confirm that the depth of discharge does not affect battery capacity but the cycles to failure and relative throughput still determine its lifespan [99]. The life time curve of the modelled battery in terms of cycles to failure is expressed in Figure 5.19.

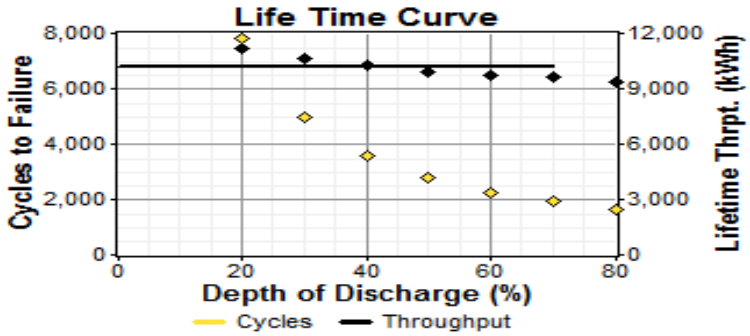

Figure 5.18 Life Time Curve of the Battery with Respect to battery discharge Cycles to Failure

Figure 5.19 shows that the battery used can be replaced once it has reached the end of its lifespan or it has reached its throughput limit. Figure 5.19 shows that the battery used will need to be replaced at least once during the simulation. Based on this observation the comparison between the BSS and HBS can be made clearer in this study. The HBS modelling procedure in HOMER is explained in the following section.

5.3.7 Modelling of the HBS

In case of HBS modelling, the selected battery is already available in HOMER and has been presented in section 5.3.6. Unfortunately, no supercapacitor models or block sets are available in the software [129], [151]. Hence, this section explains how the supercapacitor

properties are modelled indirectly in combination with the battery to achieve a model for the HBS. Before the HBS model can be defined it is important to understand the proven technical provisions of the supercapacitor. The supercapacitor has a high power density and can respond to power fluctuations, be it in the load demand or RES resource (wind or solar disturbances). This benefits the storage strategy in four primary ways:

1. Improvements in general power security of the system [74], [132].
2. By increasing the storage power rating (HBS), batteries are not oversized [47], [164].
3. Reduction in RES generated additional capacity used during fluctuations in supply (operating reserve) [3], [16], [165].
4. Extends battery lifespan through limiting frequent shallow cycles [58], [111], [136].

The fundamental benefits of supercapacitors is the provision of operating reserve and prominent impulse response [85]. The procedure followed for the modelling of the supercapacitor is explained.

a) Technical Parameters of Supercapacitor

Supercapacitor impact on operating reserve is modelled by adjusting the system constraints tab in HOMER. Previous research on HOMER simulations shows that a general operating reserve modelling consensus has been established for wind solar and load parameters. These values can be seen in Table 5.16 and are based on the consensus reached in the following references used for HOMER modelling [35], [53], [57], [128], [152], [153], [156], [157].

Table 5.16 POR Required for Disturbances Experienced

Disturbance Type	Operating Reserve in BSS	Operating Reserve in HBS
Wind Generation	50%	20%
PV Generation	25%	5%
Average Load	25%	5%
Annual Peak Load	20%	10%

Table 5.16 shows the operating reserve parameter entered in HOMER for the BSS and HBS. The last column shows that the required RES operating reserve capacity is reduced when a supercapacitor is used with a battery. The second basic supercapacitor provision mentioned in section 5.3.7 is also effectively modelled by reducing the average and peak load disturbances in Table 5.16. The HOMER operating reserve for wind and PV energy is set at 50% and 25%, as confirmed by literature references [35], [53], [57], [128], [152], [153], [156], [157] and HOMER modelling database [166]. Operating reserve is calculated as follows.

$$Wind\ Power\ \times\ (1 + Operating\ Reserve\ )\ =\ Wind\ Capacity_{Required} \tag{5.1}$$

$$200kW\ \times 1.5 = 300kW$$

Equation 5.1 shows an example of how the operation reserve is calculated. The wind energy operating reserve was shown as it is the most substation reserve needed. It shows that if 200kW of wind power is required the reserve capacity would be 300kW. The wind capacity would increase to below 200kW and above 200kW at times. Hence a power is kept in reserve in case of shortages. This power is now sent to the supercapacitor as mentioned

in Table 5.16. The supercapacitor cannot supply the complete operating reserve but can be used a high power density short term supply in order to reduce the peak operating reserve (POR). The required supercapacitor capacity is calculated as follows.

$$Wind\ Power_{Highest\ Peak} * (POR_{Old} - POR_{New}) = Supercapacitor_{Rated\ Power} + Battery_{Rated\ Power} \quad (5.2)$$

$$416kW * (50\% - 20\%) = 166.4kW$$

In order to ensure the operating reserve energy is available for supply and for absorption in the system a storage device is employed. The sensitivity analysis has its largest load tested at 416kW rated peak power. If this was fully supplied by wind power (which requires the maximum operating reserve) then 624kW of wind power is the maximum required to effectively meet supply. According to the Table 5.16 and Equation 5.2, the supercapacitor must supply 166.4kW to reduce the maximum operating reserve demand in the system. The combined supercapacitor bank has a maximum power of 315kW which can easily supply the wind and solar operating reserves simultaneously if need be [167]. Since hybrid systems use the secondary resource as a form of operating reserve which means the allocated supercapacitor will easily maintain the reduced POR demands in the HBS for all generation types considered.

b) Economic Parameters

The economic parameters of the supercapacitor when included in the HBS can now be explained. Before doing this the following factors are noted:

1. HOMER has no supercapacitor modelling block for simulation.
2. A second battery block with a high power density cannot be used to model the supercapacitor because HOMER only allows for one battery type per simulation.
3. The simulation period is 20 years. This is considered shorter than the lifespan of the supercapacitor which has over 500 000 cycles [67].
4. Customers required a 240V supply at AC. To ensure this was supplied, a 200V bus was designated on the DC supply side. This allowed for enough energy when being converted from DC to AC during load supply and made provisions in case of any battery cell shortage as only 142V was required. As a result, the supercapacitor, battery and PV panels supplied at this rate.

HOMER does not allow for multiple batteries types per simulation; hence the cost impacts of the supercapacitor are included in battery cost model. HBS and BSS battery cost parameters directly entered into the HOMER software are now compared in Table 5.17.

Table 5.17 Cost Comparison of the battery and Hybrid storage devices [52]

	BSS - Battery Only			HBS - Battery and Supercapacitor		
	Capital ($)	Replace ($)	O & M ($/yr)	Capital ($)	Replace ($)	O & M ($/yr)
1	1644	1644	10	2889	1644	10
100	164400	164400	1000	165645	164400	1000
1000	1644000	1644000	10000	1656450	1644000	10000
4000	6576000	6576000	40000	6625800	6576000	40000

The voltage bus requires 141.2V in order to connect with the AC when supplying the AC bus. In order to ensure the supply is met and converted, storage device and PV losses are

compensated for the uniform DC bus set at 200V. The present supercapacitor has a rated single cell voltage of 170V while the battery bank is connected with a pair of 100 series cells each rated at 2V. To meet the allocated battery storage power for all cases, 12 strings of series 100 batteries are connected to the bus and a single supercapacitor is paired with each string. A single supercapacitor costs $1245 and a pair of 100 batteries costs $1644 [85], [133], [167].

A fixed battery capacity of 1248 batteries is used for this feasibility study. This means 12 supercapacitors are used in order to match the bus voltage demands. The supercapacitor has a cycle lifespan of (over 500 000 cycles) which surpasses the 20-year simulation period, as a result, the replacement and O & M cost for the HBS and BSS remain the same in Table 5.17 [85], [133]. An illustration of how the HBS cost model is configured in HOMER is now shown in Figure 5.20.

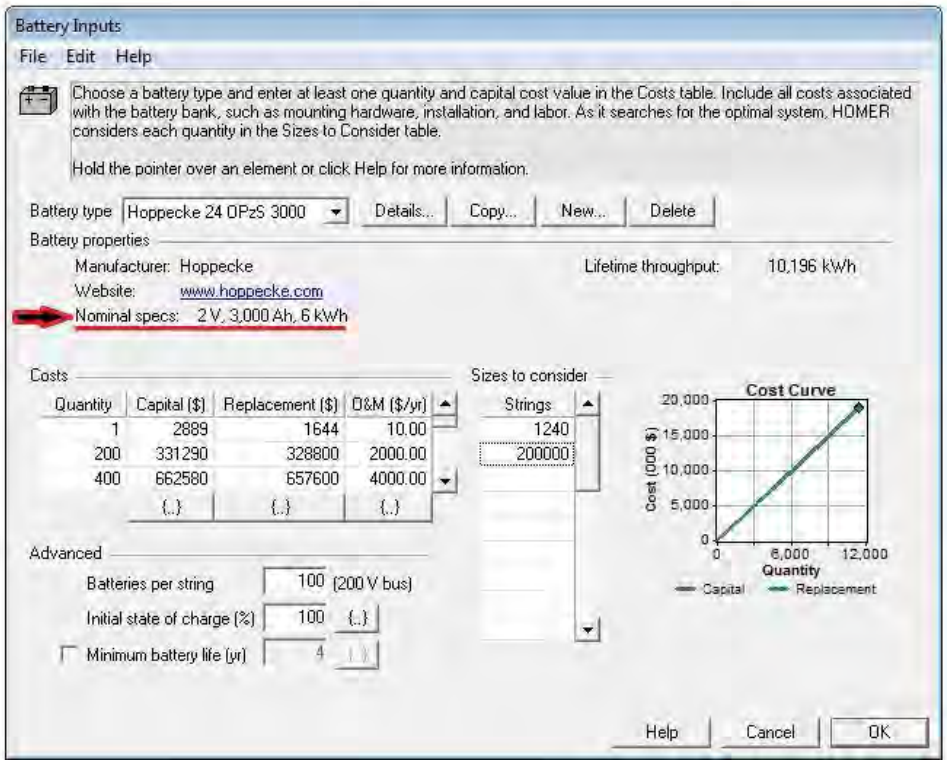

Figure 5.19 Hybrid Storage device input parameters modelled as a battery

The “Battery Inputs” block shown in Figure 5.20 is used to configure the HBS capacity and economic parameters in the software. In order to maintain continuity across simulations, the “sizes to consider” only use the selected HBS and BSS sizes, and the oversized battery which shows when storage failure has been reached. Since the technical properties of the supercapacitor are modelled through the operating reserve, the electrical specifications of the battery in HBS and BSS are now uniform. This can be seen at the “nominal specs” label underlined in Figure 5.20. Results can now be presented in Chapter 6 since the supercapacitor HOMER modelling procedure was explained.

6. Chapter 6 - Results for Economic Feasibility Analysis

Optimisation Study Results

This chapter presents and analyses the results for the economic feasibility performed in HOMER based on the data and case studies defined in Chapter 5. The results here are categorised into two sections – optimization studies and sensitivity analysis.

Sections 6.1 - 6.4 presents the optimum system configuration and component sizing for all cases, as obtained using HOMER, with detailed explanation of these results from an economic and technical perspective. As has been detailed in Chapter 5, each case study uses a different storage device and generation source combination in order to supply the average daily load of 5MWh with average power of 208kW and peak capacity 407kW. The results for all case studies are compared in order to establish the most feasible combination of renewable energy source(s) and storage device for an isolated RES. For all cases, a fixed battery capacity is set for all cases in order to compare the supply capacity extension as the load is being increased.

6.1 Solar RES Optimisation Results of Case 1a and Case 1b

The results of the solar PV panel based generation system with BSS and HBS in Cases 1a and 1b are presented in this section. The optimum sizes and costs of the PV panels, storage device and converter are presented first, followed by a detailed comparison of the BSS and HBS systems. This comparison is based on the system performance and contribution of the storage devices deployed, viz., BSS in Case 1a and HBS in Case 1b.

6.1.1 Results for Case 1a: Solar-BSS

Technical and economic parameters for the optimum solar-BSS system configuration are shown in Table 6.1.

Table 6.1 Component Size and Net Present Cost for Solar-BSS system (Case 1a)

Component	Size	Net Present Cost ($)
PV Panel	6000kW	12,000,000
Storage Devices	7,488kWh	3,310,341
Converter	600kW	268,228
Total NPC		15,578,569

Table 6.1 shows that a 6MW solar PV panel and fixed battery storage of 7.5kWh is used to supply the 5MWh/d average load. The components are very expensive showing a Net Present Cost (NPC) of over $13 million. The prescribed sizes do makes sense when one considers the fact that the load profile used for simulation has a peak of 208kW with an average of 407kW and runs over a 25 year period. A component cost summary for solar-BSS system of Case 1a is presented in Figure 6.1 followed by the breakdown of the NPC cost components in Figure 6.2.

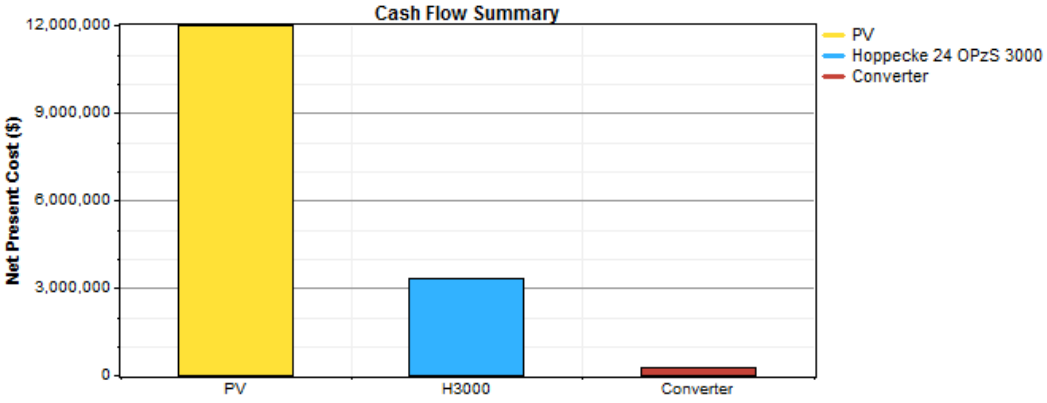

Figure 6.1 Component cost summary for solar-BSS (Case 1a)

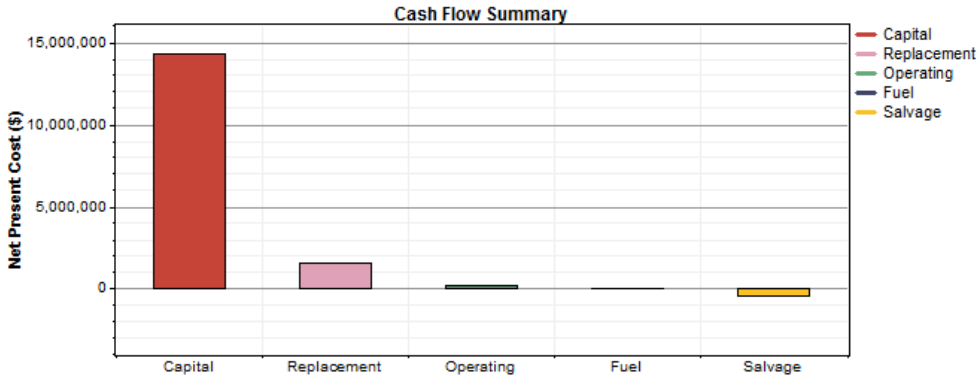

Figure 6.2 NPC cost summary for solar-BSS (Case 1a)

Figure 6.1 shows that the PV panel cost is the largest contributor to total NPC, followed by the battery. The battery bank capacity and price is fixed, which means all cases using the BSS yields the same storage device cost. The converter cost is relatively insignificant at $268,228 when compared to the total NPC of $15,578,569.

Figure 6.2 shows that the initial capital is the biggest hindrance to establishing a deployable RES. The high initial capital is mainly due to PV panel purchasing; fortunately, they require low maintenance and are not replaced often but this does mean the salvaged cost benefits are reduced. The alternative solar-HBS used in Case 1b is now presented following the same format as Case 1a.

6.1.2 Results for Case 1b: Solar-HBS

Technical and economic parameters for the optimum solar-HBS system configuration are shown in Table 6.2.

Table 6.2 Component Size and Net Present Cost for Solar-HBS system (Case 1b)

Component	Size	Net Present Cost ($)
PV Panel	5500kW	11,000,000
Storages Devices	7,488kWh	3,333,250
Converter	400kW	178,819
Solar-BSS		14,512,069

The load profile including average and peak values remains the same as in Case 1a. Since the HBS for Case 1b comprises a battery and a supercapacitor, its cost is more than the BSS. However, this improvement in storage results in a reduced PV panel capacity for the solar–

HBS and consequently less component cost. A component cost summary and a breakdown of NPC components is shown for Case 1b in Figures 6.3 and 6.4 respectively.

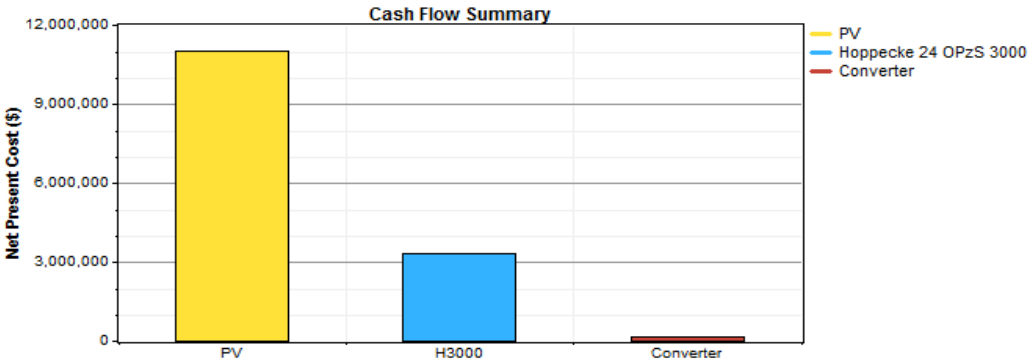

Figure 6.3 Component cost summary for Solar-HBS (Case 1b)

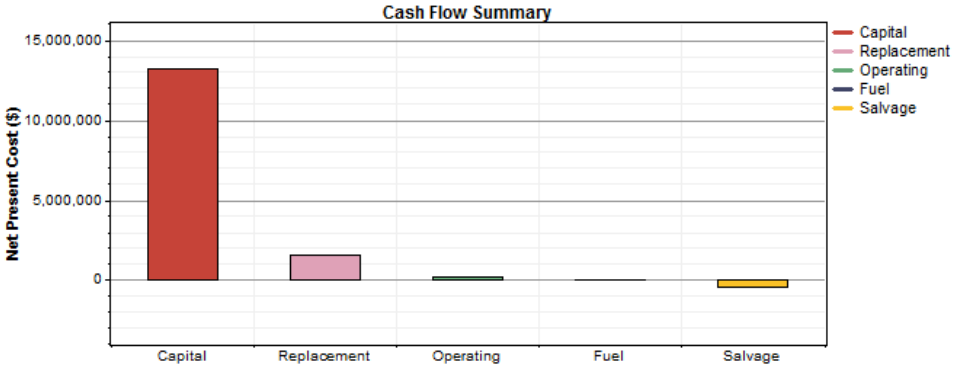

Figure 6.4 NPC cost summary for Solar-HBS (Case 1b)

Case 1b shows an increase of $200 000 in the storage component of the NPC but also yields a $1 million reduction in PV panel cost as compared to Case 1a. The new Case 1b total is reduced to $14.5 million compared to a previous NPC of $15.8 million of Case 1a. Storage and PV panel components make up the bulk capital costs once again. The technical results for Case 1 (Case 1a and 1b) are now presented in detail, in the following section.

6.1.3 Analysis of Technical Results for Case 1

The energy and component related technical parameters for the optimum solar RES system configuration as determined by HOMER simulation for Cases 1a and 1b are presented in Table 6.3. Case 1b parameters are compared with those of Case 1a and the difference between the parameters is expressed as a percentage of the ratio of the numerical difference and the Case 1a parameter value. The observations are also explained in the comments column. This is followed by a detailed analysis of these results.

Energy and component related technical parameters for optimum Solar-RES in Case 1 supplying a load of 403kW is presented in Table 6.3 below.

Table 6.3 Comparison of Energy and Component Parameters between Case 1a and Case 1b

	Case 1a BSS	Case 1b HBS	Unit	% Diff	Comments
Energy Parameters					
Energy from PV	9,695,913	8,887,910	kWh/yr	-8.3	Solar-HBS uses a supercapacitor to increase the storage power density which in turn reduces the peak operating reserve (POR) requirement of the PV panel. The reduction in POR meant that the PV energy production and rated capacity was reduced by 8.3% in Case 1b while supplying the same load.
AC Primary Load	1,812,617	1,811,744	kWh/yr	0.0	
Capacity Shortage	938	1,420	kWh/yr	51.4	The shortage percentage found in HOMER, calculates the fraction of accumulated unmet energy compared to the total energy demand over an entire year. The percentage found was below 0.0008% of the load in both solar-RES cases. This shows a near perfect power security in Case 1a and 1b which concurs with the large amounts of PV power being produced to ensure supply.
Unmet Load	546	1,420	kWh/yr	160.1	
Shortage Percentage	3e-4	7e-4	%	160.0	
Renewable Penetration	100	100	%	0.0	
PV Parameters					
Rated Capacity	6,000	5,500	kW	-8.3	A 6MW PV panel is deemed adequate for solar-BSS while the solar-HBS PV panel is rated at 5.5MW due to the POR reduction explained above. Both cases use the same type of PV panel hence the capacity factor remains uniform. Primary energy is solely produced by PV panels while the battery supplies the backup power when needed.
Mean Output	1,107	1,015	kW	-8.3	
Daily Mean Output	26,565	24,351	kWh/d	-8.3	
Capacity Factor	18.4	18.4	%	0.0	
Total Production	9,695,913	8,887,910	kWh/yr	-8.3	
Minimum Output	0	0	kW	0.0	Case 1a contains a BSS with a lower power density than the HBS thus making it more reliant on PV panels for discharge and adequately supplying the load profile with all its variations; hence its PV penetration and maximum power output from PV is higher than Case 1b.
Maximum Output	6,073	5,567	kW	-8.3	
PV Penetration	533	489	%	-8.3	
Hours of Operation	4,380	4,380	hr/yr	0.0	The solar irradiance profile of Napier resulted in PV panels only being on for half the hours of the day.
Daily on time	12	12	hours	0.0	
Battery Parameters					
String Size	100	100	units	0.0	The same size battery was used in both cases. However, the cost of the HBS storage was found to be higher due to the addition of supercapacitors.
Strings In Parallel	12	12	units	0.0	
Batteries	1,248	1,248	units	0.0	
Bus Voltage (V)	200	200	V	0.0	200V battery bus voltage is specified and adhered to in both cases. This is set to ensure supply of the 240V single phase AC load voltage.
Nominal Capacity	7,488	7,488	kWh	0.0	
Usable Nom Cap	5,242	5,242	kWh	0.0	
Autonomy	25.2	25.2	hr	0.0	This represents the rated battery maximum lifespan.
Lifetime Throughput	12,724,608	12,724,608	kWh	0.0	This shows the amount of energy passing through the battery for the entire 25 year simulation. Energy throughput can cause the battery to reach the end of its lifespan before the rated time.
Battery Wear Cost	0.174	0.174	$/kWh	0.0	Cost of allowing a single kWh of energy to pass through the battery for discharge or charge. According to [51] and [168], supercapacitor maintenance is considered negligible and it can operate for over 500 000 cycles with extremely long lifespans. Hence their O & M and replacement costs

					are not included in the price model [3], [47], [73].
Energy In	**1,146,859**	**1,150,374**	kWh/yr	0.3	Case 1b is more reliant on its storage devices due to its reduced PV panel capacity; this is reflected by the increase in HBS energy absorbed and discharged when compared to the BSS.
Energy Out	**988,214**	**991,222**	kWh/yr	0.3	
Losses	158,751	159,244	kWh/yr	0.3	A smaller PV panel is used in Case 1b which means the system now relies more on storage devices; thus the annual throughput of the HBS is increased.
Annual Throughput	**1,065,186**	**1,068,430**	kWh/yr	0.3	
Expected Life	11.9	11.9	yr	0.0	In Case 1 PV panels are only on for 12 hours of the day, storage devices autonomously supply power to the entire load for the rest of the time. As a result, expected battery lifespan is reduced to 11.9 years.
Average SOC Max	80	80	%	0.0	
Average SOC Min	60	60	%	0.0	
Converter Parameters					
Capacity	600	400	kW	-33.3	Converter power ratings are relatively small compared to the rest of the system. Case 1b shows a capacity decrease but generates the same mean output. This means the solar-BSS converter is oversized to accommodate the POR power.
Mean output	208	208	kW	0.0	
Minimum output	0	0	kW	0.0	
Maximum output	369	369	kW	0.0	
Hours of operation	8,758	8,753	hrs/yr	-0.1	
Energy in	1,849,027	1,848,137	kWh/yr	0.0	The smaller converter in Case 1b discharges slightly less energy, since less energy is sent in.
Energy out	1,818,665	1,817,791	kWh/yr	0.0	
Losses	30,362	30,346	kWh/yr	-0.1	Converter losses are relatively equal.
Capacity factor					
PV Ave Cap Used	1107	1015	kW	-8.3	The average PV capacity shows the same 8.3% rated capacity difference between cases 1a and 1b.
PV Capacity Ratio	18.4	18.4	%	0.0	
Usable Battery Cap	5,242	5,242	kWh	0.0	This is based on the percentage of usable battery capacity over the nominal capacity specified by the manufacturer. The same battery was used meaning the capacity ratio will remain the same in all cases
Battery Cap Ratio	70.01	70.01	%	0.0	
Conv Ave Cap Used	208	208	kW	0.0	Case 1b converter was sized accurately because of the reduced POR. This shows an error in the HOMER HBS model since the Case 1b converter would require the same rated power as Case 1a for the supercapacitor to discharge through. Fortunately, the converter is the cheapest component and would not affect the economic study results substantially.
Converter Cap Factor	34.6	51.9	%	50.0	
Input Energy					
Bat Daily Energy	3142.08	3151.71	kWh/d	0.3	More solar energy can be used for HBS charging in Case 1b instead of being in the operating reserve (OR)
Conv Daily Energy	5065	5063	kWh/d	0.0	
Output Energy					
PV Daily Energy	26565	24351	kWh/d	-8.3	An 8.3% reduction in PV output energy is seen for Case 1b, due to lower OR and an increased reliance on storage devices.
Conv Daily Energy	4982.64	4980.25	kWh/d	0.0	
Bat Daily Energy	2707.44	2715.68	kWh/d	0.3	
Energy Losses					
Battery	158,751	159,244	kWh/yr	0.3	Both solar RES cases yield negligible energy losses showing effective power security.
Converter	30,362	30,346	kWh/yr	-0.1	
Total	189113	189590	kWh/yr	0.3	
Power Output					

PV Average	1,107	1,015	kW	-8.3	Maximum PV power spike in solar-BSS is 1kW larger than that in solar- HBS. This shows that a larger OR is required in Case 1a because the supercapacitor in the HBS can alleviate these fluctuations in Case 1b whereas this is not possible for the battery in BSS.
PV Maximum	6,073	5,567	kW	-8.3	
Converter Average	208	208	kW	0.0	
Converter Max	369	369	kW	0.0	
Efficiency					
Battery	86.12	86.17	%	0.1	Battery efficiency is recorded at 86% which is in line with the ratings specified by the datasheet[163]. This results in a combined storage to conversion efficiency of 84.7% for both cases [163].
Converter	98.37	98.37	%	0.0	
Combined	84.71	84.77	%	0.1	
Life Throughput					
Project Lifetime	25	25	Years	0.0	This is equal to the duration of the simulation
PV daily on hours	12	12	Hours	0.0	Battery lifespan is reduced due to the increased reliance on storage due to limited PV power availability in a day.
Bat Expected Life	11.9	11.9	Years	0.0	
Battery Autonomy	25.2	25.2	Hours	0.0	
Converter on hours	23.994	23.980	Hours	-0.1	

Table 6.3 presents the technical results of the optimum solar-BSS and solar-HBS systems. Their electrical results are now interpreted in terms of system feasibility, component sizing and electrical performance.

During isolated solar RES operation, a substantial fraction of PV power capacity must be held in reserve in case of resource fluctuations. A 25% operating reserve (OR) factor, as confirmed in Chapter 5, is allocated for all isolated solar generation systems. This reserve factor is used to compensate for any irradiance reduction or disturbances caused by shading or cloud cover etc. [35], [52], [53], [57], [152]–[158]. The operating reserve demand means that the rated maximum PV power must be increased in order to keep enough energy in reserve; this is known as the peak operating reserve (POR). In Case 1a, the secondary power supply is provided by the BSS which contributes to the required operating reserve but the load parameters show that the battery power density is not high enough to effectively reduce the POR value. Hence the supply of peak load power relies considerably on solar PV generation in Case 1a while having to maintain a larger reserve power capacity. In Case 1b the POR required by the solar panel is therefore reduced on including a high power density supercapacitor with the battery. The reduced POR means the rated PV capacity in Case 1b could be reduced by 500kW but still successfully supply the load.

In terms of electrical performance, both systems match the load and maintain over 99.9992% of the annual energy demand for the duration of the simulation. Power security in both cases is extremely high which strongly validates the feasibility of solar RES.

The AC load is supplied by a DC storage device and DC PV generation source. Hence, a constant DC-AC energy conversion is required to maintain load power supply. Fortunately, the selected converter has an efficiency of over 98.5%, which means the switching losses are minimised. Unlike the converter, PV panels only operate for 12 hours of the day. At times of low solar irradiance, the storage devices are called upon which yields an increase in storage device energy throughput. This is necessary but not economically ideal when considering the 0.174 $/kWh wear cost of batteries used. In addition to the wear cost, the increased energy throughput means the batteries lifespan is reduced from 25.2 rated years

to 11.9 years. Lifespan extension properties of the supercapacitor in Case 1b cannot be accurately modelled in HOMER.

HOMER successfully models a highly efficient solar-RES using two different energy storage schemes. The power security and system efficiency is at an exceptional range and the anticipated capacity of components is deemed acceptable. The only operational concern noted is the systems' constant reliance on a converter for AC load supply. A recommendation which can be made is the potential inclusion of an AC based storage device or a dual active bridge converter design which could allocate modules during converter failures. The impact this concern has on the overall operation will be put into context in section 6.2 when an AC WECS is used to directly supply the load. The high power density of the supercapacitor solar-HBS is indeed beneficial in terms of components sizing. HOMER cannot model its lifespan extension properties but the feasibility can still be confirmed based on the economic performance analysis observed in the following section.

6.1.4 Analysis of Economic Results for Case 1

The price of the optimised system is important in establishing its feasibility. Based on the optimised component parameters found for the solar RES, the following economic results are presented and explained in Table 6.4 in terms of replacement, capital, salvage and net present costs.

Table 6.4 Comparison of Economic Parameters between Case 1a and Case 1b

	Case 1a - BSS	Case 1b- HBS	Unit	% Diff	Comment
General Cost Parameters					
Total NPC	15,578,569	14,512,069	$	**-6.8**	The total NPC considers the overall cost required for system for its installation and operation over the 25 years simulation. The NPC values of over $14.5 million does seem high initially but when put into the context of a 25 year generation scheme capable of supplying a 407kW load, this value does make sense. The solar-HBS used in Case 1b shows substantial savings compared to the solar-BSS. This is attributed to the reduced component sizes (mostly PV panels) required when POR demands to cater for load fluctuation or peak loads are allocated to the supercapacitor.
Levelised COE	0.672	0.627	$/kWh	**-6.7**	Both cases show a COE of under 0.7 $/kWh which is relatively cheap for an isolated RES. Case 1b shows a 6.7% decrease in COE which amounts to a $1 million saving in the total NPC for the project lifespan.
O & M Cost	100,667	100,507	$/yr	-0.2	Maintenance cost is exceptionally low in both cases as PV panels simply require water cleaning [39], [40].
System Cost Types					
Capital	14,291,712	13,227,250	$	**-7.4**	The reduction in initial capital can impact most of the savings in the long run for the HBS. The significant reduction in capital can draw potential investors.
Replacement	1,579,563	1,568,297	$	-0.7	
O & M	167,206	164,650	$	-1.5	
Salvage	-459,912	-448,127	$	-2.6	The aforementioned capital decline in Case 1b was as

System	15,578,569	14,512,069	$	-6.8	a result of reduced POR requirements. This brought about a decline in the required replacement costs as well. Since fewer panels were used (and replaced) the salvaged cost benefits observed are lower in Case 1b. However, the reduction in Case 1b capital still results in a total NPC saving of over $1 million.
Capital					
PV Panels	12,000,000	11,000,000	$	**-8.3**	Case 1a has a lower storage capital cost since no supercapacitor bank is purchased. However, PV panel and converter savings in the solar-HBS largely outweigh its additional supercapacitor cost; hence a 7.4% overall capital reduction is observed in Case 1b.
Battery	2,051,712	2,067,250	$	**0.8**	
Converter	240,000	160,000	$	**-33.3**	
System	14,291,712	13,227,250	$	**-7.4**	
Replacement					
PV Panels	0	0	$	0.0	The simulation parameters enforced a 100% power security; hence PV panel capacity was increased. As a result of this large capacity, the energy throughput was distributed amongst panels. This meant the average energy passing through a single panel was low hence they are not replaced. The supercapacitor used in Case 1b has a lifespan of over 500 000 cycles, since it is used in a bank the supercapacitor is not replaced over the simulation period hence the storage replacement cost is uniform for both cases. Solar-BSS uses a larger converter which slightly increases replacement cost.
Battery	1,532,792	1,537,116	$	0.3	
Converter	46,771	31,181	$	-33.3	
System	1,579,563	1,568,297	$	-0.7	
Operation & Maintenance					
PV Panels	0	0	$	0.0	Replacement and maintenance cost profiles are strongly linked. This is why the PV and storage O & M costs are the same as in Case 1a and 1b. A 1.5% reduction in Case 1b overall O & M costs is found since it requires a smaller converter.
Battery	159,536	159,536	$	0.0	
Converter	7,670	5,113	$	-33.3	
System	167,206	164,650	$	-1.5	
Salvaged					
PV Panels	0	0	$	0.0	The solar-BSS has 2.6% more salvaged cost savings since it deployed and replaced a larger converter.
Battery	-433,700	-430,653	$	-0.7	
Converter	-26,212	-17,475	$	-33.3	
System	-459,912	-448,127	$	**2.6**	
Levelised costs					
PV Panels	0.0968	0.0968	$/kWh	0.0	Levelised cost of individual components is the same since this value is aggregated as a ratio. The system COE is different as it considers the total NPC and magnitude of components. What is noted here is that a unit (kWh) of PV based energy is far cheaper than a unit for battery energy.
Battery wear cost	0.174	0.174	$/kWh	0.0	
System	0.672	0.627	$/kWh	**-6.7**	
Total Net Present Cost					
PV Panels	12,000,000	11,000,000	$	**-8.3**	PV panel initial capital is the biggest contributing cost of the total NPC. Panel maintenance is cheap but its large initial capital can easily discourage investment. Using a HBS does pose an indirect solution to the initial capital problem. Including a supercapacitor

					means that the secondary storage device can reduce the operating reserve peak ratings hence allowing for fewer PV panel cells to be used. This is demonstrated by the $1 million savings seen in the NPC.
Battery (super capacitor)	3,310,341	3,333,250	$	**0.7**	The second biggest contribution to the total NPC is made by the battery bank. The HBS brings a supercapacitor capital increase of $22 900 which is well worth the observed PV savings. Especially considering the fact that it does not need to be replaced over the project lifespan.
Converter	268,228	178,819	$	-33.3	The converter is cheap and barely influences cost
System	15,578,569	14,512,069	$	-6.8	The result shows that the additional cost of $22909 for supercapacitor in the HBS is well compensated for by the savings of over $1 million. Despite this overall COE in both solar RES cases can be reduced.

The HBS allows for accurate component sizing, most notably in the PV panels and converter. The initial capital required to start up a solar RES is $13.3 million in Case 1a and $12.3 in the solar-HBS model used in Case 1b. This shows a substantial reduction of 8.3% in the HBS configuration which amounts to a $1 million reduction of the total initial capital cost. The biggest contributor to capital cost is the PV panel price, which means that the reduction in POR (and subsequently in the PV panel capacity) is the main contributor to the savings in Case 1b. The additional supercapacitor cost of $22 909 is far offset by the savings of $1 million observed through the reduction of reserve generation capacity in the solar-HBS.

Replacement, operation and maintenance costs were reduced in the solar-HBS because the smaller components used are cheaper to maintain. Despite the simulation span of 25 years and smaller PV and converter components, the running costs savings observed did not constitute a substantial difference across cases. Case 1a does show the benefit of increased salvaged costs since larger components are being replaced herein.

The high initial capital observed in Case 1 is attributed to the high power security required in a single source isolated generation system. Since no alternative generation source is available the additional capacity required to secure power supply is attributed to more PV panels. The storage devices are used for secondary supply but their unit COE is far more than that for the PV panel power. As a result of these purchases, the systems show initial capital costs of over $14.5 million for the 25 year simulation.

The initial capital does allow for some benefits since the oversized PV panel bank can effectively distribute its energy throughput which meant panels were not replaced or heavily maintained. These cost benefits coupled with the large load supply of 5MWh/d yielded a levelised cost of 0.672 $/kWh for the solar-BSS and 0.627 $/kWh for the solar-HBS.

The HBS is once again the cheaper option but both cases actually pose competitively priced renewable energy based electricity. The total NPC is recorded at $15.57 million for the solar-BSS and $14.51 million for the solar-HBS which is very close to the capital costs mentioned. Based on this results it is clear that if the initial capital is made available the solar RES are indeed feasible and competitively priced once they are established. The HBS is clearly preferred over the BSS when implementing solar based generation.

6.2 Wind RES Optimisation Results of Case 2a and Case 2b

The wind RES technical and economic results are now presented following the same format as section 6.1. Case 2 refers to both wind RES which are divided into two different storage cases viz. BSS in Case 2a and HBS in Case 2b.

6.2.1 Case 2a: Wind-BSS Electric Optimisation Results

Generalised technical and economic parameters for the optimally sized components used in the wind-BSS configuration are shown in Table 6.5.

Table 6.5 Component Size and Net Present Cost for Wind-BSS system (Case 2a)

Component	Electrical Size	Net Present Cost ($)
WES 5 Tulipo	4375 kW	15,744,522
Storage Devices	7,488kWh	2,492,448
Converter	600kW	268,228
Wind-BSS		18,505,196

Storage device cost and capacity is fixed across BSS cases, while the same converter capacity previously deployed in Case 1a was selected here. One of the reasons for this is that a uniform load is used across all cases of the optimisation study. However, the new wind turbine cluster used for generation in Case 2a has an NPC of $15.7 million which is more expensive than the PV panel bank used in Case 1a with an NPC of $12 million. The more expensive wind turbine cluster results in a total NPC of $18.5 million for Case 2a. A NPC cost breakdown is now shown in Figure 6.5, followed by a component cost summary.

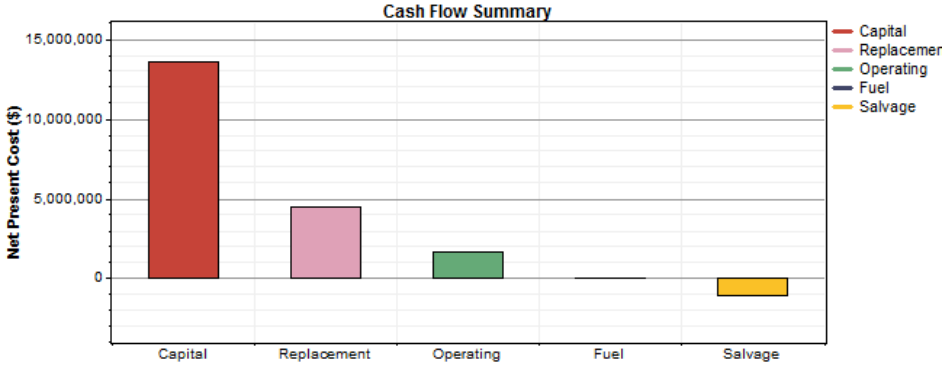

Figure 6.5 NPC cost summary for wind-BSS (Case 2a)

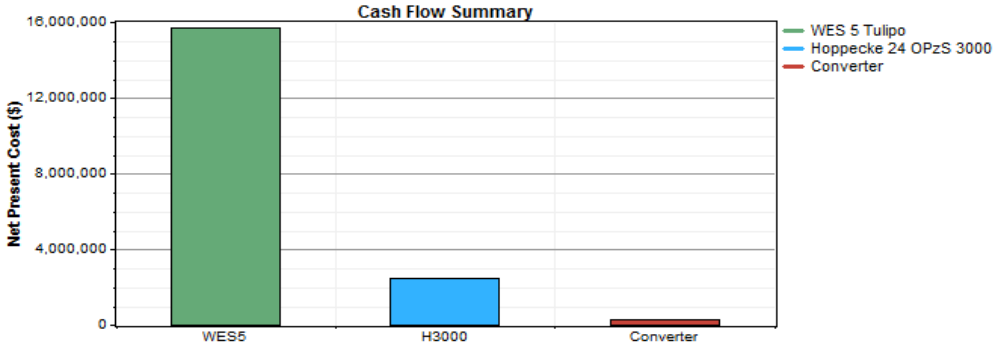

Figure 6.6 Component cost summary for wind-BSS (Case 2a)

Initial capital is still the paramount cost type but the replacement and operation cost in Figure 6.5 is more influential compared to previous cases. A cluster of small scale 2.5kW

wind turbines is used in this system due to the load size, noise reduction and component popularity [162]. The wind turbine cluster constitutes majority of the total NPC in Case 2a. This is due to the increased POR required when working with wind energy. The standard HOMER allocated POR is 50% in the WECS and 25% for solar. Since the same load is used for the optimisation study the optimised converter and battery components remain the same as Case 1a in section 6.1.1.

6.2.2 Case 2b: Wind-HBS Electric Optimisation Results

Generalised technical and economic parameters of the optimised wind-HBS components deployed are shown in Table 6.6.

Table 6.6 Component Size and Net Present Cost for Wind-HBS system (Case 2b)

Component	Electrical Size	Net Present Cost ($)
WES 5 Tulipo	4,375kW	12,245,738
Storage Devices	7,488kWh	2,507,985
Converter	400kW	178,819
Wind- HBS		14,932,543

The wind-HBS total NPC is substantially reduced to $14.9 million compared to the wind-BSS which amounted to $18.5 million. Despite savings across the wind case comparison, the HBS inclusion in the WECS reduced the expensive wind turbine cluster cost making it cheaper than the wind-BSS and the solar-BSS with a total NPC of $15.6 million observed. A cash flow summary of Case 2b is now presented in Figure 6.7 followed by the component cost breakdown in Figure 6.8.

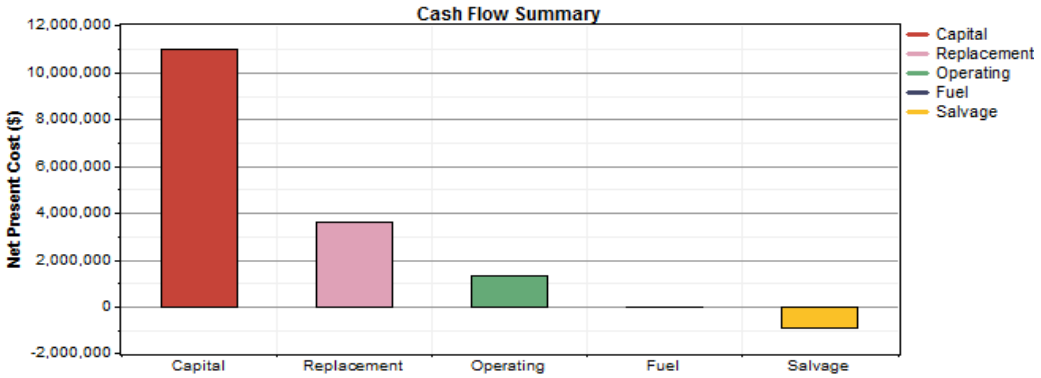

Figure 6.7 NPC cost summary for wind-HBS (Case 2b)

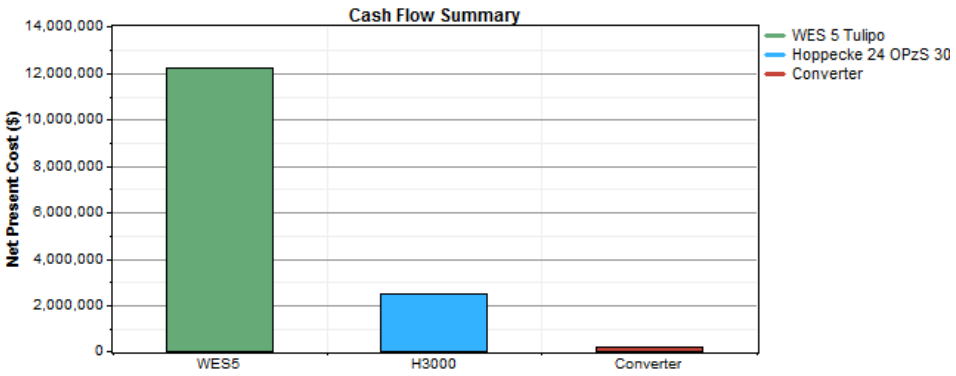

Figure 6.8 Component cost summary for wind-HBS (Case 2b)

Figure 6.7 shows that the initial capital is still the largest cost type, followed by the replacement and operating costs. The component cost breakdown shows that the wind turbine NPC is still the most expensive component in Case 2b but its price has been substantially reduced due to the POR reduction provided by the HBS. This resulted in a NPC saving of $3.6 million compared to the wind-BSS used in Case 2a. The electrical component optimisation results of Case 2a and 2b are now presented and compared.

6.2.3 Analysis of Technical Results for Case 2

The technical results of the optimally sized components used in the wind-HBS and wind-BSS for supply of the 407kW peak load are presented in Table 6.7. The results table and analysis follow the same format as Case 1, as seen in section 6.1.3.

Table 6.7 Comparison of Energy and Component Parameters between Case 2a and Case 2b

	Case 3 BSS	Case 4 HBS	Unit	% Diff	Comment
Energy Parameters					
Energy from WECS	25,474,874	19,810,292	kWh/yr	-22.2	The WECS produces more energy than the PV panels seen in Table 6.3, as it is a more intermittent resource which subsequently requires a larger POR of 50%. In addition, the present study requires 100% power security for all optimisations. Thus, additional wind energy was generated and kept in reserve. The wind-HBS manages to reduce its POR through supercapacitor discharge and subsequently reduces its required energy generation capacity by 22%.
AC Primary Load	1,812,352	1,811,467	kWh/yr	0.0	
Peak Load	346	328	kW	-5	
Capacity Shortage	1,804	1,722	kWh/yr	-4.5	
Unmet Load	816	1,722	kWh/yr	111	
Shortage %	**0.045**	**0.095**	%	111	
Renewable Penetration	100	100	%	0.0	
Wind Turbine Parameters					
Rated Capacity	5,625	4,375	kW	-22.2	The average, maximum and total output power required by the WECS used in Case 2b is reduced by 22.2%, which agrees with the previous POR reduction explanation. Capacity factor is specified by the WES 5 Tulipo manufacture based on an operable supply ratio [162]. The strong wind profile and 100% power security specification means part of the wind turbine cluster is on for 21.6 hours of the day. WECS AC generation makes it ideal for supply of the AC load.
Mean Output	2,908	2,261	kW	-22.2	
Minimum Output	0	0	kW	0	
Maximum Output	5,871	4,566	kW	-22.2	
Capacity Factor	51.7	51.7	%	0.0	
Total Production	25,473,784	19,809,344	kWh/yr	-22.2	
Hours of Operation	7,878	7,878	hr/yr	0.0	
	21.58	21.58	hr/day	0.0	
Battery					
String Size	100	100	units	0.0	Case 2a and 2b use the same battery specifications. The difference in terms of the supercapacitor will be more apparent when considering its additional cost.
Strings In Parallel	12	12	units	0.0	
Batteries	1,248	1,248	units	0.0	
Bus Voltage	200	200	V	0.0	Remains fixed for supply of the 240 AC.
Nominal Capacity	7,488	7,488	kWh	0.0	As anticipated, the reliance on storage is decreased in Case 2 due to the large volumes of available AC WECS energy. Battery wear cost describes the cost of storing and passing energy through the battery. This price will be compared to the wind turbine COE in Table 6.8.
Usable Nom Cap	5,242	5,242	kWh	0.0	
Autonomy	25.2	25.2	hr	0.0	
Lifetime Throughput	12,724,608	12,724,608	kWh	0.0	
Battery Wear Cost	0.174	0.174	$/kWh	0.0	
Energy In	353,041	377,583	kWh/yr	7.0	A smaller turbine cluster is used in the wind-HBS resulting in an increase of storage reliance. This is shown by the larger energy throughput observed.
Energy Out	303,622	324,738	kWh/yr	7.0	
Losses	50,854	54,278	kWh/yr	6.7	
Annual Throughput	327,511	350,268	kWh/yr	6.9	The maximised wind power available for direct load supply for 21.6 hours of the day has reduced battery reliance in Case 2. Thus battery throughput energy is
Expected Life	20.0	20.0	yr	0.0	
Average SOC Max	80	80	%	0.0	

Average SOC Min	60	60	%	0.0	reduced thereby extending its lifespan / replacement time to 20 years instead of 11.9 years seen in Case 1.
Inverter					
Capacity	600	400	kW	-33.3	Wind-HBS uses smaller inverter despite having an 8.8% larger average output inverter power, meaning it is more efficiently sized.
Mean output	**34**	**37**	kW	8.8	
Minimum output	0	0	kW	0.0	
Maximum output	369	369	kW	0.0	The increased load capacity results in an increase in rated WECS capacity which subsequently requires an increase in converter rated capacity. This is why the BSS rating is higher for both components. Despite the larger BSS rated capacity, the HBS converter has a higher throughput which means it is more accurately sized. The HBS POR reduction allows for more WECS energy to be used for storage device charging.
Energy in	303,622	324,738	kWh/yr	7.0	
Energy out	299,153	319,938	kWh/yr	6.9	
Losses	4,469	4,801	kWh/yr	7.4	Once again the increase in HBS throughput results in an increase in converter losses.
Hours of operation	1,554	1,678	hrs/yr	8.0	
Rectifier					
Capacity	600	400	kW	-33.3	The same principle applies for rectifier ratings provided. Case 2b is more reliant on the storage devices, therefore more DC energy is discharged and converted to AC for load power supply, which results in an increased rectifier throughput.
Mean output	40	43	kW	7.5	
Minimum output	0	0	kW	0	
Maximum output	600	400	kW	-33.3	
Hours of operation	7,189	7,063	hrs/yr	-1.8	
Energy in	363,963	389,153	kWh/yr	6.9	
Energy out	353,041	377,583	kWh/yr	7.0	
Losses	10,922	11,570	kWh/yr	5.9	
Capacity Used – Sizing Quality					
WECS Ave Cap Used	2908.13	2261.88	kW	-22.2	Wind-HBS turbine rating is 22.2% smaller than BSS. Battery capacity remains the same for Case 2a and 2b as the supercapacitors technical parameters are illustrated through the POR reduction.
WECS Cap Ratio	51.7	51.7	%	0.0	
Usable Battery Cap	5,242	5,242	kWh	0.0	
Battery Cap Ratio	70.01	70.01	%	0.0	
Inverter Ave Cap Used	34.2	36.4	kW	6.4	Inverter capacity has been explained
Rectifier Ave Cap Used	40.2	43.2	kW	7.5	Rectifier capacity has been explained
Inverter Cap Factor	5.7	9.1	%	59.6	A reduced HBS converter size and increased energy throughput means more of its capacity is being used.
Rectifier Cap Factor	6.7	10.8	%	61.2	
Daily Input Energy					
Battery	967.23	1034.47	kWh/d	7.0	WECS generates at AC which passes through the inverter in order to charge the battery. Conversely, the battery discharges through the rectifier.
Inverter	831.84	889.69	kWh/d	7.0	
Rectifier	997.16	1066.17	kWh/d	6.9	
Daily Output Energy					
Battery	831.84	889.69	kWh/d	7.0	Same principle applies as above with the regard to charge-discharge ratio. A reduction in WECS output power is understandably observed in Case 2b due to a reduced POR.
Inverter	819.6	876.54	kWh/d	6.9	
Rectifier	967.24	1034.47	kWh/d	7.0	
WES	69791	54272	kWh/d	-22.2	
Energy Losses					
Battery	50,854	54,278	kWh/yr	6.7	Despite the increased reliance on the WECS, both cases show losses of below 0.001% of the load energy making them very secure as power supply sources.
Inverter	4,469	4,801	kWh/yr	7.4	
Rectifier	10,922	11,570	kWh/yr	5.9	
Total	66245	70658	kWh/yr	6.7	

Power Output					
WECS Mean	2,908	2,261	kW	-22.2	**Average, maximum and total output power required by the WECS is reduced when using the HBS** in Case 2b. This is a fundamental benefit of POR reduction.
WECS Min	0	0	kW	0	
WECS Max	5,871	4,566	kW	**-22.2**	
Inverter Max	369	369	kW	0.0	The inverter output is the same but the max WECS energy rectified in Case 1a is understandably more.
Rectifier Max	600	400	kW	-33.3	
Efficiency					
Battery	86.00	86.00	%	0.0	Efficiency values are specified by the component manufactures [153], [163]. Excess energy generated ensure that storage and conversion losses are accounted for hence ensuring power supply.
Inverter	98.53	98.52	%	0.0	
Rectifier	97.00	97.03	%	0.0	
Combined	82.19	82.21	%	0.0	
Life Throughput					
Project Lifetime	25	25	years	0.0	The WECS generates for 21.58 hours per day, reducing storage reliance and increasing its lifespan to 20 years. Which is an improvement on the storage reliant PV cases which requires battery replacement every 11 years.
WES daily on time	21.58	21.58	hours	0.0	
Bat Expected Life	20	20	years	0.0	
Battery Autonomy	25.2	25.2	hours	0.0	
Invert daily on time	4.26	4.6	hours	8.0	
Rectifier daily on time	19.7	19.35	hours	-1.8	

The optimised electrical components used in Case 2a and 2b were presented and compared, based on the overall electrical performance of using an isolated WECS connected with either a BSS or HBS. As done in Case 1b, the wind-HBS supercapacitor is employed in order to reduce the POR required by the generation source. As a result, Case 2b shows a 22% decrease in wind turbine capacity when compared to Case 2a. The reduction of POR in Case 2b results in a WECS power rating decrease of 1250kW. The wind-HBS uses 500 fewer turbines than the BSS. Despite this reduction, the wind-HBS still generates more energy than the PV panels in Case 1 since wind power requires a 25% higher operating reserve.

The WECS benefits from a strong wind speed profile and extended generation time of 21.58 hours a day, while posing the convenience of direct connection to the load via an AC bus. These benefits have increased the Case 2 reliance on WECS energy and reduced the need for expensive battery energy. However, this is accompanied by more turbine replacement and maintenance. The converter is used on a near continuous basis in Case 2 despite the direct AC connection between load and WECS. This is because storage devices are still frequently used for charging and discharging. In Case 2a the wind-BSS required a higher rated converter to successfully interface the battery and WECS. The HBS had a lower WECS power rating hence it is connected to a smaller converter.

The use of the HBS does show an improvement in component sizing whilst maintaining power security and system efficiency. Both WECS cases supply 99.999% of the load but are oversized to compensate for operating reserve. Based on the electrical results the wind-HBS is feasible but an increase in storage power density (through supercapacitor) will make this RES more practical for deployment.

6.2.4 Analysis of Economic Results for Case 2

The economic impact of the wind-RES optimisation study is now presented in explained and analysed in Table 6.8.

Table 6.8 Wind Generation Economic Parameters Comparison Tables of Case 2a and Case 2b

	Case 2a BSS	Case 2b HBS	Unit	% Diff	Comment
General System Parameters					
Total NPC	**18,505,196**	**14,932,543**	$	-19.3	The large wind turbine capacity makes Case 2a wind - BSS the most expensive RES seen thus far in terms of total NPC. The HBS used in Case 2b shows a 19.3% reduction in total NPC. This results in a total of $3.5 million saved over the 25 year project due to the initial wind turbine capacity reduction.
Levelised COE	**0.799**	**0.645**	$/kWh	-19.3	The high NPC is reflected in Case 2a through its COE of 0.799 $/kWh. It is clear that battery storage connected to an islanded WECS is impractical for load supply. The wind-HBS capacity reduction provides a competitive price of 0.645 $/kWh, which is cheaper than the solar-BSS used in Case 1a but still slightly higher than the solar-HBS.
Operating Cost	**388.28**	**309.41**	$/yr	-20.3	Wind turbines are rotating for 21.58 hours of the day which results in component strain. This makes Case 2 more expensive to maintain compared to stationary PV panels.
System Cost Types					
Capital	13,541,712	10,977,250	$	-18.9	Initial capital still constitutes majority of the NPC but turbine replacement and maintenance shows increased significance in Case 2. These costs are reduced in Case 2b as it requires less WECS POR capacity. This does mean more components are salvaged in Case 2a. Overall a total NPC saving of $3.5 million is seen when using the wind-HBS.
Replacement	4,441,894	3,591,773	$	-19.1	
O & M	1,605,335	1,283,194	$	-20.1	
Salvage	-1,083,744	-919,674	$	15.1	
System	18,505,196	14,932,543	$	-19.3	
Capital					
WECS	**11,250,000**	**8,750,000**	$	-22.2	WECS constitutes majority of the capital savings in Case 2b. While the battery and converter differences are the same as Case 1. Case 2 has more accumulated costs. Hence, its initial capital is lower which can attract potential investors.
Battery	2,051,712	2,067,250	$	0.8	
Converter	240,000	160,000	$	-33.3	
System	13,541,712	10,977,250	$	-18.9	
Replacement					
WECS	3,755,389	2,920,858	$	-22.2	The battery and converter are the same as Case 1 (Refer to Table 6.4). WECS contributes 85% of the replacement costs incurred. If the turbine lifespan is extended, Case 2 feasibility will increase.
Battery	639,734	639,734	$	0.0	
Converter	46,771	31,181	$	-33.3	
System	**4,441,894**	**3,591,773**	$	-19.1	
Operation & Maintenance					
WECS	1,438,128	1,118,544	$	-22.2	O & M costs of wind turbines contribute to the total NPC but should not be reduced. An increase in O & M investment may extend WECS lifespan, resulting in total NPC savings.
Battery	159,536	159,536	$	0.0	
Converter	7,670	5,113	$	-33.3	
System	1,605,335	1,283,194	$	-20.1	
Salvaged					
WECS	-698,997	-543,664	$	-22.2	The wind-BSS shows an increase in salvaged costs due to its increased generation capacity.
Battery	-358,535	-358,535	$	0.0	
Converter	-26,212	-17,475	$	-33.3	

System	-1,083,744	-919,674	$	-15.1	
Levelised costs					
WECS	0.0483	0.0484	$/kWh	0.2	The WECS shows a very low unit COE at 0.0484 $/kWh which is 3.6 times cheaper than a unit of battery energy. This emphasizes the increased reliance on the WECS energy in Case 2.
Battery wear cost	0.174	0.174	$/kWh	0.0	
System	0.799	0.645	$/kWh	**-19.3**	
Total Net Present Cost					
WECS	15,744,522	12,245,738	$	-22.2	Total NPC of the wind-HBS is indeed more feasible but turbine lifespan must be extended to increase system feasibility. This can be done through improved maintenance and a larger reduction of WECS POR by using a larger supercapacitor bank.
Battery	2,492,448	2,507,985	$	0.6	
Converter	268,228	178,819	$	-33.3	
System	18,505,196	14,932,543	$	-19.3	

a) Economic Results Analysis of Case 2

Table 6.8 has illustrated the economic impact of the components selected in the HOMER based wind RES optimisation study. The total NPC required for operating a wind-BSS is substantially high at $18.5 million over 25 years. This is mainly attributed to the WECS purchase, replacement and maintenance costs which translates to a COE of 0.799 $/kWh for Case 2a. Despite the strong winds observed in Napier and the convenience of direct AC supply to the load, the oversized wind-BSS of Case 2a is impractical for isolated RES.

The wind-HBS used in Case 2b showed substantial NPC savings of $3.5 million when compared to the wind-BSS. The total NPC in Case 2b is reduced by 22% to $14.9 million by simply using a supercapacitor bank to compensate for the high WECS POR capacity. The POR reduction meant that the wind turbine cluster capacity was reduced which resulted in a more competitive COE of 0.645 $/kWh. Case 2b is cheaper than the solar-BSS with a COE of 0.672 $/kWh but still higher than the solar-HBS at 0.627 $/kWh.

The large cluster of wind turbines provided a very cheap cost of unit throughput energy generated at 0.0484 $/kWh, once it was established. This was almost 3.6 times cheaper than using battery energy at a cost of 0.174 $/kWh. This factor coupled with the electrical benefits (of AC bus supply and 21.6 hour on time) substantially increased the reliance on the WECS in Case 2. As a result, turbines required more replacements (of $3.5 million for BSS and $2.9 million for HBS over 25 years) and had maintenance costs of roughly $0.3 million per year. Once it is established the wind turbine cluster generates the cheapest energy at 0.0484 $/kWh compared to the PV COE of 0.0968 $/kWh. Despite the lower COE observed in the solar-HBS, the WECS has lower initial capital costs which may be more attractive to investors which favours the feasibility of the wind-HBS.

6.3 Hybrid Wind & Solar RES Optimisation Results

The final case combines the benefits of solar and wind resources available in Napier by constructing a hybrid PV - WECS generation model. The results are presented and analysed in the same format and considers the hybrid-BSS in Case 3a and hybrid-HBS as Case 3b.

6.3.1 Results for Case 3a: Hybrid-BSS

Technical and economic parameters used for the optimised hybrid-BSS are shown in Table 6.9.

Table 6.9 Component Size and Net Present Cost for Hybrid-BSS system (Case 3a)

Component	Electrical Size	Net Present Cost ($)
PV Array	1000kW	2,000,000
WECS	625kW	1,749,391
Storage Devices	7,488kWh	2,492,448
Converter	600kW	268,228
Hybrid-BSS		6,510,067

The results of Table 6.9 show a substantial reduction in generation capacity with a 1MW PV bank, 625kW WECS and fixed 7.5kWh battery required to supply the same 407kW rated load. The reduced WECS and PV capacity resulted in a total NPC of $6.5 million in the hybrid-BSS. Despite using two generation sources the hybrid-BSS out ranks its closest competition (the solar-HBS of Case 1b) by the $8 million in total NPC. The component cost summary for the hybrid-BSS of Case 3a is now presented in Figure 6.9, followed by the breakdown of total NPC component costs in Figure 6.10.

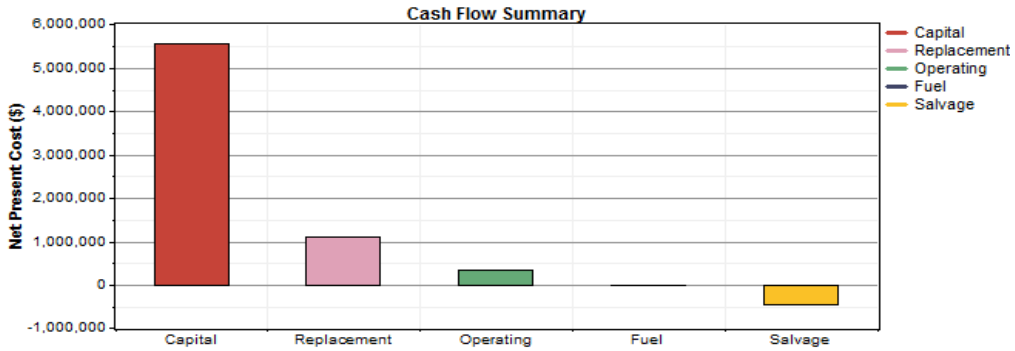

Figure 6.9 NPC cost summary for hybrid-BSS (Case 3a)

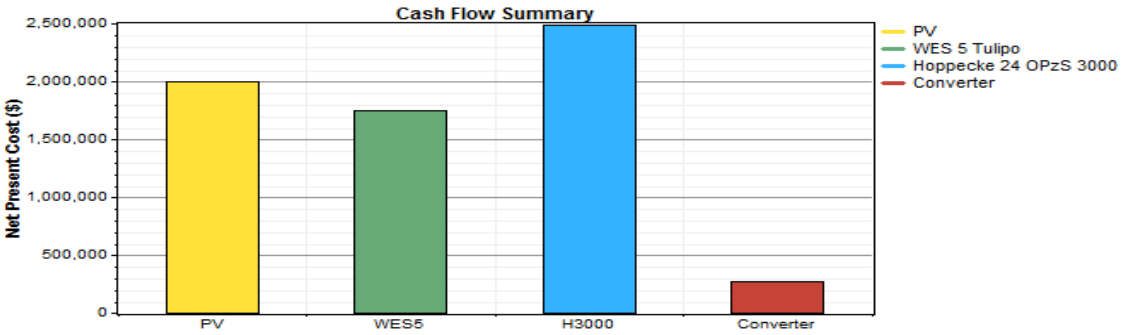

Figure 6.10 Component cost summary for hybrid-BSS (Case 3a)

The largest cost type is the initial capital, followed by replacement cost and then salvaged funds regained. Figure 6.10 puts the Case 3a savings into perspective when comparing the scale of the present fixed battery price to previous cost summaries of Figure 6.1 and 6.5. Despite remaining fixed the battery price is now the largest component cost, this shows the relative reduction in PV and WECS costs for the hybrid-BSS. The monthly average electric production is now presented to survey the PV panel - wind turbine generation ratio.

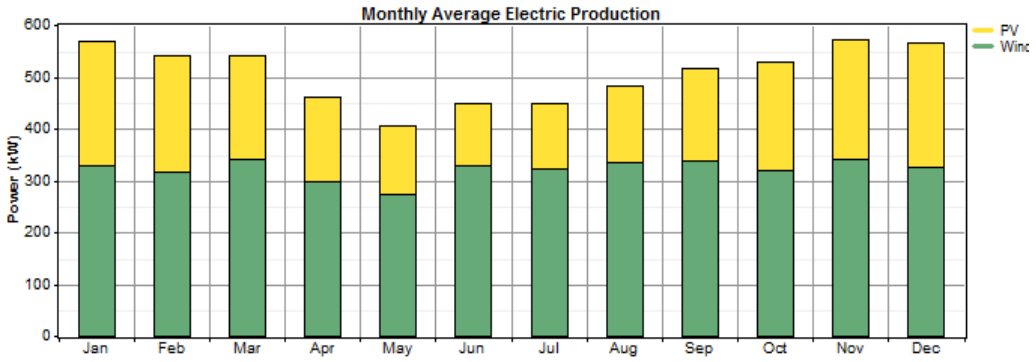

Figure 6.11 Monthly Average Electric Production In terms of Wind and PV power of Case 3a

The hybrid RES must allocate energy based on resource availability, electrical parameters and price of energy. Figure 6.11 shows the influence of seasonal changes on generation capacity. WECS generation is relatively constant but in the summer months PV generation becomes cheaper and is therefore relied upon more. By exploiting resource availability the required energy can be generated at the cheapest possible times.

6.3.2 Results for Case 3b: Hybrid-HBS

Technical and economic parameters for the last case of the optimum hybrid-HBS configuration are shown in Table 6.10.

Table 6.10 Component Size and Net Present Cost for Hybrid-HBS system (Case 3b)

Component	Electrical Size	Net Present Cost ($)
PV Array	750kW	1,500,000
WES	625kW	1,749,391
Storage Devices	7,488kWh	2,492,448
Converter	400kW	178,819
Hybrid-HBS		5,936,195

Table 6.10 confirms a further reduction in generation component capacity for the hybrid-HBS through POR reduction provisions of the supercapacitor. Case 3b shows a $0.6 million NPC reduction of the already cheap Case 3a. This is done by reducing the PV bank capacity to 750kW which is 25% lower than the hybrid-BSS. The very low WECS capacity of 625kW has remained the same in Case 3a and 3b. A component cost summary and a breakdown of NPC components is now shown for the last case in Figures 6.3 and 6.4 respectively.

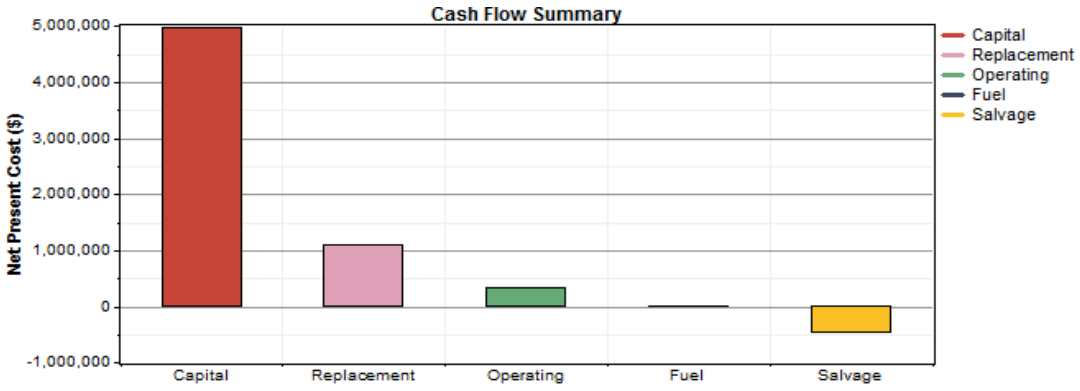

Figure 6.12 NPC cost summary for Hybrid-HBS (Case 3b)

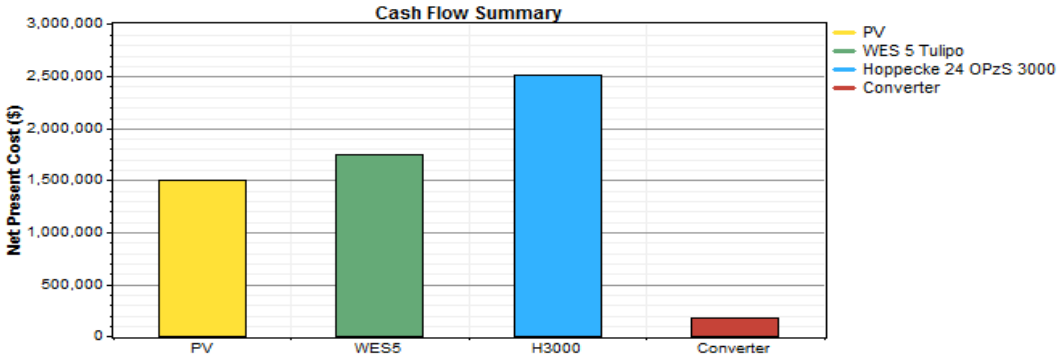

Figure 6.13 Component cost summary for Hybrid-HBS (Case 3b)

The cash flow summary for Case 3b strongly aligns with the cash flow layout of Case 3a. Figure 6.13 shows the first time that the battery price is far higher than the price of generation components. Despite acquiring a larger PV power capacity the WECS was still responsible for the primary load in Case 3a. The new generation ratio is presented for Case 3b in Figure 6.14.

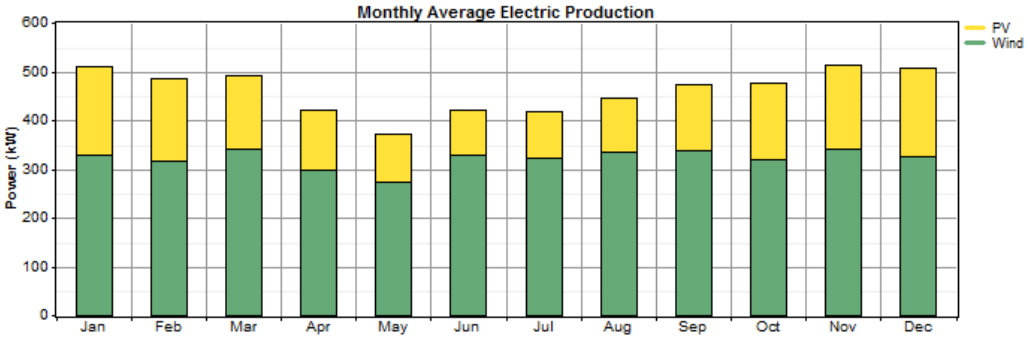

Figure 6.14 Monthly Average Electric Production In terms of Wind and PV power of Case 3b

The monthly average electricity layout shows the influence of season variations on RES. For the hybrid-HBS, the WECS is once again used as the primary power supply with the solar PV panel bank mainly used as a secondary supply. The same WECS capacity is used here in Case 3b but its influence on generation ratio has increased compared to the hybrid-BSS.

6.3.3 Analysis of Technical Results for Case 3

Based on the electrical observations made the electrical components selected and system parameters are now shown in specific detail below. It is important to note that this table considers a PV and wind generation for both cases hence an alternative means of supply is readily available before the storage device is required.

Table 6.11 Comparison of Energy and Component Parameters between Case 3a and Case 3b

	Case 3a - BSS	Case 3b - HBS	Unit	% Diff	Comment
Electrical Parameters					
WECS Production	2,829,183	2,829,183	kWh/yr	0.0	WECS capacity is considerably reduced compared to cases 1a-2b. Interestingly, Case 3a and 3b have identical WECS generation capacities and are predominantly wind power based, despite deploying more PV power. This is because of the increased WECS on time of 21.6 hours compared to
WES Energy ratio	64	70	%	9.4	
PV Production	1,616,016	1,211,989	kWh/yr	-25	
PV Energy ratio	36	30	%	-16.7	
AC Primary Load	1,813,163	1,811,773	kWh/yr	-0.1	

Capacity Shortage	0.00	1,397	kWh/yr	0.0	PV on time of 12 hours a day. Additionally, wind energy is cheaper once established at 0.0484 $/kWh compared to PV COE of 0.0968 $/kWh. Both cases generate the same amount of WECS energy but it constitutes 64% of hybrid-BSS generated capacity and 70% of hybrid-HBS. This is because of the HBS POR reduction, which allows for a 250kW reduction in PV capacity, thus 70% of the Case 3b load is provided by wind power. Case 3a and 3b show that an effectively sized combination of generation sources can be used to maintain a power security of 100%.
Unmet Load	0.0134	1,397	kWh/yr	10e6	
Shortage percentage	0.0	0.08	%	0.0	
Renewable Penetration	100	100	%	0.0	
PV Parameters					
Rated Capacity	1,000	750	kW	-25.0	Rated PV capacity is substantially reduced in Case 3a by at least 5000kW compared to single source generation cases and further reduced by 250kW in Case 3b, relative to hybrid generation cases. In Case 3 the rated PV capacity is higher than the WECS but is still used as the secondary supply source due to its limited on time. The combination of generation sources means energy can be produced at the cheapest possible off peak rates [13], [169]. A major contributor to the reduced Case 3 component sizes is the fact that the secondary generation source i.e. PV power can act as an operating reserve while the WECS is being used and vice versa while also reducing reliance on the more expensive storage device energy.
Mean Output	184	138	kW	-25.0	
Daily Mean Output	4,428	3,321	kWh/d	-25.0	
Capacity Factor	18.4	18.4	%	0.0	
Total Production	1,616,016	1,211,989	kWh/yr	-25.0	
Minimum Output	0	0	kW	0.0	
Maximum Output	1,012	759	kW	-25.0	
Hours Of Operation	4,380	4,380	hr/yr	0.0	
Wind Turbine Parameters					
Rated Capacity	625	625	kW	0.0	The WECS is already AC based which makes it easier to supply the AC load. As a result it is used as the primary power producer. HBS POR improvements are seen through reduced PV capacity requirements while the (primary source) WECS capacity remains the same for both cases.
Mean Output	323	323	kW	0.0	
Capacity Factor	51.7	51.7	%	0.0	
Total Production	2,829,962	2,829,962	kWh/yr	0.0	
Minimum Output	0	0	kW	0.0	
Maximum Output	652	652	kW	0.0	
Hours Of Operation	7,878	7,878	hr/yr	0.0	
Battery					
String Size	100	100	units	0.0	The observed storage component ratings are the same as Case 1a and Case 2a for the hybrid-BSS and Case 1b and 2b for the hybrid-HBS. Refer to Table 6.3 and 6.7. Storage device energy throughput of Case 3 is more than wind Case 2 but less than solar Case 1. The PV RES operates at DC hence it easily connected with the battery, thus increasing battery throughput. In Case 2 the WECS prefers to directly supply the load and only connects with the battery via converter. Since Case 3 uses both generation sources and its reliance on the battery is in-between.
Strings In Parallel	12	12	units	0.0	
Batteries	1,248	1,248	units	0.0	
Bus Voltage (V)	200	200	V	0.0	
Nominal Capacity	7,488	7,488	kWh	0.0	
Usable Nominal Cap	5,242	5,242	kWh	0.0	
Autonomy	25.2	25.2	hr	0.0	
Lifetime Throughput	12,724,608	12,724,608	kWh	0.0	
Battery Wear Cost	0.174	0.174	$/kWh	0.0	
Energy In	539,454	555,713	kWh/yr	3.0	
Energy Out	463,974	477,938	kWh/yr	3.0	
Losses	76,895	79,187	kWh/yr	3.0	
Annual Throughput	500,350	515,402	kWh/yr	3.0	
Expected Life	20.0	20.0	yr	0.0	
Average SOC Max	100	100	%	0.0	
Average SOC Min	80	80	%	0.0	
Inverter					

Capacity	600	400	kW	-33.3	The HBS to BSS capacity ratio remains the same in Case 3 but what is interesting is the energy throughput observed. The inverter shows a 645kWh/yr AC-DC energy conversion. This means the AC WECS is charging the storage devices more than the devices are discharging throughout the year.
Mean output	73	73	kW	0.0	
Minimum output	0	0	kW	0.0	
Maximum output	369	369	kW	0.0	
Hours of operation	3,501	3,496	hrs/yr	-0.1	
Energy in	647,311	645,892	kWh/yr	-0.2	
Energy out	637,644	636,237	kWh/yr	-0.2	
Losses	9,668	9,655	kWh/yr	-0.1	
Rectifier					
Capacity	600	400	kW	-33.3	Maximum output converter power required shows a 31% increase in Case 3a at 579kW. This is the sole reason behind the 33.3% increase in the Case 3a converter capacity. This shows the importance of reducing the peak power demand via HBS supercapacitor inclusion.
Mean output	24	28	kW	16.7	
Minimum output	0	0	kW	0.0	
Maximum output	579	400	kW	-30.9	
Hours of operation	2,821	2,989	hrs/yr	6.0	
Energy in	213,674	249,891	kWh/yr	16.9	Only 210kWh/yr of DC energy is converted to the AC load which once again shows that Case 3 is predominantly WECS based.
Energy out	207,255	242,407	kWh/yr	17.0	
Losses	6,419	7,484	kWh/yr	16.6	
Capacity Used – Sizing Quality					
WECS Cap Ratio	51.7	51.7	%	0.0	The Hoppecke wind turbine is used thus the capacity ratio is specified by the manufacture[163].
Usable Bat Cap	5,242	5,242	kWh	0.0	Same capacity and battery cells are used in the battery banks of both cases.
Battery Cap Ratio	70.01	70.01	%	0.0	
Inverter Ave Cap Used	34.2	36.4	kW	6.4	Understandably, more power is being is used to charge the batteries than for discharge.
Rectifier Ave Cap Used	40.2	43.2	kW	7.5	
Inverter Cap Factor	5.7	9.1	%	59.6	HBS in Case 3b is sized more accurately than the BSS converter used in Case 3a.
Rectifier Cap Factor	6.7	10.8	%	61.2	
Daily Input Energy					
Battery	1477.96	1522.50	kWh/d	3.0	More DC energy is being inverted for discharge by the PV panels and battery to the load.
Inverter	1773.46	1769.57	kWh/d	-0.2	
Rectifier	585.41	684.63	kWh/d	16.9	
Daily Output Energy					
Battery	1271.16	1309.42	kWh/d	3.0	Once again only noteworthy energy difference here is the increased inverter energy throughput used for power supply via DC energy sources. Case 3a discharges 25% more PV energy per day compared to Case 3b. This aligns with the PV generation difference mentioned.
Inverter	1746.97	1743.12	kWh/d	-0.2	
Rectifier	567.82	664.13	kWh/d	17.0	
PV	4427.44	3320.52	kWh/d	-25.0	
WECS	7753.32	7753.32	kWh/d	0.0	
Energy Losses					
Battery	76,895	79,187	kWh/yr	3.0	The capacity shortage observed is still below 0.0001% of the required energy which shows an effective security of power supplied.
Inverter	9,668	9,655	kWh/yr	-0.1	
Rectifier	6,419	7,484	kWh/yr	16.6	
Total	92,982	96,326	kWh/yr	3.6	
Power Output					
PV Average	184	138	kW	-25.0	HBS improvements are illustrated through the reduced maximum PV power required in Case 3b. WECS capacity remains the same for each case while the reserve energy is found through battery or hybrid storage and PV panels.
PV Maximum	1,012	759	kW	-25.0	
WECS Average	323	323	kW	0.0	
WECS Maximum	652	652	kW	0.0	
Inverter Average	73	73	kW	0.0	The inverter average power shows that more PV and

Inverter Maximum	369	369	kW	0.0	battery power is being transferred to the load for discharge. However, the maximum power is higher in the rectifier since the AC is the highest rated energy source.
Rectifier Average	24	28	kW	16.7	
Rectifier Maximum	579	400	kW	-30.9	
Efficiency					
Battery	86	86	%	0.0	All overall efficiency is the same in terms of electrical energy in and out. The HOMER software is clearly limited in terms of dynamic electrical output modelling but the sizing and costing is more informative for this study.
Inverter	98	98	%	0.0	
Rectifier	97	97	%	0.0	
Combined	81.8	81.8	%	0.0	
Life Throughput					
Project Lifetime	25	25	years	0.0	Despite using a smaller power rated WECS it supplies majority of the load due to the 21.6 hour operational time instead of the limited 12 hours seen in the PV power.
WECS daily on time	21.58	21.58	hours	0.0	
PV daily on time	12	12	hours	0.0	
Battery Expected Life	20	20	years	0.0	Reliable wind power and a secondary PV supply reduces battery throughput thus allowing for a 20 year lifespan
Battery Autonomy	25.2	25.2	hours	0.0	
Inverter daily on time	9.59	9.57	hours	-0.2	More DC energy being converted for storage and PV discharge at wind power shortages i.e. operating reserve.
Rectifier daily on time	7.73	8.19	hours	6.0	

Case 3 shows electrical capacity reductions of at least 5000kW in both PV and WECS rated power when compared to Case 1 and 2. Hybrid generation has allowed for effective resource deployment and component sizing whilst maintaining a 100% power security. The alternative energy source acts as the operating reserve which prevents components from being oversized while minimising the reliance on expensive storage device energy.

The WECS has been designated as the primary power producer responsible for 64-70% of renewable energy generated. The WECS was selected as the primary source for the following reasons: it is directly connected to the AC bus for load supply; it can generate for 21.6 hours per day (instead of the 12 hours of PV power) and had the lowest component throughput COE at 0.0484 $/kWh which is half the price of the PV COE.

Short PV operating hours contributed to an increased reliance on storage in Case 1. Similar to Case 2, the hybrid generation system used in Case 3 is more wind power based which meant the off times were reduced; hence a decrease in storage reliance was observed. The ideal benefit of using PV energy was the fact that the peak load demand times strongly aligned with the daily irradiance profile. This makes the present hybrid RES cases exceptionally feasible.

The observed peak power of the battery bank based on the usable nominal capacity is 105kW while the supercapacitor banks usable peak power is 500kW. Supercapacitor inclusion leads to an increase in power density and subsequent reductions in the POR required usually by generation sources. By reducing this rating, the HBS allowed for smaller generation capacity as illustrated through a 250kW PV panel capacity reduction.

More energy was rectified than inverted since the DC power of the PV panel and battery could be used to supply the load. The inverter was still rated higher in both storage devices cases since the AC WECS rated power used as the inverter input was higher than the storage and panel ratings. Despite the same WECS capacity being used here a smaller converter was deployed in the hybrid-HBS of Case 3b.

Table 6.11 shows that the hybrid-HBS will improve electrical sizing through PV panels and converter sizes. However, it has been discovered that a far more practical component reduction takes place by effectively combining and deploying generation sources as done in

Case 3. This result confirms that both hybrid generation cases are indeed very feasible for deployment based on its impressive resource allocation strategy. The economic impact of hybrid generation is evaluated in section 6.3.4.

6.3.4 Analysis of Economic Results for Case 3

Electrical sizing results of Case 3 showed substantial reductions in the required generation capacity. Based on previous results it is well established that generation capacity is the pertinent contributing factor to the total NPC. The anticipated cost reductions and economic feasibility of the new hybrid RES is presented in Table 6.12.

Table 6.12 Comparison of Economic Parameters between Case 3a and Case 3b

	Case 3a - BSS	Case 3b - HBS	Unit	% Diff	Comment
General System Parameters					
Total NPC	**6,510,067**	**5,936,195**	$	-8.8	Total NPC in both hybrid RES cases are substantially reduced compared to the single source generation systems (Cases 1a - 2b). The hybrid-HBS used in Case 3b shows a cost reduction of $0.6 million compared to Case 3a due to a 25% reduction in required PV panel capacity.
Levelised COE	**0.281**	**0.256**	$/kWh	-8.9	The cost of energy has plummeted to under 0.3 $/kWh in both cases. The hybrid-HBS (Case 3b) maintains an 8.9% lower COE than the already cheap hybrid-BSS case.
Operating Cost	75,751	75,015	$/yr	-1.0	Both hybrid systems are cheap to operate once they are established.
Complete System Cost Types					
Capital	**5,541,712**	**4,977,250**	$	-10.2	The initial capital constitutes the largest contribution to total NPC as shown in Figure 6.9 and 6.12. Case 3b has a 250kW reduction in PV capacity resulting in a total NPC of $5.9 million. This is the cheapest RES observed in the RES optimisation study.
Replacement	1,103,770	1,088,180	$	-1.4	
O & M	326,998	324,442	$	-0.8	
Salvage	-462,414	-453,676	$	1.9	
Whole System	**6,510,067**	**5,936,195**	**$**	**-8.8**	
Capital					
PV	**2,000,000**	**1,500,000**	$	-25	As anticipated, PV constitutes the largest cost difference between Case 3a and 3b. Interestingly, the PV panels generate less energy but are more expensive than the WECS.
WECS	1,250,000	1,250,000	$	0.0	
Battery	2,051,712	2,067,250	$	0.8	
Converter	240,000	160,000	$	-33.3	
System	5,541,712	4,977,250	$	-10.2	
Replacement					
PV	0	0	$	0.0	Replacement cost is similar in Case 3a and 3b since their only differentiating components (supercapacitor and PV panels) did not reach the end of lifespan. The battery discharged up to 13% of the load but is cost more to replace than the WECS which supplies 64%.
WECS	417,265	417,265	$	0.0	
Battery	639,734	639,734	$	0.0	
Converter	46,771	31,181	$	-33.3	
System	1,103,770	1,088,180	$	-1.4	
Operation & Maintenance					
PV	0	0	$	0.0	WECS and battery are the major contributors to maintenance costs because of the large WECS energy throughput, and strict SOC limits of lead acid batteries. Since their capacities are the same in Case 3a and 3b the O & M cost between them is the same.
WECS	159,792	159,792	$	0.0	
Battery	159,536	159,536	$	0.0	
Converter	7,670	5,113	$	-33.3	
System	326,998	324,442	$	-0.8	

Salvaged					
PV	0	0	$	0.0	Not replaced yet so nothing needs to be salvaged.
WECS	-77,666	-77,666	$	0.0	The same observation is made when comparing the salvaged cost amongst hybrid generation components. This is because the salvaged price benefits are directly related to the replacement costs.
Battery	-358,535	-358,535	$	0.0	
Converter	-26,212	-17,475	$	-33.3	
System	-462,414	-453,676	$	-1.9	
Levelised costs					
PV	0.0968	0.0726	$/kWh	-25	As previously mentioned, COE in Case 3 is remarkably lower than any other case. Battery wear cost is far more expensive than the generation components per unit kWh. This explains the substantial COE reduction observed in Case 3 when a generation source is used as the secondary power supply instead of a storage device.
WECS	0.0484	0.0484	$/kWh	0.0	
Battery wear cost	0.174	0.174	$/kWh	0.0	
System	0.281	0.256	$/kWh	-8.9	
Total Net Present Cost					
PV	2,000,000	1,500,000	$	-25	PV capacity difference yields 25% savings for the HBS
WECS	1,749,391	1,749,391	$	0.0	WECS supplies primary load in both cases.
Battery	2,492,448	2,507,985	$	0.6	Case 3b shows minor HBS improvements on generation capacity but both cases are exceptionally feasible with competitive RES prices.
Converter	268,228	178,819	$	-33.3	
System	**6,510,067**	**5,936,195**	**$**	**-8.8**	

The importance of hybrid storage implementation in islanded RES applications has been well established in the literature review and in the results of Cases 1a-2b [82], [135], [170]. However, in Case 3 it is made abundantly clear that **hybrid generation is far more important to islanded RES** as it makes use of the wealth of available renewable resources found in Napier. A brief comparison and ranking of the NPC and COE of each case is shown in Table 6.13 below.

Table 6.13 NPC and COE comparison for 5MWh average load

Case Number	NPC ($)	COE ($/kWh)	Ranking
Case 1a : Solar- BSS	15,578,569	0.672	5th
Case 1b : Solar- HBS	14,512,069	0.627	3rd
Case 2a : Wind- BSS	18,505,196	0.799	6th
Case 2b : Wind- HBS	14,932,543	0.645	4th
Case 3a : Hybrid- BSS	6,510,067	0.281	2nd
Case 3b : Hybrid- HBS	5,936,195	0.256	1st

Table 6.13 compares the COE and total NPC of each case and confirms the success of Case 3b. The HBS storage device reduced the required generation capacity in each case considered but the savings observed through effective hybrid generation is far more substantial. Since the additional generation source is used as a power supply and operating reserve source, the components deployed in Case 3 are accurately sized and maintain accurate power security.

WECS is selected as the primary power producer and allows for a cheaper baseline supply (at 0.0484$/kWh) and an effective way of deploying using PV power during the daytime peak commercial-residential load demand hours [57], [126]. Furthermore, by restricting PV panel capacity to 30%, the initial capital costs are reduced to $5.5 million for Case 3a and $4.9 million for Case 3b. This allows for a cheaper PV supply (at 0.0968 $/kWh) and

minimised the use of expensive storage device energy at 0.174$/kWh. The storage devices are still essential to power supply as their removal would once lead to oversized components used for POR. In Case 3b the HBS manages to reduce the operating reserve peak which allows for smaller sized PV panels. This then reduces the converter capacity since storage and PV panels are DC operators. The electrical results shown in Table 6.3, 6.7 and 6.11 show that the supercapacitors simply reduce the peak reserve power requirements by 200-300kW but in this case translates to a total NPC saving of $0.6 million.

Hybrid generation yields a total NPC of between $6.5 million in the BSS and $5.9 million for the HBS over a 25 year period, which is very attractive to potential investors. This makes it the most feasible solution observed thus far. It is important to note that the following optimisation study only considers the 5MWh average daily load with a peak power of 407kW. However, a more generalised body of knowledge is now presented across all sensitivity loads (1-10MWh/d).

Sensitivity Analyses Results

The optimisation study considered all six cases performance across a single 407kW rated load. The same optimisation is now conducted across 14 different loads to provide a wider test matrix of results; this is known as a sensitivity analysis. The results of the sensitivity analysis will undoubtedly establish the feasibility of islanded RES deployment with storage in remote areas. Firstly the electrical results are presented in table format and then shown in MS Excel plots. After which the economic results are presented and analysed.

6.4 Electrical Results of the Sensitivity Analysis for all Cases

The technical results of the optimised components are presented in the sensitivity analysis.

6.4.1 PV Capacity Used

PV panel capacity has the largest influence on a systems initial capital since it represents majority of the panel cost. The capacity used for each case is now illustrated in Figure 6.15.

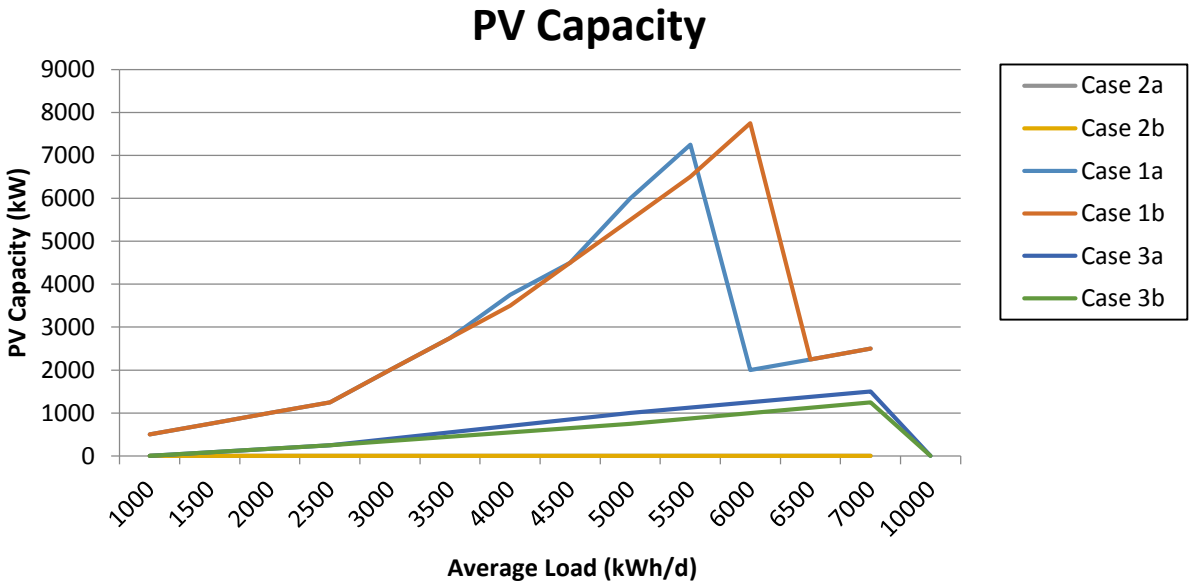

Figure 6.15 PV Capacity Comparisons of Cases

Solar irradiance exposure is only available for 12 hours a day consequently, restricting PV panel generation time. The wind turbine and PV capital cost per kW are closely aligned but more panels are required to generate the same amount of WECS energy per day. Thus hybrid RES seen in Case 3a and 3b have higher PV power ratings (compared to the WECS) but they are only responsible for generating 30-36% of the renewable energy. Restricted on time also means the island PV systems in Case 1 are more reliant on storage devices thus increasing battery replacement and the purchase of battery energy at 0.174 $/kWh.

Once the load demand is too high for the BSS or HBS battery to supply power, the oversized battery is deployed as an indication of battery supply failure. It is clear that the solar-HBS battery reached failure after the solar-BSS, which means its supercapacitor contributions to POR and high power discharge, extended the battery range of operation. This means a smaller battery can be used to supply a larger load in Case 1b. The PV capacity

difference between Case 1a and 1b shows that the solar-HBS also requires fewer panels to meet load demand.

Improvements of the solar-HBS are cancelled out when using an oversized battery, thus the PV capacity is equally sized after battery failure is reached in Figure 6.15. The figure also shows that HBS provisions before the 3.5MWh/d load are unnecessary since the power capacity is enough to supply the load and maintain a sufficient operating reserve. The HBS shows substantial technical benefits but they are only apparent when deployed with the load capacity is kept in mind.

6.4.2 Wind Turbines Capacity

Wind turbine power capacity is now compared at different loads in Figure 6.16.

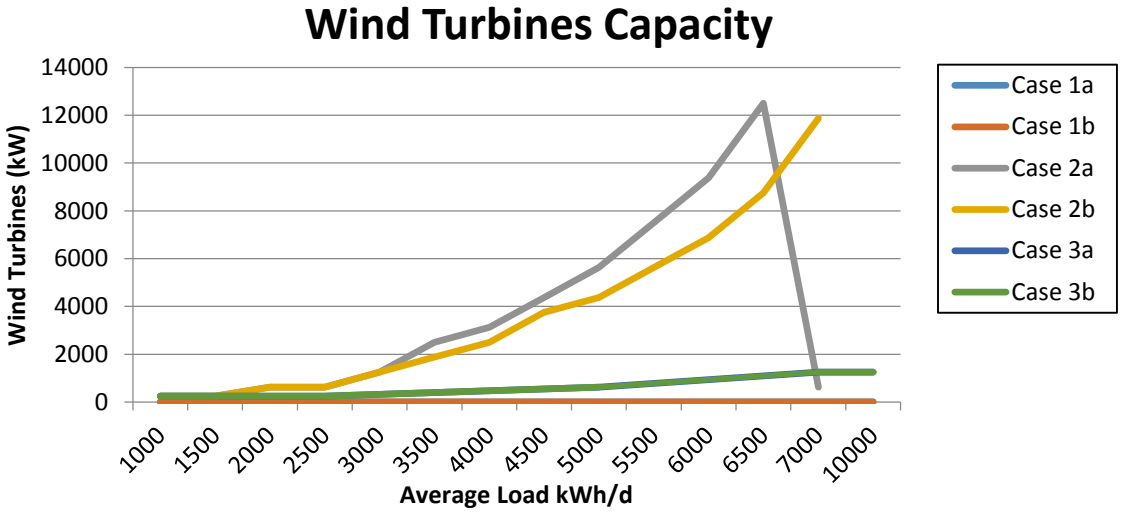

Figure 6.16 Wind Turbine Generation Capacity Comparison of cases

The wind turbine capacity presented in Figure 6.16 shows that the wind-BSS has the largest amount of power since it needs to maintain the 50% operating reserve demand. From the average load of 3.5MWh/d onwards the HBS begins to show capacity reductions in the wind-HBS, eventually reaching a reduction of up to 2MW in Case 2b. The hybrid-HBS reduced its PV capacity in Figure 6.15, thus wind turbine capacity was the same for Case 3a and 3b as confirmed by matching blue and green curves in Figure 6.16.

The point of battery failure is reached at a 6.5MWh/d load for the wind-BSS. However, the wind-HBS battery successfully supplied the load for the entire sensitivity region of 0-7MWh/d. This extension shows how substantial the HBS contribution to wind energy is.

6.4.3 Converter Capacity

Converter capacity is now compared at different loads in Figure 6.17.

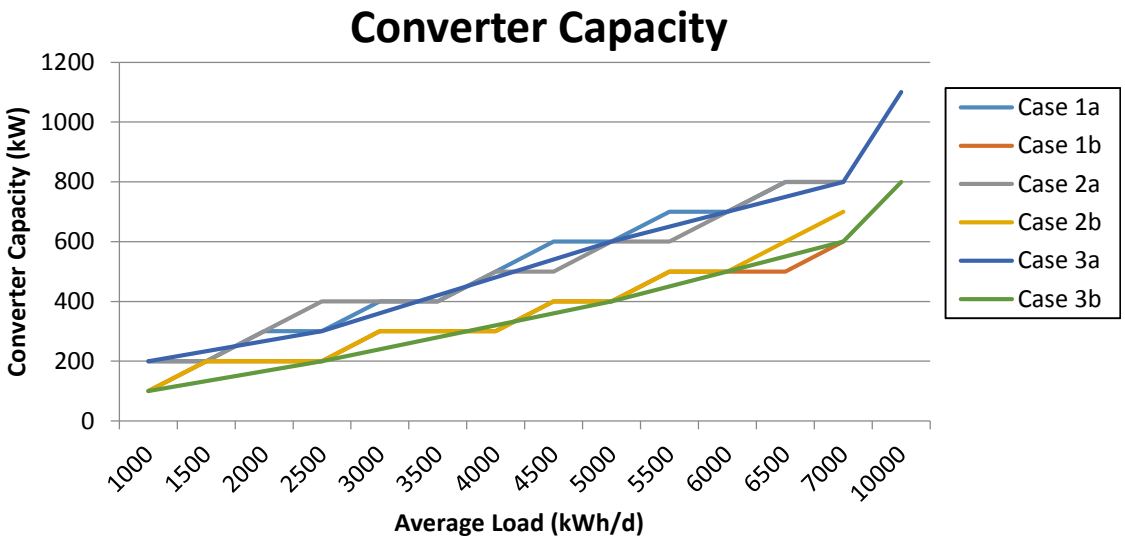

Figure 6.17 Converter capacity Comparison of cases

Figure 6.17 show that all BSS cases have capacity curves which lay slightly above their HBS counterpart. Using the HBS instead of the BSS shows an average reduction of 100kW in converter capacity. The converters are sized based on the peak capacity of the generation source. In Case 1, the PV panel required a larger rectifier (for DC-AC conversion) and in Case 2, the inverter capacity (AC-DC) was based on the WECS power rating. Furthermore, the energy throughput was not as influential as rated capacity when sizing the converter which shows the importance of reducing the rated power required.

6.4.4 Annual Battery Throughput

Annual battery throughput describes the mass of accumulated energy being transferred through the battery in a single year. This will shed light on the battery lifespan and failure observations, as well as the systems reliance on storage as illustrated in Figure 6.18.

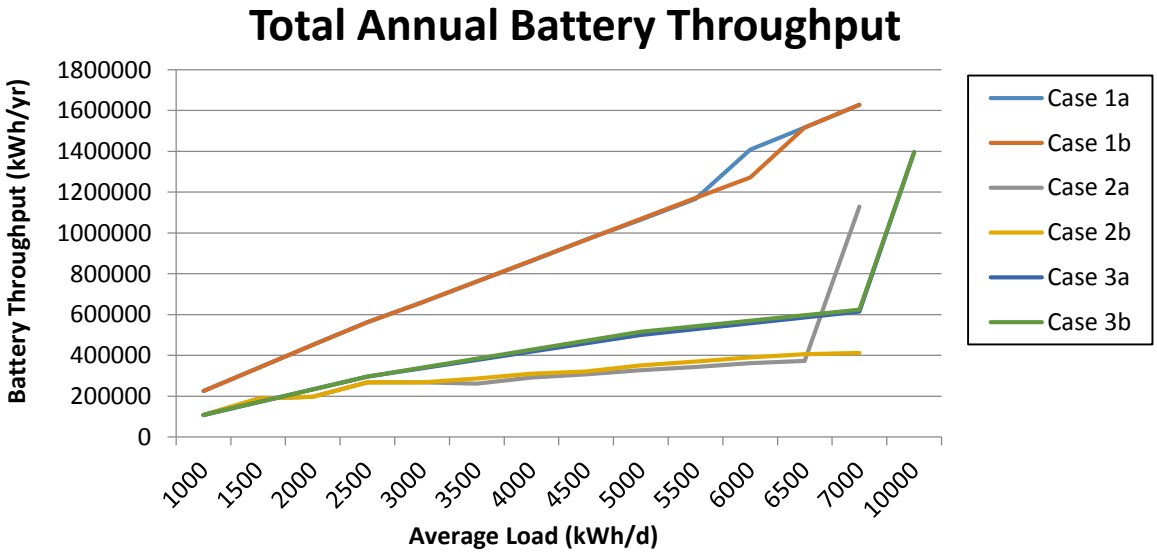

Figure 6.18 Comparison of Total Annual Battery Throughput Energy

It is important to note that supercapacitor cost is allocated in the battery model but its electrical properties on the system are modelled through a reduction of operating reserve requirements. Therefore total battery throughput curves of Figure 6.18 strictly show battery energy discharge.

Islanded PV cases show a constant increase in battery throughput due to the high reliance on storage. This enforces the purchase of expensive battery energy while increasing the replacement and O & M demands of the battery. In Case 2a and 2b, battery throughput is minimised, since the WECS is not as reliant on storage since it is AC based and operates for 21 hours per day, hence it can easily supply the load with minimum storage intervention. The wind-BSS only reaches supply failure at 6.5MWh/d and the wind-HBS further extends the battery supply to beyond the 7MWh/d simulation. All other cases reach battery failure at a specific load which can be seen by the sudden jump in annual battery throughput.

It is important to distinguish between battery supply failure and battery replacement. Battery replacement must takes place when cycle life or accumulated energy throughput capacity is reached, while battery failure, refers to when the battery deployed in HOMER is simply too small to meet the required power demands of the system. This is shown in Figure 6.18 through the sudden spikes in energy. It is has not reached the end of its total energy throughput capacity or cycle life but is simply too small to alleviate the load. As a result the battery energy spikes in Figure 6.18 when the oversized battery is deployed. The HBS manages to delay battery failure thereby extending the battery supply region.

The battery supply region extension facilitated by the HBS can bring about great capacity reductions and can reduce the reliance on more expensive storage energy. The hybrid-HBS in Figure 6.18 shows an effective distribution of power supply across sources as it exploits the benefits of the HBS for POR reduction but also restricts its storage device deployment to times when the WECS and PV panels cannot provide power. This results in the most effective deployment and sizing of generation and storage devices.

6.4.5 Overall Electrical Results Presentation

A sensitivity analysis was conducted at different loads varying from 1MWh/d to 7MWh/d for single source generation systems (case 1a-2b) while five the hybrid generation cases are modelled across 1MWh/d to 10MWh/d as presented in Table 6.14.

Table 6.14 Summary of Electrically Optimised components across all Load Sensitivity Analysis

Case		Load kWh/d													
		1000	1500	2000	2500	3000	3500	4000	4500	5000	5500	6000	6500	7000	10e3
PV Cells (kW)	1a	500	750	1000	1250	2000	2750	3750	4500	6000	7250	2000	2250	2500	X
	1b	500	750	1000	1250	2000	2750	3500	4500	5500	6500	7750	2250	2500	X
	2a	X	X	X	X	X	X	X	X	X	X	X	X	X	X
	2b	X	X	X	X	X	X	X	X	X	X	X	X	X	X
	3a	1	N/A	N/A	250	N/A	N/A	N/A	N/A	1000	N/A	N/A	N/A	1500	1
	3b	1	N/A	N/A	250	N/A	N/A	N/A	N/A	750	N/A	N/A	N/A	1250	1
WECS (kW)	1a	X	X	X	X	X	X	X	X	X	X	X	X	X	X
	1b	X	X	X	X	X	X	X	X	X	X	X	X	X	X
	2a	250	250	625	625	1250	2500	3125	4375	5625	7500	9375	12500	625	X
	2b	250	250	625	625	1250	1875	2500	3750	4375	5625	6875	7500	11875	X
	3a	250	N/A	N/A	250	N/A	N/A	N/A	N/A	625	N/A	N/A	N/A	1250	1250
	3b	250	N/A	N/A	250	N/A	N/A	N/A	N/A	625	N/A	N/A	N/A	1250	1250
Storage Device (units)	1a	1248	1248	1248	1248	1248	1248	1248	1248	1248	1248	20e3	20e3	20e3	X
	1b	1248	1248	1248	1248	1248	1248	1248	1248	1248	1248	1248	20e3	20e3	X
	2a	1248	1248	1248	1248	1248	1248	1248	1248	1248	1248	1248	1248	20e3	X
	2b	1248	1248	1248	1248	1248	1248	1248	1248	1248	1248	1248	1248	1248	X
	3a	1248	N/A	N/A	1248	N/A	N/A	N/A	N/A	1248	N/A	N/A	N/A	1248	20e3
	3b	1248	N/A	N/A	1248	N/A	N/A	N/A	N/A	1248	N/A	N/A	N/A	1248	20e3
Converter (kW)	1a	200	200	300	300	400	400	500	600	600	700	700	800	800	X
	1b	100	200	200	200	300	300	300	400	400	500	500	500	600	X
	2a	200	200	300	400	400	400	500	500	600	600	700	800	800	X
	2b	100	200	200	200	300	300	300	400	400	500	500	600	700	X
	3a	200	N/A	N/A	300	N/A	N/A	N/A	N/A	600	N/A	N/A	N/A	800	1100
	3b	100	N/A	N/A	200	N/A	N/A	N/A	N/A	400	N/A	N/A	N/A	600	800

HBS deployment is especially beneficial in single source generation cases (1a, 1b, 2a, 2b). This is because the optimisation study of each case was forced to maintain a 100% power security in HOMER i.e. fully meet all load power demands. For the RES to ensure constant supply it required a cheap form of reserve off peak energy. However, the battery used here had an energy throughput wear cost of 0.174 $/kWh which was more expensive than PV energy at 0.0968 $/kWh or WECS energy at only 0.0484 $/kWh. The single source generation systems which used the BSS therefore increased generation capacity to maintain power security and meet operation reserve demands. The single source HBS cases used the supercapacitor to increase the peak power storage capacity which reduced the peak operating reserve requirements of the PV or WECS. By reducing the POR in wind-HBS and solar-HBS, the hybrid storage cases brought great capital reductions in single generation source Cases 1b and 2b. Sizing improvements are observed from 3.5MWh/d in the wind-HBS used in Case 2b, at 4MWh/d in the solar-HBS used in Case 1b and at 5MWh/d for the hybrid-HBS of Case 3a. The operating reserve progressively influences the generation capacity as the load increases. The WECS was not very reliant on the storage device as an energy

generation source but benefitted most from the supercapacitor peak power supply in Case 2b. The first generation capacity reduction was seen in Case 2b at 3.5MWh/d since the WECS required the largest operating reserve. The capacity reduction due to the HBS inclusion was the smallest in Case 3b since the WECS and PV components deployed were already effectively sized in the hybrid-BSS. This was because the secondary power supply was already considered an operating reserve source when not supplying the load.

The optimisation region where the sized battery reaches failure is highlighted in red; at this point the battery bank employed was incapable of supplying the load. The battery supply failure point was compared for the HBS and BSS battery across all cases. Table 6.14 shows that for every generation source (PV, WECS or Hybrid) the BSS battery reached supply failure load by one sensitivity increment before its respective HBS connected alternative. The HBS connection maximises the potential supply region of the battery by compensating for infrequent high power density demands with the supercapacitor. The fixed battery capacity of 1248 cells managed to effectively supply most of the load sensitivities tested (up until 6-10MWh/d), showing that it was adequately sized for majority of the study.

For the present set of electrical results it is clear that HBS deployment strongly benefits the sizing of components in single source generation systems. However, the benefits of multi-source generation through hybrid-BSS and hybrid-HBS are far more substantial. This is due to the cheaper unit COE observed for PV panels and WECS when compared to the battery. The principal benefit of hybrid storage was the ideal interfacing of both generation systems this was illustrated by allocating PV power during peak daytime demand hours and the WECS for the baseline generation hours. The results show that the hybrid-HBS used in Case 3b is the most feasible deployment strategy in terms of its technical benefits. The economic results are now presented.

6.5 Economic Results of Sensitivity Analysis

The different electrical component sizes for optimised system were found for all cases and load sensitivities in section 6.3. The economic impact of these components are now explained in terms of RES deployment feasibility.

6.5.1 Layout of Economic Results of Sensitivity Analysis

The sensitivity analysis has revealed that the economic breakdown of all costs surrounding the 6 different case studies. Each case was compared based on component sizes and now the resultant economic cost types of each system is presented across varying loads. Table 6.15 below compares these parameters allowing for clear illustration on the significance of different energy resources and the importance of the storage device coupled with it. As observed in the Table 6.15 the highlighted block will indicate when the sized battery used reaches supply failure.

Table 6.15 Economic Results of Optimised Components for Each Case in the Sensitivity Analyses

Case		Load kWh/d													
		1000	1500	2000	2500	3000	3500	4000	4500	5000	5500	6000	6500	7000	10000
Capital ($)	1a	3131712	3631712	4171712	4671712	6211712	7711712	9751712	11291712	14291712	16831712	37160000	37700000	38200000	N/A
	1b	3107250	3647250	4147250	4647250	6187250	7687250	9187250	11227250	13227250	15267250	17767250	37829000	38369000	N/A
	2a	2631712	2631712	3421712	3461712	4711712	7211712	8501712	11001712	13541712	17291712	21081712	27371712	34450000	N/A
	2b	2607250	2647250	3397250	3397250	4687250	5937250	7187250	9727250	10977250	13517250	16017250	19807250	26097250	N/A
	3a	2631712	N/A	N/A	3171712	N/A	N/A	N/A	N/A	5541712	N/A	N/A	N/A	7871712	35820000
	3b	2607250	N/A	N/A	3147250	N/A	N/A	N/A	N/A	4977250	N/A	N/A	N/A	7307250	35949000
Replacement ($/yr)	1a	22533	22533	22801	22801	27064	42803	57774	72535	87587	105453	354397	354665	354665	N/A
	1b	22265	22533	22533	22533	26796	42535	57604	71999	87627	105609	122304	353861	354129	N/A
	2a	33160	33160	49367	49635	76201	129332	156166	209297	262697	342394	422359	555456	381230	N/A
	2b	32892	33160	49099	49099	75933	102498	129064	182464	209029	262429	315560	395525	528622	N/A
	3a	33160	N/A	N/A	33428	N/A	N/A	N/A	N/A	50171	N/A	N/A	N/A	77273	408600
	3b	32892	N/A	N/A	33160	N/A	N/A	N/A	N/A	49635	N/A	N/A	N/A	76737	407796
O & M ($/yr)	1a	12680	12680	12780	12780	12880	12880	12980	13080	13080	13180	200700	200800	200800	N/A
	1b	12580	12680	12680	12680	12780	12780	12780	12880	12880	12980	12980	200500	200600	N/A
	2a	17680	17680	25280	25380	37880	62880	75480	100480	125580	163080	200680	263280	213300	N/A
	2b	17580	17680	25180	25180	37780	50280	62780	87880	100380	125480	150480	188080	250680	N/A
	3a	17680	N/A	N/A	17780	N/A	N/A	N/A	N/A	25580	N/A	N/A	N/A	38280	226100
	3b	17580	N/A	N/A	17680	N/A	N/A	N/A	N/A	25380	N/A	N/A	N/A	38080	225800
Annual Cost ($/yr)	1a	280197	319310	361921	401034	525866	658945	833598	968929	1218660	1435323	3462001	3504612	3543725	N/A
	1b	277915	320526	359639	398752	523584	656663	789072	963150	1135231	1312896	1525158	3513599	3556209	N/A
	2a	256710	256710	342316	345813	482663	756361	896707	1170405	1447601	1858148	2272192	2959935	3289441	N/A
	2b	254428	257925	340035	340035	480381	617230	754079	1031274	1168124	1445319	1719017	2133062	2820804	N/A
	3a	256710	N/A	N/A	299320	N/A	N/A	N/A	N/A	509261	N/A	N/A	N/A	731331	3436781
	3b	254428	N/A	N/A	297039	N/A	N/A	N/A	N/A	464369	N/A	N/A	N/A	686439	3445768
COE ($)/kWh	1a	0.77	0.585	0.497	0.443	0.482	0.519	0.573	0.593	0.672	0.719	1.585	1.478	1.394	N/A
	1b	0.763	0.587	0.494	0.44	0.48	0.517	0.542	0.589	0.627	0.658	0.699	1.481	1.399	N/A
	2a	0.705	0.47	0.47	0.382	0.442	0.595	0.616	0.716	0.799	0.931	1.041	1.249	1.294	N/A
	2b	0.699	0.472	0.467	0.375	0.44	0.486	0.518	0.631	0.645	0.724	0.788	0.9	1.111	N/A
	3a	0.705	N/A	N/A	0.33	N/A	N/A	N/A	N/A	0.281	N/A	N/A	N/A	0.288	0.948
	3b	0.699	N/A	N/A	0.328	N/A	N/A	N/A	N/A	0.256	N/A	N/A	N/A	0.27	0.95
Total NPC ($)	1a	3581857	4081857	4626561	5126562	6722331	8423523	10656182	12386163	15578569	18348242	44255996	44800700	45300704	N/A
	1b	3552689	4097394	4597395	5097394	6693164	8394356	10086989	12312292	14512068	16783220	19496640	44915584	45460292	N/A
	2a	3281613	3281613	4375953	4420657	6170048	9668829	11462925	14961706	18505194	23753366	29046240	37837900	42050092	N/A
	2b	3252446	3297151	4346785	4346785	6140881	7890271	9639662	13183149	14932539	18476026	21974808	27267686	36059344	N/A
	3a	3281613	N/A	N/A	3826318	N/A	N/A	N/A	N/A	6510066	N/A	N/A	N/A	7871712	43933600
	3b	3252446	N/A	N/A	3797151	N/A	N/A	N/A	N/A	5936195	N/A	N/A	N/A	8774995	44048480

Considering the economic table of optimised results, different figures are now shown based on Table 6.15

6.5.2 Capital Cost Comparison

Capital cost constitutes the bulk of the total NPC and poses one of the major hindrances to RES investment. The capital cost for each case is now presented in Figure 6.19.

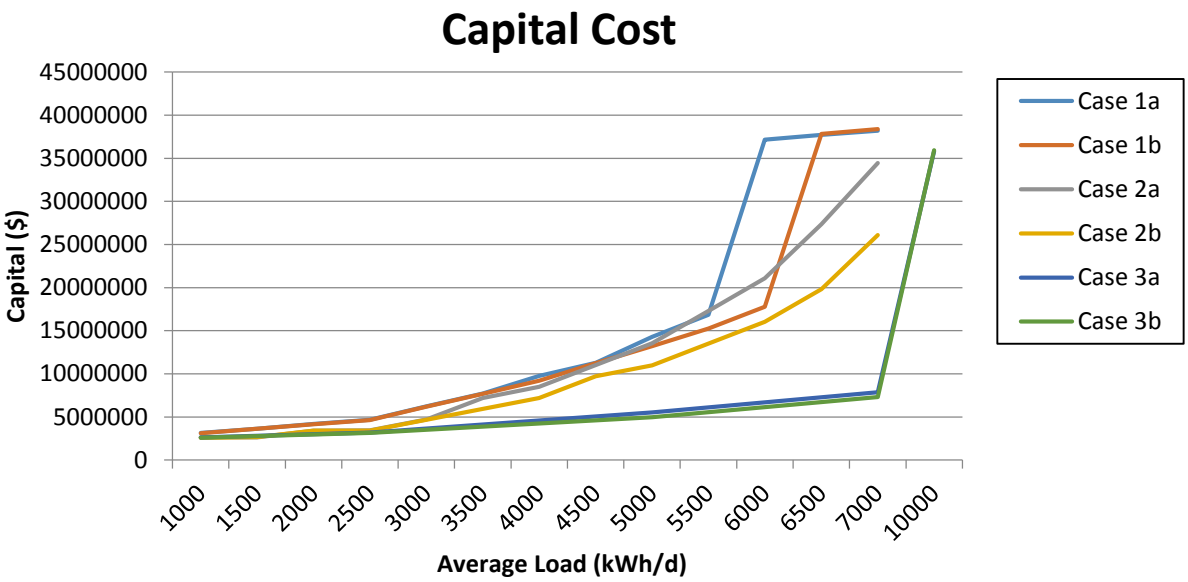

Figure 6.19 Capital cost for each case across different daily averaged loads

As mentioned in the electrical results, the HBS begins to effectively reduce the generation capacity of the PV panels or WECS after a load of 3.5MWh/d. This component capacity reduction is now reflected in Figure 6.19 by the reduced initial capital in all HBS cases.

Case 1 has the highest initial capital since the PV panels biggest cost type is its initial capital. Case 1a and 1b curves show the same initial capital up until the 4MWh/d load. From this point the solar-HBS requires a smaller PV panel bank which results in initial capital savings of up to $1.5 million before the battery failure point is reached.

Case 2 shows significant reductions in HBS capital from loads as low as 3.5MWh/d. Since wind power requires a larger operating reserve, the HBS intervention in Case 2b is seen at lower loads and provides capital savings of up to $7.5 million before reaching battery failure. It is important to note that the WECS initial capital cost is far lower than the PV panels in Figure 6.19, but the turbines used do require more replacement and maintenance.

Case 3 showed that using PV panels as a secondary power supply source with a unit COE of 0.0726 $/kWh is far cheaper than battery energy which costs 0.174 $/kWh. PV panels acted as an operating reserve source when the WECS supplied load power and vice versa during PV load supply. Generation sources were already effectively sized which meant the HBS could only provide capital savings of up to $0.5 million. However, the hybrid generation system shows substantial capital reductions from the average load of 3MWh/d. Upon comparing the hybrid generation cases to the next best alternative, namely the wind-HBS the capital margin observed is between $1-18 million based on Table 6.15.

6.5.3 Replacement Cost

The replacement cost in this system does signify a substantial percentage of the total NPC. They are now compared for different load in Figure 6.20.

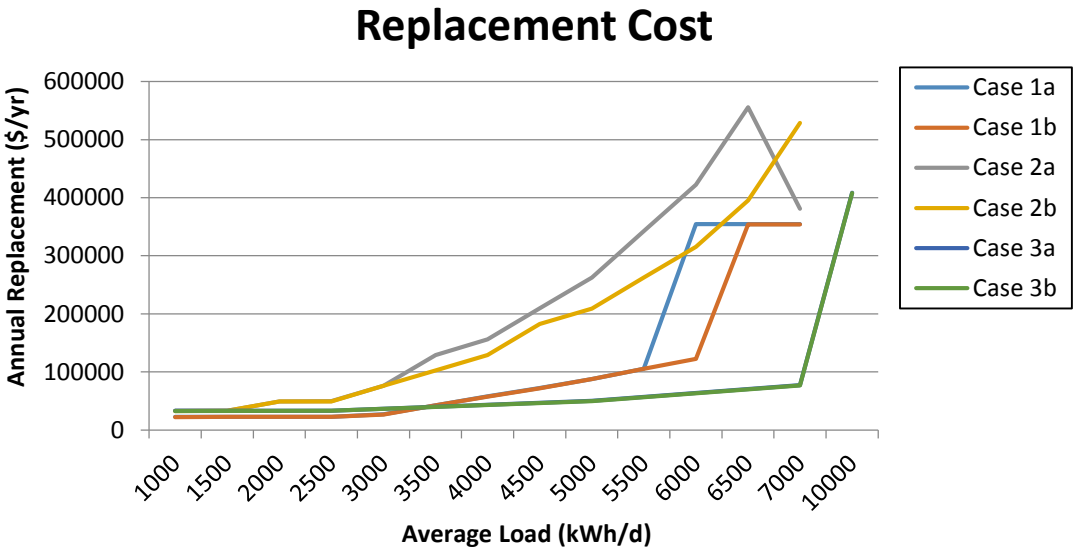

Figure 6.20 Replacement Cost of each Sensitivity Analysis

When comparing Case 1 to Case 2, it is clear that the PV panels are not replaced as frequently; thus their replacement cost are significantly lower than the WECS cases. Restricted generation time means the PV panel bank capacity must be increased (refer to capital cost in Figure 6.19), resulting in low energy throughput per unit panel thus it is not replaced often in Figure 6.20.

Case 2 uses the WECS which generates at AC for direct supply to the load for 21.58 hours of the day. Storage devices are not relied upon often in the WECS in terms of energy throughput for load supply but they still assist with reducing power ratings of the POR. The HBS reduces component sizing but the WECS still supplies majority of the average load, consequently is must be regularly replaced and maintained.

The hybrid generation systems use more accurately sized generation systems by reallocating the operating reserve to the PV panels and storage devices employed. By doing so the components selected are smaller than previous cases but still manage to supply the same load demands. The wind and storage devices do contribute to the replacements costs incurred here but once again the accurate sizing results in the lowest observed costs.

6.5.4 Operation and Maintenance Cost

The operation and maintenance (O & M) of components is extremely important to the cost analysis. This is not because of its scaled contribution to the total NPC but because of its implications on other costs. It is now shown in Figure 6.21.

Case 1 shows the lowest costs since PV panels are very easy to maintain. The wind based generation systems pose the highest maintenance costs which strongly align with the previous replacement cost curve. Hybrid generation cases are comprised of 64-70% wind turbines and subsequently show more O & M costs than Case 1.

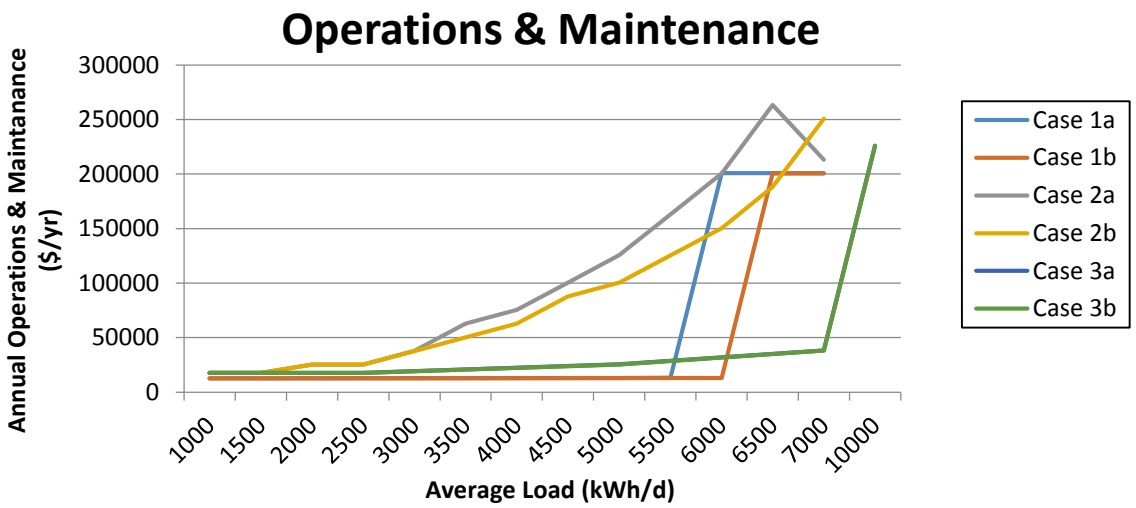

Figure 6.21 Operation and Maintenance Cost Comparison

Figure 6.21 show that maintenance cost is based on the component which is most often replaced i.e. wind turbines. As shown in Figure 6.20, the HBS contribution is fundamentally based on reducing the initial capital by employing smaller generation components hence replacement and O & M costs remain relatively unaffected by the storage device selected. This is because only the unused components are replaced and maintained. Since operating reserve components are mainly there in case of shortages, they are not used as much and therefore are not replaced.

6.5.5 Final Observations on Total NPC and COE

The cost of unit energy provides the best overall economic feasibility criteria from a customer's perspective. The total NPC represents the most important feasibility criteria from an investor's perspective as it encompasses the capital, replacement, and maintenance costs over the entire project lifespan. Total NPC is divided by the average load which then yields the levelised cost of energy. The NPC and COE are presented concurrently for a more balanced economic feasibility comparison in the following figures.

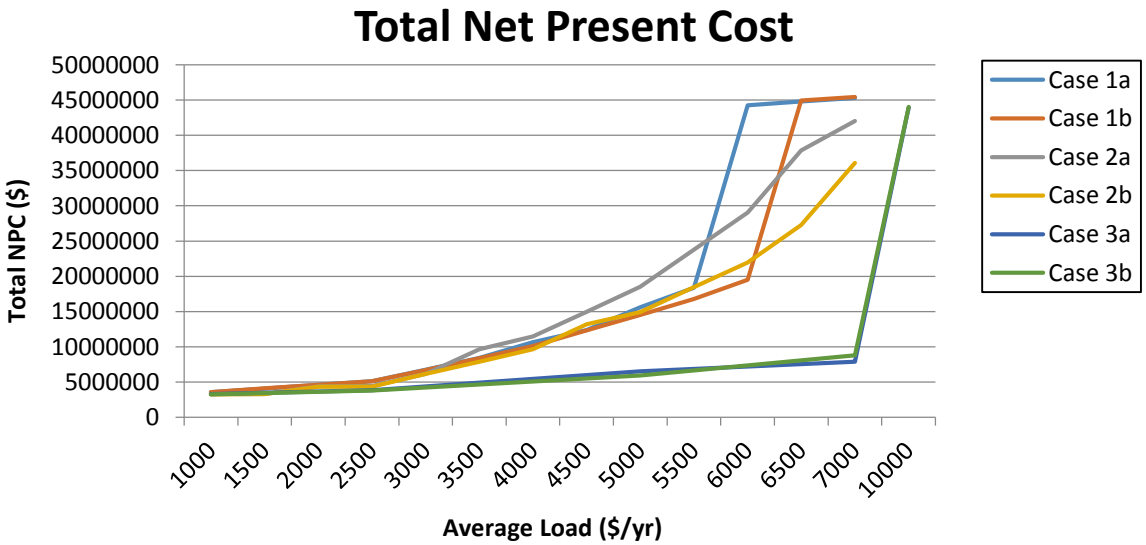

Figure 6.22 Total Net Present Cost Comparison

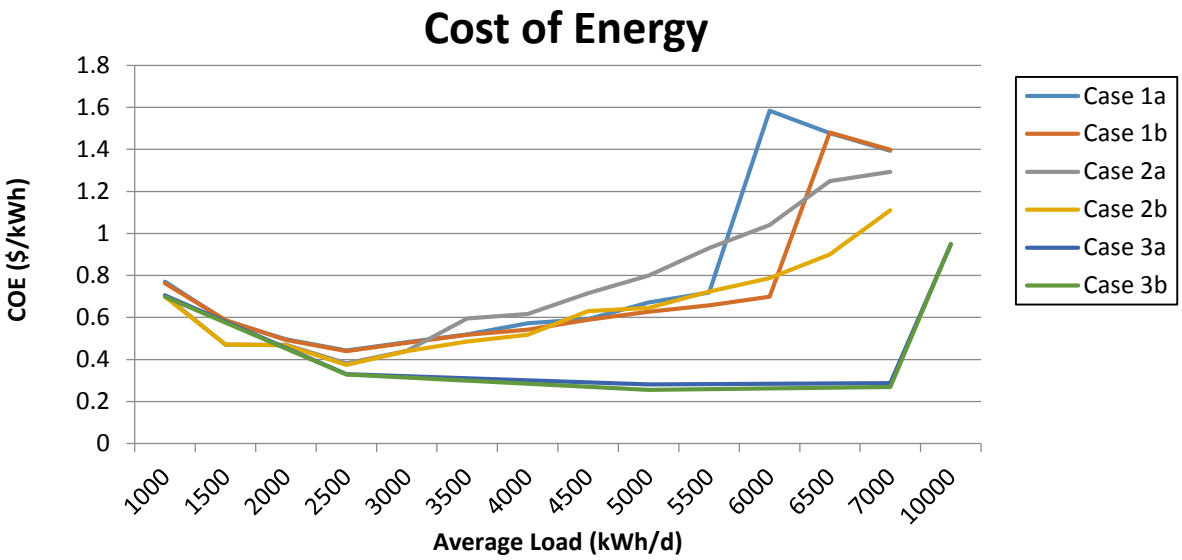

Figure 6.23 Cost of Energy Comparison

The solar-BSS has an exorbitant initial capital which poses a problem to investor interest and market penetration. Visible NPC and COE reductions are clearly illustrated in Figure 6.22 and 6.23 when using the solar-HBS with NPC savings of up to $1.56 million observed. In addition, the solar-BSS COE of 0.719 $/kWh was reduced to 0.658 $/kWh in the solar-HBS for the maximum load tested before battery failure is reached. At a load of 2.5MWh/d the system managed a COE of 0.44 $/kWh which was definitely feasible but was still more expensive than the wind and hybrid cases. Based on the systems dependence on storage, high initial capital and poor irradiance profile, Case 1a and 1b are not considered feasible for islanded RES deployment.

Since the load operated at AC it was directly supplied with the WECS in Case 2, thus the DC storage devices were called upon less. As a result of the increased WECS responsibility, replacement and maintenance costs were increased, as indicated by the steep gradients of their NPC and COE curves. Since wind (energy) is very intermittent the supercapacitor reduction in POR for Case 2b resulted in substantial NPC savings of up to $7.5 million when compared to the wind-BSS. It is important to keep in mind that the wind-HBS saving still amounted to a total NPC of $26.5 million for the 6.5MWh/d load which showed an equivalent COE of 0.9$/kWh. Despite HBS savings the total COE for Case 2b on average was 0.595$/kWh. This value is respectable, but must be reduced to make wind-HBS more feasible.

The sensitivity analysis results illustrate the relationship which states that as the load demand increases, the required operation reserve escalates since it is based on a percentage of the power capacity generated. As a result, the single source Cases 1a-2b purchase generation components at a higher rate than the load demand increasing gradient. This is the fundamental problem observed with single source generation since the cost of energy actually increases as the load increases. This is illustrated in Figure 6.23 which explains why the HBS shows more COE savings as the load increases.

In the hybrid wind-solar supply used in Case 3, the alternative generation source (PV panels) acts as the operating reserve. This reduces the need for excess generation capacity and shows the only instance where the COE steadily declines as the load increases. The hybrid-HBS used in Case 3b does show some POR reductions which brings the COE to

0.3$/kWh on average, with the hybrid-BSS COE at 0.35$/kWh. The NPC and COE prices of the hybrid-BSS are slightly higher (than the hybrid-HBS), but has a reduced complexity which makes it more inviting to engineering firms. Thus, both hybrid cases are very feasible for RES deployment.

7. Chapter 7 - Conclusions and Recommendations

Conclusions of work

Finally in this chapter, the conclusions and inferences derived from this dissertation are presented. A review of the study motivation and research question is provided, and is followed by penultimate conclusions based on the previous chapters. Contributions to this thesis, in the form of conference and journal publications, are then presented. Lastly, all general conclusions made from the research and results found, as well as recommendations for future work and research in this domain, are offered.

7.1 Review of Argument and Research Question

The motivation behind this study was the concurrent observation of unelectrified remote areas found in South Africa, all of which possess an abundance of natural wind and solar irradiance resources. A study based on the deployment of islanded RES in these remote areas was conducted in terms of electric performance, and technical and economic feasibility.

RES have shown tremendous growth worldwide, but its success is often limited to the reliability of its supply. PV and WECS are reliant on intermittent wind and sunlight resources, which often leads to a reliance on a connection with the utility grid in order to maintain an uninterrupted electricity supply. Unfortunately, many remote areas in South Africa simply do not extend to the utility grid, and thus have no electricity access [9]. The most common storage methods used as alternatives to utility grid connection is PHS or CAES. However, they are often limited to a specific terrain and landscape, which are not as prominent in South Africa. Battery storage and Hybrid storage systems have been identified in literature as the most common alternatives, but questions still arise on whether or not they can successfully replace complete connection with the grid and thereby allow for autonomous RES supply in South Africa. Based on the observations, this study sought to answer the following three fundamental questions:

1. Can remote area RES be successfully implemented in South Africa without connection with the utility grid, via the implementation of battery or hybrid battery supercapacitor storage systems?
2. Are remote area RES economically feasible in South Africa through the use of battery or hybrid battery supercapacitor storage systems?
3. If feasible, what is the best storage device and generation combination for deployment?

7.2 Contributions of Research

The author is currently employed as an engineer at South Africa's largest energy generation utility, Eskom. Contributions to this dissertation, in the form of conference and journal publications, are listed as follows:

- C_1. I. Chotia, S. Chowdhury, "Battery Storage and Hybrid Battery Supercapacitor Storage Systems: A Comparative Critical Review*," IEEE Innov. Smart Grid Technol., 2015*
- C_2. H. Tayob, I. Chotia and S. Chowdhury, "Design and Simulation of a Charging Algorithm for Lithium Ion Batteries,*" SAUPEC, 2016*
- J_1. I. Chotia, S. Chowdhury, *Technical and Economic Feasibility Analyses of Hybrid and Battery Storage Devices for Remote Area Renewable Energy Systems.* This article is in its developmental stages, and is being prepared for timeous submission.

7.3 Conclusions on Electrical Performance of Islanded RES

7.3.1 Electrical Model Development

The literature review, conducted in Chapter 2, established the potential PV and WECS based energy in South Africa, and identified that certain challenges accompany them. The importance of storage device implementation in islanded RES was highlighted, and a review of different batteries and their benefits was conducted. After reviewing several battery types, the lead acid battery was chosen due to its high energy density, establishment in industry and cheap cost. The supercapacitor was suggested as a means to compensate for the identified lead acid battery weaknesses. A comparative review of both devices explained their electrical provisions in RES applications and how their combination can be beneficial. The review showed that the supercapacitor can extend battery lifespan and provide high power density, but the extent of this benefit has not been considered in depth in terms of electrical and economic feasibility.

Chapter 3 consisted of the theory development and methodology followed for the electrical modelling of the RES and storage devices. The chapter was aimed at establishing an accurate and realistic model, which can effectively show the battery and supercapacitor contributions to RES. The mathematical and electrical models of the storage devices were considered and compared to the Matlab-Simulink models provided. By establishing a background in storage modelling theory, the Matlab storage models were effectively compared and improved upon where necessary. Based on the identified strengths and weaknesses of Matlab, relevant assumptions, constraints and improvements on the RES models were made. Once design constraints and requirements were established, the solar panel, wind turbine, converter, controller blocks, commercial-residential load descriptions, battery and supercapacitor parameters were modelled in different subsystems. The electrical study was divided into three cases studies, based on their input power supply source viz. ideal voltage source, PV panel and wind PMSG. The three cases studies were then divided into different BSS or HBS storage strategy pairs. A schematic breakdown of each case was drawn, and the justifications of all parameters selected for modelling was presented in Table 3.13.

7.3.2 Electrical Performance of RES Cases

Chapter 4 considered the electric performance results of three RES cases, tested with HBS and BSS. The results were compared in terms of load matching accuracy, power security and system efficiency, as well as battery lifespan and SOC monitoring. Ideal voltage source, used in Case 1, showed impressive load matching properties, but came at the expense of storage device errors and exhaustion in terms of lifespan and power security. This was due to the direct storage device connection to the ideal voltage source. The ideal voltage source with BSS showed a system efficiency of 94.1%, while the ideal HBS system had a 95% load supply efficiency. The slight increase was attributed to the supercapacitor's effective supply of load disturbances that were tested. The lifespan extrapolation results, shown in Table 4.15, compared the extension of battery lifespan observed when using a supercapacitor buffer, ideal for high power discharge requirements. Case 1 showed that the system's reliance on storage led to the observed BSS battery reaching capacity failure 5 years earlier than the HBS battery.

The solar-BSS and solar-HBS was modelled and tested in Case 2 under the same criteria. This system effectively distributed the load power demand to the PV panel or storage device,

using the charge algorithms defined in section 3.7.4 for the BSS and section 3.8.3 for the HBS. Through this combination of power sources, Case 2 managed to effectively match the load through excess energy absorptions. The solar-HBS used in Case 2a showed an improved system response to load disturbances and PV power fluctuations, due to the high power density of the supercapacitor. The improved high power supercapacitor response to these fluctuations was reflected through a 9 year extension of the HBS's battery lifespan, when compared to the BSS's battery. Both systems in Case 2 showed a load supply power shortage of less than 6.5W when supplying an 848W average load. This made the PV panel based system the most secure form of remote area power supply, when connected with either BSS or HBS.

The WECS deployed in Case 3 fails to accurately match the load demand for the first 6 hours of operation. In the first hour, the battery bank (used in the BSS and HBS) showed an abrupt power spike during the WECS start-up phase. The system manages to recover by 3.5 hours, and the load demand is met from 4 hours onwards. By 6 hours, the WECS power generated reaches its maximum value and the system's power is stable. After 6 hours the storage devices operate effectively, and can discharge (load response) and charge (excess energy) as instructed. This problem was observed due to the redundant design employed. The results showed that the DC charging algorithm used was not applicable for the AC based WECS system. This resulted in a reduced power security and efficiency of load supply, of 80.3% for the wind-BSS and 80.5% in the wind-HBS. The HBS supercapacitor still managed to extend the battery lifespan by 9 years due to the improved high power buffering once again. However, this case has shown that the success of generation components are limited to the applicability of the controller design and interfacing technology used.

7.3.3 Success of Islanded RES and Storage

Based on the development of the conceptual, designed and simulated model in Matlab, the electrical performance test has confirmed that RES implementation in South Africa is possible without connection from the grid, through interfacing with BSS or HBS. Case 1 established the importance of storage as a base case, while the solar-RES in Case 2 showed promising load matching properties and managed to autonomously maintain load supply by effectively relying on the PV and storage power. The importance of isolating the load and communication with the supply and storage device was exhibited through the separate storage device and PV power profile analysis. In Case 3 the initial discharge error meant that the WECS could only effectively supply the load once the power stability was established. From 6 hours onwards the charge algorithm managed to effectively provide an operable power supply, but the use of an equivalent DC wind power signal resulted in power losses. The contrast in results of the DC based PV power used in Case 2, and AC WECS deployed in Case 3, has highlighted the importance of allocating an appropriate control charge algorithm when combining storage devices with RES in islanded power supply.

Furthermore, the performance of the aforementioned storage systems successfully extracted excess energy, which would otherwise be sent to a dump load or sold back to the utility grid at low prices. The HBS benefitted from the supercapacitor's high power provisions through improved power security and load matching. It also showed that its inclusion in the HBS can allow for financial benefits through high power buffering, which allowed for an extension of the battery lifespan via SOC maintenance.

The success of any project is based on its ability to fulfil the objectives and goals set forth. Considering the research objectives of this study, an islanded connected RES, which relied on

South African natural resources to supply electricity without connection from the grid, was established through the effective interfacing with BSS and HBS storage. In addition, the results showed that using the HBS for high power responses is a more applicable electrical alternative for islanded RES. The current study has indeed shown that islanded RES in remote areas of South Africa are electrically viable; therefore the financial feasibility is addressed in the HOMER techno economic study.

7.4 Conclusions on Economic Feasibility of Islanded RES

7.3.1 Techno Economic Model Development

The techno economic study was based on establishing the feasibility of battery or hybrid based RES deployment in South Africa. A socio economic investigation took place with the object of establishing the ideal location for islanded RES. The location justification was made by firstly finding un-electrified nearby areas. After consulting the WASA, NASA and Solar GIS data bases the landscape, terrain, population, solar and wind data was acquired and the Western Cape Napier area was selected as a favourable RES location [44], [117], [147]. This was due to the accurate and recent high speed wind data found, in addition to an un-electrified area located near an open clear area ideal for RES deployment in terms of terrain. Furthermore, the solar and wind data was collected at the exact same Napier coordinates, which allows for a potential hybrid generation test model.

After location selection and data acquisition the potential limitations of the HOMER software was identified and proposed, assumptions and constraints for successful modelling were drawn and justified. It was discovered that HOMER did not possess a supercapacitor model in its storage properties, which led to the design of a new supercapacitor modelling algorithm which was implemented in the software. The supercapacitor modelled the electrical effects of the supercapacitor through operating reserve reduction, by editing the system parameters of the software. The economic effects of the supercapacitor were modelled by including its additional capital cost into the battery bank cost profile. The system was confirmed by HOMER software developers, and assumptions made in previous HOMER research papers were investigated to establish a general consensus. From this, the operating reserve parameters were established as 25% for PV supply, 50% for wind supply and 10% for irregular loads when modelled in HOMER [159]. The economic study was once again divided into three case studies with different input power supply sources. These cases were then further separated in terms of HBS and BSS once again.

7.3.2 Optimisation Study Results

The six case studies were laid out into three main supply categories of solar, wind and hybrid generation, and then further divided based on the BSS or HBS selection. The optimisation of each model was considered under the fixed average load of 5MWh/d, with a peak load demand of 407kW. Each supply type was compared, and the results showed that the HBS sufficiently reduced the cost of operation for both the solar and wind generation cases when compared to BSS. Its effect was more prominent in the wind cases (Case 2a and 2b) compared to the solar, due to the wind resource intermittency and hence a further operating reserve reduction. In the single source generation systems, the COE was in the region of 0.799 - 0.627 $/kWh. The observed improvement was clear in the cases implementing HBS storage, due to the supercapacitors reduction of POR, which subsequently reduced the rated generation capacity. This resulted in a total NPC saving of $1.07 million (or 0.45 $/kWh) in the solar-HBS and an impressive cost reduction of $3.6 million (or $1.54

$/kWh) in the wind-HBS over the 25 year project. The observed savings emphasised the importance of implementing an HBS islanded RES.

The HBS storage device reduced the required generation capacity in each case considered, but the savings observed through effective hybrid generation are far more substantial. Since the additional generation source is used as a power supply and operating reserve source, the components deployed in Case 3 are accurately sized and maintain accurate power security.

WECS is selected as the primary power producer and allows for a cheaper baseline supply (at 0.0484$/kWh) and an effective way of deploying PV power during the daytime peak commercial/residential load demand hours [57], [126]. Furthermore, by restricting PV panel capacity to 30%, the initial capital costs are reduced to $5.5 million for Case 3a and $4.9 million for Case 3b. This allows for a cheaper PV supply (at 0.0968 $/kWh) and minimised the use of expensive storage device energy at 0.174$/kWh. The storage devices are still essential to power supply, as their removal would lead to oversized components used for POR. In Case 3b, the HBS manages to reduce the POR which allows for smaller sized PV panels. Hybrid generation yields a total NPC of between $6.5 million in the BSS and $5.9 million for the HBS over a 25 year period, which is very attractive to potential investors. This makes it the most feasible solution based on the optimisation study results.

7.3.3 Sensitivity Analysis Results

The optimisation study considered all six cases' performance across a single 407kW rated load. The same optimisation was conducted across 14 different loads to provide a wider test matrix of results. Across the varying loads, the solar-BSS showed an exorbitant initial capital due to PV panel capacity purchased. Since PV panels only have a 12 hour on time they require more panels to increase the required energy throughput. Furthermore, the short on time increases the system's reliance on battery power which results in frequent storage replacements and increased maintenance costs. The initial capital was reduced when using the solar-HBS due to the POR reduction, but the reliance on storage and high PV capacity still made this option expensive at higher loads of above 5MWh/d.

The intermittent wind energy, coupled with its 50% operating reserve requirement and high replacements and maintenance costs, made the wind-BSS the most expensive case overall. The intermittency and operating reserve favoured the inclusion of the supercapacitor, which amounted to large POR reductions in Case 2b. This meant fewer wind turbines were purchased, which resulted in total NPC savings of up to $7.5 million when compared to the wind-BSS. The wind-HBS showed an average COE of 0.595$/kWh which was low enough to make it feasible for deployment.

The sensitivity analysis shows that as the load demand increases the required operation reserve escalates since it is based on a percentage of the power generated. As a result, the single source cases (1a-2b) purchase generation components at a higher rate than the observed increase in load demand. This is the fundamental problem of single source generation since the cost of energy actually increases as the load increases. This can be seen in Figure 6.23, and explains why the HBS shows more savings as the load increases.

In the hybrid generation system used in Case 3, the secondary generation sources acts as the operating reserve, which reduces the need for excess generation capacity and shows the only instance where the COE declines as the load increases, evident in Figure 6.23. The hybrid-HBS used in Case 3b shows some POR reductions which brings the COE to 0.3$/kWh on average, with the hybrid-BSS at 0.35$/kWh. The hybrid-BSS is slightly more expensive but

has a reduced complexity, which can be more appealing, and so both hybrid cases are very feasible for RES deployment.

7.4.2 Success of RES Feasibility Study

It is without question that the isolated cases present a feasible venture in terms of sustainable energy provisions to remote areas. In addition to this, using the HBS can be extremely beneficial in reducing the strategic capital and replacement costs for system deployment and attracting investors. Despite this fact, it is clear that Hybrid storage is beneficial but Hybrid generation is far more significant, and undoubtedly presents the most feasible economic RES venture based on this thesis.

Hybrid-HBS showed an average COE of 0.3$/kWh, which presents a very attractive cost of RES. Extracting the benefits of strategic deployment of energy is essential, especially in South African areas where hybrid generation would be the most environmentally, socially and economically beneficial and competitive option for RES deployment. This sustainable price helps overcome the limitations of terrain and grid connection, which often exclude remote / rural areas from electricity. Based on the confirmed technical and economic results, this study has confirmed multi resource hybrid and battery storage RES as a very feasible solution to remote area distribution. In addition, with the current global trend in sustainable energy and the identified potential for hybrid generation in terms of South African natural resources, this solution is not only feasible but is also a promising venture for current and future generations.

Recommendations for Future Work

7.5 Electrical Performance Analysis Recommendations

Based on the observed constrains and results found, the following design and modelling recommendations are made for future electrical performance analyses.

1. The Matlab simulation tool was proven to be ideal for technical lead acid battery and supercapacitor modelling, as a result of the in depth theory development conducted before simulation. However, further research into the contributions of HBS via hybrid generation, as done in the HOMER Techno Economic study of Case 3b, is recommend for Matlab electric performance.
2. The electric performance analysis conducted in Matlab, can be implemented on a larger scale using the exact same loads as sensitivity analysis conducted in HOMER. If the relevant hardware is available the system can be tested at the same 14 sensitivities of the HOMER software. Furthermore, an interfacing tool for these software's is currently under research and is highly recommend for feasibility studies conducted across academic fields.
3. The use of a larger supercapacitor bank to test wider spans of load and supply disturbances is recommended. This can be conducted under a 1 year simulation if the applicable hardware is made available. This will show more extensive lifespan extension properties.
4. In Case 3, reactive power contributions of the AC based WECS was overlooked since the uniform DC charge algorithm was applied for system simplicity. An AC based charging algorithm is imperative to future work, in order to establish the feasibility of the storage interfaced WECS. The PV and WECS systems can then be tested, for AC and DC loads (using the present charging algorithm), in order to establish which system is more robust in terms of undergoing energy conversion.
5. A hysteresis block limit or more advanced limiting protocols such as fuses must be implemented with the new charging algorithm applied to AC systems in order to prevent storage devices from yielding high discharge errors which can compromise or delay power stability.
6. The BSS and HBS can be compared to flywheel storage technology. This is a more fated storage device, but may be more feasible if substantially cheaper. Furthermore, it may be more applicable as a form of AC storage with the WECS. If its performance is inferior, its validity can still be shown in HOMER in terms financial feasibility.

7.6 Economic Feasibility Study Recommendations

The present mode exceeded the observed objectives in terms of proving the feasibility of RES. However, it can still be improved by implementing or considering the following recommendations:

1. The economic feasibility study was the first designed supercapacitor model in the HOMER software but is not immune to improvements. Firstly, the test matrix in HOMER can always be made more accurate by using even smaller increments of component prices that are entered into the parameters of each component tested. This would allow for more potential options and therefore increase the chances of finding an even cheaper combination.

2. More sensitivity variables can be considered in HOMER to gauge the influence of varying irradiance inputs, wind speeds over times or curvatures of the load. These improvements are subject to the growth of computer processors in future studies since they will significantly increase the potential combinations, and thereby increasing the simulation time to find the optimised solution.
3. Instead of lumping the environmental costs incurred into component costs, the system parameters for inflation, land and emission costs can be individually entered and compared to the assumptions made in this model.
4. In future research a supercapacitor model will be implemented by the HOMER software developers. It will be interesting to observe the effects of said model when it becomes available to consumers.
5. Since the sizing capacity extension and constant storage performance on the load study has been verified in the study, future research can implement a wide test matrix of battery kWh capacity and tests its influence on the COE as well.
6. As mentioned in section 7.5, the Flywheel storage technology can be tested and compared to the BSS and HBS or even combined to make a new hybrid storage system. It is already available in HOMER and may show promising solutions since it is primarily an operating reserve based storage device.
7. More recent prices and designs of solar panels, wind turbines and power electronic converters can be used when modelling the system. This in combination with inflation will yield an interesting result.
8. Lastly, a survey on the results of present local RES COE and the observed COE can be conducted to establish a benchmark for how pertinent the observed improvements and results are.

List of References

[1] E. Ziramba, "Disaggregate energy consumption and industrial production in South Africa," *Energy Policy*, vol. 37, no. 6, pp. 2214–2220, 2009.

[2] H. Chen, T. N. Cong, W. Yang, C. Tan, Y. Li, and Y. Ding, "Progress in electrical energy storage system: A critical review," *Prog. Nat. Sci.*, vol. 19, no. 3, pp. 291–312, 2009.

[3] H. Ibrahim, A. Ilinca, and J. Perron, "Energy storage systems -Characteristics and comparisons," *Renew. Sustain. Energy Rev.*, vol. 12, no. 5, pp. 1221–1250, 2008.

[4] A. Amare, "Local Government Budgets and Expenditure Review: 2001/02 – 2007/08," Addis Ababa University, 2010.

[5] J. Krupa and S. Burch, "A new energy future for South Africa: The political ecology of South African renewable energy," *Energy Policy*, vol. 39, no. 10, pp. 6254–6261, 2011.

[6] R. A. F. de Groot, V. G. van der Veen, and A. B. Sebitosi, "Comparing solar PV (photovoltaic) with coal-fired electricity production in the centralized network of South Africa," *Energy*, vol. 55, pp. 823–837, 2013.

[7] M. Kohler, "Differential electricity pricing and energy efficiency in South Africa," *Energy*, vol. 64, pp. 524–532, 2014.

[8] A. Lombard and S. Ferreira, "Residents' attitudes to proposed wind farms in the West Coast region of South Africa: A social perspective from the South," *Energy Policy*, vol. 66, pp. 390–399, 2014.

[9] ScottishPower, "Community Electricity in Rural South Africa : Renewable mini-grid assessment," *Glob. Sustain. Electr. Partnersh.*, pp. 1–39, 2004.

[10] O. M. Longe, F. I. Oluwajobi, and F. Omowole, "Electricity access in Sub-Saharan Africa - Case for renewable energy sources microgrid," *2nd Int. Conf. Emerg. Sustain. Technol. Power ICT a Dev. Soc. IEEE NIGERCON 2013 - Proc.*, pp. 253–257, 2013.

[11] S. Ruiz-Romero, A. Colmenar-Santos, F. Mur-Pérez, and Á. López-Rey, "Integration of distributed generation in the power distribution network: The need for smart grid control systems, communication and equipment for a smart city - Use cases," *Renew. Sustain. Energy Rev.*, vol. 38, pp. 223–234, 2014.

[12] O. a. Olanrewaju, a. a. Jimoh, and P. a. Kholopane, "Assessing the energy potential in the South African industry: Acombined IDA-ANN-DEA (Index Decomposition Analysis-Artificial Neural Network-Data Envelopment Analysis) model," *Energy*, vol. 63, pp. 225–232, 2013.

[13] R. Dufo-López and J. L. Bernal-Agustín, "Techno-economic analysis of grid-connected battery storage," *Energy Convers. Manag.*, vol. 91, pp. 394–404, 2015.

[14] K. Menyah and Y. Wolde-Rufael, "Energy consumption, pollutant emissions and economic growth in South Africa," *Energy Econ.*, vol. 32, no. 6, pp. 1374–1382, 2010.

[15] A. K. Basu, S. P. Chowdhury, S. Chowdhury, and S. Paul, "Microgrids: Energy management by strategic deployment of DERs - A comprehensive survey," *Renew. Sustain. Energy Rev.*, vol. 15, no. 9, pp. 4348–4356, 2011.

[16] L. Sigrist, E. Lobato, and L. Rouco, "Energy storage systems providing primary reserve and peak shaving in small isolated power systems: An economic assessment," *Int. J. Electr. Power Energy Syst.*, vol. 53, no. 1, pp. 675–683, 2013.

[17] H. Zhao, Q. Wu, S. Hu, H. Xu, and C. N. Rasmussen, "Review of energy storage system for wind power integration support," *Appl. Energy*, 2014.

[18] H. You, V. Vittal, and Z. Yang, "Self-healing in power systems: An approach using islanding and rate of frequency decline-based load shedding," *IEEE Trans. Power Syst.*,

vol. 18, no. 1, pp. 174–181, 2003.
[19] M. Soshinskaya, W. H. J. Graus, J. M. Guerrero, and J. C. Vasquez, “Microgrids: experiences, barriers and success factors,” *Renew. Sustain. Energy Rev.*, vol. 40, pp. 659–672, 2014.
[20] B. G. Pollet, I. Staffell, and K.-A. Adamson, “Current energy landscape in the Republic of South Africa,” *Int. J. Hydrogen Energy*, vol. 40, no. 46, pp. 16685–16701, 2015.
[21] A. M. Foley, P. G. Leahy, A. Marvuglia, and E. J. McKeogh, “Current methods and advances in forecasting of wind power generation,” *Renew. Energy*, vol. 37, no. 1, pp. 1–8, 2012.
[22] P. Liu, M. C. Georgiadis, and E. N. Pistikopoulos, “An energy systems engineering approach for the design and operation of microgrids in residential applications,” *Chem. Eng. Res. Des.*, vol. 91, no. 10, pp. 2054–2069, 2013.
[23] V. Devabhaktuni, M. Alam, P. Boyapati, P. Chandna, A. Kumar, L. Lack, D. Nims, and L. Wang, “Wind Energy: Trends and Enabling Technologies,” vol. 53, pp. 1–15, 2016.
[24] K. Hagemann, “Mesoscale wind atlas of South Africa,” Cape Town, 2008.
[25] B. Dursun and C. Gokcol, “Impacts of the renewable energy law on the developments of wind energy in Turkey,” *Renew. Sustain. Energy Rev.*, vol. 40, pp. 318–325, 2014.
[26] J. K. Kaldellis and D. Zafirakis, “The wind energy (r)evolution: A short review of a long history,” *Renew. Energy*, vol. 36, no. 7, pp. 1887–1901, 2011.
[27] S. Kim, J. Jeon, C. Cho, J. Ahn, and S. Kwon, “Dynamic Modeling and Control of a Grid-Connected Hybrid Generation System With Versatile Power Transfer,” vol. 55, no. 4, pp. 1677–1688, 2008.
[28] C. Abbey, S. Member, F. Katiraei, C. Brothers, G. Joos, and S. Member, “Integration of Distributed Generation and Wind Energy in Canada,” 2006.
[29] S. & W. Energy, “Vaisala 3TIER Services Global Solar Dataset.”
[30] a. B. Sebitosi and P. Pillay, “Grappling with a half-hearted policy: The case of renewable energy and the environment in South Africa,” *Energy Policy*, vol. 36, no. 7, pp. 2513–2516, 2008.
[31] Department of Energy, “Integrated Resource Plan for Electricity 2010 - 2030,” no. March, pp. 2010–2030, 2011.
[32] D. R. Walwyn and A. C. Brent, “Renewable energy gathers steam in South Africa,” *Renew. Sustain. Energy Rev.*, vol. 41, pp. 390–401, 2015.
[33] C. L. Azimoh, F. Wallin, P. Klintenberg, and B. Karlsson, “An assessment of unforeseen losses resulting from inappropriate use of solar home systems in South Africa,” *Appl. Energy*, vol. 136, pp. 336–346, 2014.
[34] G. E. Gilligan, D. Qu, M. P. Paranthaman, H. Liu, S. Dai, M. Brown, O. Ridge, T. M. Lim, M. Ulaganathan, and Q. Yan, “Advances in Batteries for Medium and Large-Scale Energy Storage . Woodhead Publishing Series in Energy.”
[35] G. Bekele and G. Tadesse, “Feasibility study of small Hydro/PV/Wind hybrid system for off-grid rural electrification in Ethiopia,” *Appl. Energy*, vol. 97, pp. 5–15, 2012.
[36] S. Giglmayr, A. C. Brent, P. Gauché, and H. Fechner, “Utility-scale PV power and energy supply outlook for South Africa in 2015,” *Renew. Energy*, vol. 83, pp. 779–785, 2015.
[37] P. Basak, S. Chowdhury, S. Halder Nee Dey, and S. P. Chowdhury, “A literature review on integration of distributed energy resources in the perspective of control, protection and stability of microgrid,” *Renew. Sustain. Energy Rev.*, vol. 16, no. 8, pp. 5545–5556, 2012.

[38] X. Liu, P. Wang, P. C. Loh, F. Gao, and F. H. Choo, “Control of hybrid battery/ultra-capacitor energy storage for stand-alone photovoltaic system,” *2010 IEEE Energy Convers. Congr. Expo. ECCE 2010 - Proc.*, pp. 336–341, 2010.
[39] T. Sarver, A. Al-Qaraghuli, and L. L. Kazmerski, “A comprehensive review of the impact of dust on the use of solar energy: History, investigations, results, literature, and mitigation approaches,” *Renew. Sustain. Energy Rev.*, vol. 22, pp. 698–733, 2013.
[40] A. O. Mohamed and A. Hasan, “Effect of Dust Accumulation on Performance of Photovoltaic Solar Modules in Sahara Environment,” *J. Basic. Appl. Sci. Res*, vol. 2, no. 11, pp. 11030–11036, 2012.
[41] C. D. Parker, “Lead-acid battery energy-storage systems for electricity supply networks,” *J. Power Sources*, vol. 100, no. 1–2, pp. 18–28, 2001.
[42] M. Capellaro, “Prediction of site specific wind energy value factors,” *Renew. Energy*, vol. 87, pp. 430–436, 2016.
[43] M. Ross, R. Hidalgo, C. Abbey, and G. Joós, “Energy storage system scheduling for an isolated microgrid,” *IET Renew. Power Gener.*, vol. 5, no. 2, p. 117, 2011.
[44] N. G. Mortensen, J. C. Hansen, and M. C. Kelly, “Wind Atlas for South Africa (WASA) Observational wind atlas for 10 met. stations in Northern, Western and Eastern Cape provinces,” 2012.
[45] M. Brower, “Ontario Power Authority (OPA),” pp. 1–14, 2007.
[46] M. Asmine, J. Brochu, J. Fortmann, R. Gagnon, Y. Kazachkov, C.-E. Langlois, C. Larose, E. Muljadi, J. MacDowell, P. Pourbeik, S. a. Seman, and K. Wiens, “Model Validation for Wind Turbine Generator Models,” *IEEE Trans. Power Syst.*, vol. 26, no. 3, pp. 1769–1782, Aug. 2011.
[47] H. Jia, Y. Mu, and Y. Qi, “A statistical model to determine the capacity of battery-supercapacitor hybrid energy storage system in autonomous microgrid,” *Int. J. Electr. Power Energy Syst.*, vol. 54, pp. 516–524, 2014.
[48] X. Wang, M. Yue, E. Muljadi, and W. Gao, “Probabilistic Approach for Power Capacity Specification of Wind Energy Storage Systems,” *Ind. Appl. IEEE Trans.*, vol. 50, no. 2, pp. 1215–1224, 2014.
[49] C. Spataru, Y. C. Kok, and M. Barrett, “Physical Energy Storage Employed Worldwide,” *Energy Procedia*, vol. 62, pp. 452–461, 2014.
[50] W. Li and G. Joós, “Comparison of Energy Storage System Technologies and Configurations in a Wind Farm,” *Power Electron. Spec. Conf.*, pp. 1280–1285, 2007.
[51] B. Zakeri and S. Syri, “Electrical energy storage systems : A comparative life cycle cost analysis,” *Renew. Sustain. Energy Rev.*, vol. 42, pp. 569–596, 2015.
[52] T. Ma, H. Yang, and L. Lu, “A feasibility study of a stand-alone hybrid solar-wind-battery system for a remote island,” *Appl. Energy*, vol. 121, pp. 149–158, 2014.
[53] K. Y. Lau, M. F. M. Yousof, S. N. M. Arshad, M. Anwari, and a. H. M. Yatim, “Performance analysis of hybrid photovoltaic/diesel energy system under Malaysian conditions,” *Energy*, vol. 35, no. 8, pp. 3245–3255, 2010.
[54] F. Díaz-González, A. Sumper, O. Gomis-Bellmunt, and R. Villafáfila-Robles, “A review of energy storage technologies for wind power applications,” *Renew. Sustain. Energy Rev.*, vol. 16, no. 4, pp. 2154–2171, 2012.
[55] H. Zhou, “Composite Energy Storage System using dynamic energy management in microgrid applications,” *Power Electron. …*, pp. 1163–1168, 2010.
[56] W. F. Pickard, A. Q. Shen, and N. J. Hansing, “Parking the power: Strategies and physical limitations for bulk energy storage in supply-demand matching on a grid

whose input power is provided by intermittent sources," *Renew. Sustain. Energy Rev.*, vol. 13, no. 8, pp. 1934–1945, 2009.
[57] S. M. Shaahid, "Review of research on autonomous wind farms and solar parks and their feasibility for commercial loads in hot regions," *Renew. Sustain. Energy Rev.*, vol. 15, no. 8, pp. 3877–3887, 2011.
[58] Y. Z. Y. Zhang, Z. J. Z. Jiang, and X. Y. X. Yu, "Control Strategies for Battery/Supercapacitor Hybrid Energy Storage Systems," *2008 IEEE Energy 2030 Conf.*, pp. 5–10, 2008.
[59] C. D. Parker, "Lead acid battery energy storage systems for electricity supply networks," *J. Power Sources*, vol. 100, pp. 18–28, 2001.
[60] A. Oudalov and D. Chartouni, "Value analysis of battery energy storage applications in power systems," *Power Syst. …*, pp. 2206–2211, 2006.
[61] R. M. Dell and D. a J. Rand, "Energy storage - A key technology for global energy sustainability," *J. Power Sources*, vol. 100, no. 1–2, pp. 2–17, 2001.
[62] M. Karimi, H. Mokhlis, K. Naidu, S. Uddin, and a. H. a. Bakar, "Photovoltaic penetration issues and impacts in distribution network – A review," *Renew. Sustain. Energy Rev.*, vol. 53, pp. 594–605, 2016.
[63] B. Kroposki, R. Lasseter, T. Ise, S. Morozumi, S. Papatlianassiou, and N. Hatziargyriou, "Making microgrids work," *Power Energy Mag. IEEE*, vol. 6, no. june, p. 40,53, 2008.
[64] A. Kirchev, L. Serra, S. Dumenil, G. Brichard, M. Alias, B. Jammet, and L. Vinit, "Carbon honeycomb grids for advanced lead-acid batteries. Part III: Technology scale-up," *J. Power Sources*, vol. 299, pp. 324–333, 2015.
[65] A. Cooper, J. Furakawa, L. Lam, and M. Kellaway, "The UltraBattery-A new battery design for a new beginning in hybrid electric vehicle energy storage," *J. Power Sources*, vol. 188, no. 2, pp. 642–649, 2009.
[66] M. E. Glavin, P. K. W. Chan, S. Armstrong, and W. G. Hurley, "A stand-alone photovoltaic supercapacitor battery hybrid energy storage system," *2008 13th Int. Power Electron. Motion Control Conf. EPE-PEMC 2008*, pp. 1688–1695, 2008.
[67] I. Hadjipaschalis, A. Poullikkas, and V. Efthimiou, "Overview of current and future energy storage technologies for electric power applications," *Renew. Sustain. Energy Rev.*, vol. 13, no. 6–7, pp. 1513–1522, 2009.
[68] D. H. Doughty, P. C. Butler, A. a Akhil, N. H. Clark, and J. D. Boyes, "Batteries for Large-Scale Stationary Electrical Energy Storage," *Electrochem. Soc. Interface*, pp. 49–53, 2010.
[69] J. Wang, P. Liu, J. Hicks-Garner, E. Sherman, S. Soukiazian, M. Verbrugge, H. Tataria, J. Musser, and P. Finamore, "Cycle-life model for graphite-LiFePO4 cells," *J. Power Sources*, vol. 196, no. 8, pp. 3942–3948, 2011.
[70] K. Zaghib, M. Dontigny, a. Guerfi, P. Charest, I. Rodrigues, a. Mauger, and C. M. Julien, "Safe and fast-charging Li-ion battery with long shelf life for power applications," *J. Power Sources*, vol. 196, no. 8, pp. 3949–3954, 2011.
[71] A. Price, "Technologies for energy storage-Present and future: flow batteries," *2000 Power Eng. Soc. Summer Meet. (Cat. No.00CH37134)*, vol. 3, no. c, pp. 1541–1545, 2000.
[72] S. B. Peterson, J. Apt, and J. F. Whitacre, "Lithium-ion battery cell degradation resulting from realistic vehicle and vehicle-to-grid utilization," *J. Power Sources*, vol. 195, no. 8, pp. 2385–2392, 2010.
[73] R. Drummond, D. a. Howey, and S. R. Duncan, "Low-Order Mathematical Modelling of

Electric Double Layer Supercapacitors Using Spectral Methods," *J. Power Sources*, vol. 277, pp. 317–328, 2014.
[74] P. Sharma and T. S. Bhatti, "A review on electrochemical double-layer capacitors," *Energy Convers. Manag.*, vol. 51, no. 12, pp. 2901–2912, 2010.
[75] T. Shimizu and C. Underwood, "Super-capacitor energy storage for micro-satellites: Feasibility and potential mission applications," *Acta Astronaut.*, vol. 85, pp. 138–154, 2013.
[76] F. Rafik, H. Gualous, R. Gallay, a. Crausaz, and a. Berthon, "Frequency, thermal and voltage supercapacitor characterization and modeling," *J. Power Sources*, vol. 165, no. 2, pp. 928–934, 2007.
[77] P. K. Soori, S. C. Shetty, S. Chacko, P. O. Box, and U. a E. Email, "Application of Super Capacitor Energy Storage in Microgrid System," *2011 IEEE GCC Conf. Exhib.*, pp. 581–584, 2011.
[78] K. B. Oldham, "A Gouy-Chapman-Stern model of the double layer at a (metal)/(ionic liquid) interface," *J. Electroanal. Chem.*, vol. 613, no. 2, pp. 131–138, 2008.
[79] H. Zhou, T. Bhattacharya, D. Tran, T. S. T. Siew, and A. M. Khambadkone, "Composite energy storage system involving battery and ultracapacitor with dynamic energy management in microgrid applications," *IEEE Trans. Power Electron.*, vol. 26, no. 3, pp. 923–930, 2011.
[80] C. L. Benson and C. L. Magee, "On improvement rates for renewable energy technologies: Solar PV, wind turbines, capacitors, and batteries," *Renew. Energy*, vol. 68, pp. 745–751, 2014.
[81] Y. Zhan, Y. Guo, J. Zhu, and L. Li, "Power and energy management of grid/PEMFC/battery/supercapacitor hybrid power sources for UPS applications," *Int. J. Electr. Power Energy Syst.*, vol. 67, pp. 598–612, 2015.
[82] Y. Y. Chia, L. H. Lee, N. Shafiabady, and D. Isa, "A load predictive energy management system for supercapacitor-battery hybrid energy storage system in solar application using the Support Vector Machine," *Appl. Energy*, vol. 137, pp. 588–602, 2015.
[83] Zaheeruddin and M. Manas, "Renewable energy management through microgrid central controller design: An approach to integrate solar, wind and biomass with battery," *Energy Reports*, vol. 1, pp. 156–163, 2015.
[84] I. Chotia and S. Chowdhury, "Battery Storage and Hybrid Battery Supercapacitor Storage Systems : A Comparative Critical Review," *IEEE Innov. Smart Grid Technol.*, 2015.
[85] R. Karangia, M. Jadeja, C. Upadhyay, and H. Chandwani, "Battery-supercapacitor hybrid energy storage system used in Electric Vehicle," *2013 Int. Conf. Energy Effic. Technol. Sustain. ICEETS 2013*, pp. 688–691, 2013.
[86] Y. Luo, L. Shi, and G. Tu, "Optimal sizing and control strategy of isolated grid with wind power and energy storage system," *Energy Convers. Manag.*, vol. 80, pp. 407–415, 2014.
[87] M. Masih-Tehrani, M. R. Ha'iri-Yazdi, V. Esfahanian, and A. Safaei, "Optimum sizing and optimum energy management of a hybrid energy storage system for lithium battery life improvement," *J. Power Sources*, vol. 244, pp. 2–10, 2013.
[88] A. J. Fairweather, D. A. Stone, and M. P. Foster, "Evaluation of UltraBattery™ performance in comparison with a battery-supercapacitor parallel network," *J. Power Sources*, vol. 226, pp. 191–201, 2013.
[89] T. Ma, H. Yang, and L. Lu, "Development of hybrid battery–supercapacitor energy

storage for remote area renewable energy systems," *Appl. Energy*, 2014.
[90] I. Prodan and E. Zio, "A model predictive control framework for reliable microgrid energy management," *Int. J. Electr. Power Energy Syst.*, vol. 61, pp. 399–409, Oct. 2014.
[91] J. J. Ming Kwok, N. Yu, I. a. Karimi, and D. Y. Lee, "Microgrid scheduling for reliable, cost-effective, and environmentally friendly energy management," *Ind. Eng. Chem. Res.*, vol. 52, no. 1, pp. 142–151, 2013.
[92] S. Morozumi, "Micro-grid demonstration projects in Japan," *Fourth Power Convers. Conf. PCC-NAGOYA 2007 - Conf. Proc.*, pp. 635–642, 2007.
[93] J. Furukawa, T. Takada, D. Monma, and L. T. Lam, "Further demonstration of the VRLA-type UltraBattery under medium-HEV duty and development of the flooded-type UltraBattery for micro-HEV applications," *J. Power Sources*, vol. 195, no. 4, pp. 1241–1245, 2010.
[94] Y. Yuan, C. Sun, M. Li, S. S. Choi, and Q. Li, "Determination of optimal supercapacitor-lead-acid battery energy storage capacity for smoothing wind power using empirical mode decomposition and neural network," *Electr. Power Syst. Res.*, vol. 127, pp. 323–331, 2015.
[95] Z. Ding, C. Yang, Z. Zhang, C. Wang, and S. Xie, "A novel soft-switching multiport bidirectional dc-dc converter for hybrid energy storage system," *IEEE Trans. Power Electron.*, vol. 29, no. 4, pp. 1595–1609, 2014.
[96] A. Mansour, B. Faouzi, G. Jamel, and E. Ismahen, "Design and analysis of a high frequency DC-DC converters for fuel cell and super-capacitor used in electrical vehicle," *Int. J. Hydrogen Energy*, vol. 39, no. 3, pp. 1580–1592, 2014.
[97] S. R. Cain, A. Anderson, E. Tasillo, W. Infantolino, and P. Wolfgramm, "Empirical evaluation of the improvement of battery output when coupled with a capacitor bank," *J. Power Sources*, vol. 268, pp. 640–644, 2014.
[98] N. Omar, J. Van Mierlo, B. Verbrugge, and P. Van Den Bossche, "Power and life enhancement of battery-electrical double layer capacitor for hybrid electric and charge-depleting plug-in vehicle applications," *Electrochim. Acta*, vol. 55, no. 25, pp. 7524–7531, 2010.
[99] A. Bouharcho, E. M. Berkouk, T. Ghunnam, and B. Tabbache, "Modeling and control of a Doubly Fed Induction Generator With Battery-Supercapacitor Hybrid Energy Storage for Wind Power Applications," no. May, pp. 13–17, 2013.
[100] N. Devilliers, M.-C. Péra, D. Bienaimé, and M.-L. Grojo, "Influence of the energy management on the sizing of Electrical Energy Storage Systems in an aircraft," *J. Power Sources*, vol. 270, pp. 391–402, 2014.
[101] F. Ongaro, S. Saggini, and P. Mattavelli, "Li-Ion battery-supercapacitor hybrid storage system for a long lifetime, photovoltaic-based wireless sensor network," *IEEE Trans. Power Electron.*, vol. 27, no. 9, pp. 3944–3952, 2012.
[102] S. Koohi-Kamali, V. V. Tyagi, N. a. Rahim, N. L. Panwar, and H. Mokhlis, "Emergence of energy storage technologies as the solution for reliable operation of smart power systems: A review," *Renew. Sustain. Energy Rev.*, vol. 25, pp. 135–165, 2013.
[103] J. F. Manwell and J. G. McGowan, "Lead acid battery storage model for hybrid energy systems," *Sol. Energy*, vol. 50, no. 5, pp. 399–405, 1993.
[104] R. A. Jackey, "A Simple, Effective Lead-Acid Battery Modeling Process for Electrical System Component Selection," *SAE Pap.*, pp. 01–0778, 2007.
[105] O. Tremblay and L. a. Dessaint, "Experimental validation of a battery dynamic model

for EV applications," *World Electr. Veh. J.*, vol. 3, no. 1, pp. 289–298, 2009.
[106] C. Tammineedi, "Modelling battery-ultracapacitor hybrid systems for solar and wind applications," The Pennsylvania State University, 2011.
[107] M. Dürr, A. Cruden, S. Gair, and J. R. McDonald, "Dynamic model of a lead acid battery for use in a domestic fuel cell system," *J. Power Sources*, vol. 161, no. 2, pp. 1400–1411, 2006.
[108] M. Ceraolo, "New dynamical models of lead-acid batteries," *IEEE Trans. Power Syst.*, vol. 15, no. 4, pp. 1184–1190, 2000.
[109] Mathworks, "Stateflow™ User ' s Guide R 2015 b," 2015.
[110] N. Xu and J. Riley, "Nonlinear analysis of a classical system: The double-layer capacitor," *Electrochem. commun.*, vol. 13, no. 10, pp. 1077–1081, 2011.
[111] A. M. Gee, F. V. P. Robinson, and R. W. Dunn, "Analysis of battery lifetime extension in a small-scale wind-energy system using supercapacitors," *IEEE Trans. Energy Convers.*, vol. 28, no. 1, pp. 24–33, 2013.
[112] R. de Levie, "On porous electrodes in electrolyte solutions—IV," *Electrochim. Acta*, vol. 9, no. 9, pp. 1231–1245, 1964.
[113] P. C. Blaud, "Développement d'un modèle de simulation de supercondensateur Et validation expérimentale," ÉCOLE DE TECHNOLOGIE SUPÉRIEURE UNIVERSITÉ DU QUÉBEC, 2012.
[114] N. Achaibou, M. Haddadi, and a. Malek, "Modeling of lead acid batteries in PV systems," *Energy Procedia*, vol. 18, pp. 538–544, 2012.
[115] G. T. Burstein, "A hundred years of Tafel's Equation: 1905–2005," *Corros. Sci.*, vol. 47, no. 12, pp. 2858–2870, 2005.
[116] P. Johansson and P. Johansson, "Comparison of Simulation Programs for Supercapacitor Modelling," *Electr. Eng.*, 2008.
[117] NASA, "Surface meteorology and Solar energy," 2015. [Online]. Available: https://eosweb.larc.nasa.gov/sse/RETScreen/. [Accessed: 25-Jul-2015].
[118] A. A. H. Hussein and I. Batarseh, "An overview of generic battery models," *IEEE Power Energy Soc. Gen. Meet.*, no. 4, pp. 4–9, 2011.
[119] L. T. Lam, N. P. Haigh, C. G. Phyland, and a. J. Urban, "Failure mode of valve-regulated lead-acid batteries under high-rate partial-state-of-charge operation," *J. Power Sources*, vol. 133, no. 1, pp. 126–134, 2004.
[120] G. Cau, D. Cocco, M. Petrollese, S. Knudsen Kær, and C. Milan, "Energy management strategy based on short-term generation scheduling for a renewable microgrid using a hydrogen storage system," *Energy Convers. Manag.*, vol. 87, pp. 820–831, 2014.
[121] E. Hittinger, T. Wiley, J. Kluza, and J. Whitacre, "Evaluating the Value of Batteries in Microgrid Electricity Systems Using a Novel Energy System Model," *Energy Convers. Manag.*, vol. 89, p. 21, 2015.
[122] L. T. Lam and R. Louey, "Development of ultra-battery for hybrid-electric vehicle applications," *J. Power Sources*, vol. 158, no. 2 SPEC. ISS., pp. 1140–1148, 2006.
[123] matlabideas, "matlab ideas," 2011. [Online]. Available: https://matlabideas.wordpress.com/2011/10/31/connecting-solar-cells-to-electrical-circuits-designed-with-blocks-from-simpowersystems-library/. [Accessed: 15-Jun-2015].
[124] M. Siva, "PMSG based Wind Power Generation System," 2012. [Online]. Available: http://www.mathworks.com/matlabcentral/fileexchange/36116-pmsg-based-wind-power-generation-system/content/Wind_PMSG.mdl. [Accessed: 20-Dec-2015].

[125] S. Milla, “view_license,” *mathworks*, 2012. [Online]. Available: http://www.mathworks.com/matlabcentral/fileexchange/view_license?file_info_id=36116. [Accessed: 20-Dec-2015].
[126] N. Iwai, N. Kurahashi, Y. Kishita, Y. Yamaguchi, Y. Shimoda, S. Fukushige, and Y. Umeda, “Scenario analysis of regional electricity demand in the residential and commercial sectors - Influence of diffusion of photovoltaic systems and electric vehicles into power grids - Influence o,” *Procedia CIRP*, vol. 15, pp. 319–324, 2014.
[127] Eskom, “What is a kilowatt hour,” 2014. [Online]. Available: http://www.eskom.co.za/sites/idm/Documents/Appliance_Usage_rev41.pdf. [Accessed: 29-Jan-2016].
[128] T. Lambert, P. Gilman, and P. Lilienthal, “Micropower System Modeling with Homer,” *Integr. Altern. Sources Energy*, pp. 379–418, 2006.
[129] Gsma, “HOMER Software: Training Guide for Renewable Energy Base Station Design | Mobile for Development,” *Green Power Mob.*, 2010.
[130] L. Ferrer-Martí, A. Garwood, J. Chiroque, B. Ramirez, O. Marcelo, M. Garfí, and E. Velo, “Evaluating and comparing three community small-scale wind electrification projects,” *Renew. Sustain. Energy Rev.*, vol. 16, no. 7, pp. 5379–5390, 2012.
[131] M. Cheng and Y. Zhu, “The state of the art of wind energy conversion systems and technologies : A review,” *Energy Convers. Manag.*, vol. 88, pp. 332–347, 2014.
[132] J. J. Awerbuch and C. R. Sullivan, “Control of ultracapacitor-battery hybrid power source for vehicular applications,” *2008 IEEE Energy 2030 Conf. ENERGY 2008*, no. November, 2008.
[133] M. B. Camara, H. Gualous, F. Gustin, A. Berthon, and B. Dakyo, “DC / DC Converter Design for Supercapacitor and Battery Power Management in Hybrid Vehicle Applications — Polynomial Control Strategy,” *Technology*, vol. 57, no. 2, pp. 587–597, 2010.
[134] A. Burke, “Batteries and Ultracapacitors for Electric, Hybrid, and Fuel Cell Vehicles,” *Proc. IEEE*, vol. 95, no. 4, pp. 806–820, 2007.
[135] G. Zhang, X. Tang, and Z. Qi, “Research on battery supercapacitor hybrid storage and its application in MicroGrid,” *Asia-Pacific Power Energy Eng. Conf. APPEEC*, pp. 5–8, 2010.
[136] R. A. Dougal, S. Liu, and R. E. White, “Power and life extension of battery-ultracapacitor hybrids,” *IEEE Trans. Components Packag. Technol.*, vol. 25, no. 1, pp. 120–131, 2002.
[137] F. Touati, M. a. Al-Hitmi, N. A. Chowdhury, J. A. Hamad, and A. J. R. San Pedro Gonzales, “Investigation of solar PV performance under Doha weather using a customized measurement and monitoring system,” *Renew. Energy*, vol. 89, pp. 564–577, 2016.
[138] P. Kundur, J. Paserba, V. Ajjarapu, G. Andersson, a Bose, C. Canizares, N. Hatziargyriou, D. Hill, a Stankovic, C. Taylor, T. Van Cutsem, and V. Vittal, “Definition and classification of power system stability,” *IEEE Trans. Power Syst.*, vol. 19, pp. 1387–1401, 2004.
[139] J. Liang, Y. Qiu, M. Zhao, S. Kang, and H. Lu, “The modeling and numerical simulations of wind turbine generation system with free vortex method and simulink,” *Energy Convers. Manag.*, vol. 103, pp. 762–777, 2015.
[140] P. G. Arul, V. K. Ramachandaramurthy, and R. K. Rajkumar, “Control strategies for a hybrid renewable energy system : A review,” *Renew. Sustain. Energy Rev.*, vol. 42, pp.

597–608, 2015.
[141] S. L. Sanjuan, “Voltage Oriented Control of Three-Phase Boost PWM Converters,” 2010.
[142] S. S. Choi and H. S. Lim, “Factors that affect cycle-life and possible degradation mechanisms of a Li-ion cell based on LiCoO2,” *J. Power Sources*, vol. 111, no. 1, pp. 130–136, 2002.
[143] Z. Xu and S. Chowdhury, “A Review of Rural Electrification through Micro- grid Approach: South African context,” pp. 1–6.
[144] a. B. Sebitosi and P. Pillay, “Renewable energy and the environment in South Africa: A way forward,” *Energy Policy*, vol. 36, no. 9, pp. 3312–3316, 2008.
[145] S. GeoModel, “Solar GIS,” 2015. [Online]. Available: http://solargis.info/. [Accessed: 20-Nov-2015].
[146] Google, “GoogleMaps,” 2015. [Online]. Available: https://www.google.co.za/maps/place/Napier,+7270/@-34.4715281,19.8866553,14z/data=!4m2!3m1!1s0x1dd1ec51fdd5f407:0x629b7149efcf82b. [Accessed: 21-Nov-2015].
[147] Google, “Google Maps Job street.” [Online]. Available: https://www.google.co.za/maps/@-34.4745964,19.8869803,3a,75y,163.59h,80.91t/data=!3m6!1e1!3m4!1ssC1-LpHS1sOVXQGkoW3K3g!2e0!7i13312!8i6656. [Accessed: 21-Nov-2015].
[148] Vaisala, “5km Wind Map 7 13,” 2015. [Online]. Available: http://www.vaisala.com/en/energy/support/Resources/Pages/Free-Wind-And-Solar-Resource-Maps.aspx.
[149] Eskom, “Renewable Energy,” 2015. [Online]. Available: http://www.eskom.co.za/AboutElectricity/RenewableEnergy/Pages/Renewable_Energy.aspx. [Accessed: 29-Dec-2015].
[150] G. Geißler, J. Köppel, and P. Gunther, “Wind energy and environmental assessments - A hard look at two forerunners’ approaches: Germany and the United States,” *Renew. Energy*, vol. 51, pp. 71–78, 2013.
[151] Kayako, “Homer Support Knowledgebase,” 2015. [Online]. Available: http://support.homerenergy.com/index.php?/Knowledgebase/List. [Accessed: 10-Oct-2015].
[152] M. S. Ngan and C. W. Tan, “Assessment of economic viability for PV/wind/diesel hybrid energy system in southern Peninsular Malaysia,” *Renew. Sustain. Energy Rev.*, vol. 16, no. 1, pp. 634–647, 2012.
[153] S. K. Nandi and H. R. Ghosh, “Prospect of wind-PV-battery hybrid power system as an alternative to grid extension in Bangladesh,” *Energy*, vol. 35, no. 7, pp. 3040–3047, 2010.
[154] M. Hoogwijk, B. de Vries, and W. Turkenburg, “Assessment of the global and regional geographical, technical and economic potential of onshore wind energy,” *Energy Econ.*, vol. 26, no. 5, pp. 889–919, 2004.
[155] T. Ma, H. Yang, and L. Lu, “Study on stand-alone power supply options for an isolated community,” *Int. J. Electr. Power Energy Syst.*, vol. 65, pp. 1–11, 2015.
[156] G. J. Dalton, D. a. Lockington, and T. E. Baldock, “Feasibility analysis of stand-alone renewable energy supply options for a large hotel,” *Renew. Energy*, vol. 33, no. 7, pp. 1475–1490, 2008.
[157] G. J. Dalton, D. a. Lockington, and T. E. Baldock, “Case study feasibility analysis of

renewable energy supply options for small to medium-sized tourist accommodations," *Renew. Energy*, vol. 34, no. 4, pp. 1134–1144, 2009.
[158] J. L. Bernal-Agustín and R. Dufo-López, "Simulation and optimization of stand-alone hybrid renewable energy systems," *Renew. Sustain. Energy Rev.*, vol. 13, no. 8, pp. 2111–2118, 2009.
[159] J. Awerburch, "HOMER Knowledgebase 10565 - Required operating capacity, operating reserve," 2015. [Online]. Available: http://support.homerenergy.com/index.php?/Knowledgebase/Article/View/573/90/10565---required-operating-capacity-operating-reserve. [Accessed: 22-Nov-2015].
[160] J. Cotrell and W. Pratt, "Modeling the Feasibility of Using Fuel Cells and Hydrogen Internal Combustion Engines in Remote Renewable Energy Systems," *Contract*, no. September, 2003.
[161] IBC-solar, "ibc-solar," 2010. [Online]. Available: https://www.ibc-solar.pt/fileadmin/content/homepage/produtos/Download/Datasheet_Suntech_Power_STP_200_205_210_18Ud_(101029)_EN.pdf. [Accessed: 08-Aug-2015].
[162] Wind Energy Solutions, "WES5 Tulipo," *Cell Energy International*. [Online]. Available: http://cellenergyinternational.co.uk/pdf/WES5_Tulipo_brochure_ds1.pdf. [Accessed: 10-May-2015].
[163] Hoppecke, "OPzS Vented lead-acid battery." [Online]. Available: http://currentautomation.co.za/files/cur/1410249429_OPzS.pdf?cache=4120. [Accessed: 16-Aug-2015].
[164] M. T. Lawder, V. Viswanathan, and V. R. Subramanian, "Balancing Autonomy and Utilization of Solar Power and Battery Storage for demand based Microgrids," *J. Power Sources*, vol. 279, pp. 645–655, 2015.
[165] P. A Ruiz, C. R. Philbrick, E. Zak, K. W. Cheung, and P. W. Sauer, "Uncertainty Management in the Unit Commitment Problem," *Power Syst. IEEE Trans.*, vol. 24, no. 2, pp. 642–651, 2009.
[166] J. Awerburch, "10565 - Required operating capacity, operating reserve," 2015. [Online].Available:http://support.homerenergy.com/index.php?/Knowledgebase/Article/View/573/90/10565---required-operating-capacity-operating-reserve. [Accessed: 07-Jul-2015].
[167] Mouser Electronics, "Maxwell 160V Module." [Online]. Available: http://www.mouser.com/ds/2/257/Maxwell_160VModule_DS_3000246-5-341193.pdf. [Accessed: 12-Nov-2015].
[168] L. Gao, S. Liu, and R. A. Dougal, "Dynamic lithium-ion battery model for system simulation," *IEEE Trans. Components Packag. Technol.*, vol. 25, no. 3, pp. 495–505, 2002.
[169] J. McDowall, "Integrating energy storage with wind power in weak electricity grids," *J. Power Sources*, vol. 162, no. 2 SPEC. ISS., pp. 959–964, 2006.
[170] Y. Wang, S. Member, K. T. Tan, P. L. So, and S. Member, "Coordinated Control of Battery Energy Storage System in a Microgrid," 2013.

Appendices

Appendix A

Selected solar panel dimensions taken from data sheet.

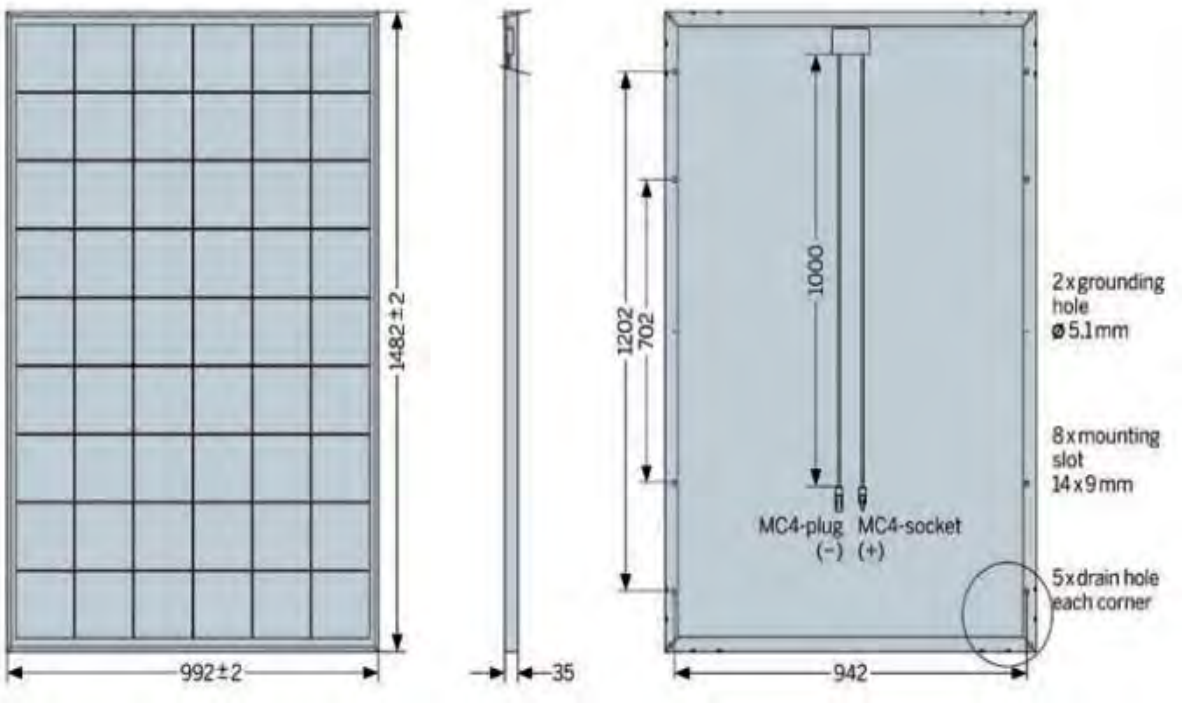

Appendix A Suntech STP210-18 / Ud PV panel dimensions [161]

Appendix B1

Energy and Power Voltage Curve taken from turbine datasheet

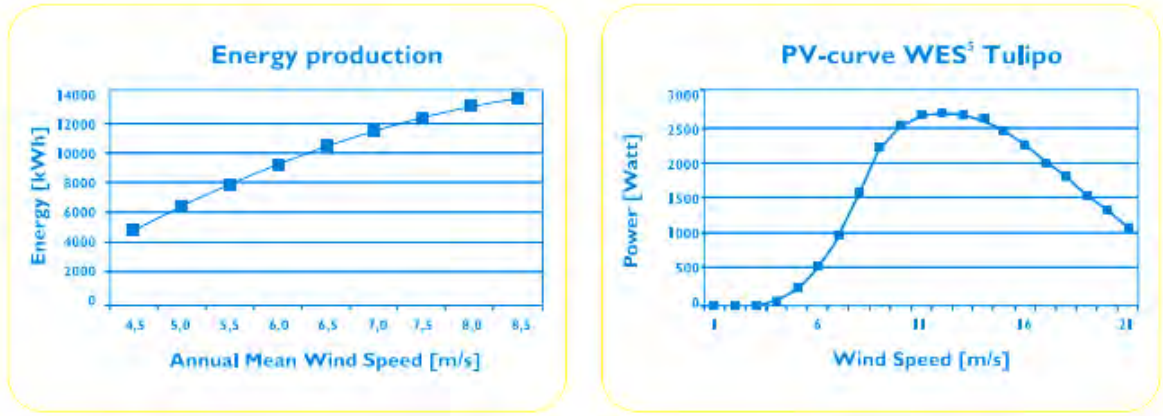

Appendix B1 Energy Production and Power-Voltage Curve of WES Tulipo datasheet [162]

Appendix B2

Selected Turbine Modelled in HOMER

Power curve

	Wind Speed (m/s)	Power Output (kW)
1	0.00	0.000
2	1.00	0.000
3	2.00	0.000
4	3.00	0.068
5	4.00	0.243
6	5.00	0.530
7	6.00	0.958
8	7.00	1.553
9	8.00	2.159
10	9.00	2.474
11	10.00	2.595
12	11.00	2.625
13	12.00	2.598
14	13.00	2.552
15	14.00	2.382
16	15.00	2.192

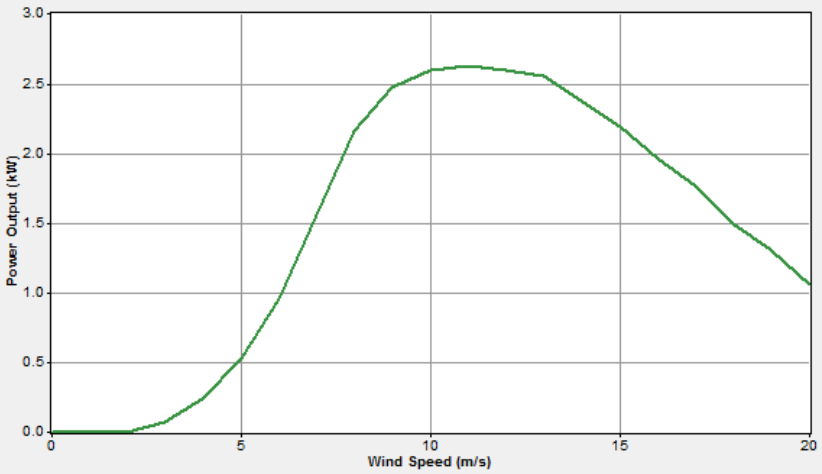

Appendix B2 HOMER Software WES Power Curve model

EBE Faculty: Assessment of Ethics in Research Projects (Rev2)

Any person planning to undertake research in the Faculty of Engineering and the Built Environment at the University of Cape Town is required to complete this form before collecting or analysing data. When completed it should be submitted to the supervisor (where applicable) and from there to the Head of Department. If any of the questions below have been answered YES, and the applicant is NOT a fourth year student, the Head should forward this form for approval by the Faculty EIR committee: submit to Ms Zulpha Geyer (Zulpha.Geyer@uct.ac.za; Chem Eng Building, Ph 021 650 4791).
NB: A copy of this signed form must be included with the thesis/dissertation/report when it is submitted for examination

This form must only be completed once the most recent revision EBE EiR Handbook has been read.

Name of Principal Researcher/Student: Imran Chotia Department: Electrical Engineering

Preferred email address of the applicant: chtimr001@myuct.ac.za

If a Student: Degree: MSc Electrical Engineering Supervisor: Dr S Chowdhury

If a Research Contract indicate source of funding/sponsorship: National Research Fund Scholarship

Research Project Title: Simulation of a Microgrid Energy storage system simulation using a Hybrid of Battery and Super capacitor system

Overview of ethics issues in your research project:

Question 1: Is there a possibility that your research could cause harm to a third party (i.e. a person not involved in your project)?	YES	(NO)
Question 2: Is your research making use of human subjects as sources of data? If your answer is YES, please complete Addendum 2.	YES	(NO)
Question 3: Does your research involve the participation of or provision of services to communities? If your answer is YES, please complete Addendum 3.	YES	(NO)
Question 4: If your research is sponsored, is there any potential for conflicts of interest? If your answer is YES, please complete Addendum 4.	YES	(NO)

If you have answered YES to any of the above questions, please append a copy of your research proposal, as well as any interview schedules or questionnaires (Addendum 1) and please complete further addenda as appropriate. Ensure that you refer to the EiR Handbook to assist you in completing the documentation requirements for this form.

I hereby undertake to carry out my research in such a way that

- there is no apparent legal objection to the nature or the method of research; and
- the research will not compromise staff or students or the other responsibilities of the University;
- the stated objective will be achieved, and the findings will have a high degree of validity;
- limitations and alternative interpretations will be considered;
- the findings could be subject to peer review and publicly available; and
- I will comply with the conventions of copyright and avoid any practice that would constitute plagiarism.

Signed by:

	Full name and signature	Date
Principal Researcher/Student:	Imran Chotia Signed	29 January 2015

This application is approved by:

Supervisor (if applicable):	SUNETRA CHOWDHURY Signed	29-1-15
HOD (or delegated nominee): *Final authority for all assessments with NO to all questions and for all undergraduate research.*	E BOTT Signed	17/3/15
Chair : Faculty EIR Committee For applicants other than undergraduate students who have answered YES to any of the above questions.		

Declaration

1. I know that plagiarism is wrong. Plagiarism is to use another's work and pretend that it is one's own.
2. I have used the IEEE convention for citation and referencing. Each contribution to, and quotation in, this final year project report from the work(s) of other people, has been attributed and has been cited and referenced.
3. This final year project report is my own work.
4. I have not allowed, and will not allow, anyone to copy my work with the intention of passing it off as their own work or part thereof

Name: Imran Chotia

Signature: Signed

Date: 30 March 2016